

DEVELOPMENT OF FLEXIBLE PAVEMENT RUT PREDICTION MODELS FROM
THE NCAT TEST TRACK STRUCTURAL STUDY SECTIONS DATA

Except where reference is made to the work of others, the work described in this dissertation is my own or was done in collaboration with my advisory committee.

This dissertation does not include propriety or classified information.

Suresh Immanuel Selvaraj

Certificate of Approval:

Mary Stroup-Gardiner
Professor
Civil Engineering

David H. Timm, Chair
Associate Professor
Civil Engineering

E. Ray Brown
Professor
Civil Engineering

Pradeep Lall
Professor
Mechanical Engineering

George T. Flowers
Interim Dean
Graduate School

DEVELOPMENT OF FLEXIBLE PAVEMENT RUT PREDICTION MODELS FROM
THE NCAT TEST TRACK STRUCTURAL STUDY SECTIONS DATA

Suresh Immanuel Selvaraj

A Dissertation
Submitted to
the Graduate Faculty of
Auburn University
in Partial Fulfillment of the
Requirements for the
Degree of
Doctor of Philosophy

Auburn, Alabama
August 4, 2007

DEVELOPMENT OF FLEXIBLE PAVEMENT RUT PREDICTION MODELS FROM
THE NCAT TEST TRACK STRUCTURAL STUDY SECTIONS DATA

Suresh Immanuel Selvaraj

Permission is granted to Auburn University to make copies of this dissertation at its discretion, upon request of individuals or institutions and at their expense.
The author reserves all publication rights.

Signature of Author

Date of Graduation

VITA

Suresh Immanuel Selvaraj, son of Mr. Jacob J. Selvaraj and Mrs. Sumathi Hebzebah, was born in Tamilnadu, India. He completed his Bachelor of Engineering (B.E) degree in Civil Engineering from the College of Engineering-Guindy (CEG), Anna University, India in 2001. After graduation, he worked as an engineer in Secon Surveys Private Limited, Bangalore in transportation infrastructure projects for one year. In August 2002, he returned back to graduate school and received his Master of Engineering (M.E) degree in Highway and Transport Management, with honors from the College of Engineering-Guindy (CEG), Anna University, India in 2004. In August 2004, he entered the Graduate School at Auburn University to pursue the Doctor of Philosophy (PhD) degree in Civil Engineering with specialization in Pavements and Materials.

DISSERTATION ABSTRACT

DEVELOPMENT OF FLEXIBLE PAVEMENT RUT PREDICTION MODELS FROM
THE NCAT TEST TRACK STRUCTURAL STUDY SECTIONS DATA

Suresh Immanuel Selvaraj

Doctor of Philosophy, August 4, 2007
(M.E., College of Engineering, Anna University, Chennai, India, 2004)
(B.E., College of Engineering, Anna University, Chennai, India, 2001)

233 Typed Pages

Directed by David H. Timm

This research study was attempted to address two of the most important aspects of mechanistic-empirical (M-E) pavement design. As M-E design continues to advance toward full implementation by state agencies, there is a need to assess the accuracy of the load-response models under dynamic truck loading. The load response model is a core component of flexible pavement M-E design and the common practice is to use a layered elastic approach to predict pavement responses under load. Concerns regarding accuracy of this type of model arise when considering unbound materials exhibiting non-linear behavior, viscoelastic hot-mix asphalt (HMA) materials and dynamic loads applied by moving traffic. Despite this, layered elastic models continue to be the state-of-the-practice for most pavement design and analysis applications. Considering this, one of the objectives of this study was to assess the accuracy of a layered elastic model with respect to measured pavement responses under live truck traffic.

Specifically, eight test sections at the National Center for Asphalt Technology (NCAT) Test Track were instrumented to measure vertical pressures in the unbound base and subgrade layers. The test sections consisted of various HMA thicknesses and used modified and unmodified asphalt binders. Material properties were established using backcalculation of falling weight deflectometer (FWD) data. The test sections were then simulated with the layered elastic computer program, WESLEA. Comparisons between theoretical and measured pavement responses were made over a wide range of environmental conditions and the two different truck load configurations. The measured responses were generally within 15% of theoretical with a strong correlation between the two sets of data.

After validating the load response model, an effort was made to develop a rut prediction model that can accurately predict field rutting. HMA layer rutting was the only source of rutting observed in all eight sections. During the development of the rut prediction model, two different approaches were evaluated and compared. First, a vertical strain-based rut model was built by relating the measured rutting to the vertical strain on the top of granular layers and the number of truck axle passes. In the second approach, rutting was linked with maximum shear strain in the HMA layer and the number of truck axle passes. The model coefficients were analyzed for both approaches and their validity was evaluated. It was concluded that the shear strain model predicted rutting realistically and the model coefficients distinguished rutting in polymer-modified and unmodified asphalt sections.

ACKNOWLEDGEMENTS

The author would like to express his deepest gratitude to his advisor Dr.David Timm, for all the support, patience, and encouragement he received throughout the course of his graduate study. The author feels very fortunate to have Dr.Timm as his advisor who gave him complete freedom to explore on his own and at the same time offered watchful guidance whenever required. Sincere thanks are due to Dr.Timm for all the discussions that helped the author to sort out the technical details of this work.

The author would like to acknowledge the doctoral committee members, Dr.Ray Brown, Dr.Mary Stroup Gardiner and Dr.Pradeep Lall for their many valuable, thought-provoking comments and constructive criticisms on this research that helped to improve the overall quality of this dissertation. Special thanks are to Dr.Nedret Billor for reviewing the dissertation and acting as an outside reader.

Also, the author wishes to acknowledge his appreciation to Dr.Buzz Powell, Test Track Manager for providing the required data for this research and the NCAT staff members for sharing their experience and advice during the course of this research. The author wishes to acknowledge all members of the Test Track structural study research team for their assistance in all possible ways during the course of this research.

Style manual or journal used Auburn University Graduate School Guide to Preparation of Doctoral Dissertation & NCAT Research Report Style

Computer software used Microsoft Word[™], Microsoft Excel[™], DATAQ[™], DADiSP[™] and Datafit[™]

TABLE OF CONTENTS

LIST OF TABLES	xii
LIST OF FIGURES	xiii
1 INTRODUCTION	1
1.1 BACKGROUND	1
1.1.1 Flexible Pavement Rutting.....	5
1.1.2 Load Response Mechanistic Model and Transfer Function	7
1.1.3 National Center for Asphalt Technology (NCAT) Test Track	9
1.2 OBJECTIVES	11
1.3 SCOPE OF STUDY	11
1.4 ORGANIZATION OF DISSERTATION	12
2 LITERATURE REVIEW	13
2.1 INTRODUCTION	13
2.2 HISTORY OF PAVEMENT DESIGN.....	13
2.2.1 Empirical Design	13
2.2.2 Mechanistic-Empirical Design.....	15
2.3 LOAD RESPONSE MODEL VALIDATION	18
2.3.1 Development of Multilayer Layer Elastic Theory	18
2.4 MULTILAYER ELASTIC THEORY VALIDATION STUDIES.....	21
2.4.1 TRRL Study (1962)	21
2.4.2 Shell Research Study (1967).....	23
2.4.3 TRRL Study (1967)	25
2.4.4 Shell Laboratory Study (1967).....	26
2.4.5 Dutch Road Research Study (1967).....	30
2.4.6 San Diego Test Road Study (1970)	33
2.4.7 TRRL Study (1972)	36
2.4.8 WSU Test Track Study (1972)	38
2.4.9 Nottingham (TRRL) Study (1979).....	40
2.4.10 Amsterdam Study (1982).....	42
2.4.11 Minnesota Road Research Study (1997)	43
2.4.12 NCAT Study (2005)	46
2.4.13 European Study Results (2002)	48
2.4.14 Advanced Models	49
2.4.15 Summary.....	50

2.5	FLEXIBLE PAVEMENT RUTTING	51
2.5.1	Rutting Progression.....	52
2.6	RUT PREDICTION MODELS	53
2.6.1	Historical Trend on the Development of Rut Prediction Models	54
2.7	SIGNIFICANT RUT PREDICTION MODELS	56
2.7.1	Finn et al. Model (1977)	57
2.7.2	TRRL Equation (1979)	58
2.7.3	Shell (1977) & Asphalt Institute Model (1982).....	59
2.7.4	Allen & Deen Model (1980).....	60
2.7.5	Leahy's Model (1989).....	61
2.7.6	WesTrack Model (1999).....	63
2.7.7	M-E based Rut models from LTPP Data	63
2.7.8	Rut Prediction Model from In-Service Pavements	64
2.7.9	MEPDG Model (2004)	66
2.7.10	Three Stage Model.....	67
2.7.11	Other Rut Prediction Models	69
2.7.12	Summary.....	69
3	TEST FACILITY AND DATA COLLECTION	70
3.1	INTRODUCTION	70
3.2	NCAT TEST TRACK.....	70
3.3	STRUCTURAL SECTION INSTRUMENTATION	76
3.3.1	Earth Pressure Cells	77
3.3.2	Temperature Probes	80
3.4	DATA ACQUISITION.....	81
3.5	TRUCKING.....	83
3.6	HIGH SPEED DATA COLLECTION AND PROCESSING	86
3.6.1	Data Collection	86
3.6.2	Data Processing.....	88
3.7	MATERIAL PROPERTY DATA COLLECTION	90
3.8	PERFORMANCE DATA COLLECTION.....	93
3.9	SUMMARY	98
4	LOAD RESPONSE MODEL VALIDATION	99
4.1	INTRODUCTION	99
4.2	DYNAMIC DATA VALIDATION	100
4.2.1	Trend in Base and Subgrade Pressure.....	101
4.3	PRESSURE PREDICTION MODEL.....	113
4.4	THEORETICAL PRESSURE CALCULATION.....	122
4.4.1	Material Characterization.....	122
4.4.2	Selection of Pavement Cross Section	122
4.4.3	HMA Modulus Characterization.....	124
4.4.4	Base Modulus.....	129
4.4.5	Subgrade Modulus	131
4.4.6	Pressure Computation	134
4.5	VALIDATION OF LAYERED ELASTIC RESPONSE MODEL	135
4.6	SUMMARY AND CONCLUSION	137

5	RUT PREDICTION MODEL DEVELOPMENT	138
5.1	BACKGROUND	138
5.2	RUTTING PROGRESSION IN THE NCAT TEST TRACK.....	140
5.3	MODEL METHODOLOGY: VERTICAL STRAIN BASED MODEL	142
5.4	VERTICAL STRAIN BASED RUTTING MODEL DEVELOPMENT	144
5.4.1	Need for Base and Subgrade Strain Calculation.....	144
5.4.2	Strain Prediction Models.....	145
5.4.3	Trucking Data	149
5.5	VERTICAL STRAIN BASED RUT PREDICTION MODEL RESULTS..	150
5.5.1	Rut Prediction Model Form	150
5.5.2	Analysis on Model Coefficients.....	157
5.6	SHEAR STRAIN BASED RUTTING MODEL DEVELOPMENT	161
5.6.1	Background.....	161
5.6.2	Methodology	162
5.6.3	Maximum Shear Strain Computation	163
5.7	RUT PREDICTION MODEL: SHEAR STRAIN APPROACH	168
5.7.1	Analysis of Model Coefficients	174
5.7.2	Grouped Model Based on Binder Modification.....	176
5.8	SUMMARY	179
6	CONCLUSIONS AND RECOMMENDATIONS	180
6.1	CONCLUSIONS.....	180
6.2	LIMITATIONS AND RECOMMENDATIONS	183
	REFERENCES	186
	APPENDIX.....	203

LIST OF TABLES

Table 2.1 Measured and Computed Responses (Terrel and Krukar, 1970).....	40
Table 2.2 Comparison of Model Results to Measured Response (Ullidtz, 2002)	49
Table 2.3 Causes of Rutting (Monismith et al., 1972).....	51
Table 3.1 Structural Study Section HMA Mix Parameters.....	75
Table 3.2 Axle Weight Data by Truck (Priest and Timm, 2006)	83
Table 3.3 FWD Data Cut Off Dates for Analysis	92
Table 4.1 Pressure Prediction Model Coefficients for Triple Trailer Truck.....	116
Table 4.2 Pressure Prediction Model Coefficients for Box Trailer Truck.....	116
Table 4.3 Final Pressure Model Coefficients for Triple Trailer	117
Table 4.4 Final Pressure Model Coefficients for Box Trailer	117
Table 4.5 HMA Modulus Prediction Model Coefficients	126
Table 4.6 Backcalculated Modulus Values for Modified Binder Sections.....	128
Table 4.7 Backcalculated Modulus Values for Unmodified & SMA Binder Sections .	128
Table 5.1 Vertical Strain Model Results for Triple and Box Trailer	149
Table 5.2 Subgrade Vertical Strain Based Rut Prediction Model Coefficients.....	151
Table 5.3 Shear Strain Model Results for Triple and Box Trailer.....	167
Table 5.4 Shear Strain Model Coefficients.....	168

LIST OF FIGURES

Figure 1.1 M-E Design Framework.....	3
Figure 1.2 Typical Flexible Pavement Rutting Profile (LTPP, 2003).....	6
Figure 2.1 Flow chart for M-E Design Scheme (After Timm et al., 1998).....	17
Figure 2.2 Comparison of Experimental and Theoretical Values of Stress on Subgrade Whiffin and Lister, 1962).....	23
Figure 2.3 Comparison Between Measured Strain and Calculated Strain at Different Depths (Klomp and Niesman, 1967).....	25
Figure 2.4 Measured and Calculated Strain at the Bottom of Asphalt Layer for Varying Asphalt Stiffness (Gusfeldt and Dempwolff, 1967).....	27
Figure 2.5 Measured and Calculated Strains at 9.5 cm in Asphalt Layer for Varying Asphalt Stiffness (Gusfeldt and Dempwolff, 1967).....	28
Figure 2.6 Measured and Calculated Vertical Stress in Gravel Layer for Varying Asphalt Stiffness (Gusfeldt and Dempwolff, 1967).....	29
Figure 2.7 Measured and Calculated Strains at the Top of Asphalt Layer & at the Bottom of Asphalt Layer (Nijboer, 1967).....	31
Figure 2.8 Measured and Calculated Deflections (Nijboer, 1967).....	32
Figure 2.9 Measured and Calculated Vertical Pressure Values (Nijboer, 1967).....	32
Figure 2.10 Comparison of Measured and Computed Surface Longitudinal Strain (Hicks and Finn, 1967).....	35

Figure 2.11 Comparison of Measured and Computed Surface Transverse Strain (Hicks and Finn, 1967).	36
Figure 2.12 Comparison of Calculated and Measured Values For Road Machine Section 1 Vertical Normal Stress (Thrower et al., 1972).....	37
Figure 2.13 Comparison of Calculated and Measured Deflections For Road Machine Section 1 Surface Deflection (Thrower et al., 1972).	38
Figure 2.14 Comparison of Predicted and Measured Permanent Strains in Pavement Sections 1 and 2 (Brown and Bell, 1979).	41
Figure 2.15 Comparison of Predicted and Measured Permanent Strains in Pavement Section 3 (Brown and Bell, 1979).....	42
Figure 2.16 Measured and Calculated Strains from Mn/Road (Bao, 2000).	45
Figure 2.18 Measured Vs Theoretical Asphalt Strain (Barrett and Timm, 2005).	47
Figure 2.19 Measured Vs Theoretical Stress in Base and Improved Subgrade Layer (Barrett and Timm, 2005).	48
Figure 2. 20 Rut Progression for Increasing Load Repetitions (El-Basyouny et al., 2005).	52
Figure 3.1 Overview of the NCAT Test Track.	71
Figure 3.2 Location of Structural Study Sections.	72
Figure 3.3 Structural Experiment Sections Layer Cross Section (Timm et al., 2004). ...	74
Figure 3.4 HMA Layer Composition of Structural Experiment Sections (Timm and Priest, 2006).	75
Figure 3.5 Structural Experiment Sections Instrumentation Layout.	76
Figure 3.6 Geokon 3500 Earth Pressure Cell Used at the Test Track.	78

Figure 3.7 Subgrade Earth Pressure Cell Placed on the Top of Subgrade.....	78
Figure 3.8 The Base Pressure Cell on Top of Base Layer.	79
Figure 3.9 Temperature Probes Bundled Together.....	80
Figure 3.10 Data Acquisition System Used at the Test Track.	82
Figure 3.11 Road Side Data Logger Box Used at the Test Track.....	82
Figure 3.12 NCAT Test Track Test Vehicles – Triple Trailer.	84
Figure 3.13 NCAT Test Track Test Vehicles – Box Trailer.....	84
Figure 3.14 Average Strain by Truck and Pass (Priest and Timm, 2006).	87
Figure 3.15 Typical Pressure Response Trace for a Triple Trailer.....	89
Figure 3.16 FWD Testing on the Structural Study Sections.....	91
Figure 3.17 DIPSTICK Profile Measurement at the Test Track.	94
Figure 3.18 Automated Profile Measurement at the Test Track using ARAN.....	94
Figure 3.19 Six Foot Straight Edge Transverse Profile Measurement.	95
Figure 3.20 Computation of Rutting from DIPSTICK Profiler.....	96
Figure 4.1 Pressure vs Temperature Relationship (Section N3, Triple Trailer).	101
Figure 4.2 Trend of Base and Subgrade Pressures in Section N1-Triple Trailer.	102
Figure 4.3 Trend of Base and Subgrade Pressures in Section N2-Triple Trailer.	103
Figure 4.4 Trend of Base and Subgrade Pressures in Section N3-Triple Trailer.	103
Figure 4.5 Trend of Base and Subgrade Pressures in Section N4-Triple Trailer.	104
Figure 4.6 Trend of Base and Subgrade Pressures in Section N5-Triple Trailer.	104
Figure 4.7 Trend of Base and Subgrade Pressures in Section N6-Triple Trailer.	105
Figure 4.8 Trend of Base and Subgrade Pressures in Section N7-Triple Trailer.	105
Figure 4.9 Trend of Base and Subgrade Pressures in Section N8-Triple Trailer.	106

Figure 4.10	Trend of Base and Subgrade Pressures in Section N3-Box Trailer.....	106
Figure 4.11	Trend of Base and Subgrade Pressures in Section N4-Box Trailer.....	107
Figure 4.12	Trend of Base and Subgrade Pressures in Section N5-Box Trailer.....	107
Figure 4.13	Trend of Base and Subgrade Pressures in Section N6-Box Trailer.....	108
Figure 4.14	Trend of Base and Subgrade Pressures in Section N7-Box Trailer.....	108
Figure 4.15	Trend of Base and Subgrade Pressures in Section N8-Box Trailer.....	109
Figure 4.16	Base Pressure by Truck and Pass.	111
Figure 4.17	Subgrade Pressure by Truck and Pass.	111
Figure 4.18	Maximum Base and Subgrade Pressure Response for Truck Pass.....	112
Figure 4.19	Example shows the HMA Thickness and Pressure Relation.....	115
Figure 4.20	Measured and Predicted Pressures - Modified binder Sections (Triple)....	119
Figure 4.21	Measured and Predicted Pressures - Unmodified Test Sections (Triple)...	119
Figure 4.22	Measured and Model Predicted Pressures - SMA Test Sections (Triple)..	120
Figure 4.23	Measured and Predicted Pressures – Modified Test Sections (Box).....	120
Figure 4.24	Measured and Predicted Pressures - Unmodified Test Sections (Box).....	121
Figure 4.25	Measured and Predicted Pressures - SMA Test Sections (Box).....	121
Figure 4.26	Pavement Cross Section for Backcalculation.....	123
Figure 4.27	HMA Modulus vs. Temperature Relationship.	125
Figure 4.28	Backcalculated Average Base Modulus by Section.	129
Figure 4.29	Backcalculated Base Modulus Values Used in Mechanistic Analysis.....	130
Figure 4.30	Backcalculated Average Subgrade Modulus by Section.....	131
Figure 4.31	Computed Base Pressure for Varying Subgrade Moduli.	132
Figure 4.32	Computed Subgrade Pressure for Varying Subgrade Moduli.	133

Figure 4.33 Measured and Theoretical Pressure Comparison for Triple Trailer.	136
Figure 4.34 Measured and Theoretical Pressure Comparison for Box Truck.	136
Figure 5.1 Rutting Progression in Structural Test Sections.	141
Figure 5.2 Vertical Strain Based Rut Prediction Methodology Flow Chart.	143
Figure 5.3 Base Strain Vs Temperature (Eq 5.2) - Triple Trailer.	147
Figure 5.4 Subgrade Strain Vs Temperature (Eq 5.2) - Triple Trailer.	147
Figure 5.5 Base Strain Vs Temperature (Eq 5.2) - Box Trailer.	148
Figure 5.6 Subgrade Strain Vs Temperature (Eq 5.2) - Box Trailer.	148
Figure 5.7 Predicted and Measured Rutting for Section N1.	153
Figure 5.8 Predicted and Measured Rutting for Section N2.	153
Figure 5.9 Predicted and Measured Rutting for Section N3.	154
Figure 5.10 Predicted and Measured Rutting for Section N4.	154
Figure 5.11 Predicted and Measured Rutting for Section N5.	155
Figure 5.12 Predicted and Measured Rutting for Section N6.	155
Figure 5.13 Predicted and Measured Rutting for Section N7.	156
Figure 5.14 Predicted and Measured Rutting for Section N8.	156
Figure 5.15 HMA Thickness vs Rutting Model Coefficients.	158
Figure 5.16 Rutting Model Coefficients for Modified and Unmodified Sections.	159
Figure 5.17 Shear Strain Based Rut Prediction Methodology Flow Chart.	162
Figure 5.18 Typical Shear Strain Profile (Section N1 at 40 Deg F-Triple Trailer).	164
Figure 5.19 Maximum Shear Strain Vs Temperature Relation (Triple Trailer).	166
Figure 5.20 Maximum Shear Strain Vs Temperature Relation (Box Trailer).	166
Figure 5.21 Shear Strain Model: Predicted and Measured Rutting for Section N1.	169

Figure 5.22 Shear Strain Model: Predicted and Measured Rutting for Section N2.....	170
Figure 5.23 Shear Strain Model: Predicted and Measured Rutting for Section N3.....	170
Figure 5.24 Shear Strain Model: Predicted and Measured Rutting for Section N4.....	171
Figure 5.25 Shear Strain Model: Predicted and Measured Rutting for Section N5.....	171
Figure 5.26 Shear Strain Model: Predicted and Measured Rutting for Section N6.....	172
Figure 5.27 Shear Strain Model: Predicted and Measured Rutting for Section N7.....	172
Figure 5.28 Shear Strain Model: Predicted and Measured Rutting for Section N8.....	173
Figure 5.29 HMA Thickness vs Shear Strain Based Rutting Model Coefficients.....	174
Figure 5.30 Shear Strain Based Model Coefficients for Modified and Unmodified Sections.....	175
Figure 5.31 Shear Strain: Rut prediction for Modified Sections (N1, N4, N5).....	177
Figure 5.32 Shear Strain: Rut Prediction For Unmodified Sections (N2, N3, N6).	177
Figure 5.33 Shear Strain: Rut Prediction For SMA Sections (N7 and N8).	178

CHAPTER 1

INTRODUCTION

1.1 BACKGROUND

The empirically-based Guide for Design of Pavement Structures published by the American Association of State Highway and Transportation Officials (AASHTO) in 1972, 1986 and 1993 is currently used by almost 80 percent of the U.S. state departments of transportation (DOTs) to design flexible pavements (ERES, 2004). This design guide uses empirical equations developed from the AASHO Road Test (HRB, 1962) to relate pavement characteristics with pavement performance.

To design flexible pavements using the 1993 AASHTO Guide, the designer has to input specific values for reliability, variability, change in serviceability, subgrade modulus, and predicted future traffic in terms of equivalent single axle loads (ESALs). The structural number is calculated from the AASHO equation from which the required pavement thickness is determined. The structural number is an abstract number expressing the structural strength of a pavement required for a given combination of soil support, total traffic in ESALs and allowable change in serviceability over the period of pavement life.

Though the design guide has been used for traffic loadings greater than 50 million equivalent single-axle loads (ESALs), the basic design equations in the guide were developed from traffic loadings of less than 2 million ESALs (Seeds, 2000). The developed equations were based on the specific pavement materials and roadbed soil present at the AASHO Road Test and they are suitable for the environment equivalent to the AASHO Road Test site only. Identical axle loads and configurations, as opposed to mixed traffic were used to develop the empirical design equation. The limited nature of the AASHO Road Test in terms of pavement layer configuration, loading pattern, and environmental conditions forced pavement engineers to look beyond existing empirical-based design and move toward mechanistic-empirical (M-E) design procedures.

M-E design is an efficient method of pavement design in which pavement responses such as stress and strain are determined from the load, material properties and climate, which are then empirically related to field performance. The result leads to more robust analysis and design approach that is applicable over a much wider range of environmental conditions. Further, M-E design can adapt to new materials and different types of loading conditions.

Generally, M-E design combines the elements of mechanistic modeling and performance observations to determine the required pavement thickness for a set of design conditions (Timm et al., 1998). The environmental conditions, different pavement layers and traffic loading, are the primary inputs into the mechanistic model. The model predicts the mechanistic pavement responses in terms of stress and strain, which are then used to calculate the pavement damage (rutting and fatigue cracking) with the help of transfer functions. If the pavement damage is not within the predetermined permissible

limit, then the pavement thickness is increased and the process is repeated. A simple M-E design framework is shown in Figure 1.1.

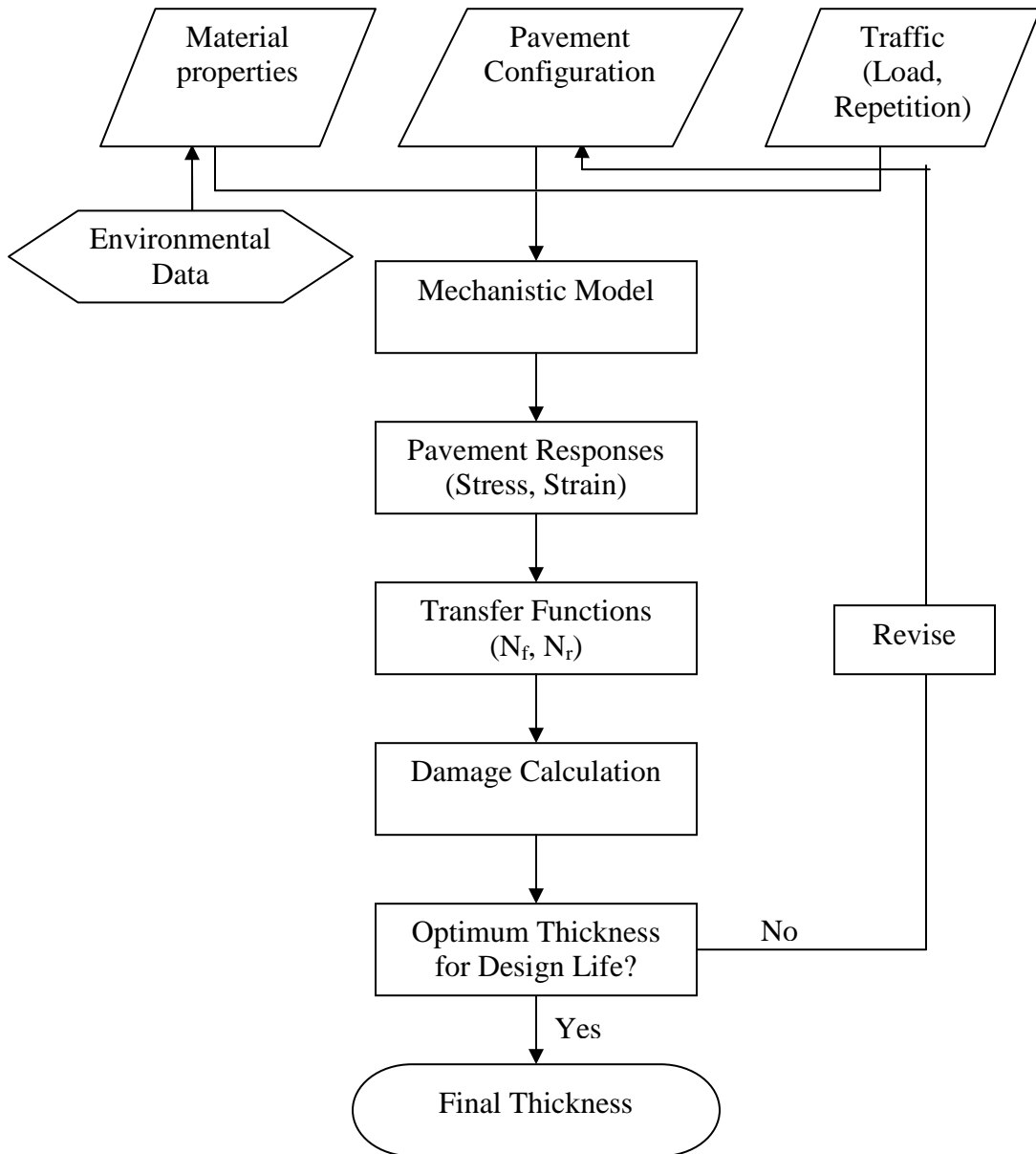


Figure 1.1 M-E Design Framework.

Transfer functions are the performance equations that are used to predict pavement life and are a critical empirical component in M-E design. They are typically derived from statistically-based correlations of pavement responses with observed performance from laboratory test specimens or from full-scale road test data. These transfer functions need local calibration, since the equations generated for a particular climate and location may not be applicable for another region (Priest, 2005). Extensive field and laboratory calibrations are of paramount importance for the success of the M-E design approach (Ioannides, 1992).

Examples of some of the new M-E based procedures used by states are those that have been developed for the Minnesota Department of Transportation (Timm et al., 1998) and the Washington State Department of Transportation (WSDOT, 1995). There is also a group of lead states working toward a successful implementation of M-E design. These include: Arizona, Florida, Kentucky, Maryland, Minnesota, Mississippi, Missouri, Montana, New York, New Jersey, New Mexico, Pennsylvania, Texas, Utah, Virginia, Washington and Wisconsin (FHWA, 2006). Other countries, such as Canada, the United Kingdom, the Netherlands, Australia, India and South Africa, have also adopted M-E design methods in whole or in part (Hajek et al., 2001; AUSTRROADS, 2001; Das, 2004; Theyse et al., 1996)

As the M-E design approach for designing flexible pavements is in the process of evaluation by many state agencies and researchers, there is a need to assess the accuracy of the load-response model and performance prediction models under dynamic truck loading which are the core components in the M-E design process. The research study

reported in this dissertation explored two important aspects of M-E design; namely, the mechanistic load response model and the pavement performance model to predict rutting.

1.1.1 Flexible Pavement Rutting

Historically, the term “pavement rutting” or “permanent deformation” was used to describe any distortion in the pavement surface, including shoving and pushing due to mix instability (Goetz et al., 1957). The distress identification manual for the long term pavement performance program (LTPP) defines rutting as a longitudinal surface depression along the wheel path (LTPP, 2003). Flexible pavement rutting is also called “permanent deformation”. It represents an accumulation of small amounts of unrecoverable deformation that occur whenever the traffic load is applied on the pavement.

Research and trench studies at the AASHO Road Test proved that rutting does not occur only in HMA layers, but can also occur in any of the underlying pavement layers. However in most pavements, rutting appears only as a change in transverse surface profile and it is often contributed to surface instability (Southgate et al., 1988; Dawley et al., 1990; Sousa et al., 1993; Archilla and Madanat, 2001; Chen et al., 2003; Fwa et al., 2004; Zhou et al., 2004; Gokhale et al., 2005).

There are two basic types of rutting common in the field; they are structural rutting and mix densification or consolidation. Structural rutting occurs when one or more pavement layers show permanent deformation due to excessive loadings or insufficient shear strength. Mix densification occurs when the pavement surface exhibits wheel path depressions as a result of compaction/mix design problems. Usually, rutting

occurs predominantly under the action of heavy vehicles in hot climates and under slow moving traffic conditions. It is mostly found in the surface layer of asphalt pavement near the loading area. Shear deformation and densification are the main reasons for flexible pavement rutting. A typical rutting profile is shown in Figure 1.2.

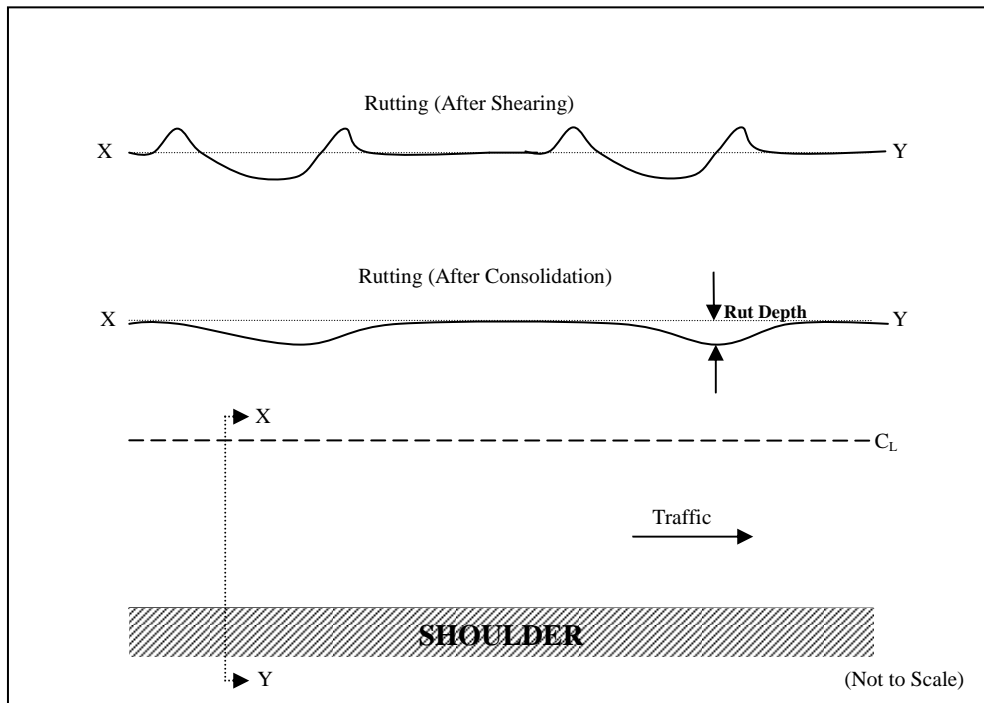


Figure 1.2 Typical Flexible Pavement Rutting Profile.

Rutting is a serious safety issue for road users. When the vehicle moves along the rutted portion of the pavement, steering becomes difficult and it reduces driving comfort. If rain water pools in the rutted wheel path, it can result in the hydroplaning of vehicles. Further, the decreased thickness in the rutted portions may accelerate fatigue cracking. So, accurate rutting prediction of pavements is very important to pavement design.

1.1.2 Load Response Mechanistic Model and Transfer Function

The mechanistic model that computes pavement responses in different locations of a pavement is the core component in the M-E design procedure. Hence, the validity of response models is an important prerequisite for reliable evaluation of structural pavement condition. Historically, analyses have been limited to static loads resting on layered elastic systems.

Generally speaking, these approaches are reasonably accurate for design purposes; however, there is a need to further validate layered elastic models with the help of field-measured responses. Though there were some questions about the assumptions made in the layered elastic theory in pavement applications, such as uniform contact pressure, isotropic layers, interface conditions, loading pattern etc., the layered elastic theory predict pavement responses reasonably well (Chadbourn et al., 1997; Hildebrand, 2002; Epps et al., 2003; Barrett and Timm, 2005; Immanuel and Timm, 2006). Ullidtz (2002) compared the available software results with the measured response and the comparison shows that the layered elastic packages predict the pavements responses reasonably well in most cases. The current mechanistic empirical pavement design guide (MEPDG) also uses a layered elastic analysis package, JULEA to compute the pavement responses. A questionnaire conducted to study the available accelerated pavement testing (APT) sites around the world show that elastic layer analysis is the most frequently used procedure to compute pavement responses in APT (Hugo and Epps, 2004).

Currently, many available computer packages help the pavement designer to calculate pavement responses by inputting the load configuration and material properties. WESLEA, VESYS, KENLAYER, CIRCLY4, BISAR, VEROAD, ELSYM, PDMAP,

JULEA, ILLIPAVE, FENLAP are some of the important available computer programs that are used in pavement analysis and design (Monismith, 2004). In some cases, the models have been further refined to estimate pavement performance in terms of rutting and fatigue by incorporating appropriate transfer functions (e.g., WESLEA for Windows 3.0 and KENLAYER).

Finite Element (FE) models are also very good for predicting pavement response and are capable of considering both dynamic wheel and environmental loading. But they are complicated to operate and time consuming. Therefore, they are not typically used in M-E design for flexible pavements. However at this time, the state of the art is to use the multilayer elastic theory which has been implemented in most of the available software packages.

The pavement response parameters in terms of stress and strain are included in the transfer function to relate the mechanistic and empirical parts of pavement design. The transfer function to predict the number of load cycles for rutting failure typically has the following form (Shook et al., 1982; Timm et al., 1998; Newcomb and Von Quintus, 2002; Priest, 2005):

$$N_r = k_1 \left(\frac{1}{\epsilon_v} \right)^{k_2} \quad (1.1)$$

Where:

N_r = Number of load repetitions until rutting failure

ϵ_v = Maximum vertical compressive strain at the top of the subgrade

k_1, k_2 = Empirically derived constants

While the vertical compressive strain can be mechanistically determined through a load-response model, the empirical constants have to be determined from laboratory or field performance data. Including an accurate mechanistic model to predict pavement response in the design approach is very important for accurate rut prediction. Further, it would be advantageous to derive the empirical constants mentioned in Equation 1.1 directly from field data since they do not need any shift factors. Shift factor accounts for differences between laboratory and field conditions, when a model is built purely from lab data to reflect field behavior.

1.1.3 National Center for Asphalt Technology (NCAT) Test Track

Accelerated pavement testing is a useful tool to accomplish the above-mentioned task of calibrating the load response model with field response data. Here the pavement is subjected to accelerated traffic and the empirical constants can be directly derived from the field. In addition, before laying any new mixtures in the field or adopting new pavement design methods, they have to be tested for their usefulness. It would take at least 20 or more years to effectively test and verify the materials and design methods in existing highways. However, full scale accelerated testing facilities such as the NCAT Test Track and WesTrack can safely verify these within two or three years of accelerated loading. Further, the outcome of these test road results, in addition to facilities such as Virginia Smart Road and Minnesota Road Research Project help to verify the available theoretical models for pavement design.

The NCAT Test Track has now been in use since 2000. The experimental sections on the 1.7 mile oval-shaped accelerated pavement testing facility are being funded by a number of state DOTs and Federal Highway Administration (FHWA). The first research cycle in 2000 focused primarily on performance evaluation in terms of surface rutting of the available 46 HMA test sections when they were subjected to 10 million equivalent single axle load (ESAL) in two years. The ESAL is defined as the total number of a standard 18 kip standard axle load applications required to produce the same damage or loss of serviceability as a number of applications of one or more different axle loads and/or configurations over the life of pavement.

In 2003, twenty three of the original 46 test sections were left in place for further traffic loading of another 10 million ESALs and 22 new sections were built. Of the 22 new sections, 8 sections were used for M-E design validation and analysis. The eight sections that were especially dedicated for M-E design were called structural study sections. The main objectives of the structural study experiment were to validate mechanistic pavement models, develop transfer functions for typical asphalt mixtures and pavement cross-sections, studying the dynamic effects on pavement deterioration from a mechanistic viewpoint and to evaluate the effect of thickness and polymer modification on structural performance (Timm et al., 2004). The structural study sections were sponsored by the Alabama DOT, Indiana DOT and the FHWA.

Various sensors were embedded in the structural study sections to fully capture the pavement responses and environmental characteristics. A detailed explanation of the instrumentation and the structural study sections are provided in Chapter 3.

1.2 OBJECTIVES

The primary objectives of this research study were to:

1. Develop a field-calibrated rut performance model from the NCAT Test Track structural experiment sections.
2. Assess the accuracy and validate the layered elastic model relative to measured pavement responses.

1.3 SCOPE OF STUDY

To fulfill these objectives, eight 200 ft test sections were instrumented in the structural study sections to measure vertical pressures in the unbound base and subgrade layers.

High speed pavement response data, pavement performance data, environmental data and traffic data were collected at regular intervals. With the help of collected instrumented responses (vertical pressure) comparisons were made between measured and predicted pavement responses under a variety of environmental conditions. This attempt falls under fulfilling the secondary objective of load-response mechanistic model validation.

The measured pavement rutting was studied in detail and a fully field-calibrated model to predict rutting was developed. In this rut prediction model, the conventional vertical strain rut model approach was compared against the proposed new shear strain rut model approach. A fully field-calibrated rut prediction model that can be easily used in the M-E design guide was presented as a final outcome of this research.

1.4 ORGANIZATION OF DISSERTATION

This dissertation is organized into six remaining chapters. Chapter 2 presents a literature review of M-E design, available rut performance models, field rutting characterization and measurements and effect of binder modification on pavement performance with respect to rutting. Chapter 3 mainly details the NCAT pavement testing facility. The main focus of this chapter is to explain structural study sections, embedded instrumentation, trucking operation and data collection efforts. Chapter 4 deals with the layered elastic pavement response model validation. The dynamic data collection and processing are also presented in this chapter along with the material characterization. In Chapter 5, the development of vertical strain based rut model and the new fully field calibrated shear strain based rut model development is explained. A detailed study on the model coefficients is also presented. The conclusions and recommendations for future work related to load response model validation and rut prediction model are given in Chapter 6.

CHAPTER 2

LITERATURE REVIEW

2.1 INTRODUCTION

In this chapter, available literature on the development of mechanistic empirical design concepts, pavement load response model validation, flexible pavement rutting phenomenon and rut prediction models are explained in detail.

2.2 HISTORY OF PAVEMENT DESIGN

2.2.1 Empirical Design

Over the years, test road results have been used for efficient design of pavements and for better understanding of pavement performance over time under traffic loading. Some key findings from earlier road tests such as Maryland Road Test (HRB, 1945), AASHO Road Test (HRB 1962), San Diego Road Test (Hicks and Finn, 1970), WesTrack Test Track (Epps et al., 1998), the Minnesota Road Research project (Mn/Road, 1990) and NCAT Test Track (Brown et al., 2002) helped designers to develop more efficient pavement design procedures. The foremost among these test roads was the AASHO Road Test conducted in Ottawa, Illinois from 1958 to 1960. The data gathered from the test road form the basis of the AASHTO Design Guide for Pavement Structures (AASHTO, 1993).

Historically used pavement design methods in the past such as California Bearing Ration (CBR) method of design, and other empirical based designs relied more on empirical correlations with past performance, index-value-based characterizations of material properties and engineering judgment for design strategy selection (Seeds, 2000). Further, the empirical design method which was developed from the AASHO road test had many shortcomings. The developed empirical equations in the design guide only related loss in serviceability, traffic, and pavement thickness. Since the equations were developed from specific conditions at the AASHO Road Test, they have some significant limitations. The main limitations are given below (WSDOT, 2003):

1. The design equations were developed for specific pavement materials and roadbed soil present at the AASHO Road Test.
2. The equations were developed only based on the environment at the AASHO Road Test conditions.
3. The final design equations are based on an accelerated two-year testing period rather than for a longer, more typical pavement life that normally ranges from 20 to 40 years. Therefore, environmental factors were difficult if not impossible to extrapolate out for longer periods.
4. The traffic loading applied during the testing cycle was only 1.1 million ESAL. The loads used to develop the equations were operating vehicles with identical axle loads and configurations, as opposed to mixed traffic.
5. The truck tire pressures used to apply accelerate loading was only 80 psi.

In order to apply the equation developed as a result of the AASHO Road Test, some unrealistic assumptions are needed:

1. The characterization of subgrade soil support may be extended to other subgrade soils by an abstract soil support scale.
2. The mixed traffic loading may be characterized by the ESAL concept.
3. Material characterizations may be applied to other surfaces, bases, and subbases by assigning appropriate layer coefficients.
4. The two year period accelerated testing done at the AASHO Road Test can be extended for longer design periods.

2.2.2 Mechanistic-Empirical Design

The limited nature of the AASHO Road Test in terms of loading pattern, environmental conditions and the unrealistic assumptions forced pavement engineers to look beyond existing empirical-based design and move towards the M-E design procedure. Increased axle loading and tire pressures, different axle configurations, new materials for pavement construction, advances in mix design methods, varying climatic condition with in and between regions, make the current 1993 empirically-based AASHTO design guide less applicable for present conditions.

Further, advancements in computing technology and pavement performance prediction models enable designers to consider specific distress modes such as rutting and fatigue cracking as a function of mechanistic pavement responses. The M-E design concept has been in practice for quite some time and the basic principles and framework of mechanistic design method was laid out during the First International Conference on Structural Design of Asphalt Pavements (Dornon, 1962). In an attempt to demonstrate that mechanistic design methods were complete and available, several substantial papers

were solicited during the Fourth International Conference on Structural Design of Asphalt Pavements to describe such systems. Peattie (1962) and Dormon (1962) and Dormon and Edwards (1967) presented several concepts, based on such analyses, which would later become a part of the M-E based design developed by Shell researchers and later by other organizations and researchers.

Though there are existing M-E pavement design approaches developed by various organizations, the M-E Pavement Design Guide (MEPDG) developed under NCHRP 1-37A has brought international attention to M-E design. A typical M-E design approach is depicted in Figure 2.1. The M-E design procedure relies on predicting pavement responses such as stresses, strains and deflections under load and empirically relating these to field performance. The pavement responses are then converted through transfer functions into pavement life predictions (N_f) and damage (D) is computed through Miner's hypothesis. The concept of seasonal changes in material properties is also shown in the Figure 2.1 whereby the design method can accommodate changes in properties as a function of changing temperatures and moisture contents where applicable (Timm et al., 1998). Further, the M-E design is a more robust analysis and design approach that is applicable over a much wider range of climatic conditions and this method adapt new materials and varying traffic patterns.

One important aspect of M-E design method is the load response model which predicts stress and strains in various layers of pavement structure. The other core component in the M-E design process is the performance prediction models that predict pavement distresses in terms of rutting and fatigue cracking.

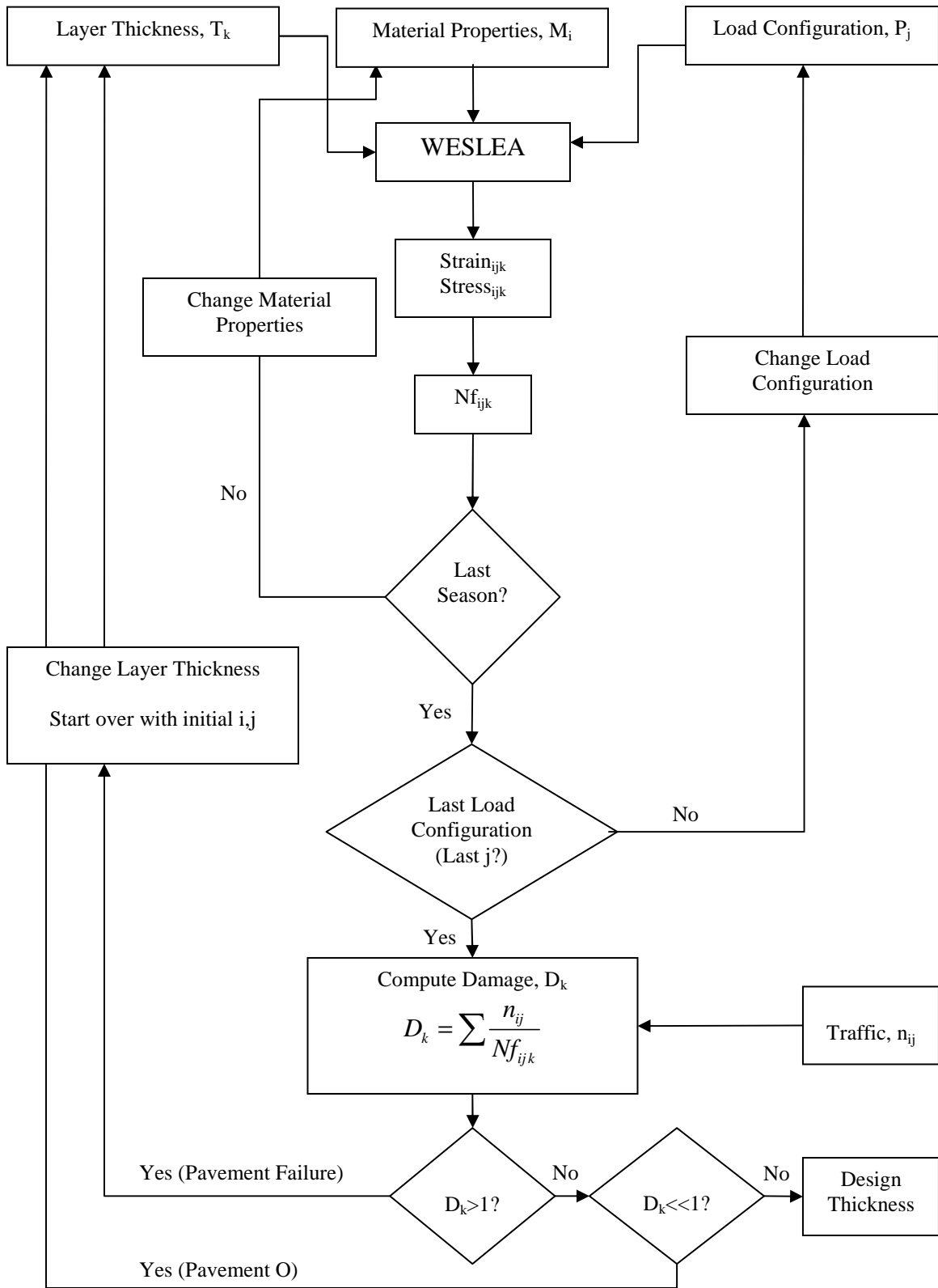


Figure 2.1 Flow chart for M-E Design Scheme (After Timm et al., 1998).

2.3 LOAD RESPONSE MODEL VALIDATION

2.3.1 Development of Multilayer Layer Elastic Theory

Modeling pavement responses is central in mechanistic pavement analysis and design. Hence, the validity of response models is an important prerequisite for efficient design and reliable evaluation of pavement condition. An important consideration in M-E design is the accuracy of load response model that predicts pavement response under wheel loads. An accurate mechanistic model is required to determine the pavement response that may be used in the performance equation (Timm and Newcomb, 2003).

After Boussinesq's elastic theory was developed to describe single layer structures of infinite width and depth in early 1880's, for over half a century their applicability to pavement structures as a layered system was not explored. The original Boussinesq's elastic theory was based on a concentrated load applied on an elastic half space. The solutions are based on the assumption that the material that constitutes the half space is linear elastic. The stresses, strains, and deflections due to a concentrated load can be integrated to obtain those due to a circular loaded area (Huang, 1993).

Before the development of Burmister's layered theory in 1943, much attention was paid to Boussinesq's solutions because they were the only ones available (Huang, 1993). In 1943, Donald M. Burmister expanded Boussinesq's formulations to derive elastic response for two layered systems. In 1945, Burmister developed three-layer elastic theory. It was then possible to treat pavements as layered systems in order to compute responses at layer interfaces under representative loading conditions. This development of multilayer elastic theory was a milestone for pavement analysis and

design. The main assumptions involved in the layered elastic theory are explained in the later part of this chapter.

Burmister's multi-layered theory to predict pavement response did not receive widespread attention until the First International Conference on the Structural Design of Asphalt Pavements in 1962. In that conference, important contributions were made by many researchers (Whiffin and Lister, 1962; Skok and Finn, 1962; Peattie, 1962; Dormon, 1962). They illustrated how the layered elastic analysis could be used for pavement response computation and to analyze pavement distress. A number of general solutions for determination of stresses and deformations in multilayered elastic solids also were presented at the 1962 conference. These general solutions, coupled with rapidly advancing computer technology, fostered the development of current generation multi-layer elastic and other advanced programs such as viscoelastic and finite element based computer programs.

Currently, available computer packages help the pavement designer to calculate pavement responses by inputting the load configuration and material properties. WESLEA, VESYS, KENLAYER, CIRCLY4, BISAR, VEROAD, ELSYM, PDMAP, JULEA, ILLIPAVE, FENLAP are some of the important available computer programs that are used to compute pavement responses (Monismith, 2004). Some computer programs (WESLEA, KENLAYER, BISAR, CIRCLY and JULEA) use the multilayer elastic theory assuming all pavement layers are linearly elastic. Few computer programs (VESYS, VEROAD) consider the HMA layer as visco-elastic, and some packages use the finite element approach (ILLIPAVE and FENLAB) to compute pavement responses.

In currently used analytical based pavement design procedures, layered elastic analysis is the primary method for defining pavement response under traffic loading. The use of finite element approach (ILLIPAVE, FENLAB) has limited application to date because of its complexity and computational time constraints. At this time, it has been used primarily for research purposes. It is tempting to believe that a more complex model will produce better results than a simple model, but that is not necessarily the case. If the results from the simple model are as good (or better) than those from more complex models, the simpler model has to be preferred (Ullidtz, 2002).

The current MEPDG uses layered elastic analysis package JULEA to compute pavement responses (ERES, 2004). A questionnaire conducted in various APT facilities shows that elastic layer analysis is most frequently being used in APT facilities for pavement response calculation (Hugo and Epps, 2004).

The elastic layer theory employs some assumptions to calculate mechanistic responses at different depths in a pavement system. Some of the main assumptions are (Ullidtz, 2002):

1. The pavement layers are isotropic, homogenous and elastic in nature.
2. Each layer has a finite thickness except for the lower layer, and all layers are infinite in lateral directions.
3. The loading pattern is static over a circular area.
4. Full friction is developed between layers at each interface.

Though the assumptions are questionable for calculating pavement responses, layered elastic theory has been in practice because of its simplicity. Even though the assumptions on which a model are based are simplifications of reality, the model may

still be useful if the stresses and strains it produce are reasonably close to stresses and strains in real pavements (Ullitz, 2002). To find out whether a particular model is useful or not, the response predicted by the model has to be compared to the response measured from actual pavement structures.

2.4 MULTILAYER ELASTIC THEORY VALIDATION STUDIES

As mentioned above, in order to validate the theory the response needs to be compared against field measurement. This section details similar research done to validate layered elastic models. The accuracy and validation from reliable field measurements are of vital importance for load response models. With the help of instrumentation embedded in pavements, actual pavement responses can be measured directly from the field. The First International Conference on the Design of Asphalt Pavements held at the University of Michigan (Ann Arbor) in 1962 was the starting point for studies on validation of elastic layer theory with field measured responses.

2.4.1 TRRL Study (1962)

In a study conducted at the Transportation Road Research Laboratory (TRRL) in London, 3" diameter and 5/8" thick piezoelectric gauges were used to measure vertical stress on base and subgrade pavement layers (Whiffin and Lister, 1962). The tested pavement structures had an HMA thickness of 4" and the base thickness varied from 6 to 8". The base layer was composed of different materials such as lean concrete, soil-cement, crushed stone and asphalt treated base. A 15 kilometer per hour (km/h) moving wheel load of 2,300 lb was applied and the vertical stress on top of pavement layers was

measured by the embedded piezoelectric gauges. The wave propagation technique developed by Shell researchers and dynamic modulus testing were done to compute the elastic moduli of component pavement layers.

A layered elastic model was used to calculate vertical stresses and they were compared with measured vertical stresses. Good agreement between measured and calculated responses was obtained in this study as shown in Figure 2.2. Being the first study of its kind, the researchers were not able to provide any reasons for the small differences seen between experimental and theoretical values. However this study proved to be a starting point for similar research. From this work it was also shown that the dynamic stresses applied to the soil increased with an increase in road temperature. This outcome was expected since asphalt modulus reduces with increasing temperature resulting in higher stresses transmitted to the lower pavement layers. Further, the measured stresses were found to be proportional to wheel load. The measured and calculated vertical stresses at the top of the subgrade for different base types are given in Figure 2.2.

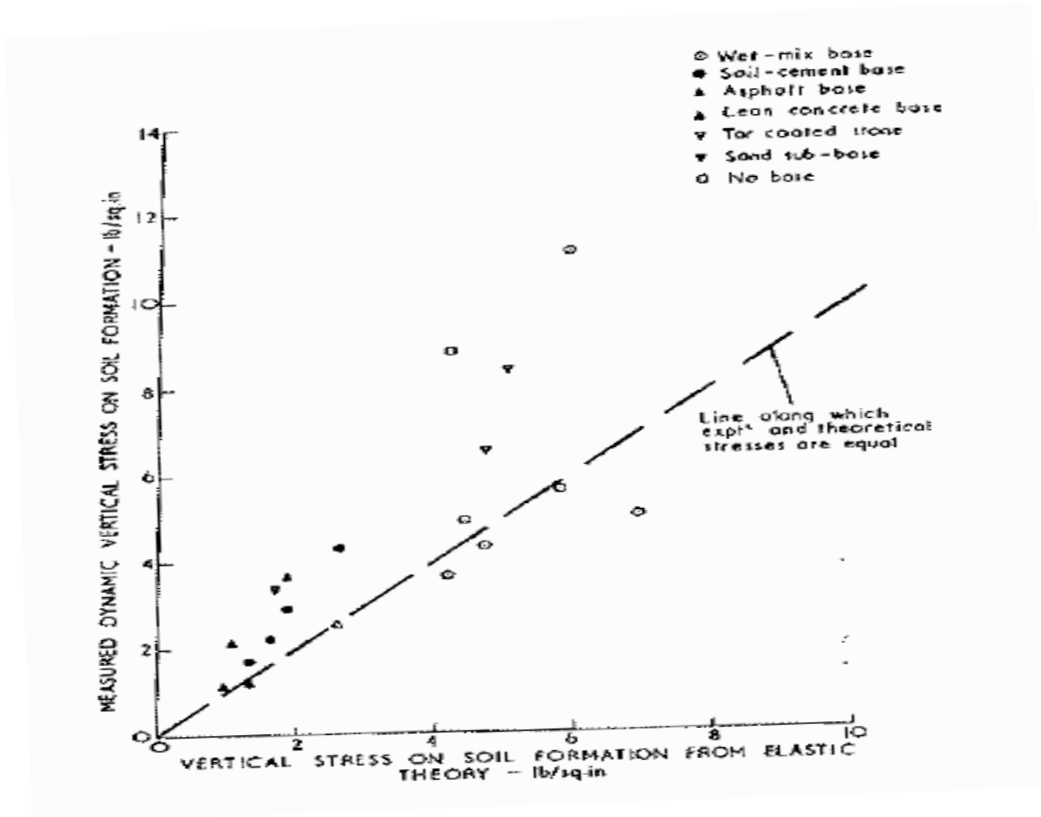


Figure 2.2 Comparison of Experimental and Theoretical Values of Stress on Subgrade (Whiffin and Lister, 1962).

2.4.2 Shell Research Study (1967)

In a similar study conducted by Shell researchers (Klomp and Niesman, 1967), field measured strain values were compared against theoretically computed strain values. The strains were measured at different depths of pavement (0, 3, 8 and 14 cm from top of pavement surface) for a wheel load of 1650 kg and at a velocity of about 30 km/h. The moduli of the asphalt materials were determined at various temperatures and various frequencies to obtain an elastic moduli curve covering a wide range of stiffness values.

In order to obtain dynamic modulus of subgrade under actual moisture content and compaction conditions, the wave propagation method was used. Wave propagation is a non-destructive method in which the propagation velocity of the wave travel is related to the layer stiffness. This method was carried out on top of the subgrade and later on top of all the layers. For theoretical strain calculation, a layered elastic computer program developed by researchers at the Shell Thornton Research Center was used. Two different Poisson ratios (0.35 and 0.50) were assumed for the asphalt layer during computation.

Figure 2.3 shows the comparison between measured strain and calculated strain values at different depths. Except strain measurements at the very top of the structure, reasonable agreement was observed between measured and theoretical values, though the simulated values were generally lower than measured. Deeper in the structure, at 11 cm, the simulation and measurement showed very good agreement. This signifies potential problems with both simulation and measurement near the pavement surface that should be further investigated. Also, as shown in Figure 2.3, the calculated pavement response varies with Poisson's ratio, which signifies the importance of accurate estimation of Poisson's ratio in the analysis.

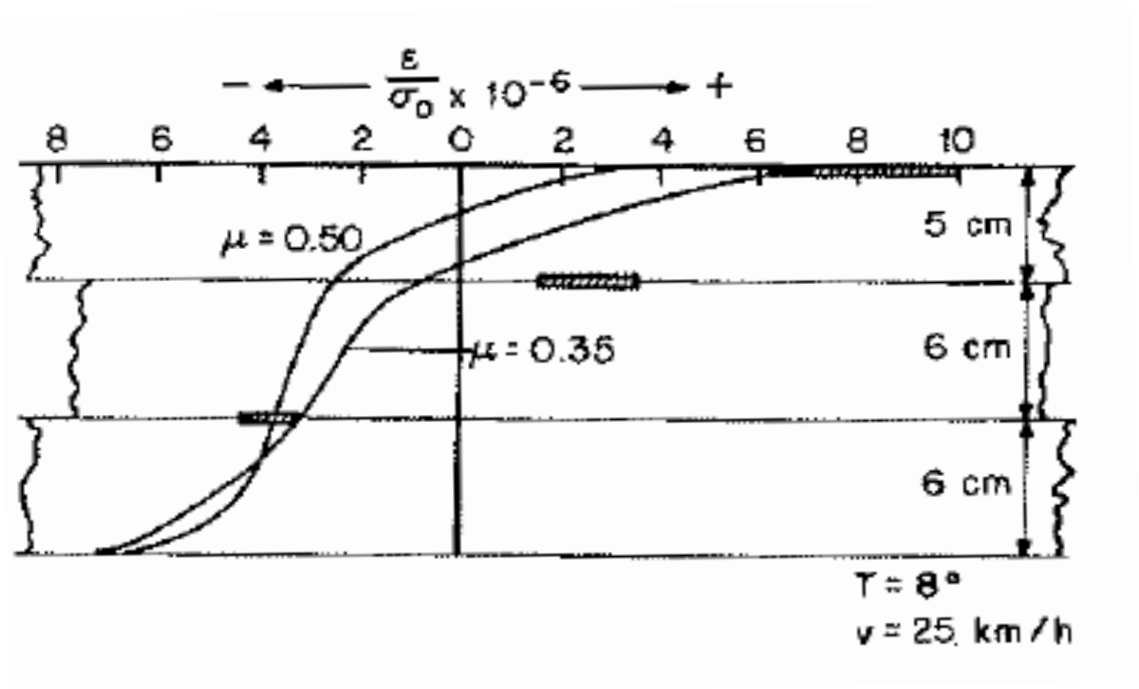


Figure 2.3 Comparison Between Measured Strain and Calculated Strain at Different Depths (Klomp and Niesman, 1967).

2.4.3 TRRL Study (1967)

In a research study conducted at TRRL (Brown and Pell, 1967), 2.5” diameter and 0.43” thick diaphragm type pressure cells were used to measure vertical pressures on top of granular layers. Two different contact pressures (7.5, 17 psi) and three different loading areas (6, 9 & 12”) were used to apply the traffic load on the test pit. The pressure values calculated with elastic theory matched very well with field-measured pressure values. The satisfactory prediction of strain and deflection values by elastic layer theory was an outcome of this validation work.

2.4.4 Shell Laboratory Study (1967)

A study was conducted by researchers at Amsterdam to compare theoretical pavement responses with field measurements (Gusfeldt and Dempwolff, 1967). Two test sections (10x10 m) in the test track were used for this purpose. The test sections had an asphalt layer thickness of 14 cm and a gravel base thickness of 86 cm. Strain gauges, pressure cells and thermocouples were installed at different depths in the asphalt concrete and base layers. Dynamic elastic modulus measurements with the vibration machine developed at Amsterdam Shell Laboratory gave a subgrade modulus value of 1300 kg/cm^2 . The gravel base used in the test section had a dynamic elastic modulus value of 2600 kg/cm^2 . The dynamic HMA stiffness varied from 8000 kg/cm^2 to $100,000 \text{ kg/cm}^2$. The wheel load was varied between 400 and 2000 kg. However, to compare theoretical results with measured responses, the wheel load was kept at 1000 kg. The tire pressure was set at 5 kPa/cm^2 . The maximum speed of the loading vehicle was maintained at 50km/h and it was driven by an electric motor via a cable line.

The theoretical pavement response in terms of stress and strain was calculated using a layered elastic computer program developed by Shell researchers. The results obtained in this study (Figures 2.4-2.6) showed reasonably good agreement between direct measurement and theoretical model results. The experimental values at the bottom of asphalt concrete layer were somewhat smaller than the theoretical results (Figure 2.4). Theoretical and measurement values matched closely for strain values measured at a depth of 9.5 cm (Figure 2.5). The reasons for all these observations were not explained by the researchers.

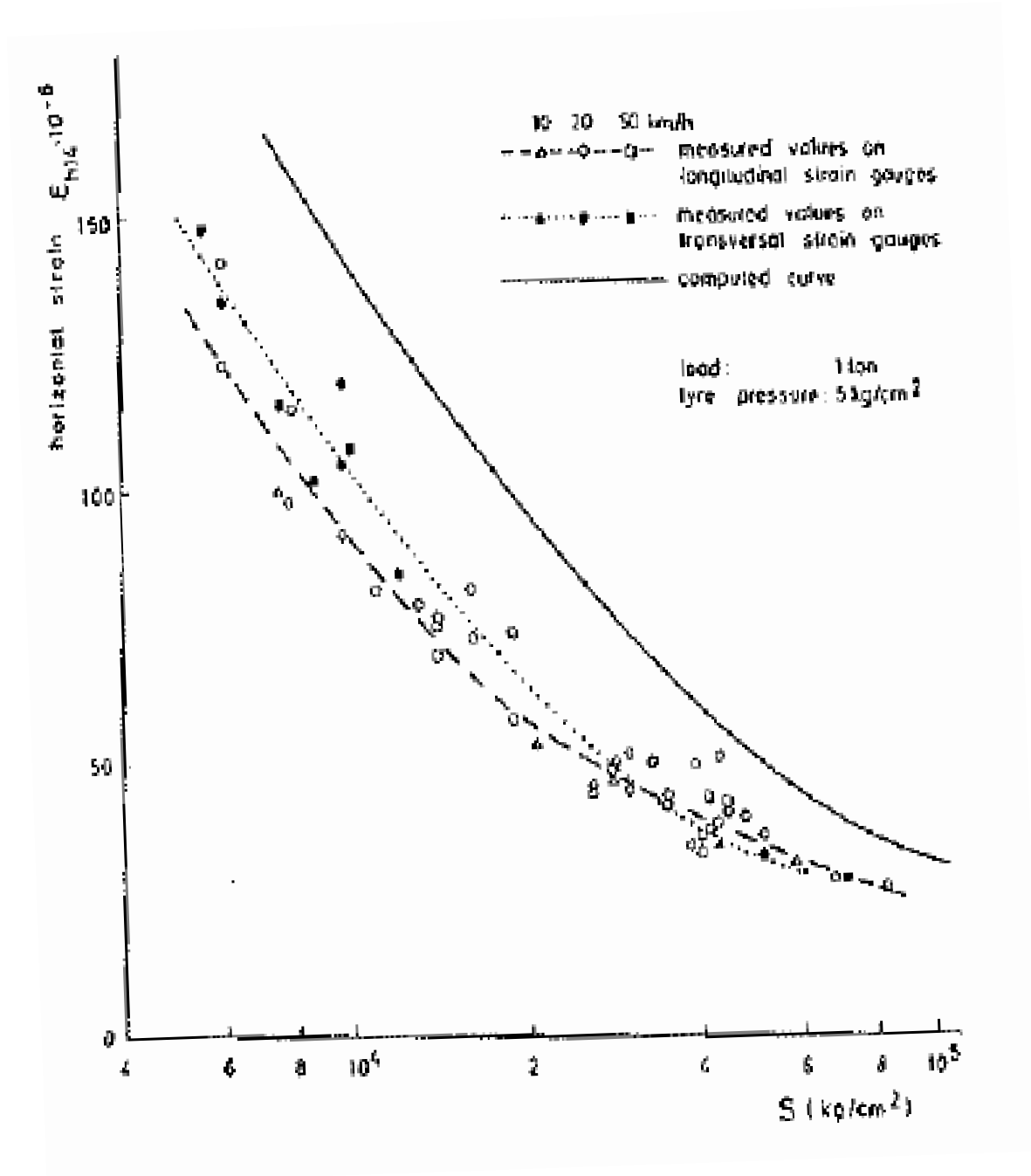


Figure 2.4 Measured and Calculated Strain at the Bottom of Asphalt Layer for Varying Asphalt Stiffness (Gusfeldt and Dempwolff, 1967).

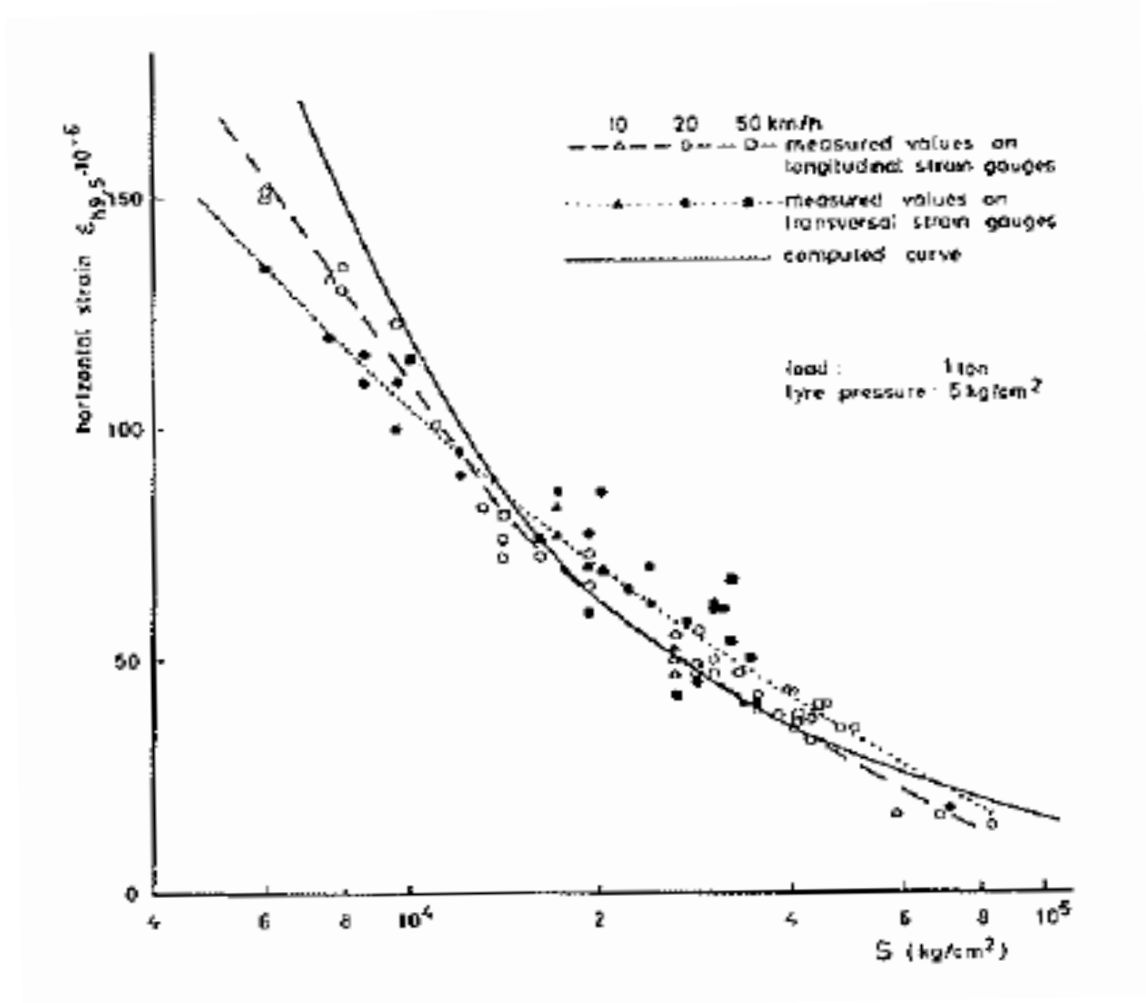


Figure 2.5 Measured and Calculated Strains at 9.5 cm in Asphalt Layer for Varying Asphalt Stiffness (Gusfeldt and Dempwolff, 1967).

In the case of pressure cells embedded at a depth of 19 cm, the conformity between measured and theoretical values was fairly good (Figure 2.6). At greater depths the deviations became somewhat greater. The measured stress values were always somewhat lower than theoretical values. Though most of the measured responses compared well with theory, appreciable deviations which did not show a systematic trend were also observed. This study recommended more detailed studies to compare theory

and measured responses with extensive/advanced measurements to eliminate systematic errors to reduce the scatter in test results.

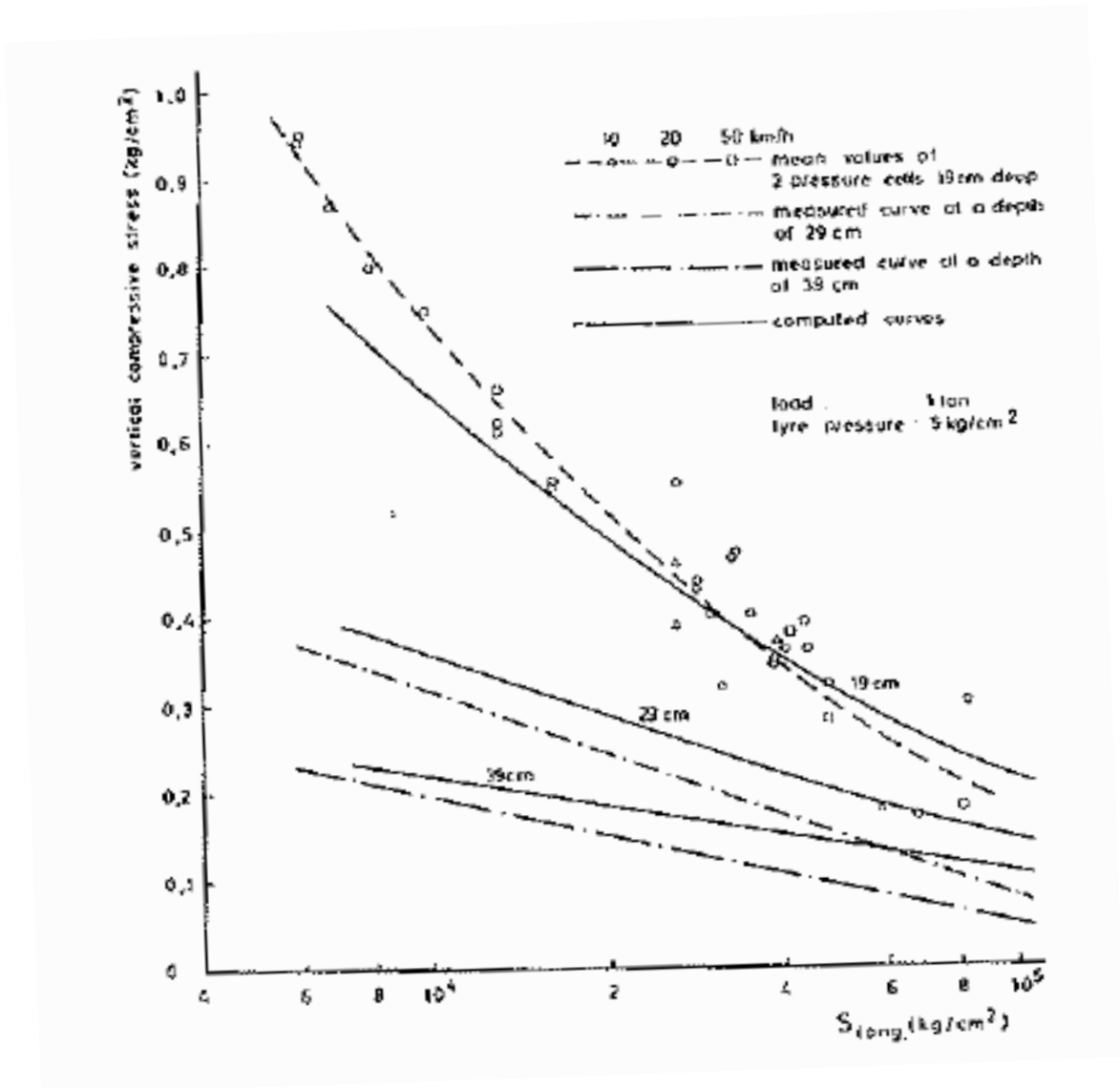


Figure 2.6 Measured and Calculated Vertical Stress in Gravel Layer for Varying Asphalt Stiffness (Gusfeldt and Dempwolff, 1967).

2.4.5 Dutch Road Research Study (1967)

In research conducted at the Dutch Road Research Center at Holland, Nijboer (1967) used the pressure cell developed in TRRL to measure vertical stress on top of base and subgrade layers. Strain gauges developed in the Shell Research Laboratory were used in this study to measure strain responses. For measuring vertical deflections, a new optical system designed by the Shell Researchers was used. The tests were carried out on State Highway No.1, a four lane undivided highway that carried 15,000 to 20,000 vehicles a day in both directions. The test road consisted of 19 cm of asphalt concrete thickness. Strain gauges were embedded at different depths in the asphalt concrete layer (0, 4, 9, and 19 cm) and pressure cells were embedded at the layer interface and at different depths in the soil.

The dynamic elastic properties of the asphalt concrete were determined by a vibration technique developed by Shell researchers, both on the road and in the laboratory. A small difference between the road measurements and the laboratory investigation was observed by the researchers. The elastic modulus (E) value of HMA varied ($20,500 \text{ kg/cm}^2$ to $135,000 \text{ kg/cm}^2$) based on vehicle speed. The soil had a stiffness of $2,400 \text{ kg/cm}^2$. The theoretical values were calculated using Burmister layer theory and good agreement was observed when the results were compared against field measured responses (Figure 2.7).

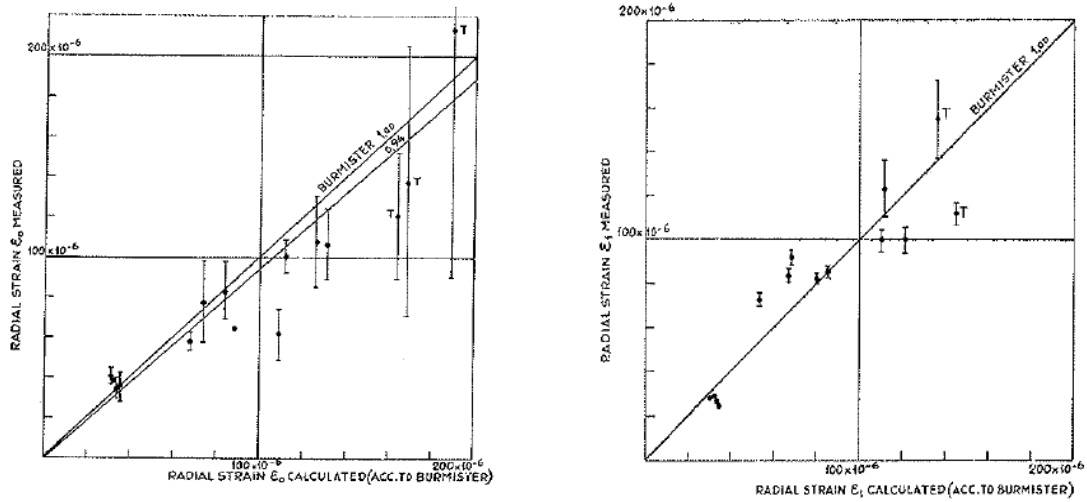


Figure 2.7 Measured and Calculated Strains at the Top of Asphalt Layer & at the Bottom of Asphalt Layer (Nijboer, 1967).

Similarly, the measured deflection was compared against calculated deflection using Burmister's elastic layer theory. Both values matched reasonably well and Figure 2.8 shows the comparison between these two values. Reasonably good agreement was found between measured and theoretically calculated vertical pressure values also (Figure 2.9).

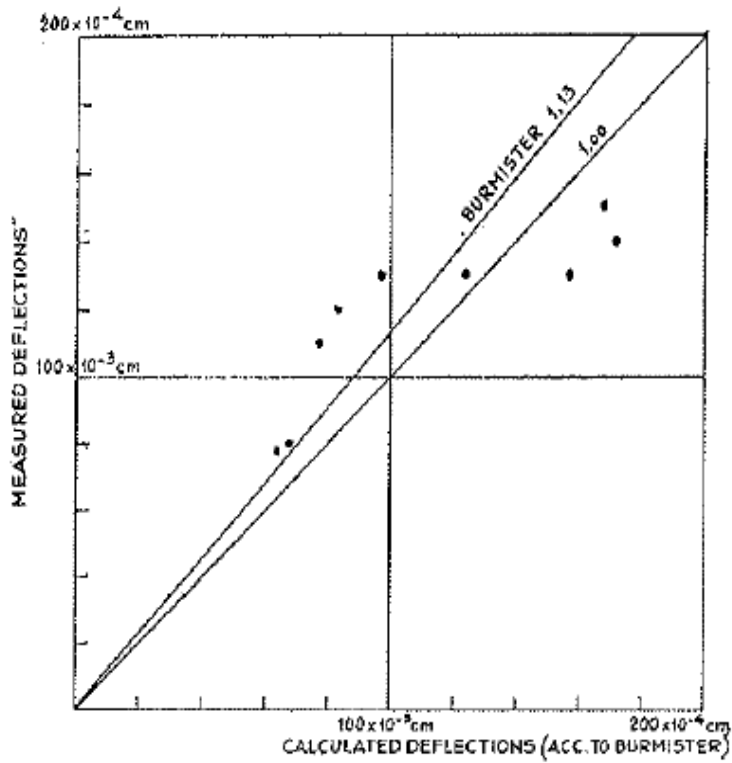


Figure 2.8 Measured and Calculated Deflections (Nijboer, 1967).

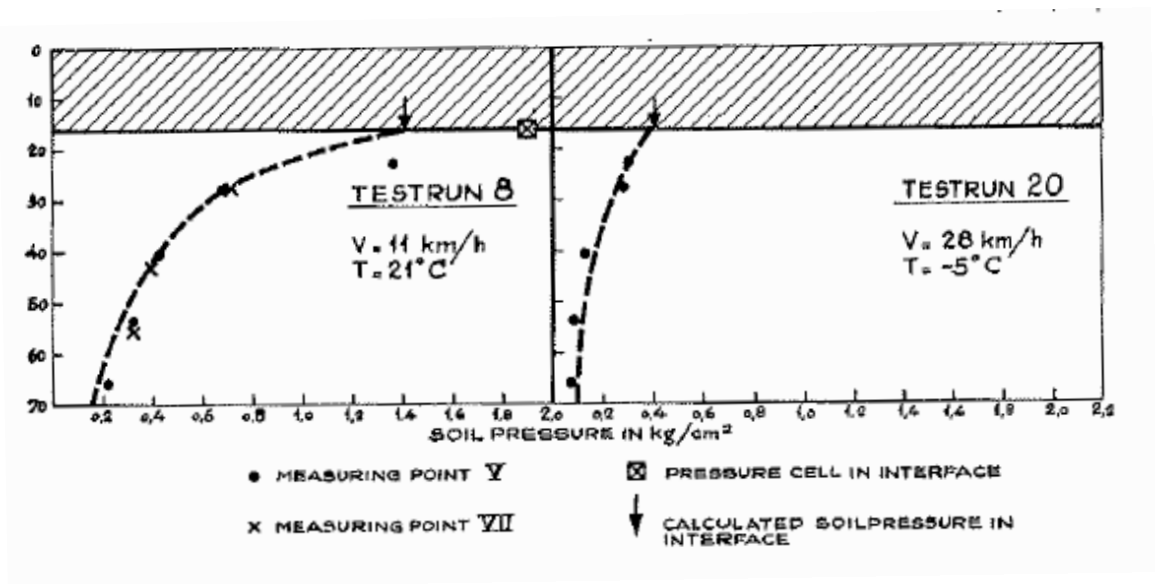


Figure 2.9 Measured and Calculated Vertical Pressure Values (Nijboer, 1967).

2.4.6 San Diego Test Road Study (1970)

One of the main objectives of the San Diego Test Road conducted in 1966 was to compare measured responses against theoretical results (Hicks and Finn, 1970). This project was considered to be the first instrumented pavement test track project in the United States. Pressure cells, strain gauges, thermocouples, and moisture gauges were installed at different locations in the pavement layers. The strain gauges were made with polyester heat resistant backing and were 7/8" long. They were placed on the top of surface, top of base and in the first lift of base. The subsurface strain gauges were installed in pairs in all asphalt treated base sections and about 50% of those were damaged during construction. Some 61% of the subsurface strain gauges were not operational during the course of this experiment. Excessive strain and weak solder connection between gauge and the lead wire were attributed as a cause for gauge failure.

The pressure cell used in this project, DC-200 Filpip Cell, was manufactured by Spitz Laboratories in Delaware. Of the 8 pressure cells installed in the top of subgrade, only 3 were operational after construction. The deflection measurements were made by linear variable differential transducer (LVDT) model 103C-200. American Wire Gauge (AWG) 20 iron and constantan thermocouples were installed in 4 locations, at the bottom of base, on top of first lift of base, on top of base and about one half inch below the surface. When compared with other instrumentation, the thermocouples were found to be generally reliable.

Measurements of stresses, strains and deflections were made at three different times, in August 1966, immediately after construction in February 1967, and in April 1968. An 18 kip test vehicle (2 axle dump truck) was used to apply loading with a tire

pressure of 70 psi. For material properties, repeated load lab tests were conducted in the University of California, Berkeley (UCB) and the Asphalt Institute Lab. After considering the variability in the stiffness values measured from lab tests, a nominal subgrade modulus value of 75 ksi was considered for theoretical computation of pavement responses. The base modulus value was varied from 8.4 to 10.3 ksi during wet conditions and 16 to 21.2 ksi during dry conditions. The HMA dynamic elastic modulus ranged from 272 ksi at 63°F to 93 ksi at 90°F.

Due to lack of manpower, out of 32 sections in the San Diego Test Road, only 4 sections were considered for measured and calculated response comparison. These test sections had HMA thickness of 3". The base material consisted of aggregate base, asphalt concrete base and emulsion treated aggregate base with thickness varying from 5.6" to 14.6". After 7 months, when the pressure cells were examined, none of them was in working condition.

Computations of stress, strain and deflection were made by use of the N-layer program developed at the Chevron Research Institute. Relatively good correlation was found between measured and theoretical responses. This project vouched for accurate field-measured material properties to be used in theoretical response calculation for future work. Though the collected vertical pressure data were limited as a result of low survivability of pressure cells, the percent deviation of pressure value between measured and theory was only 4%. From Figures 2.10 and 2.11, it can be seen that the measured and calculated strain profiles matched reasonably well. The measured transverse strain beneath the tire center was lower than computed values. The large number of instrument

failures during this study emphasizes the need for proper selection of instruments to measure responses, proper installation practices before and after construction.

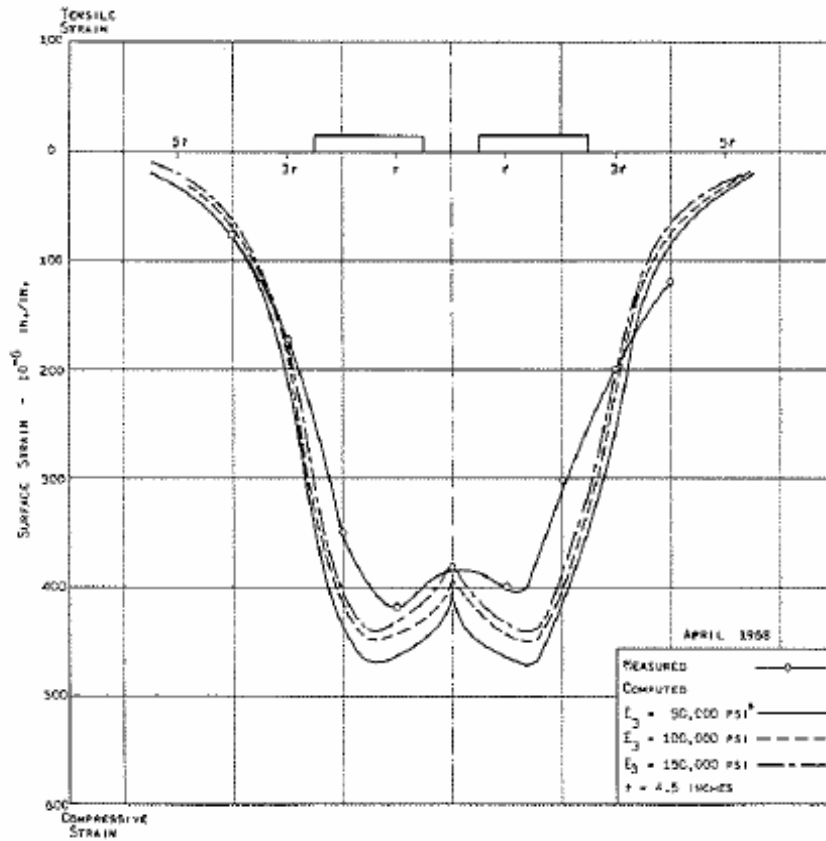


Figure 2.10 Comparison of Measured and Computed Surface Longitudinal Strain (Hicks and Finn, 1967).

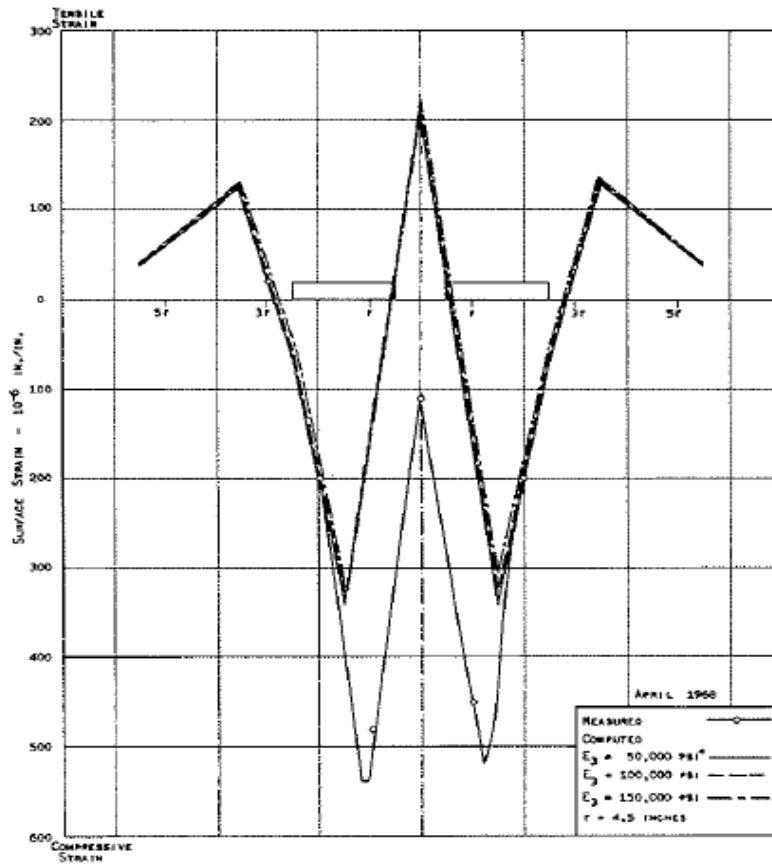


Figure 2.11 Comparison of Measured and Computed Surface Transverse Strain (Hicks and Finn, 1967).

2.4.7 TRRL Study (1972)

Laboratory-derived material properties were used to calculate pavement responses in terms of stress, strain and deflection in a research study done at the TRRL by Thrower et al. (1972). The dynamic modulus of the asphalt wearing course was calculated by cutting beam samples from the test road and testing them in the lab by subjecting a sinusoidal vibration at frequencies ranging from 1 to 100 Hz and at temperatures from 10°C to 35°C. The wave propagation method was used for base modulus and the value was found to be

7 ksi. The tire pressure of 75 psi and a wheel speed of 20 mph were kept constant and the wheel load was varied during load application.

Figure 2.12 showed good correlation between measured and calculated pavement response in terms of vertical stress in the test sections. However, at high stress levels small scatter was visible between measured and theoretical results. The computed values were reasonably close to those measured for low levels of deflection (Figure 2.13), but became progressively higher with higher levels of deflection.

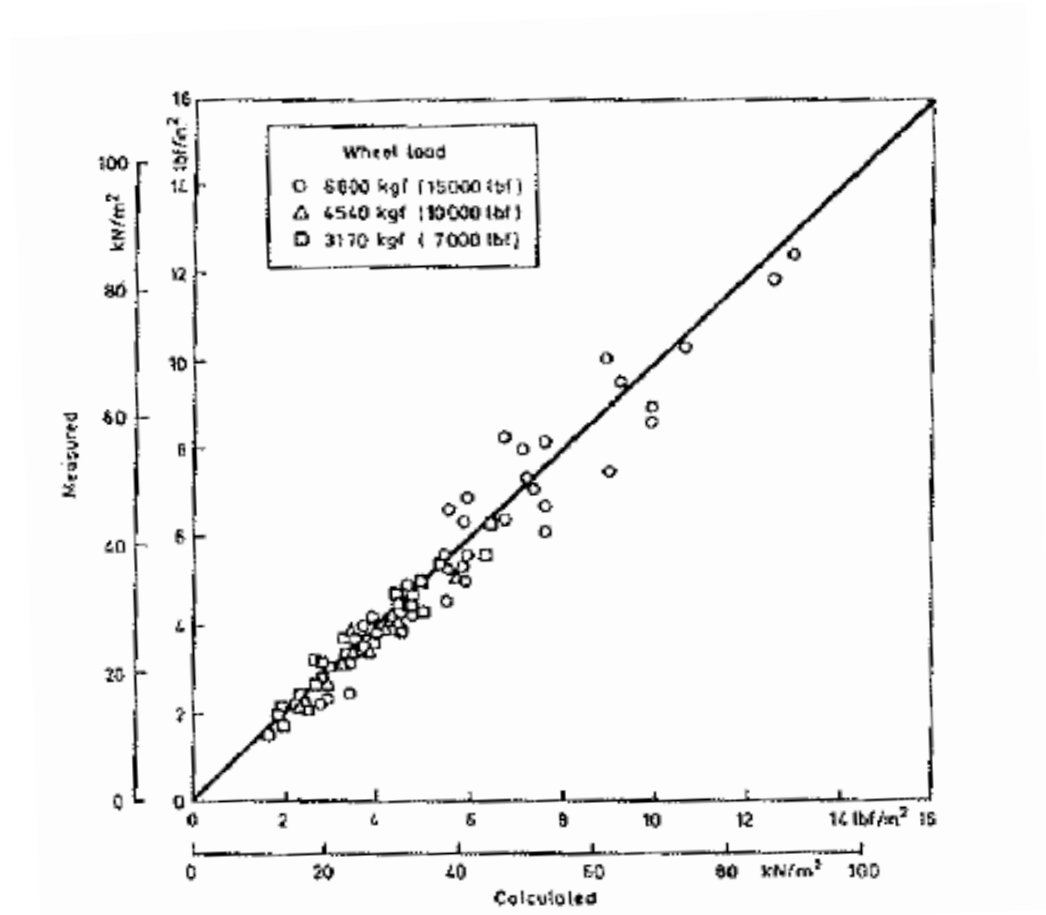


Figure 2.12 Comparison of Calculated and Measured Values For Road Machine Section 1 Vertical Normal Stress (Thrower et al., 1972).

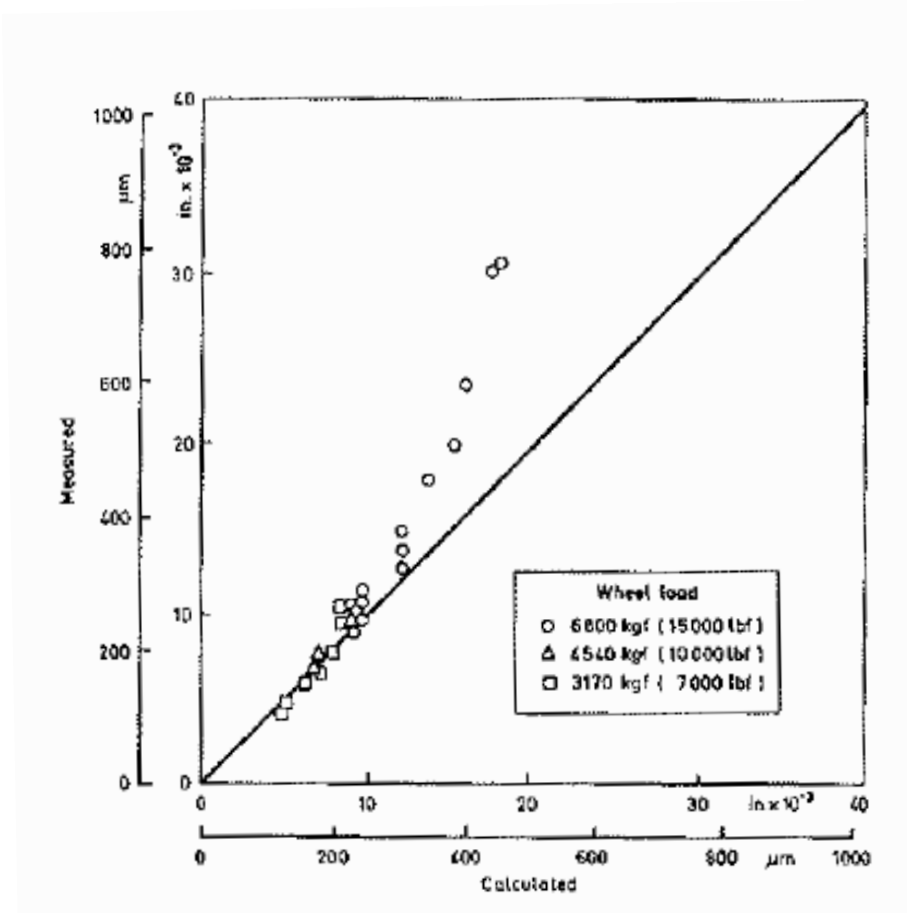


Figure 2.13 Comparison of Calculated and Measured Deflections For Road Machine Section 1 Surface Deflection (Thrower et al., 1972).

In general, when the measured responses were compared against layered elastic theory results they matched very well with 20% error between them. A reasonably accurate prediction was observed in stiff layers.

2.4.8 WSU Test Track Study (1972)

A moving dual wheel load of 10,600 lb with a tire pressure of 80 psi was applied in the Washington State University Test Track (Terrel and Krukar, 1970; Krukar and Cook, 1972) at a speed of 20 mph in the 12 sections available at the Test Track. The asphalt

concrete had a thickness 4.25 and 7.75". All sections had a standard base thickness of 5.25". Pavement instrumentation such as pressure cells and strain gauges along with other instrumentation was installed at different depths. Thermocouples were placed in all layers and moisture gauges were placed only in subgrade. Longitudinal and transverse strain gauges were placed only in 5 test sections on top of base and top of subgrade. Two test sections were instrumented with WSU hydraulic pressure cells on top of base and subgrade. Further, Filp pressure transducers were also introduced on the top of base and subgrade.

Repeated load triaxial tests were conducted to characterize base and subgrade materials. The base modulus value ranged from 11.5 to 19 ksi. Complex modulus tests were conducted to characterize the HMA at three different frequencies and temperatures. The HMA modulus had values between 1,100 and 1,500 ksi. The obtained subgrade modulus value ranged from 8 to 13.5 ksi. Layered elastic theory developed by Chevron Research Corporation was used for theoretical pavement response computation. The measured responses compared very well with the n-layer elastic theory computed responses.

From Table 2.1, it can be clearly seen that the deflection values matched reasonably well between theoretical results and measured values. However there were large differences in strain values measured on the top of base and subgrade. For example, the measured longitudinal strain on the top of subgrade at 8" was very small (15); whereas the computed value was 277. The researchers concluded saying that the instrumentation placement techniques adopted could possibly be the reason for these differences. This highlights the fact that measurements may not always be "truth."

Table 2.1 Measured and Computed Responses (After Terrel and Krukar, 1970)

Item	Section	Measured	Computed
Deflection (in, 10^{-3}) Shallow LVDT	2	8.4	5.2
	6	17.6	4
	8	9.0	5.8
	10	1	0.24
Deflection (in, 10^{-3}) Deep LVDT	2	36.0	33.8
	6	35.0	33.7
	8	22.0	24.9
	10	21.0	20.3
Longitudinal Strain (in, 10^{-3}) Surface	2	Not available	26.0
	6	15.0	309
	8	200	235
	10	100	111
Longitudinal Strain (in, 10^{-3}) Top of base	2	95	261
	6	Not available	315
	8	180	238
	10	80	8
Longitudinal Strain (in, 10^{-3}) Top of subgrade	2	40	389
	6	Not available	436
	8	15	277
	10	80	129

2.4.9 Nottingham (TRRL) Study (1979)

At the Nottingham pavement test facility (Brown and Bell, 1979), 25 mm diameter strain coils (Bison Instrument) and diaphragm type pressure cells were employed to measure strain and vertical stress, respectively. LVDTs were used to measure vertical deflection. Three pavement sections were tested in this study. The applied wheel load was varied from 11-15 kN with a speed of 14kmph. The contact pressure in pavement section 1 was kept at 660 kN/m² with a load radius of 85mm. In the other two sections, the contact pressure was maintained at 550 kN/m² with a nominal load radius of 80mm. The nominal HMA thickness in sections 1 and 2 was 150mm and test section 3 had a thickness of 230 mm.

Laboratory-derived layer moduli were used for theoretical pavement responses to be used in layered theory. When the measured responses were compared against predicted response, two of the pavement sections (Figure 2.14) did not compare well with theoretical responses. Instrument error and insufficient replicate instrumentation to measure pavement response were attributed to this deviation. In the remaining pavement section (Figure 2.15), the theory compared reasonably well with measured responses. This study recommended the use of field-measured material properties instead of laboratory-derived properties for theoretical calculation.

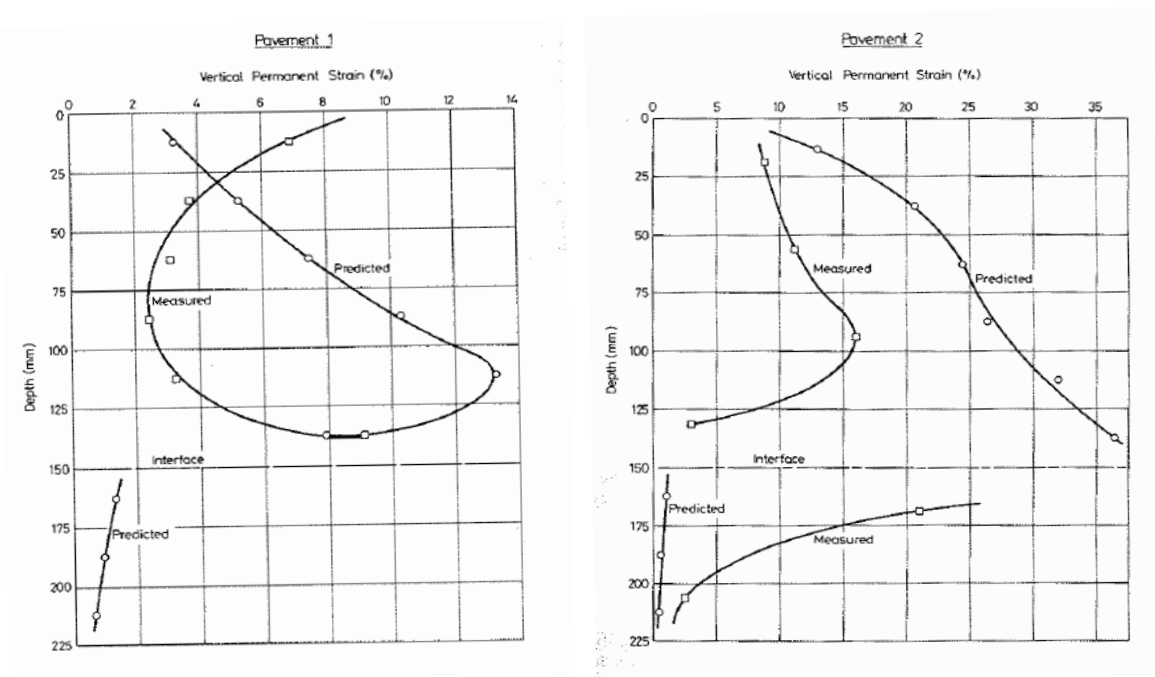


Figure 2.14 Comparison of Predicted and Measured Permanent Strains in Pavement Sections 1 and 2 (Brown and Bell, 1979).

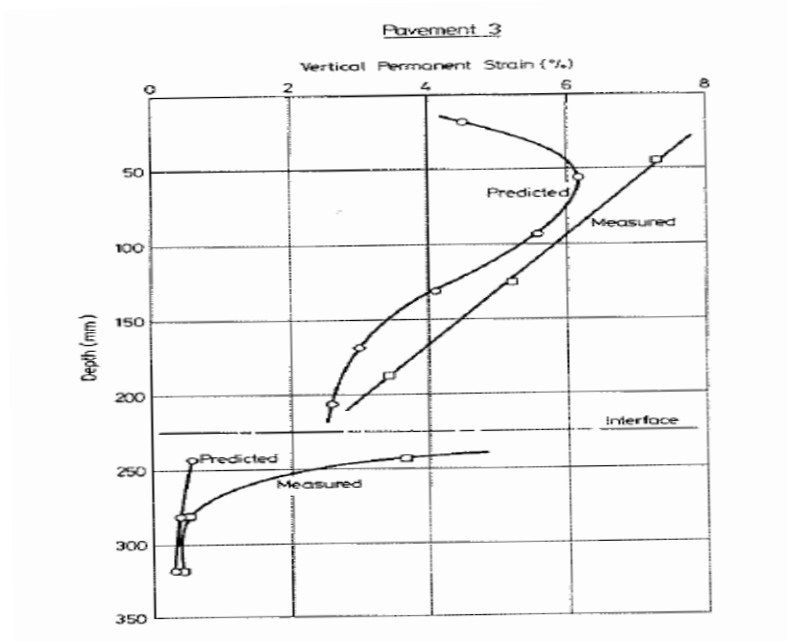


Figure 2.15 Comparison of Predicted and Measured Permanent Strains in Pavement Section 3 (Brown and Bell, 1979).

2.4.10 Amsterdam Study (1982)

In a similar research study conducted in Amsterdam (Ros et al., 1982), the Falling Weight Deflectometer (FWD) was used to measure material properties in situ. This was the first study where FWD measured values were used in theoretical pressure computations. Besides FWD measurements, wave velocity measurements, dynamic bending test and creep tests were also conducted for material property evaluation. A 100 kN load was applied at three different speeds (2.5, 10 and 45 km/h) in 9 trial sections. This Highway A15 research project was carried out on a series of trial sections between 1970 and 1980.

The BISAR linear elastic multi-layer program was used for theoretical response computation. Strain gauges (in longitudinal and transverse at the bottom of HMA layer) and soil pressure cells (in subgrade) were embedded at different depths in the pavement layers and the response was noted. According to the researchers, a good correlation between measured and computed values was observed in most of the trial sections for soil pressure values.

2.4.11 Minnesota Road Research Study (1997)

In the Minnesota Road Research project (Chadborn et al., 1997; Bao, 2000), instrumentation such as strain gauges, pressure cells, thermocouples and moisture gauges were embedded inside the pavement layers. The twenty-two bituminous test cells comprising the 5-year mainline, 10-year mainline and low-volume road (LVR) bituminous test sections at Mn/ROAD have different combinations of layer thicknesses and subbase types. Subbases consisted of granular materials and permeable asphalt stabilized bases (PASB).

Two types of strain gages were used in this study to measure pavement strain. The first, Dynatest PAST-II PCC gages, consisted of electrical resistance strain gages embedded within a strip of glass-fiber reinforced epoxy, with transverse steel anchors at each end of the strip to form an H-shape. The second gauge was a Tokyo Sokki PML-60 gauge, which consisted of standard wire gages hermetically sealed between thin resin plates and coated with coarse grit to bond the gage to the concrete. The Tokyo Sokki gauges were installed to measure longitudinal (LE) and transverse (TE) strain. Three TE strain gages and three LE strain gages were placed at six locations in each test section.

Both of two strain groups were transversely located in the outside wheel paths. Some of the flexible pavement sections were instrumented with the Schaevitz HCD-500 DT linear variable differential transformers. LVDTs were used to measure deflection at the pavement surface, base and subgrade materials due to load.

Some of the flexible pavement cells used at the Mn/ROAD was dynamic soil pressure cells that measured the vertical stress in the base and subgrade layers. The instrumentation used in this study was the Geokon 3500 dynamic soil pressure cell. Thermocouples installed at Mn/ROAD allowed the measurement of temperature gradients experienced by the HMA layers. At least one set of thermocouples was present in each cell. Resistivity probes (RPs) were used to monitor changes in soil moisture state. The resistivity probes installed at Mn/ROAD consisted of 250-cm-long tubes with concentric pairs of copper conductors located every 5 cm (2 in). Time domain reflectometer sensors (TDRs) were used to measure the unfrozen base/subgrade moisture content.

The Mn/ROAD test vehicle is a five-axle semi-tractor trailer combination with a single steering axle with single tires and two tandem axles with dual tires for the drive and trailer axles. The wheel loads applied to the pavement are expressed in terms of a particular wheel configuration.

Backcalculated modulus values from FWD measurements were used for material properties. The material properties along with the pavement configurations and truck loading were the inputs for theoretical response calculation. The layer elastic program “WESLEA” (Waterways Experiment Station Linear Elastic Analysis for Windows) was used to compute theoretical responses. WESLEA for Windows is a mechanistic analysis

program that calculates pavement response to applied tire loads through user-input tire pressure and tire load and pavement layer properties. The theoretical results and measurements for strain are given in Figure 2.16. Though small scatter at higher strain levels (exceeding $200\mu\epsilon$) were visible, according to the researcher, both measured and predicted values match closely.

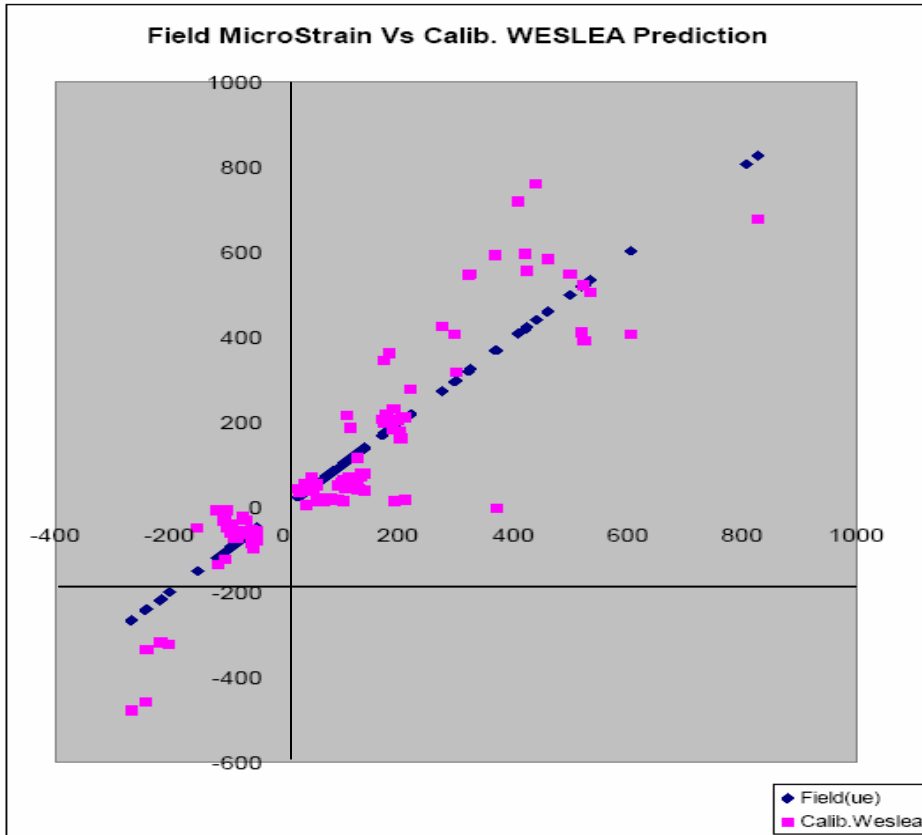


Figure 2.16 Measured and Calculated Strains from Mn/Road (Bao, 2000).

2.4.12 NCAT Study (2005)

Similar efforts to compare field measured responses with theoretical results were done at the National Center for Asphalt Technology (NCAT) Test Track under FWD loading (Barrett and Timm, 2005; Timm and Priest 2006). Instrumentation in these test sections was comprised of asphalt strain gauges and earth pressure cells. The asphalt strain gauges measured strain at the bottom of the asphalt layer, while the earth pressure cells measured stress in the top of the base and subgrade layer. The layout of the instrumentation array consisted of 12 asphalt strain gauges with four positioned to the left, four positioned to the right, and four positioned in the center of the outside wheelpath to record longitudinal and transverse strain. There were two pressure plates (Geokon 3500 Earth Pressure Cell) in each section positioned in the center of the wheelpath at the top of the base layer and at the top of the improved subgrade layer, respectively.

FWD testing was conducted on eight different cross sections at the facility. The sections represented different pavement thicknesses, and use of modified and unmodified asphalt binders. FWD loads were dropped directly on top of and in close proximity to strain gauges and pressure cells. This enabled the measurement of both surface deflections and in situ pavement responses under FWD loading. The surface deflections were used to backcalculate elastic layer properties within each test section. The properties were then used in forward calculation to compute stresses and strains at locations coinciding with embedded instrumentation.

Direct comparisons were made between predicted pavement responses and measured responses to evaluate the effectiveness of both the backcalculation and forward

calculation models. Good agreement between measured and predicted responses was observed for horizontal strain in the bottom of asphalt layer and vertical pressures on the top of base, subgrade layers. However, it was generally found that layered elastic back-and forward-calculation was sufficiently accurate for the conditions at the NCAT Test Track and also served to validate the sensor installation procedures. The strong correlation between linear-elastic and measured pavement response (Figures 2.17 and 2.18) has served as a reference point for the validation of the installation and operation of the embedded instrumentation at the 2003 NCAT Test Track Structural Experiment.

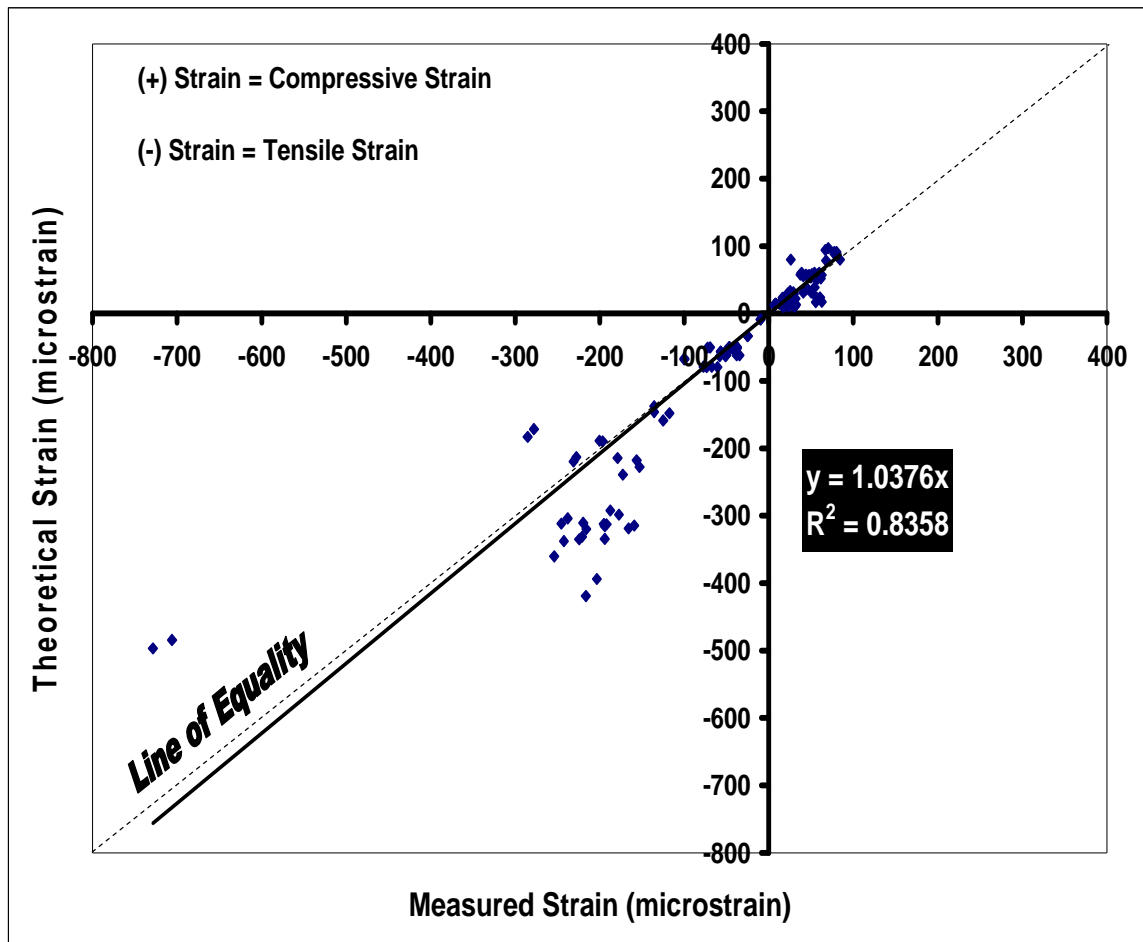


Figure 2.17 Measured Vs Theoretical Asphalt Strain (Barrett and Timm, 2005).

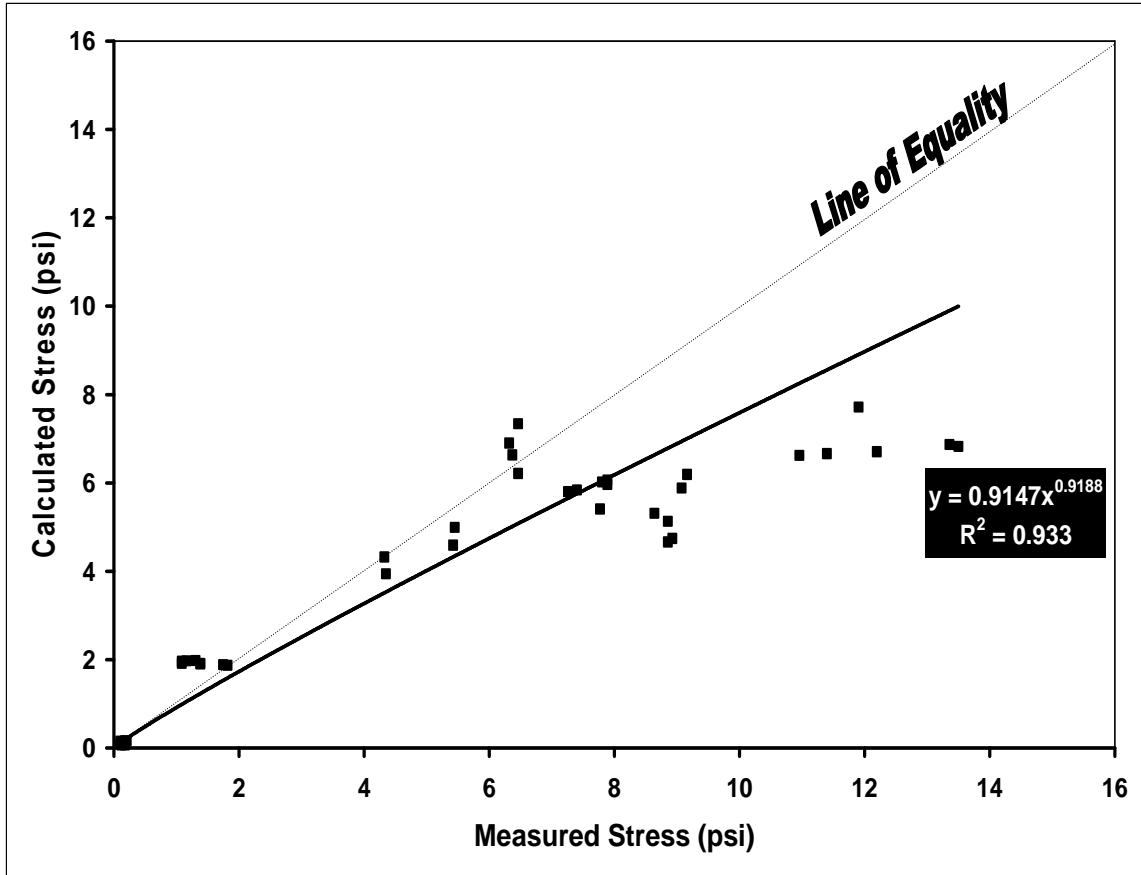


Figure 2.18 Measured Vs Theoretical Vertical Stress in Base and Improved Subgrade Layer (Barrett and Timm, 2005).

2.4.13 European Study Results (2002)

Ullidtz (2002) compared available elastic layer package results with the measured responses from three full scale pavement testing projects from Europe (CEDEX in Spain DTU in Denmark and LAVOC in Switzerland) and the comparison showed that the elastic layered theory predicted some mechanistic responses reasonably well. Table 2.2 shows the research results. In all three projects, the elastic layer programs underestimated the vertical stress in the subgrade.

Table 2.2 Comparison of Model Results to Measured Response (Ullidtz, 2002)

Model	CEDEX			DTU			LAVOC		
	ϵ_x	σ_z	d	ϵ_x	ϵ_z	σ_z	ϵ_x	ϵ_z	d
BISAR	↓	↓	↑	↓	↓	↓	↔	↓	↑
CAPA3D	↓	↓	↑	↓	↓	↓	↔	↓	↔
CIRCLY	↔	↓	↑	↓	↓	↓	↔	↓	↑
KENLAYER	↔	↓	↔	↔	↓	↔	↔	↓	↔
MICHPAVE	-	-	-	-	-	-	↔	↓	↔
NOAH	↑	↓	↔	↔	-	-	↔	↓	↑

ϵ_x = horizontal strain at the bottom of asphalt

σ_z = vertical stress in subgrade

d = deflection at the surface

↔ = predicted response close to measured response

↓ = underestimation of response

↑ = overestimation of response

2.4.14 Advanced Models

From the late 1960s, along with layered elastic systems, multi layer viscoelastic approach and finite element modeling were also explored by researchers to measure pavement response (Pister and Westman, 1962; Huang, 1967; Waterhouse, 1967; Kenis, 1977; Hornych et al., 2002; Siddharthan et al., 2002; Al-Qadi et al., 2004; Sukumaran et al., 2004; Elseifi et al., 2006). VESYS and VEROAD are some of the programs that use multilayer viscoelastic approach to calculate pavement responses. Increasingly, the finite-element method has been used to model pavement response, particularly to describe the nonlinear response characteristics of pavement materials. Examples of this approach include ILLIPAVE and FENLAP (Monismith, 2004).

2.4.15 Summary

Historically, analyses have been limited to static loads resting on layered elastic systems. Generally speaking, these approaches are reasonably accurate for design purposes; however, there is a need to further validate layered elastic models. Apart from the Nottingham (TRRL) study conducted in 1979, all reviewed literature included in this section showed good correlation between measured and theoretical pavement responses. In most of the research studies conducted for layered elastic model validation, a reduced tire pressure (75 to 80 psi) and slower speed (up to 20 mph) were used. For material properties, most of the studies utilized laboratory derived values instead of field measured properties. In almost all studies, responses in conventional HMA mixes were only studied and not much work had been done to study Superpave mix responses and the multilayer elastic theory validity for those mixes.

So a field validation study to compare elastic layer responses with field measured responses from the NCAT Test Track Structural test sections was necessary as part of this research.

2.5 FLEXIBLE PAVEMENT RUTTING

Rutting is one of the most prevalent forms of distress in flexible pavements; it is quite obvious that a thorough knowledge of rutting phenomenon is very important to control rutting. Modeling rut progression and predicting its occurrence will help pavement engineers to design pavements in such a way that the pavement can avoid excessive rutting in its expected service life.

Rutting problem should be addressed for structural and economic reasons; it is also related strongly to traffic safety. The causes of rutting may be traffic or non traffic associated. Table 2.3 gives an overall view of these two causes of rutting (Monismith et al., 1972).

Table 2.3 Causes of Rutting (Monismith et al., 1972)

Cause	Causative Factor	Example of Distress
Traffic-Load Related	<ul style="list-style-type: none">• Single or comparatively few excessive loads• Repetitive traffic loading	Plastic flow/Shear deformation Rutting
Non Traffic Associated	<ul style="list-style-type: none">• Soil Volume Change• Compressive material underlying pavement structure• Frost susceptible material	Swell/shrinkage Consolidation Settlement Heave (particularly differential settlement)

2.5.1 Rutting Progression

Flexible pavement rutting is categorized in three stages (primary, secondary and tertiary).

In the primary stage, permanent deformation accumulates rapidly. But the rate tends to decrease, reaching a constant value in the secondary stage. The stresses and strains within the pavement structure increase quite rapidly during early loading cycles and then tend to increase at a much slower rate because of shear distortion and densification of materials. Finally, at the tertiary stage, the rate starts to increase (flow point/accelerated deformation zone) and permanent deformation rapidly accumulates. A typical field rut progression curve is given in Figure 2.19.

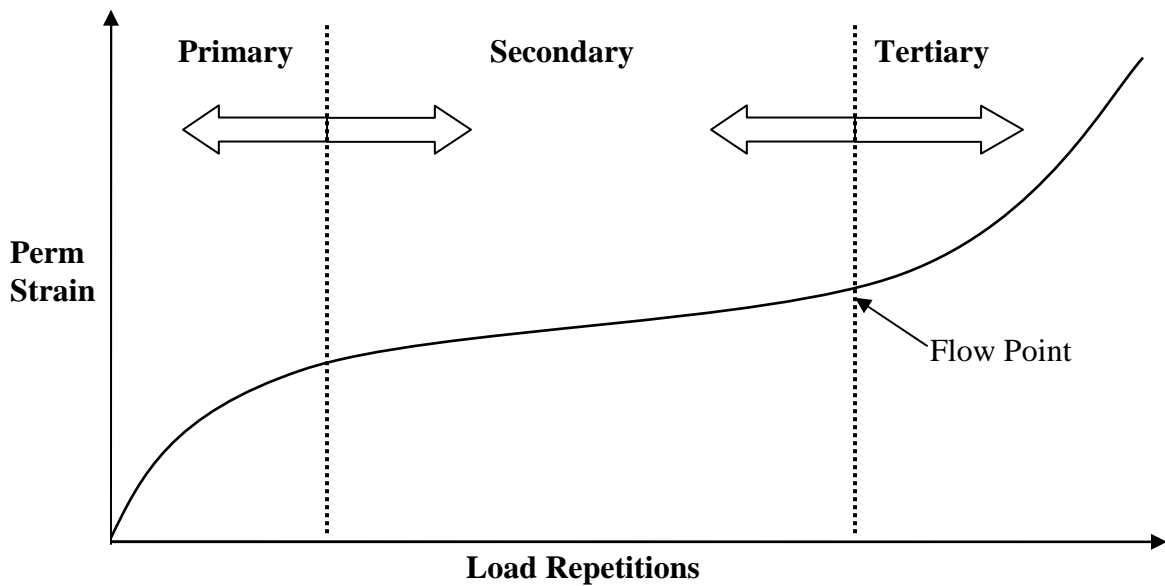


Figure 2. 19 Rut Progression for Increasing Load Repetitions (El-Basyouny et al., 2005).

It was shown that the shear movement in asphalt layers can also occur at the same time as densification and the shear deformation constitutes a major part of rutting mechanism in accelerated pavement testing (Harvey et al., 2000; Gokhale et al., 2005). Rut depths measured in more than 50 pavement structures under accelerated pavement tests were limited to rutting in asphalt layer only and no rutting in base and subgrade was evident (Zhou et al., 2002). Further it was found that HMA layer rutting is the common form of rutting in APT facilities (Hugo and Epps, 2004). So modeling the HMA layer rutting is sufficient in most cases. By modeling the HMA layer rutting alone, the rutting can be captured fully for many cases (Archilla et al., 2001; Fwa et al., 2004).

The field rutting can be measured manually and automatically. The manual measurements include straight edge method, dipstick profiler, and rut measurement from pavement cores. The automated rut measurement includes the automatic road analyzer (ARAN) which uses a laser profiler to measure rutting profile. These rut measurement techniques are discussed in detail in the next chapter.

2.6 RUT PREDICTION MODELS

Predicting actual performance of a pavement under the actions of traffic load and environmental conditions is a major part of the M-E design scheme. Further, predicting the future condition of a pavement with or without maintenance and rehabilitation is an essential element of most pavement management systems. With this in mind, an attempt of modeling the pavement deterioration must necessarily be based on simplifications of reality (Ullidtz, 1999).

Accurate prediction of pavement performance helps the state highway agencies for proper work planning and budget allocation. Inaccurate or unrealistic performance prediction will result in uneconomical pavement design and premature failures. Accelerated pavement tests are being used in many countries around the world to evaluate pavement performance and to establish failure modes for pavement life predictions (Madanat et al., 2002; Hugo and Epps, 2004). While M-E design relies heavily on mechanistic pavement modeling, the results are meaningless without accurate performance equations that allow designers to predict pavement performance and design accordingly (Timm and Newcomb, 2003).

Starting from earlier 1960's, many rut prediction models were developed by researchers from all around the world that ranged from simple linear regression equation to advanced mechanistic empirical rut prediction models. In this part of chapter, a detailed literature review on available important rut prediction models is presented.

2.6.1 Historical Trend on the Development of Rut Prediction Models

Prior to AASHO Road Test in late 1950's, the focus of most research was to develop preventive design methodologies rather than actual performance modeling. This changed with the completion of the AASHO Road Test because the test results provided a large database of useful information that allowed predictions to be compared with measured performance (Sousa et al., 1991). An abundance of information on construction, material characterization, traffic and the environment would finally allow researchers to scrutinize the effects of various factors on pavement performance.

The First International Conference on the Structural Design of Asphalt Pavements held in 1962 provided a great opportunity to discuss AASHO findings. At this time, the first pavement design approach which explicitly considered both fatigue and rutting as mechanisms of distress was presented (Dorman, 1962). As part of this design, rutting was controlled by limiting the vertical compressive strain on the top of the subgrade. With gradual increase in allowable axle loads, tire pressure and truck volume, the need for an improved approach to predict rutting, particularly in the upper part of the pavement layer became apparent (Sousa et al., 1991). The criterion for allowable subgrade strain was developed by Dorman and Metcalf (1964) based on data from the AASHO road test, and reported in 1962 by the Highway Research Board (HRB, 1962).

During the Second International Conference on the Structural Design of Asphalt Pavements held in Ann Arbor, Michigan (1967), the focus was shifted to layered elastic model validation rather than performance model development. However during the third international conference held in London in 1972, Barksdale came up with a layer strain approach for rut prediction. In the Fourth International Conference on the Structural Design of Asphalt Pavements, various approaches such as statistical techniques based on observed rut performance, limiting subgrade strain method, elastic analysis combined with creep test data and linear visco-elastic analysis were presented. The important work among others was the VESYS model developed by Kenis (Kenis, 1977). At this time, laboratory test results were normally used to build rut prediction models.

In 1980, Allen and Deen developed rutting models for HMA from repeated load tests (Allen and Deen, 1980). In 1982, research studies were directed both in material characterization and in developing models for rut prediction ranging from simple empirical methods to viscoelastic plastic considerations (Sousa et al., 1991). In 1989, the Tseng and Lytton model, which formed the basis for MEPDG rut prediction model, was developed. In the late 1990's, researchers explored the LTPP data as a potential base for M-E based rut prediction model development (Ali et al, 1998; Kim et al., 2000). Research at the University of California, Berkeley (Archilla et al., 2001) developed rut prediction models from AASHO Road Test data and a combined model from AASHO and WesTrack data. The continuous revision in the original Tseng and Lytton model resulted in the final form of MEPDG rut prediction model in 2002.

Recently, researchers from Texas Transportation Institute (Zhou at al., 2004) suggested a three stage permanent deformation prediction model. Still research efforts are going all around the world to develop a simple, easy to use field derived and calibrated rut prediction model.

2.7 SIGNIFICANT RUT PREDICTION MODELS

Since rutting poses problem to the driving public as well as affects the life of pavement, it is very important to predict accurately in advance. In the area of rut prediction model development, hundreds of models were developed by researchers over the past 45 years. Since it is impractical to discuss all available models, only a few important models that are relevant to this study are discussed in this section.

Earlier studies suggested limiting the vertical strain on the top of subgrade to control rutting at the surface. The examples include Shell design procedure (Claessen et al., 1977), and the Asphalt Institute design method (Shook et al., 1982). Some studies (Barksdale and Miller, 1977) included limiting vertical stress instead of strain as a way to minimize rutting.

The layered strain approach that predicts rutting using lab test results together with pavement analysis methods such as layer elastic theory was first proposed by Barksdale (Barksdale, 1972) and Romain (Romain, 1972). This method was considered to be a simplified engineering approach for rut prediction since it permits the flexibility of using either linear or nonlinear elastic analysis (Sousa et al., 1991).

2.7.1 Finn et al. Model (1977)

Researchers (Finn et al., 1977) relied upon statistical analysis of rutting data from the AASHO Road Test to produce a rut prediction model. Data from 32 sections in the AASHO Road Test were used in model building. Initially, a regression model that related rutting rate as a function of stress and strain in component layers, surface deflection and ESALs was evaluated. The stepwise regression analysis indicated that vertical deflection at the surface of the pavement, vertical compressive stress in asphalt concrete and cumulative traffic were the most significant variables for rutting. Finally, two prediction models were obtained; one model for conventional sections up to 6" of asphalt concrete, and one for thick or full depth asphalt concrete as follows;

For conventional construction:

$$\text{Log}(RR) = -6.866 + 4.325 \times \log(d) - 0.131 \times \log(N_{18}); R^2 = 0.974 \quad (2.1)$$

For full depth or thick (>6") pavements:

$$\text{Log}(RR) = -1.173 + 0.717 \times \log(d) - 0.658 \times \log(N_{18}) + 0.666 \times \log(\sigma_c); R^2 = 0.974 \quad (2.2)$$

Where,

RR = rate of rutting, micro inches per repetition

d = surface deflection, 10^{-3} inches

σ_c = vertical compressive stress in asphalt concrete, psi; calculated from layer elastic theory

N_{18} = total equivalent number of 18000 lb single axle load

The models given in Equations 2.1 & 2.2 are only applicable to pavements similar to AASHO Road Test and its related climatic locations. In this particular model the traffic coefficient had a negative sign which indicates decrease in rutting rate as traffic application increases. This was expected, since after some point of time, the rutting rate decreases for increasing traffic applications.

2.7.2 TRRL Equation (1979)

A layered strain based rut prediction equation was developed by researchers from TRRL, London (Brown and Bell, 1979). For the development of rut prediction model, axial repeated load tests were conducted on dense bituminous macadam samples at 30⁰C. The loading was applied as a continuous sinusoidal loading at a frequency of 1 Hz for convenience rather than simulating in-situ loading conditions. The model form is:

$$\epsilon_p = \left(\frac{q}{a}\right)^b \times N \quad (2.3)$$

Where,

ϵ_p = permanent strain

q = deviator stress

a,b = regression constants

N = number of load applications

The validity of this model was checked by comparing model results with the TRRL Test Track results for three pavement sections. A good agreement was found between model predicted rutting and the TRRL Test Track measured rutting. The main disadvantage of this model is that the model form was derived from the laboratory test results which did not replicate actual field conditions.

2.7.3 Shell (1977) & Asphalt Institute Model (1982)

Based on results from the AASHO road test, Shell researchers (Claussen et al., 1977) developed the rut model which used the subgrade vertical strain criterion.

$$N_r = 6.15 \times 10^{-7} (\epsilon_v)^{4.0} \quad (2.4)$$

Where,

N_r = allowable number of load repetitions to limit rutting to 0.5 inches

ϵ_v = Maximum vertical strain at the top of subgrade

The Asphalt Institute (Shook et al., 1982) came up with a similar model in 1982 for rut prediction.

$$N_r = 1.365 \times 10^{-9} (\epsilon_v)^{-4.477} \quad (2.5)$$

Where,

N_r = allowable number of load repetitions to limit rutting with in 0.5 inches

ϵ_v = Maximum vertical strain at the top of subgrade

Though the models developed by Shell and Asphalt Institute researchers were simple and easy to use, the validity of the subgrade strain criterion is questionable and this equation does not distinguish rutting in different layers of pavement. Further the constants in the model were derived from particular temperature conditions and loading conditions and hence they can not be applicable as a whole to other locations. This requires local calibration for different locations and the model validity to predict HMA deformation is questionable.

2.7.4 Allen & Deen Model (1980)

A model to predict permanent deformation in asphalt concrete was proposed by Allen and Deen (1980). Repeated load tests were conducted in 27 samples with three deviator stress ranges (20, 50 & 80 psi) and at three different temperatures (45, 77 & 100° F). In addition three loading times were used at each deviator stress levels. A linear regression analysis was performed on the data from each test and the following model was built.

$$\log \epsilon_p = C_0 + C_1(\log N) - C_2(\log N)^2 + C_3(\log N)^3 \quad (2.6)$$

Where,

ϵ_p = axial permanent strain

N = number of deviator stress repetitions

$C_0, C_1, C_2,$ and C_3 = regression constants

The predicted rut depth was checked against measured rut depths from two full depth asphalt concrete pavements. These sections did not have any base layers and built with HMA layers over the subgrade. The measured rut depth in the first pavement section was 1.75” and the model predicted a rut value between 1.6 and 1.9”. In the second pavement section, the predicted rutting was 1.25” and the measured rutting was 1.15”.

The inherent disadvantage of this model was that it was developed entirely from laboratory test results and has only number of stress repetition in the model form. A mechanistic based rut prediction model would be very useful to predict rutting in any field conditions.

2.7.5 Leahy’s Model (1989)

The model developed by Leahy (1989) to predict asphalt pavement rutting was the starting point for MEPDG rut prediction model development. In the study developed at the University of Maryland, College park, nearly 250 HMA specimens were tested to study their permanent deformation characteristics with the help of repeated load test machine. The experimental factorial included three asphalt content, three stress levels, two binder types, three temperatures and two aggregate types. The test results were based on unconfined repeated load permanent deformation tests. About 2,860 permanent strain data were used in the model building. The resilient strain was assumed to be reasonably constant and independent of the number of load repetitions.

The model developed by Leahy was:

$$\log\left(\frac{\varepsilon_p}{\varepsilon_r}\right) = -6.631 + 0.435 \log N + 2.767 \log T + 0.110 \log S + 0.118 \log \eta + 0.930 \log V_{beff} + 0.501 \log V_a; R^2 = 0.76 \quad (2.7)$$

Where,

ε_p = accumulated permanent strain

ε_r = resilient strain

N = number of load repetitions

T = mix temperature, deg F

S = deviatoric stress, psi

η = viscosity at 70 deg F, 10^6 poise

V_{beff} = effective asphalt content, percent by volume

V_a = air void content, percent

The sensitivity analysis showed that temperature was by far the most important variable. The model was less sensitive to loading conditions, material type and mix properties.

Though the developed model had a R^2 value of 0.76, their implementation usefulness was limited because of complex model with many parameters. Besides the model used limited number of HMA mixtures for the model development (El-Basyouny et al, 2005).

2.7.6 WesTrack Model (1999)

Research works highlighting WesTrack findings excluded densification and assumed that rutting was controlled by shear deformation. A regression model was developed to model the WesTrack rutting by considering elastic shear response and axle loadings. The developed model employed an hourly change in elastic shear strain in order to encompass time hardening. The model form is (Hand et al., 1999):

$$\gamma^p = a e^{(b \cdot \tau^e)} \gamma^e N^c \quad (2.8)$$

Where,

γ^p = plastic shear strain at a depth of 2" from HMA top

τ^e = elastic shear stress at a depth of 2" from HMA top

γ^e = elastic shear strain at a depth of 2" from HMA top

N = Number of 18kip load applications

a,b,c = regression coefficients

Though the methods proved that elastic shear stress and shear strain can be used in a model to predict plastic deformation, the model is only applicable to WesTrack mixes.

2.7.7 M-E based Rut models from LTPP Data

An M-E rutting model was developed and calibrated from LTPP data (Ali et al., 1998).

The subgrade strain approach was used to predict rutting in 61 LTPP test sections and the actual load spectrum was used to build the model. The developed model only considered vertical strain in different layer locations and they did not account for lateral flow resulting from horizontal shearing strain in layers. The authors suggested the use of

shearing strain in future research as potential predictor of rutting. Similar models were also developed for rutting prediction in base and subgrade layers. After mathematically deriving the model and calibrating them with 61 LTPP section data, the model form to predict rutting in HMA layer was;

$$\rho_p = 0.00011 \times h_{AC} \left[\sum_{i=1}^k n_i (\varepsilon_{i,AC})^{1.111} \right]^{0.9} \quad (2.9)$$

Where,

ρ_p = rut depth in HMA layer

h_{AC} = HMA layer thickness

n_i = number of divisions in HMA layer

$\varepsilon_{i,AC}$ = vertical compressive elastic strain in middle of each divided layer corresponding to load group 'i'.

The model was validated using a different set of data from LTPP that were obtained at different times. The model validation done for this model showed a standard error of rut depth estimate to be around 0.14". This model form did not include traffic load application and only the mechanistic response (vertical elastic strain) controls rutting in this developed model.

2.7.8 Rut Prediction Model from In-Service Pavements

Kim et al., (2000) proposed a rut prediction model developed from 39 in-service pavements from Michigan. The developed model included inventory type variables like pavement cross section, layer stiffness, ambient temperature and asphalt consistency

properties. For mechanistic response calculations, a linear layered elastic solution developed by Chevron was used. To backcalculate pavement layer moduli for use in the mechanistic model, the backcalculation program MICHBACK was used.

A nonlinear regression analysis was conducted with 760 data points from 39 test sections. After grouping all data points into 51 statistical samples that represents every test site, numerical optimization was done to build the model. The final rut prediction model had the following form;

$$RD = \left\{ \left[\begin{aligned} &[-0.016H_{AC} + 0.033\ln(SD) + 0.011T_{annual} - 0.01\ln(KV)] \times \\ &[-2.703 + 0.657(\epsilon_{v,base})^{0.097} + 0.271(\epsilon_{v,SG})^{0.883} + 0.258\ln(N) - 0.034\ln\left(\frac{E_{AC}}{E_{SG}}\right)] \end{aligned} \right] \right\} (2.10)$$

Where,

RD = rut depth, in

H_{AC} = thickness of asphalt concrete, in

SD = pavement surface deflection

T_{annual} = annual ambient temperature, deg F

KV = kinematic viscosity

$\epsilon_{v,base}$ = vertical elastic compressive strain at the top of base layer, 10^{-3}

$\epsilon_{v,SG}$ = vertical elastic compressive strain at the top of subgrade, 10^{-3}

N = cumulative traffic volume, ESAL

E_{AC} = resilient modulus of asphalt concrete, psi

E_{SG} = resilient modulus of subgrade, psi

The rut model was validated with data from 24 LTPP sections and two test sites in Michigan. The plot of observed versus predicted rut depth indicated reasonable agreement between them and the variation ranged from 5-7mm. In the developed model the variables such as temperature, stiffness and vertical strain in different layers are dependant of each other and there was no proper explanation given by the researchers for including all variables separately in the model. The model is applicable only to cold temperature regions and the model is complex in form and had many variables.

2.7.9 MEPDG Model (2004)

From the laboratory derived permanent strain data, the MEPDG rut model to predict HMA rutting was built. Test data from Leahy's model (Leahy, 1989) was taken and some more test results were also added which yielded 3476 permanent strain data points for regression analysis. The developed model was calibrated with the help of seven sections of Mn/ROAD trench rutting data. The field calibrated form of HMA rut prediction model used in the design guide was (ERES, 2004):

$$\frac{\epsilon_p}{\epsilon_r} = k_1 \beta_{r1} 10^{-3.1552} T^{1.734 * \beta_{r2}} N^{0.39937 * \beta_{r3}} \quad (2.11)$$

Where,

ϵ_p = accumulated permanent strain

ϵ_r = resilient strain

T = mix temperature, deg F

N = number of load repetitions

K_1 = function of total asphalt layer thickness and depth to computational point

$\beta_{r1}, \beta_{r2}, \beta_{r3}$ = calibration factors for the asphalt mixtures in the rut model

The disadvantage of this model is that it was developed from unconfined repeated load tests and no confining pressure was considered in the model. When trial runs were done with the model, asphalt rutting increased as the thickness increased which did not conform to field observations. To overcome this limitation, the model was calibrated with trench study data from Mn/ROAD. One more disadvantage of this rutting model is that it models only the secondary stage of rutting and the primary stage was modeled as an extrapolation of the secondary stage trend (El-Basyouny et al., 2005). These limitations necessitate the development of a simple, easy to use, HMA rut prediction model developed from field data to be used in the design guide.

2.7.10 Three Stage Model

In order to characterize the three stage permanent deformation behavior of asphalt concrete, Texas Transportation Institute researchers (Zhou et al., 2004) developed three separate models to predict primary, secondary and tertiary rutting stage. An algorithm was established to determine the model parameters from repeated load test data. The transition point between different stages of rutting was identified. The authors observed all three stages of rutting in the FHWA accelerated loading facility, located in Mclean, Virginia. The proposed model given below was tested with seven different field mixes and for most mixes the model predicted rutting compared well with laboratory tested mix rutting. The developed model is:

Primary stage:

$$\varepsilon_p = aN^b \quad (2.12)$$

Where,

ε_p = permanent strain

N = number of load repetitions

a, b = material constants

Secondary stage:

$$\varepsilon_p = \varepsilon_{ps} + c(N - N_{ps}) \quad (2.13)$$

ε_{ps} = permanent strain corresponding to the initiation of secondary stage

N_{ps} = number of load repetitions corresponding to the initiation of the secondary stage

c = material constant

Tertiary stage:

$$\varepsilon_p = \varepsilon_{st} + d(e^{f(N-N_{st})} - 1) \quad (2.14)$$

ε_{st} = permanent strain corresponding to the initiation of tertiary stage

d, f = material constants

N_{st} = number of load repetitions corresponding to the initiation of the tertiary stage

The main disadvantage of this model form is that the model material constants vary based on mixes and it is very difficult to come up with a unique model to predict rutting. Along with number of loading, the model included only material parameters and the model did not include any mechanistic parameters. Further, having three models to capture rutting makes the process more complicated and it would be advantageous to have a single model that can capture the true rut progression in the field.

2.7.11 Other Rut Prediction Models

Since the objective of this study was to develop a simple M-E based rut prediction models, only related literatures were discussed above. However, very complicated and advanced models were also developed by researchers. Some researchers developed non-linear finite element models to predict rutting (Kirwan et al., 1977; Meyer and Hass., 1977). Some research studies (Kenis, 1977; Thrower, 1977; Battiato et al., 1977; Mahboub and Little, 1988; Sousa et al., 1993; Long, 2001; Blab and Harvey, 2002; Hornyk et al., 2002; Fang et al., 2004; Park, 2004; Elseifi et al., 2006) focused on including the viscoelastic and plastic characteristics of pavement layers on the model and developed rut prediction models. However, these models have employed many assumptions and further used laboratory test results for material behavior in the model development. Detailed explanations of these models are beyond the scope of this study.

2.7.12 Summary

Most rut prediction models given above included layered vertical strain on pavement layers as one the variable for rut prediction. Researchers hypothesized and later proved with laboratory test results (Bissada et al., 1982; Sousa et al., 1993; Hand and Epps, 1998; Drakos et al., 2001; Long, 2001; Park, 2004) that consideration of shear strain in the asphalt layer is a more valid approach for HMA rut prediction. In their studies, they found very good correlation between permanent deformation (rutting) and shear strain.

After reviewing the literature, the necessity of layer vertical strain approach and shear strain approaches for rut prediction model building and comparing them for their ability to predict field rutting was explored in this research.

CHAPTER 3

TEST FACILITY AND DATA COLLECTION

3.1 INTRODUCTION

There are many developments in the field of pavement engineering that needs field verification before implementation. One among the developments is the newly proposed M-E pavement design method. Further, there are many performance tests that need field verification. This field verification effort will take at least 20-25 years in existing highways. However, for accurate field verification in the shortest period of time, accelerated pavement testing facility such as the NCAT Test Track can be used very effectively. Since the research study was conducted at the NCAT Test Track, having a complete understanding of the NCAT Test facility and the data collection efforts at the Test Track are very important to understand the next two chapters.

3.2 NCAT TEST TRACK

The NCAT Test Track was built in 2000 and it has been in service since then. The Test Track is cooperatively funded by a number of DOTs and the Federal Highway Administration (FHWA), with operation and research managed by NCAT. State DOTs that have sponsored research at the Test Track include; Alabama, Florida, Georgia, Indiana, Missouri, Mississippi, North Carolina, Oklahoma, South Carolina and

Tennessee. A complete Test Track research cycle comprises one million laps on the 1.7 mile track in about two years.

The NCAT Test Track is a fully access controlled, oval shaped, full scale accelerated pavement testing (APT) facility. It is located near the campus of Auburn University in Auburn, Alabama. The Test Track consists of 46 different test sections, out of which eight sections were assigned for structural study in 2003. The construction details of these sections are given in detail elsewhere (Powell, 2001; Brown et al., 2002; Powell, 2006). The overall view of the Test Track is given in Figure 3.1.



Figure 3.1 Overview of the NCAT Test Track.

Mixture rutting was the preliminary study variable in the 2000 Test Track cycle. In 2003, twenty three of the original 46 test sections were left in place for continuous performance evaluation and twenty two new sections were built in 2003. One test section was removed to serve as a transition for new construction. In the 2003 Test Track cycle, eight sections that are located in the north tangent (Sections N1 through N8) were allocated for M-E design evaluation and to learn more about material characterization and validation of pavement responses. The locations of structural study sections in the Test Track are shown in Figure 3.2.

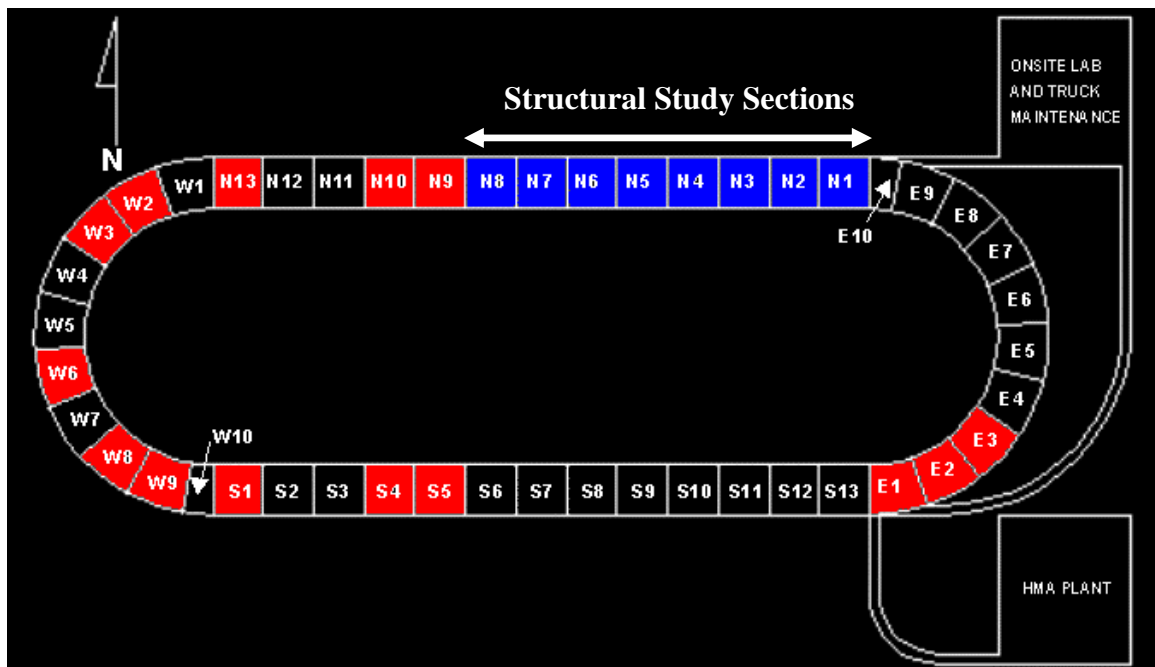


Figure 3.2 Location of Structural Study Sections.

Specifically, the 2003 structural study was conducted to address many issues pertaining to M-E design. The main objectives of the structural experiment study was to validate mechanistic pavement models, develop transfer functions for typical asphalt mixtures and pavement cross-sections, to study the dynamic effects on pavement

deterioration from a mechanistic viewpoint and to evaluate the effect of thickness and polymer modification on structural performance (Timm et al., 2004). The structural study sections were sponsored by the FHWA, Alabama Department of Transportation (ALDOT) and the Indiana Department of Transportation.

The two preliminary experimental factors in the structural study were HMA thickness and binder modification. The structural study sections utilized a modified and an unmodified binder and different HMA thicknesses. The PG 67-22 was an unmodified binder. The modified binder PG 76-22 used the same base asphalt as the PG 67-22, but was modified with Styrene-Butadiene-Styrene (SBS) polymer. Both materials have been used by ALDOT.

The eight test sections were designed for varying levels of traffic which resulted in the design of thin, medium and thick sections using unmodified PG 67-22. These three sections were replicated with SBS modified PG 76-22. The final two sections were designed for medium traffic level with stone matrix asphalt (SMA) as their wearing course in the top one inch. The last section (N8) had a rich bottom with an additional 0.5% asphalt content above optimum. The thin (N1 and N2), medium (N5 and N8), and thick HMA sections (N3 and N4) have HMA thickness of 5", 7" and 9", respectively. All eight sections have a 6" granular base course as shown in Figure 3.3. Beneath the granite base was a fill layer to bring all test sections to the same surface elevation.

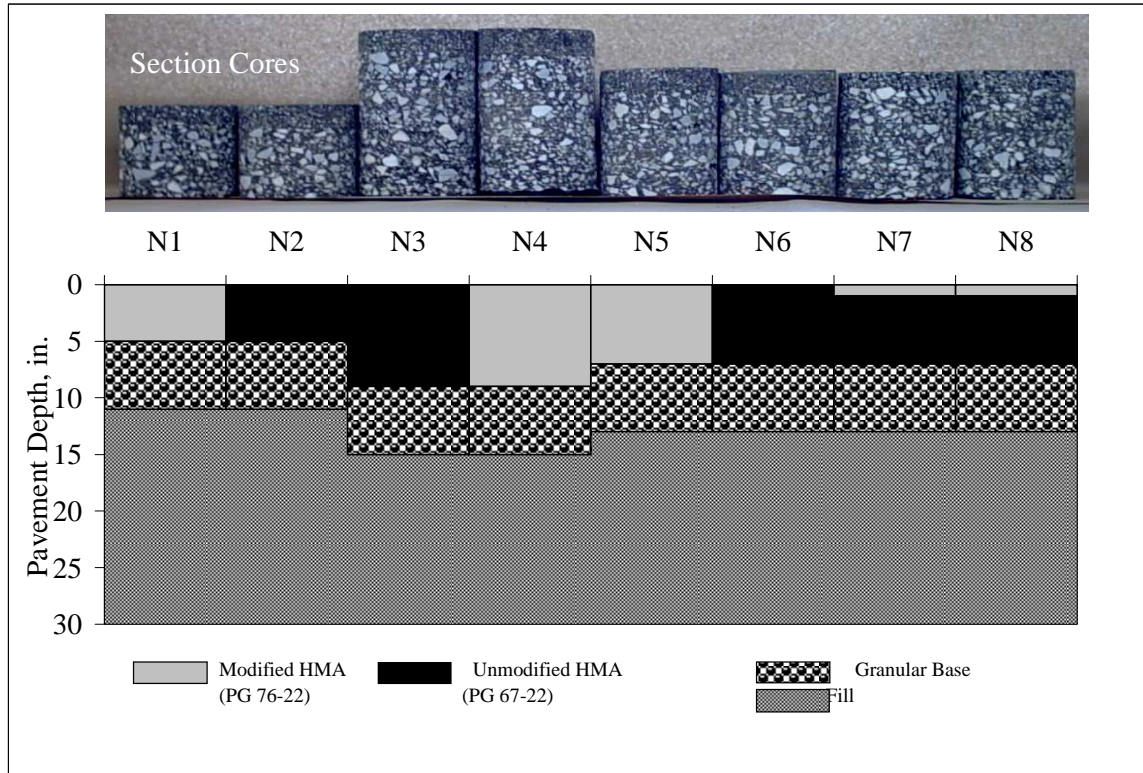


Figure 3.3 Structural Experiment Sections Layer Cross Section (Timm et al., 2004).

The top HMA layer was built with different lift thickness and the component material varied in subsequent lifts. Figure 3.4 shows the HMA sub-layer constituent information. The different mix characteristics indicated in Figure 3.4 are given in Table 3.1. From the Table, it is clearly evident that the topmost layer (wearing course) had a standard asphalt content value of 6.1% between sections. The detailed structural design of all eight test sections is given in detail in a published NCAT research report (Timm et al., 2004).

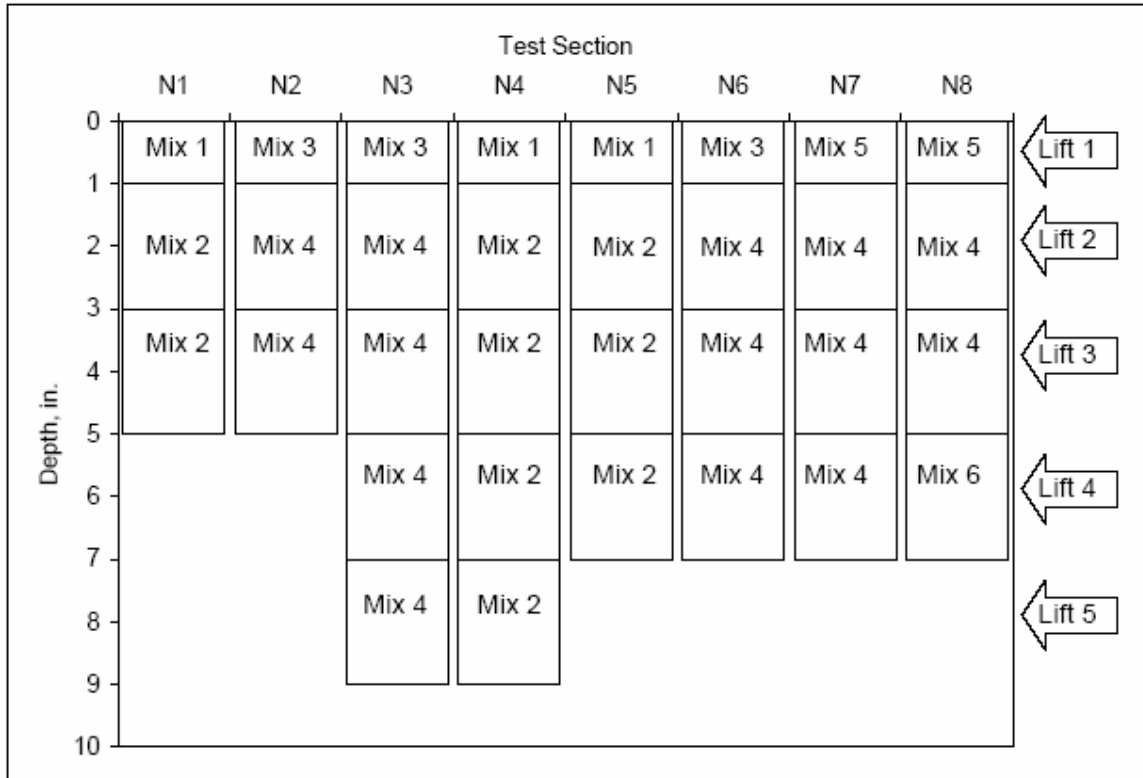


Figure 3.4 HMA Layer Composition of Structural Experiment Sections (Timm and Priest, 2006).

Table 3.1 Structural Study Section HMA Mix Parameters

Mix Number	Asphalt Grade	Gradation	Design	No of Gyration	AC, %
1	76-22	Wearing	Superpave	80 blows	6.1
2	76-22	Base	Superpave	80 blows	4.3
3	67-22	Wearing	Superpave	80 blows	6.1
4	67-22	Base	Superpave	80 blows	4.3
5	76-22	SMA	Marshall	50 blows	6.1
6	67-22	Base	Superpave	80 blows	4.8

In this research effort, all mix specific construction parameters such as asphalt content, air voids, and gradation were kept constant between test sections and the only study variables were HMA thickness and binder modification.

3.3 STRUCTURAL SECTION INSTRUMENTATION

The structural sections have asphalt strain gauges to measure longitudinal and transverse strain, pressure cells to measure vertical stress along with moisture probes and temperature probes. The general instrumentation layout is shown in Figure 3.5. Since the objective of this research was to build a rut prediction model, this study focused on the vertical pressure response derived from the embedded pressure cells. Historically, vertical responses over the granular layers in terms of stress and strain were attributed to the permanent deformation of pavement layers.

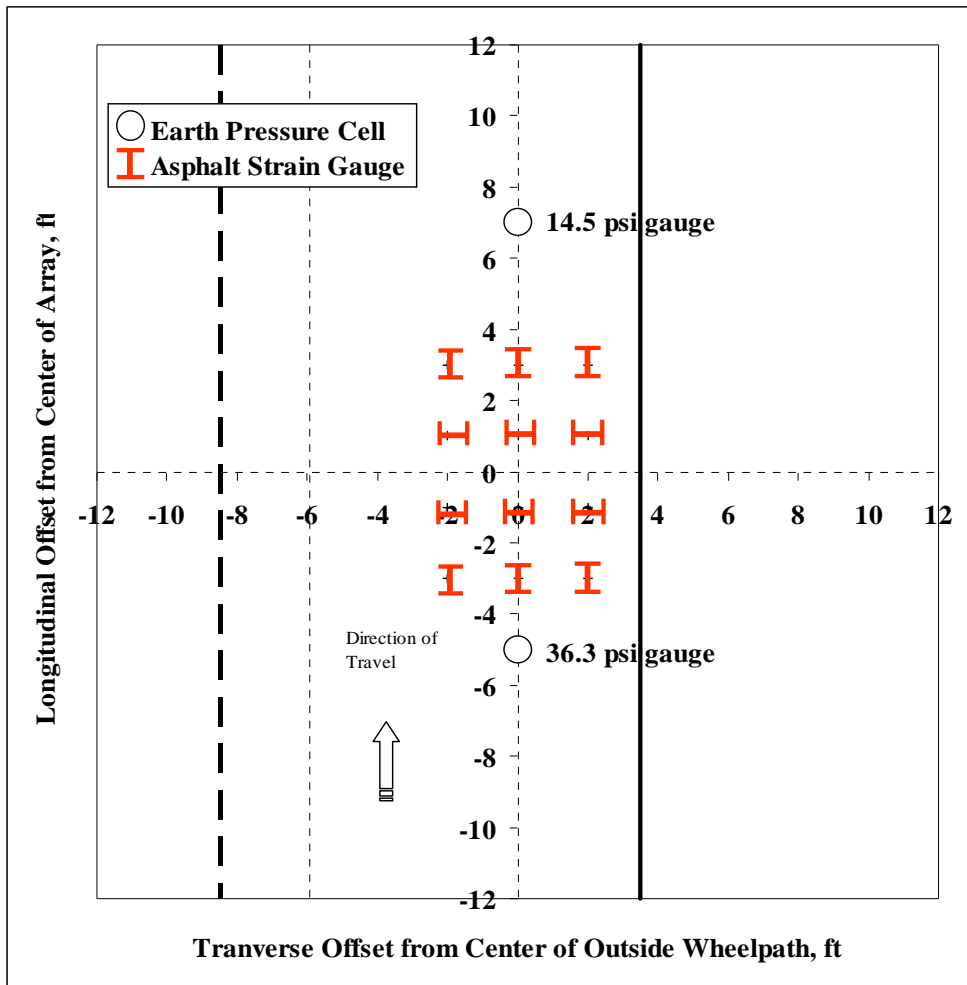


Figure 3.5 Structural Experiment Sections Instrumentation Layout.

3.3.1 Earth Pressure Cells

The earth pressure cells were placed at the top of the base layer and at the top of the subgrade layer at the center of outside wheel path. The role of the earth pressure cell was to measure dynamic vertical stresses generated under moving wheel loads. Geokon 3500 earth pressure cell (EPC) was used in this study and the same type of instrumentation had also been used at the Mn/ROAD project to collect dynamic vertical stresses successfully.

Geokon 3500 EPC consists of two 9” diameter circular 304-stainless steel plates welded together around their periphery and spaced apart by a narrow cavity filled with de-aired oil. External pressures squeeze the two plates together causing an equal internal pressure in the internal fluid. The attached semiconductor transducer then converts this pressure into an electrical signal which is transmitted as a voltage change via cable to the readout location (Geokon, 2006). Figure 3.6 shows a typical Geokon 3500 EPC used at the Test Track structural study sections. Figures 3.7 and 3.8 show the placement of a pressure cell in the test sections.

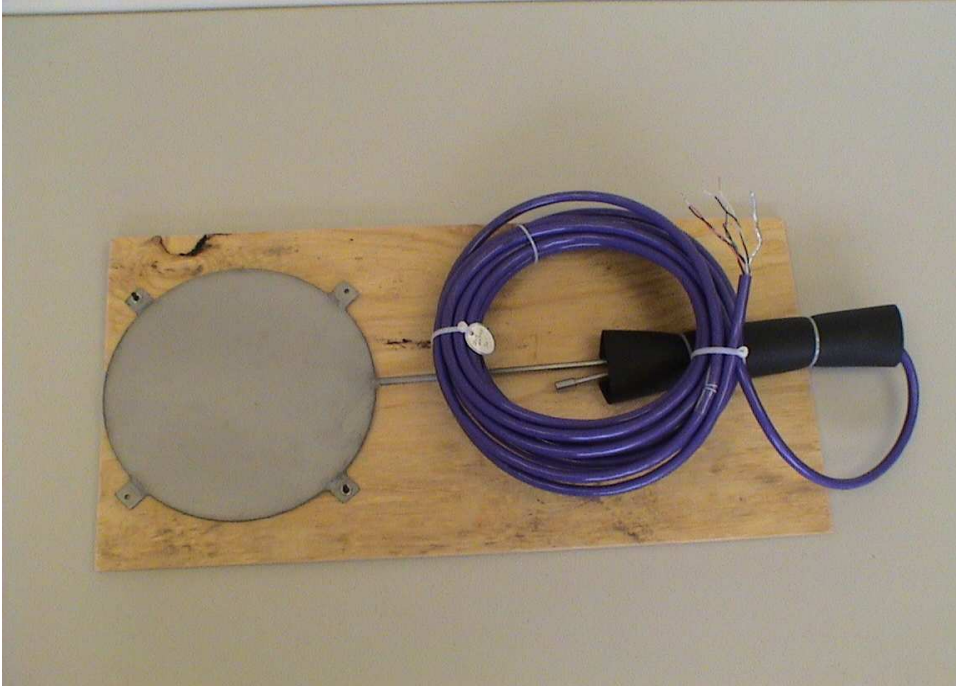


Figure 3.6 Geokon 3500 Earth Pressure Cell Used at the Test Track.



Figure 3.7 Subgrade Earth Pressure Cell Placed on the Top of Subgrade.



Figure 3.8 The Base Pressure Cell on Top of Base Layer.

The EPC 3500 type produced by Geokon is available in different ranges to measure pressures up to 10 MPa (100,250,600 kPa, 1.0, 2.5, 6.0 and 10 MPa). After conducting preliminary mechanistic analyses to find out the maximum stress values expected at the top of base and subgrade layers in the test sections, gauges with maximum limit of 100 kPa (14.5 psi) and 250 kPa (36.3 psi) were selected. During this process, estimates were made regarding material properties, wheel loadings, and stresses were calculated at the top of base and subgrade and it was found that the 14.5 psi and 36.3 psi gauges would work well for the subgrade and base, respectively. The accurate and careful installation efforts resulted in 100% survivability of the pressure cells during the 2003 Test Track cycle. The calibration of these pressure cells is documented elsewhere (Timm at al., 2004).

3.3.2 Temperature Probes

In each test section, four thermistors supplied by Campbell Scientific were bundled together (Figure 3.9) and installed in the pavement to provide temperature information near the surface, at 2", 4" and 10" depth. A hole was drilled in the pavement in such a way that the thermistor bundles could be inserted into the pavement with ease. After placing the thermistor bundles, the hole was filled with asphalt roof sealant cement and made sure that there was no trapped air within the hole.

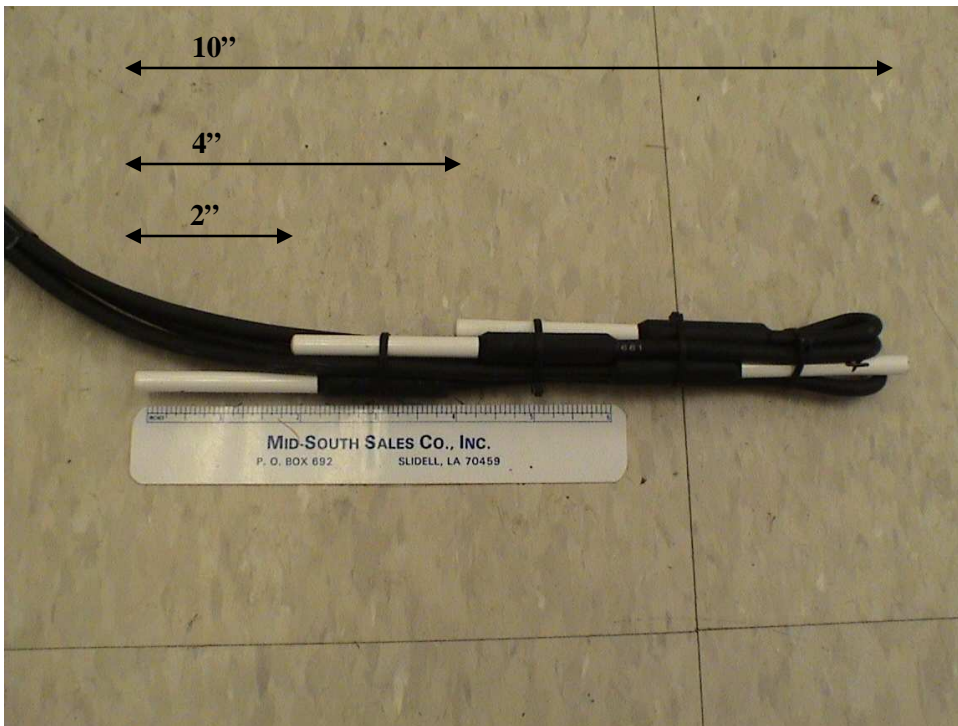


Figure 3.9 Temperature Probes Bundled Together.

3.4 DATA ACQUISITION

The temperature data was sampled at a relatively slow frequency, without missing any important information. Data collected using the slow speed system was logged at one sample per minute using a Campbell Scientific CR10X datalogger located at each test section in the roadside box. The datalogger sampled at every minute and recorded the hourly average, maximum and minimum readings. Hourly readings were transmitted through a radio modem to the data storage computer located in an onsite laboratory building throughout the duration of the test cycle

The sampling rate required for pressure cells was much higher, relative to temperature readings, due to the dynamic nature of the traffic loading. Since the trucks are driven at a higher speed (normally 45 mph), the loading duration on the gauges under live traffic is in the range of 20 to 100 milliseconds.

A high speed data acquisition system Dataq DI-510-32 was used to collect data at a higher sampling rate. The data acquisition system used at the Test Track is shown in Figure 3.10. This acquisition system has a 32 channel, 250,000 Hz capability with individual channel signal conditioning cards unique for each type of gauge. While collecting high speed data under live truck loading, the slow speed sensors were disconnected from the road side box (Figure 3.11) and wired into the high speed data acquisition system and the data were collected.

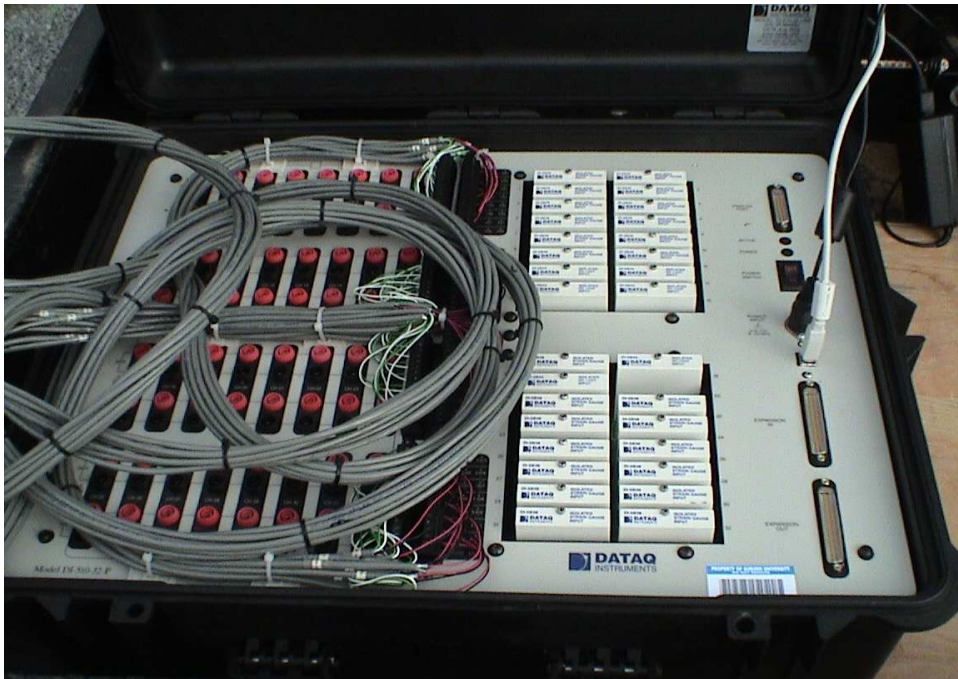


Figure 3.10 Data Acquisition System Used at the Test Track.

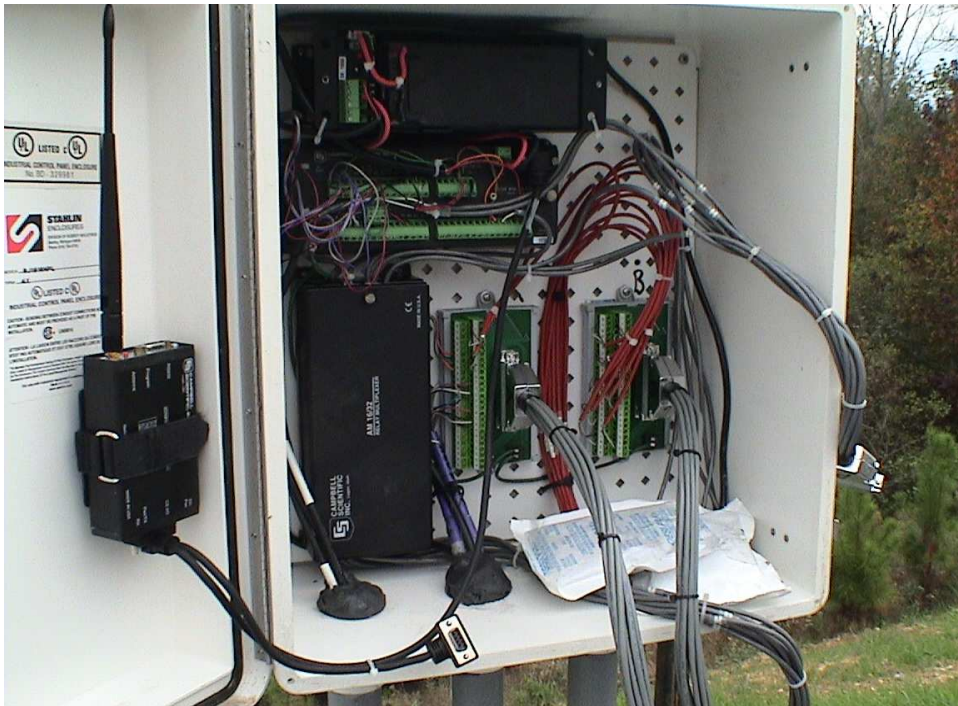


Figure 3.11 Road Side Data Logger Box Used at the Test Track.

3.5 TRUCKING

At the Test Track, one box trailer and four triple trailers were used initially to apply traffic loading. At a later stage of this traffic cycle, one more triple trailer (6-Triple) was added to accelerate the traffic. In general, the box truck had a steer axle (12 kip) and two tandem axles (34 kip/axle group); the triple trailer consisted of a steer axle (12 kip), one tandem axle (40 kip) and five single axles (20 kip/axle). However the exact loads were monitored and varied slightly from truck to truck. The exact axle weight data are given in Table 3.2. For the analysis, the triple-trailers were considered equal and duplicates of the same test vehicle, while the box trailer was considered as a separate vehicle. The test vehicles are shown in Figure 3.12 and 3.13.

Table 3.2 Axle Weight Data by Truck (Priest and Timm, 2006)

Truck ID	Steer, lb	Drive Tandem, lb		Single Axle, lb				
		1	2	1	2	3	4	5
1-Triple	10,150	19,200	18,550	21,650	20,300	21,850	20,100	19,966
2-Triple	11,000	20,950	20,400	20,950	21,200	21,000	20,900	20,900
3-Triple	10,550	20,550	21,050	21,000	21,150	21,150	21,350	20,850
4-Triple	10,500	21,050	20,700	21,100	21,050	21,050	20,900	21,050
6-Triple	11,200	19,850	20,750	20,350	20,100	21,500	19,500	20,300
Average	10,680	20,320	20,290	21,010	20,760	21,310	20,550	20,613
COV ¹	3.9%	3.9%	4.9%	2.2%	2.5%	1.7%	3.6%	2.2%
	Steer	Drive Tandem		Rear Tandem				
5-Box	11,550	16,850	17,000	16,800	16,100			

¹Coefficient of Variation



Figure 3.12 NCAT Test Track Test Vehicles – Triple Trailer.



Figure 3.13 NCAT Test Track Test Vehicles – Box Trailer.

Drivers were employed by NCAT to operate trucks to simulate real traffic. At the beginning of the 2003 Test Track cycle, a single triple trailer was operated for approximately two months and full operations began in December 2003. The main reason to begin the test cycle with a single truck was to provide some seating and aging of pavement layers before accelerating the loading.

The trucking operations were done in two shifts, each consisting of eight hours of driving around the track. The drivers were instructed to drive the trucks at a constant speed of 45 mph. From the collected pressure response signals (refer Figure 3.15); the speed of the trucks can be verified. To have a counter check on the vehicle speed, the collected pressure data were randomly selected for four different dates (11/7/2003, 4/13/2004, 7/20/2004, and 1/11/2005). The time required for an axle to cross the distance between base and subgrade pressure plates (12 feet) were measured from the collected signals. By knowing the linear distance between the two pressure plates, the velocity of the vehicles were calculated. When analysis was done on the data, it was found that the trucks were moving at an average speed of 45.76mph with a standard deviation of 1.7mph.

Traffic was applied six days a week and every Monday trucking was suspended for weekly truck maintenance and so that performance data could be collected to thoroughly document the field performance over time. The traffic volume data were recorded based on the mileage per shift and then converted to laps per hour based on the shift schedule and track length (1.7 mile/lap). At 45mph, typically each truck was able to complete 28 laps in an hour. The triple trailer laps were combined and considered together, while the box trailer was considered separately. This trucking database was

assembled manually and efforts were taken to verify that the collected data is accurate and complete with no missing data. The trucking data that were used to calibrate fatigue transfer functions for M-E pavement design (Priest, 2005; Priest and Timm, 2006) was used in this study. Trucking operations were completed in the middle of December 2005 after applying 10 million ESALs.

3.6 HIGH SPEED DATA COLLECTION AND PROCESSING

3.6.1 Data Collection

During high speed data collection, the portable data acquisition system was taken to each test section and three passes of each truck were collected. Over the two year period, the high speed data were collected once a week from the Test Track, for three passes of live traffic loads (triple trailer and box truck) and under different environmental conditions. It was necessary to collect multiple passes of each truck to account for natural wheel wander variation. The decision to record three passes was taken at the starting of this project based on a balance between having a representative distribution of pavement responses that included wheel wander and other random effects with the need to conduct testing in a relatively short amount of time for personal safety purposes.

A detailed study on wheel wander was carried out at the Test Track and the results showed that the wheel load distribution in the Test Track was consistent with the wheel wander in typical highways (Timm and Priest, 2005). The wheel wander was due to the mechanical alignment of the trailers and driving pattern of human drivers. By collecting three passes and using the maximum response for analysis, the effect of natural

wheel wander could be minimized. This strategy was proved successful with the collected pressure data and documented in the next chapter.

Further, analysis on the Test Track strain data also proved that three truck passes captured full variability of the data. A study was conducted on October 13, 2004, to investigate the effect of lateral placement on the collected strain data. For this purpose, ten consecutive passes of each truck were collected. After analyzing the collected data, it was found that the individual truck responses were fairly consistent by pass, and the range of variability was captured in about three passes. From Figure 3.14, it was evident that no additional information was drawn from the data when ten passes were compared to three passes. Therefore, it was decided to follow a testing scheme of collecting and processing three passes of trucks during the testing cycle (Priest, 2005; Priest and Timm, 2006).

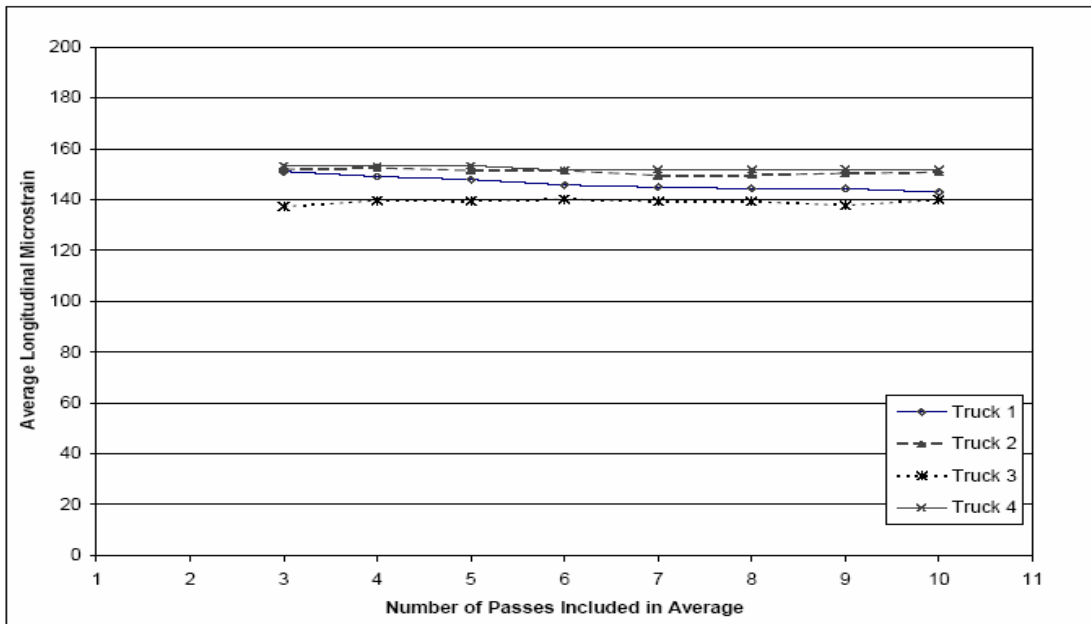


Figure 3.14 Average Strain by Truck and Pass (Priest and Timm, 2006).

3.6.2 Data Processing

In each test section, three passes of the trucks were recorded at 2,000 samples per second per channel and checked in the field to make sure that all three passes were successfully recorded. The voltage outputs of the gauges were recorded in the field, and then the conversions to pressure (psi) were later applied to the data when the data were processed.

The recorded high speed data signal were processed using a signal processing software DaDisp2002. The DaDisp 2002 is a commercially available signal processing software. Unlike the strain response (Priest, 2005), the pressure cell signal had less electrical noise. Cleaning the signals for electrical noise was required because of residual noise that is inherent with electrical signals. To clean the pressure gauge signals, a ten point moving average was more than sufficient without compromising the data.

A typical processed pressure response trace for a pass of triple trailer is given in Figure 3.15. When the collected pressure gauge response is processed by the signal processing software, it first picks the minimum and maximum inflection points. Then the average of all maximum and minimum inflection points for a single truck pass is computed. The difference between the maximum and minimum inflection points are then converted to average pressure amplitude and the steps involved in that process is explained below. In this way, an average pavement response over an entire truck pass is represented. The final output from the DaDisp software contains the test section number, gauge ID, gauge factor, truck ID, pass number, maximum, minimum and average amplitudes. The processed data were stored in a comprehensive database for further data analysis.

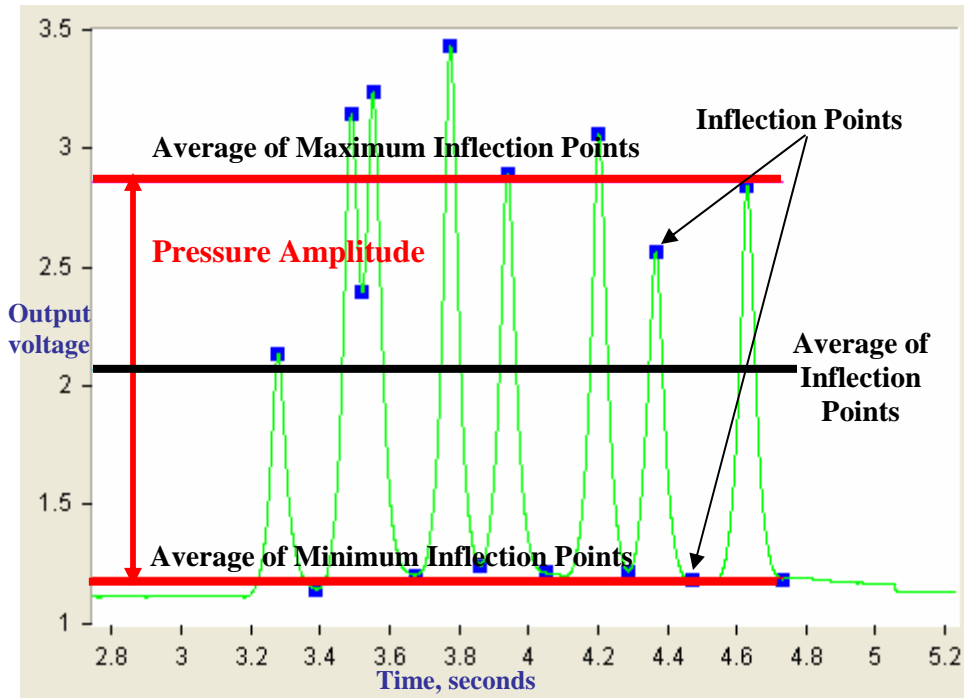


Figure 3.15 Typical Pressure Response Trace for a Triple Trailer.

The conversion of voltage difference (ΔV) between the average maximum and minimum inflection points in the processed signal is converted to average pressure amplitude (base, subgrade) for a truck pass by the following procedure.

The average of maximum and minimum inflection points for a single truck pass is indicated as a thick line in Figure 3.15. The change in output voltage between the recorded points was calculated and converted to pressure by:

$$\text{Pressure} = \Delta V * \text{Gauge Factor} \quad (3.1)$$

Where:

ΔV = change in output voltage = voltage difference between consecutive inflection points

$$\text{Gauge Factor} = \frac{P_{fullscale}}{V_{fullscale}} \quad (3.2)$$

Where,

$P_{fullscale}$ = full scale pressure of the gauge, psi

$V_{fullscale}$ = full scale output (5V)

The full scale voltage is 5V and the full scale pressure for subgrade pressure cell is 14.5 psi and for base pressure cell is 36.3 psi. So, the gauge factor for subgrade pressure plate = $14.5/5 = 2.90$ psi/V. The gauge factor for base pressure plate = $36.3/5 = 7.26$ psi/V for base pressure gauge.

When the change in voltage was multiplied with the respective gauge factor, the pressure value in psi was obtained. This voltage to pressure conversion was done in the DaDisp software when the respective gauge factor is inputted while processing the signal. All axles in a single truck pass were processed at a time and the final output from DaDisp is the average amplitude (psi) which was used in this study.

3.7 MATERIAL PROPERTY DATA COLLECTION

Accurate material properties are critical inputs in M-E design, since they govern pavement responses and performance evaluations. In the context of M-E design and analysis, field characterization of modulus is important. Further, it is important to link the material properties to their mechanistic response whenever loadings are applied on the pavement. Laboratory derived layer modulus values can also be used as an input in M-E design. However, in the laboratory it is very difficult to exactly replicate the field conditions, changing environment, loading conditions etc. For accurate mechanistic analysis, the available literature suggests the use of field derived material modulus values.

To accomplish this, FWD testing was conducted on a monthly basis by ALDOT in all eight sections. Due to scheduling conflicts and equipment problems, tests were not conducted in some months. The FWD used at the Test Track was a Dynatest 8000, (Figure 3.16) and it had seven sensors spaced at 12” on center. The load plate had a radius of 5.91” and had a split configuration to ensure good seating on the pavement surface.



Figure 3.16 FWD Testing on the Structural Study Sections

At the beginning of the test cycle, three random locations were determined for each of the eight test sections. The FWD testing was conducted at those three predetermined locations per test section in both inside and outside wheelpath, and each testing location was thumped twice with an approximate load of 9000 lb.

While the FWD testing approach is straightforward, backcalculation of the data to determine the pavement layer properties requires a great deal of care. The procedure requires a level of engineering judgment and understanding because a small error in backcalculation would yield unreasonable and inaccurate moduli.

Back calculation procedures were carried out with EVERCALC 5.0 program to arrive at material properties. The FWD data collected after the pavement showed various signs of distresses were not used in further analysis, since cracked pavements do not give accurate deflection values, which will lead to inaccurate layer moduli. The cut off dates for FWD data are given in Table 3.3. The material characterization (modulus values of HMA, base and subgrade) for all test sections is described in the next chapter. The FWD testing and backcalculation protocol are documented in detail in a NCAT report (Timm and Priest, 2006).

Table 3.3 FWD Data Cut Off Dates for Analysis

Section	Cut-Off Dates for FWD Measurement
N1	22-March 2004
N2	14-June 2004
N3	No Cracks Observed; Data Collection Continued
N4	No Cracks Observed; Data Collection Continued
N5	7-February 2005
N6	7-February 2005
N7	7-February 2005
N8	12-July 2004

3.8 PERFORMANCE DATA COLLECTION

Once a week (Monday), the performance data were collected from the field. It included rut depth measurement, crack mapping and roughness measurement. The field performance evaluations focused on the middle 150' of each 200' test section. The middle part of test section was divided into three 50' sections, each containing a stratified random location to measure transverse profile on a weekly basis.

The main focus of this study was to build models to predict rutting. The cracking was also mapped and measured in the field. Explanation of fatigue cracking measurement methods are beyond the scope of this research work. The rutting was measured using three different methods; dipstick profiler/precision level (Figure 3.17), laser profiler (Figure 3.18) and wire line measurement with the six foot straight edge (Figure 3.19). A study conducted to compare these three methods of rut measurement showed that all three methods give relatively similar results (Brown, 2004).

An accurate transverse profile is needed to serve as the primary source of information as shearing in the outside the wheel paths became more influential (Powell, 2006). The dipstick profiler captures rutting along with the exact transverse profile, so it was further used in this study. However the pavement rutting captured using the other two forms of measurements were used for other research studies.



Figure 3.17 DIPSTICK Profile Measurement at the Test Track.

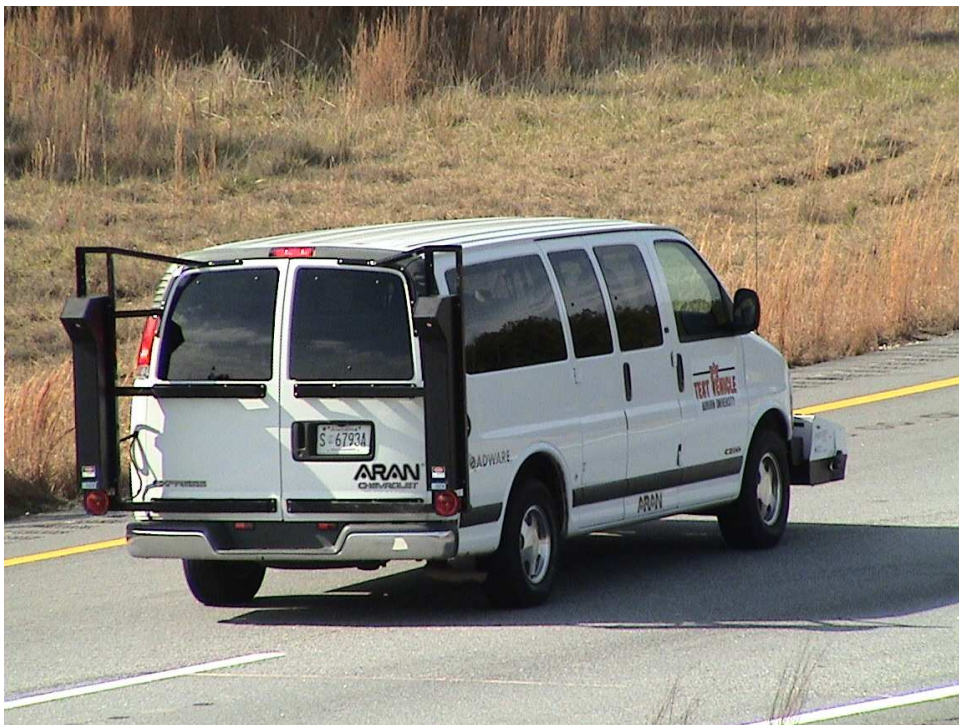


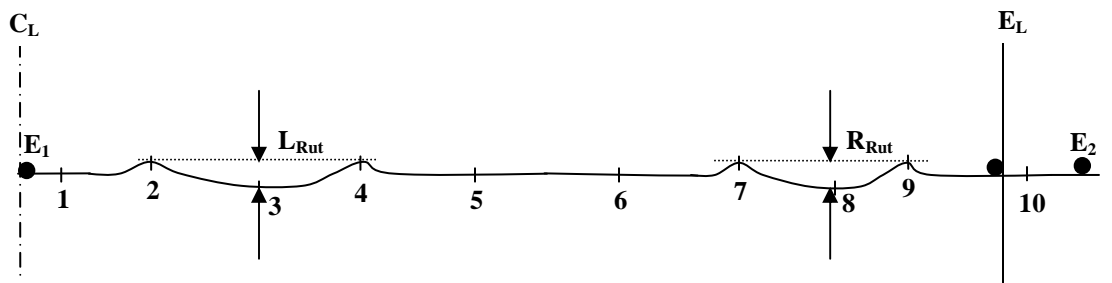
Figure 3.18 Automated Profile Measurement at the Test Track using ARAN.



Figure 3.19 Six Foot Straight Edge Transverse Profile Measurement.

The dipstick measures the transverse slope of the pavement, in increments, which changes with the presence of ruts. While using the Dipstick profiler to capture transverse profile, the profiler was walked across each stratified random locations within each section. In all three stratified locations with in a test section, a pin of known elevation (E_1 and E_2) was available as shown in Figure 3.20. The known elevations at both ends of the random locations helped to close the traverse, producing elevations that could be used to compute both left and right wheel path rutting.

At first, one end of the Dipstick profiler was kept at the known elevation E_1 . Then the Dipstick was walked across and the difference in elevation at different locations (1, 2, 3...11) were recorded. After recording the elevations at different locations across the pavement, finally the profiler was placed at the known elevation in the other end E_2 and the traverse was completed. Whenever the Dipstick measured elevation at the end E_2 , did not match with the known elevation of the pin, the difference between the known and the measured elevation was calculated and distributed equally among the number of surveyed locations.



E_1, E_2	= Known Pin Elevation, mm	
C_L	= Center of Road	
E_L	= Road Edge	
L_{Rut}	= Maximum Left Wheel Path Rutting, mm	
R_{Rut}	= Maximum Right Wheel Path Rutting, mm	
1..2..11	= Dipstick Measured Elevations, mm	(Not to Scale)

Figure 3.20 Computation of Rutting from DIPSTICK Profiler.

To compute the maximum rut depth in each wheel path, one Dipstick measured elevation was considered on each side of the wheel path. The procedure to identify the maximum rut depth is entirely manual. Six points and their average location were first assumed within the wheel path location. Then the center of the left wheel path was

moved around iteratively to achieve the maximum depth. When the center point was identified, the left peak was adjusted back and forth to find the maximum computed depth. The maximum depth at that location was recorded as the location having the highest rut depth. Similar procedure was carried out for the other side of the wheel path and the maximum rut depth was recorded manually.

After finding out the maximum rut depth in all three locations on both wheel paths within a test section, the average value was taken from six rut depth measurements and it was presented as the rut depth for that section. Considering the natural variability within a test section, the decision to have an average rut depth from all three locations was reasonable from an engineering stand point.

To supplement and accurately quantify rutting as well as to have a counter check over the measured rutting, transverse profiles were measured at the same six locations within each test section using straightedge. The measured rutting difference between these two methods was well within 0.5 to 1" (Brown, 2004).

3.9 SUMMARY

The NCAT Test Track is a state-of-the-art, full-scale accelerated test facility with the capability of conducting a variety of pavement and material testing. This research facility includes full-scale pavement sections, actual tractor-trailer test vehicles, human drivers, pavement instrumentation, environmental monitoring and the ability to conduct a wide range of performance and material characterization testing. Since most or all of the above elements are essential for a successful M-E pavement design, the contribution of the NCAT Test Track to the pavement community is paramount.

The detailed explanation of the NCAT Test Track was provided in this chapter with main emphasize on the structural study. Further the high, slow speed data collection, data processing and field performance data collection methods and efforts employed at the Test Track were explained. The usage of these data from the Test Track to fulfill the main objectives of this research study is given in subsequent chapters.

CHAPTER 4

LOAD RESPONSE MODEL VALIDATION

4.1 INTRODUCTION

As M-E design continues to advance toward full implementation by state agencies, there is a need to assess the accuracy of the load-response models under dynamic truck loading. Further, as mentioned in Chapter 2, the load response model needs to be validated in the field for increasing tire pressures, vehicle speed, loading conditions and for new mixes. So a field validation study to compare load response model (elastic layer responses) with field measured responses from the NCAT Test Track Structural test sections was necessary to accomplish one of the main objectives of this research study.

The load response model is a core component of flexible pavement M-E design and the common practice is to use a layered elastic approach to predict pavement responses under load. Concerns regarding accuracy of this type of model arise when considering unbound materials exhibiting non-linear behavior, viscoelastic hot-mix asphalt materials, and dynamic loads applied by moving traffic. Despite this, layered elastic models continue to be the state-of-the practice for most pavement design and analysis applications. For example, the new M-E pavement design guide developed under the National Cooperative Highway Research Program (NCHRP) project 1-37A relies upon layered elastic analysis for pavement response predictions (ERES, 2004). To

make sure that an accurate pavement response model is being used in M-E design, the layered elastic model has to be validated with respect to measured pavement responses under live traffic loads in real field conditions and the theoretical responses have to be verified by field measurements.

In this regard, one of the main objectives of this research effort was to assess the accuracy of a layered elastic model with respect to measured vertical stresses on top of granular layers under live traffic for eight test sections from the NCAT Test Track. Historically, the mechanistic responses on top of granular pavement layers are related strongly to the rutting performance of pavements.

4.2 DYNAMIC DATA VALIDATION

As explained in the previous chapter, the dynamic pressure response was collected over a two year period (October 2003 to November 2005) from the Test Track structural study sections. The data were collected once a week, for three passes of live traffic loads and under different environmental conditions. Though the data were collected during the entire testing cycle, only the intact pavement responses were used in the analysis. The data cutoff date considered for FWD was also applicable for dynamic pressure response data.

Before using the data for further analysis, analyses on the pressure data were done to get a better understanding of the collected data to make sure that the processed data were valid.

4.2.1 Trend in Base and Subgrade Pressure

Seasonal temperature variations had a profound effect on measured pressures and the influence of temperature was clearly visible on the collected pressure response. In winter periods, lower ambient temperatures increased the HMA modulus, which in turn reduced the pressure in the base and subgrade layers. During hot summer periods, the pressure in the base and subgrade was higher due to increased temperature and its influence on HMA modulus.

To explain this concept and to show the relation between temperature and measured pressures, Figure 4.1 is given below. From this figure, it is clearly evident that increase in temperature increases pressures in both base and subgrade layers. This behavior was a theoretically proven and well validated fact in flexible pavements.

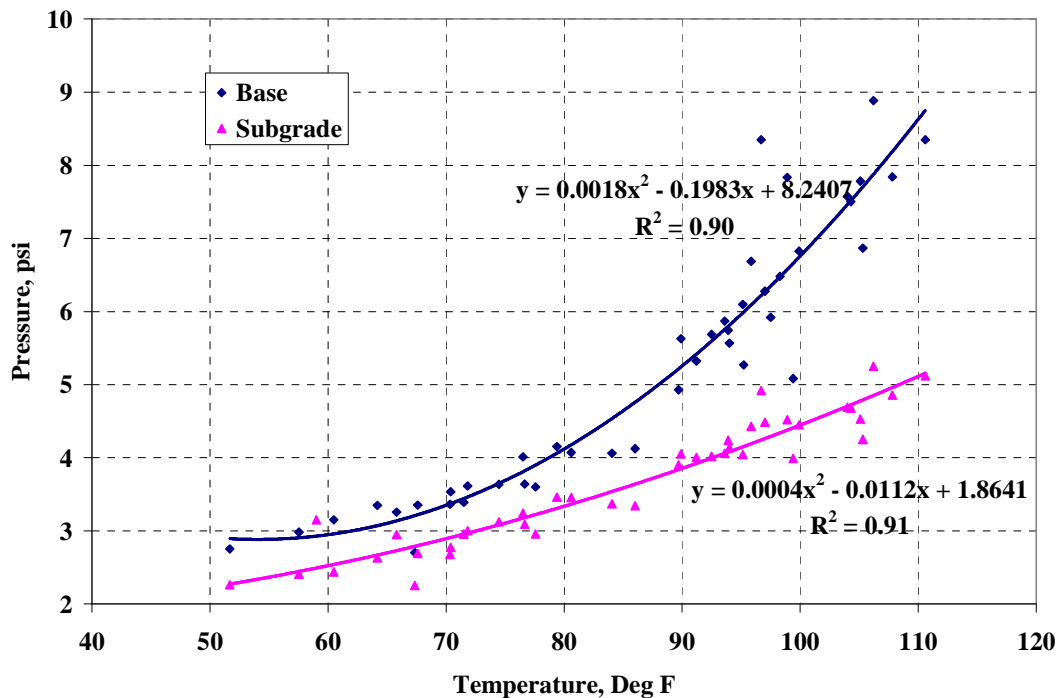


Figure 4.1 Pressure vs Temperature Relationship (Section N3, Triple Trailer).

When the processed pressure (base, subgrade) data were plotted against collected dates, a seasonal trend was clearly visible. During summer, the measured responses were higher than the winter and spring periods that are evident from Figures 4.2 to 4.15.

Similar trends were also observed for box trailer loading. For the box trailer, there were not enough data to show the trend clearly between base and subgrade pressures in sections N1 and N2.

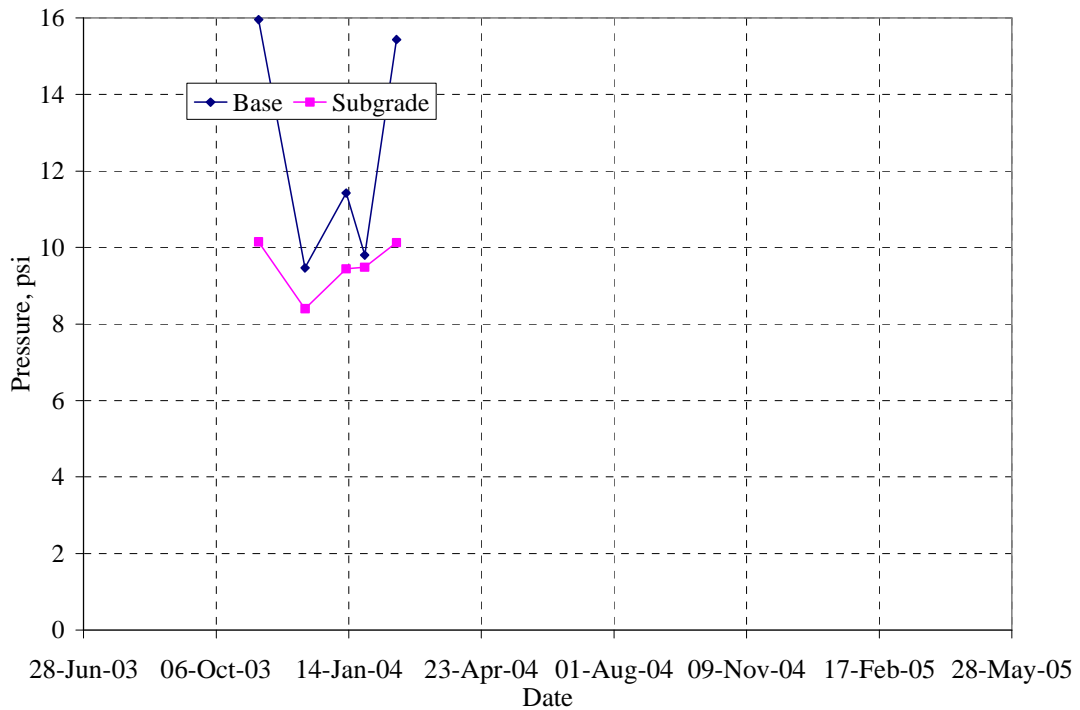


Figure 4.2 Trend of Base and Subgrade Pressures in Section N1-Triple Trailer.

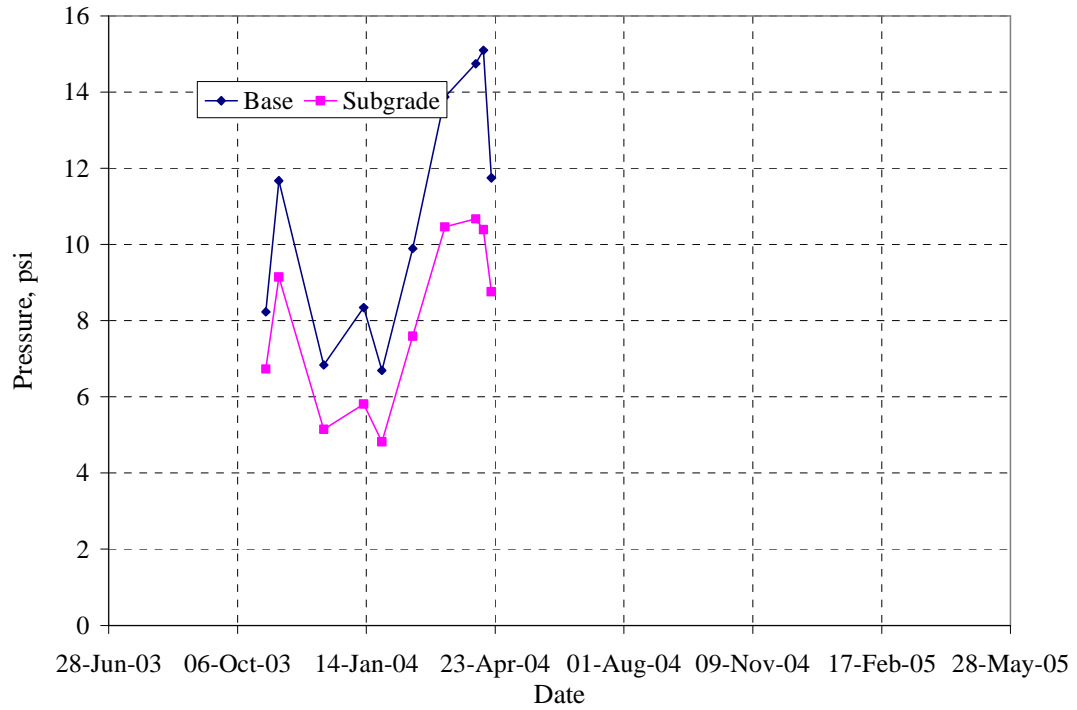


Figure 4.3 Trend of Base and Subgrade Pressures in Section N2-Triple Trailer.

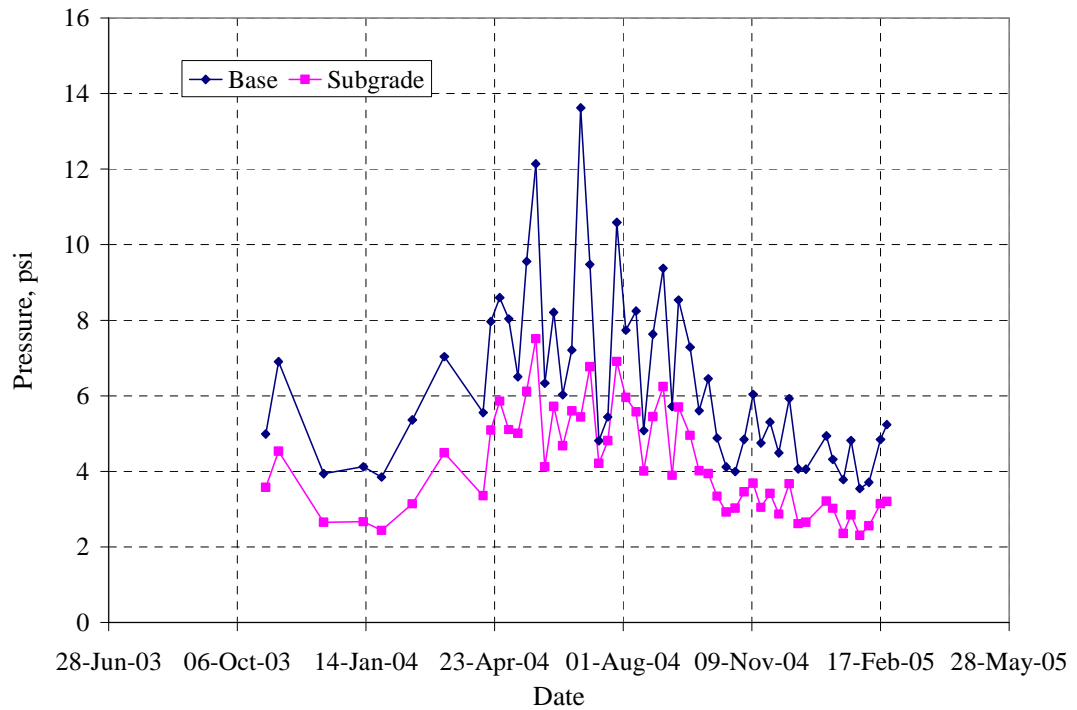


Figure 4.4 Trend of Base and Subgrade Pressures in Section N3-Triple Trailer.

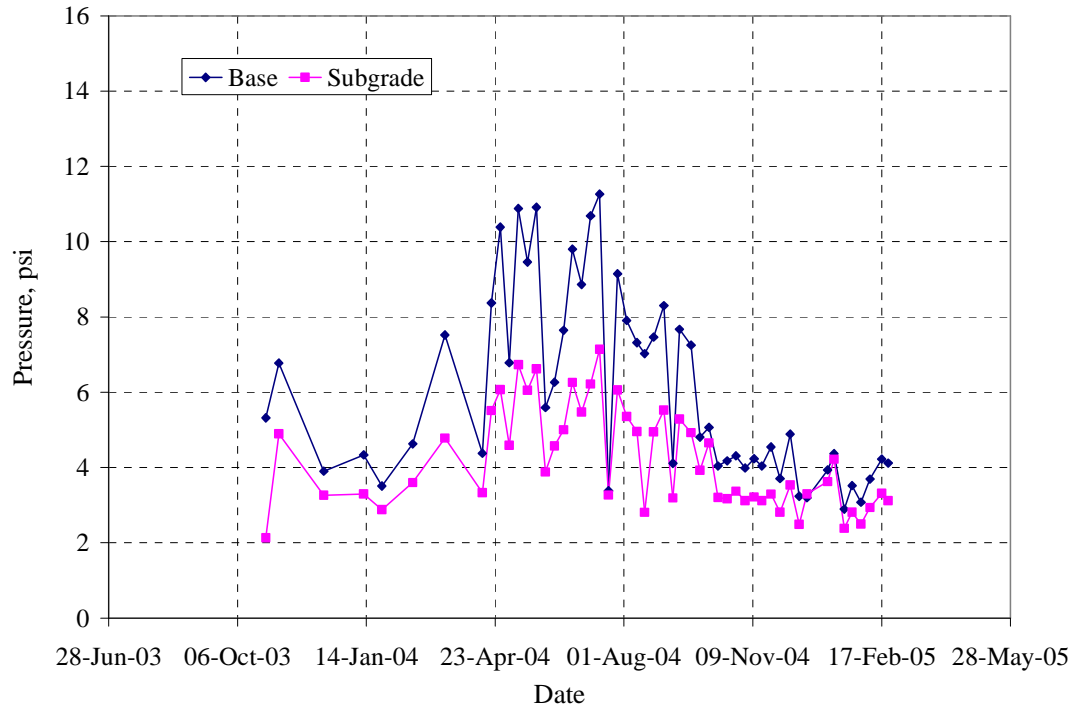


Figure 4.5 Trend of Base and Subgrade Pressures in Section N4-Triple Trailer.

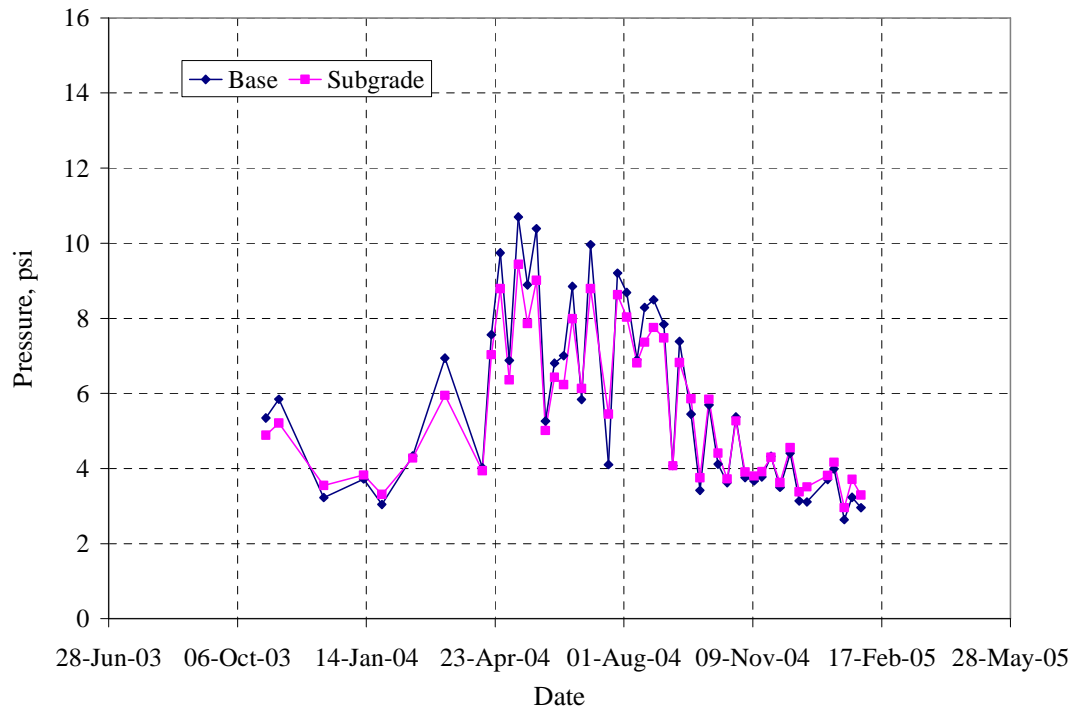


Figure 4.6 Trend of Base and Subgrade Pressures in Section N5-Triple Trailer.

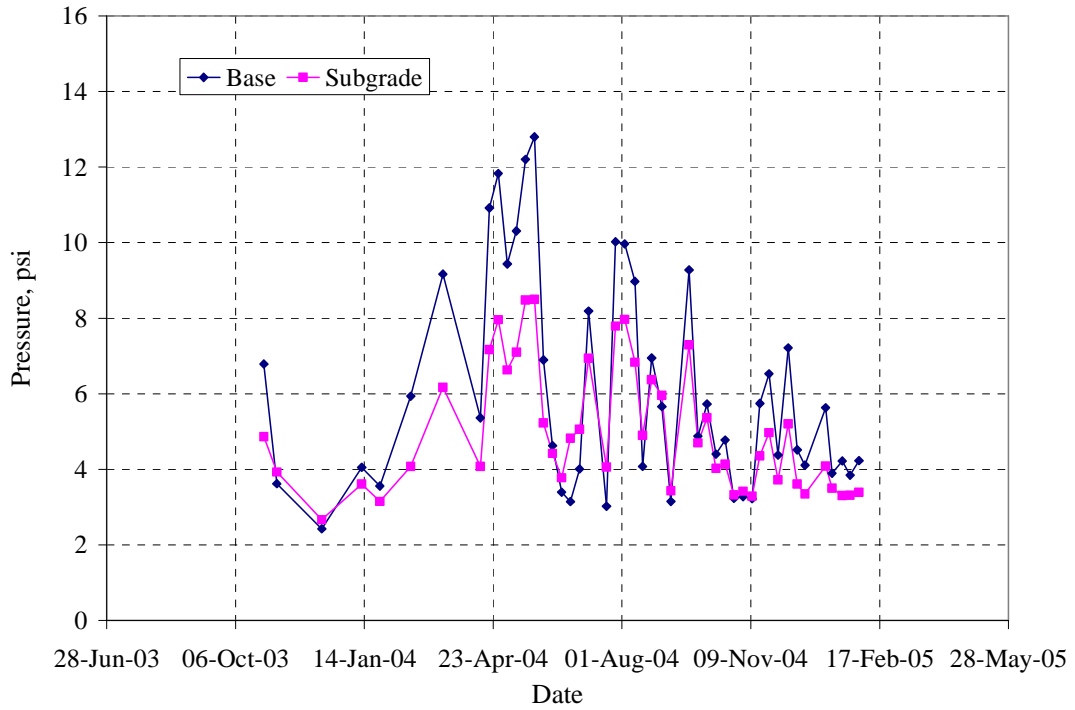


Figure 4.7 Trend of Base and Subgrade Pressures in Section N6-Triple Trailer.

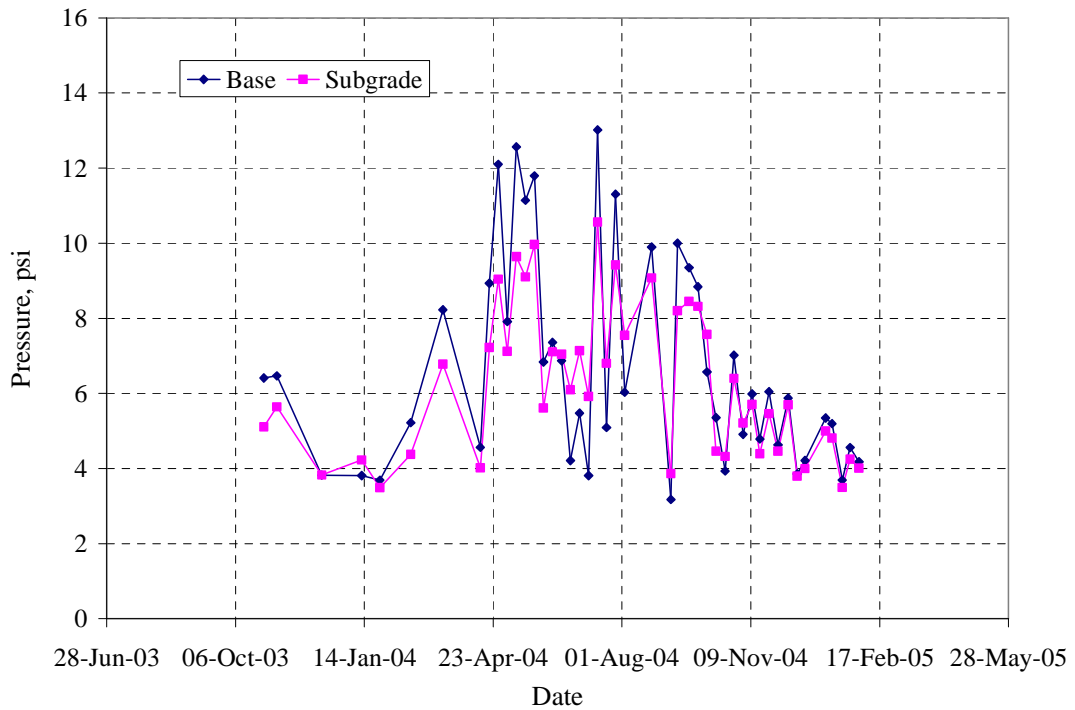


Figure 4.8 Trend of Base and Subgrade Pressures in Section N7-Triple Trailer.

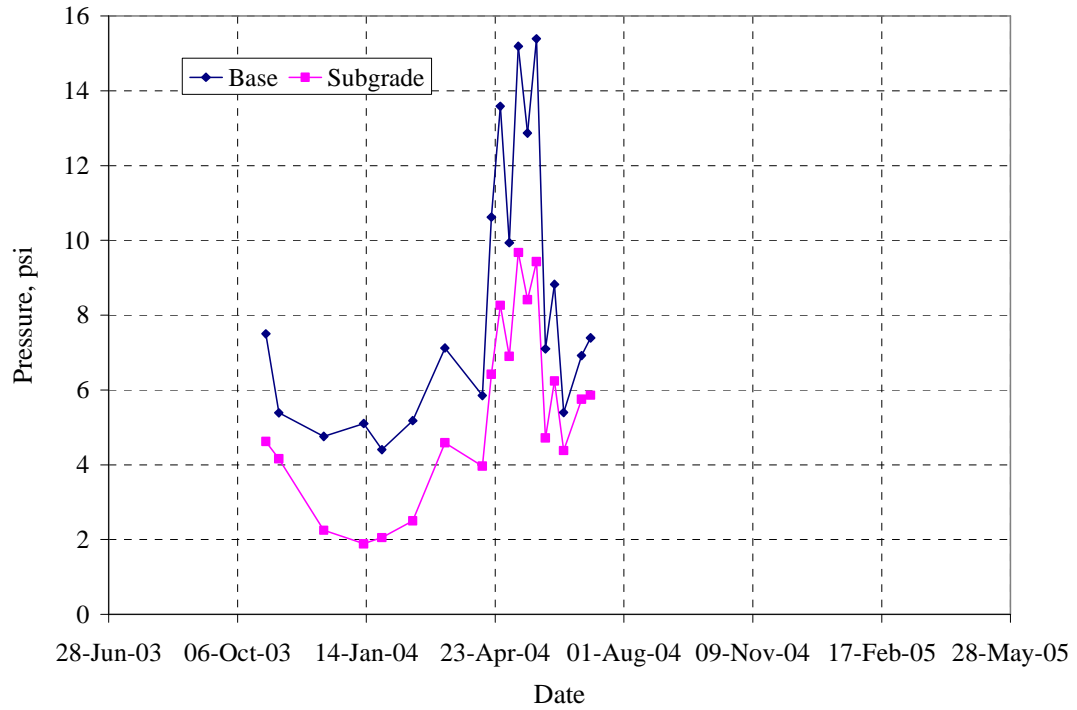


Figure 4.9 Trend of Base and Subgrade Pressures in Section N8-Triple Trailer.

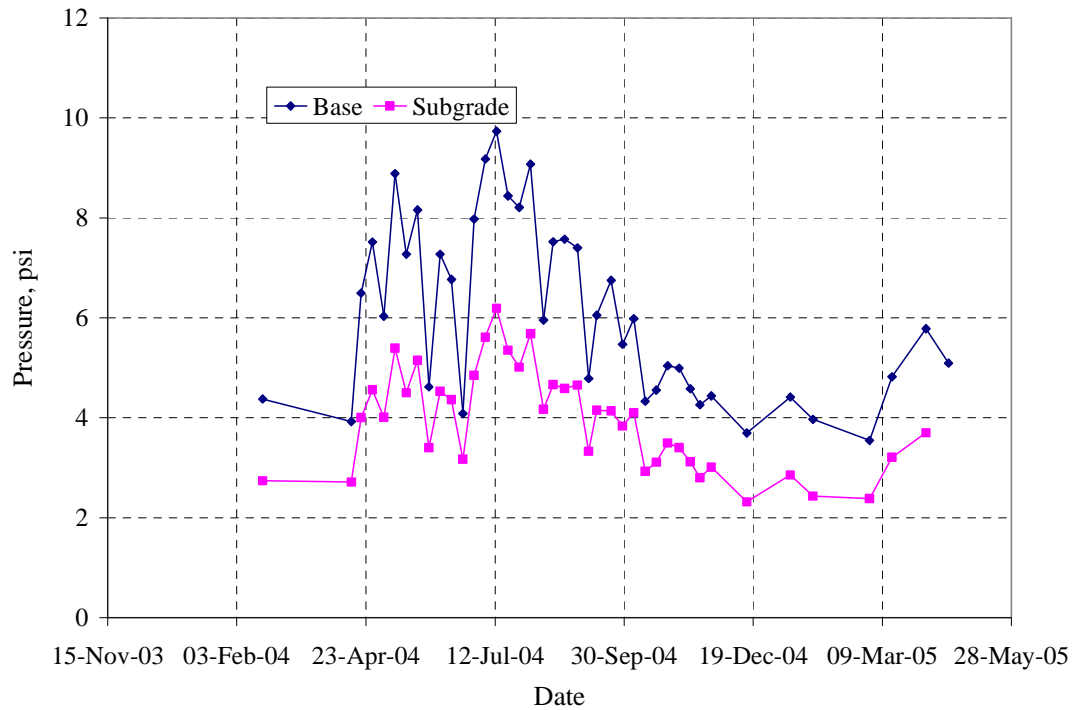


Figure 4.10 Trend of Base and Subgrade Pressures in Section N3-Box Trailer.

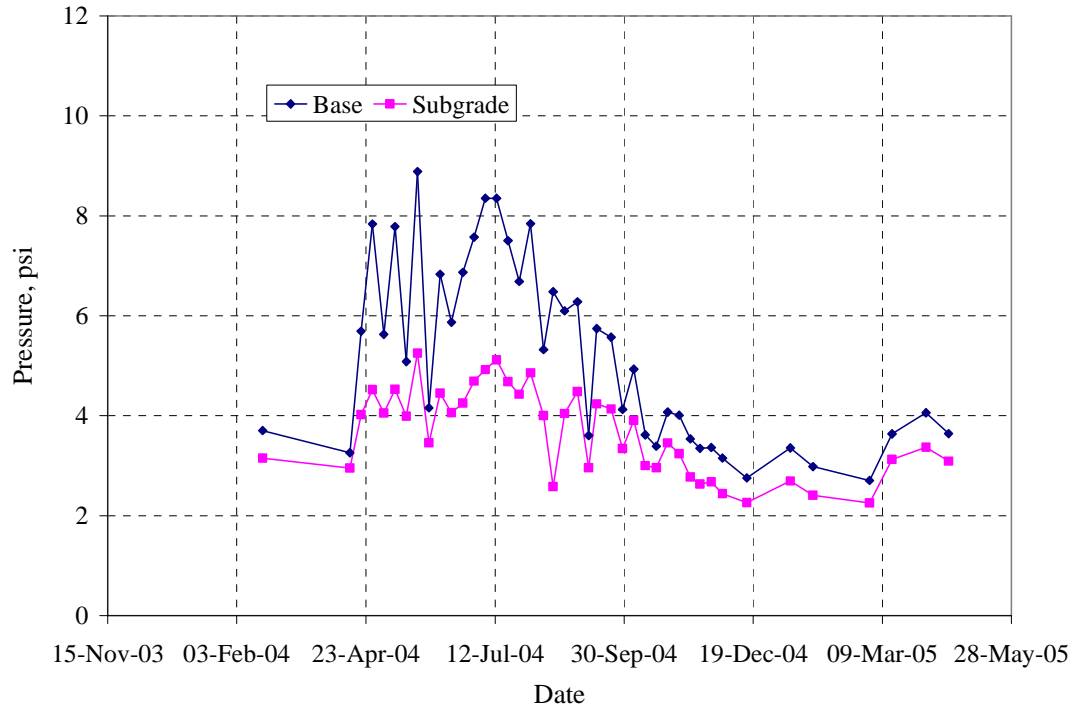


Figure 4.11 Trend of Base and Subgrade Pressures in Section N4-Box Trailer.

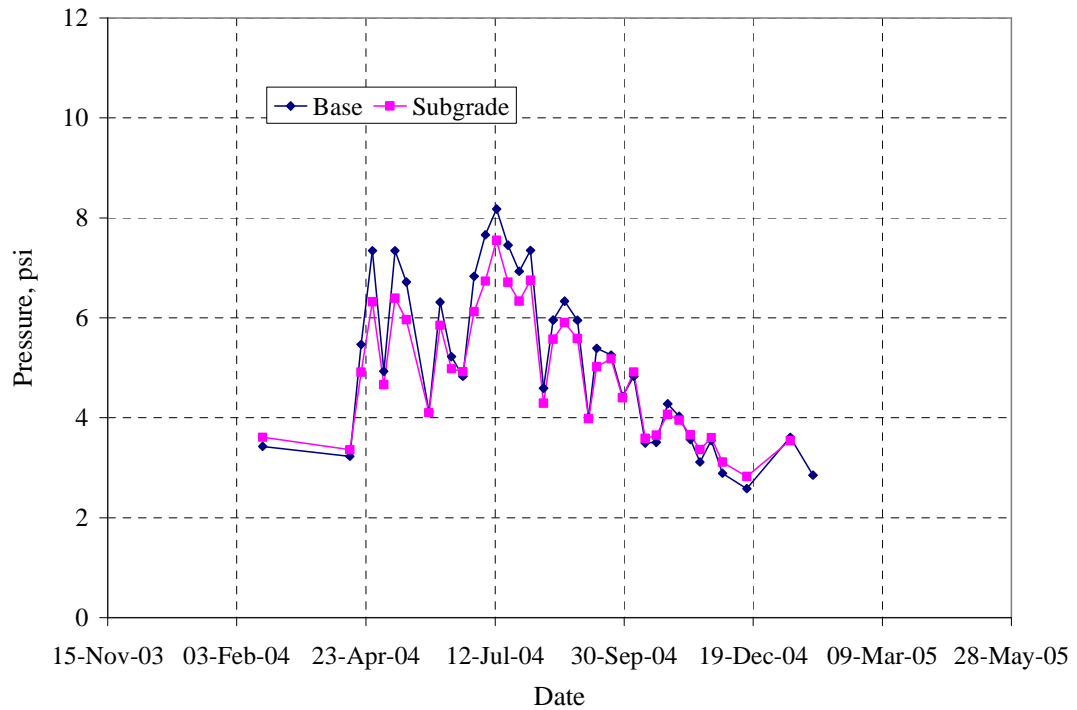


Figure 4.12 Trend of Base and Subgrade Pressures in Section N5-Box Trailer.

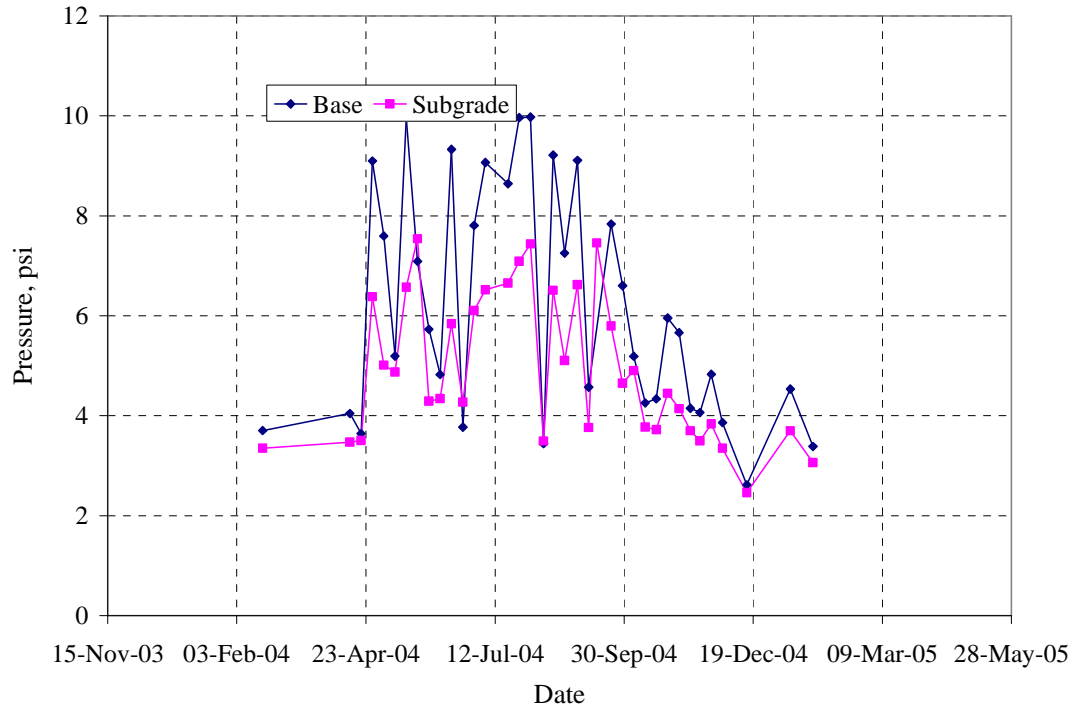


Figure 4.13 Trend of Base and Subgrade Pressures in Section N6-Box Trailer.

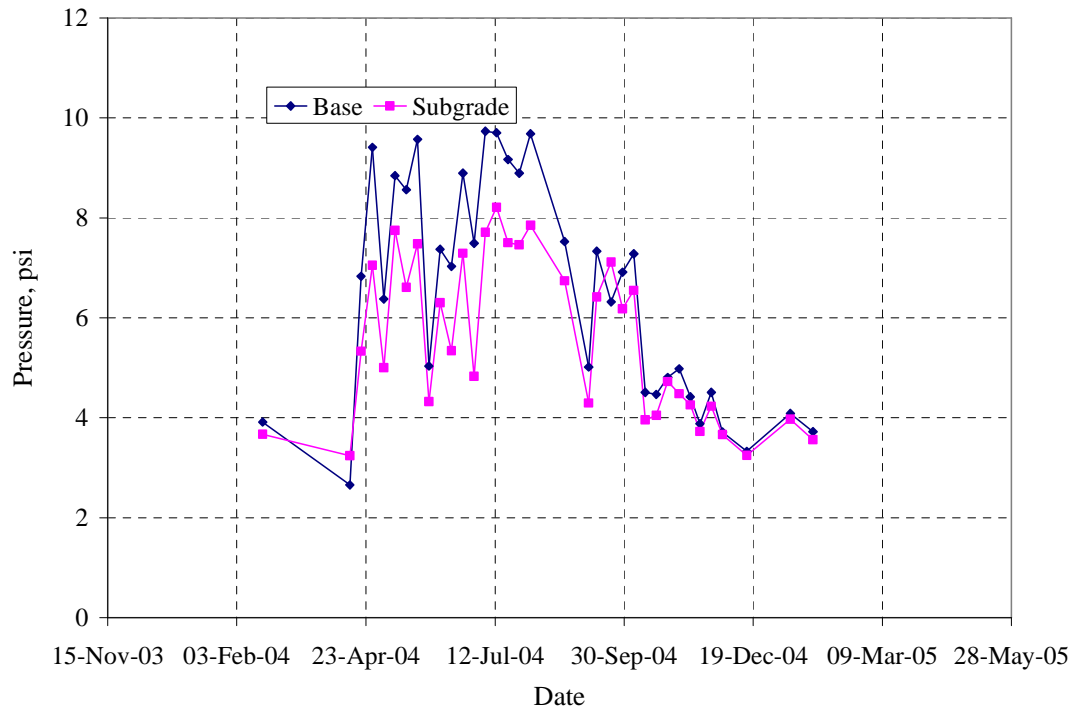


Figure 4.14 Trend of Base and Subgrade Pressures in Section N7-Box Trailer.

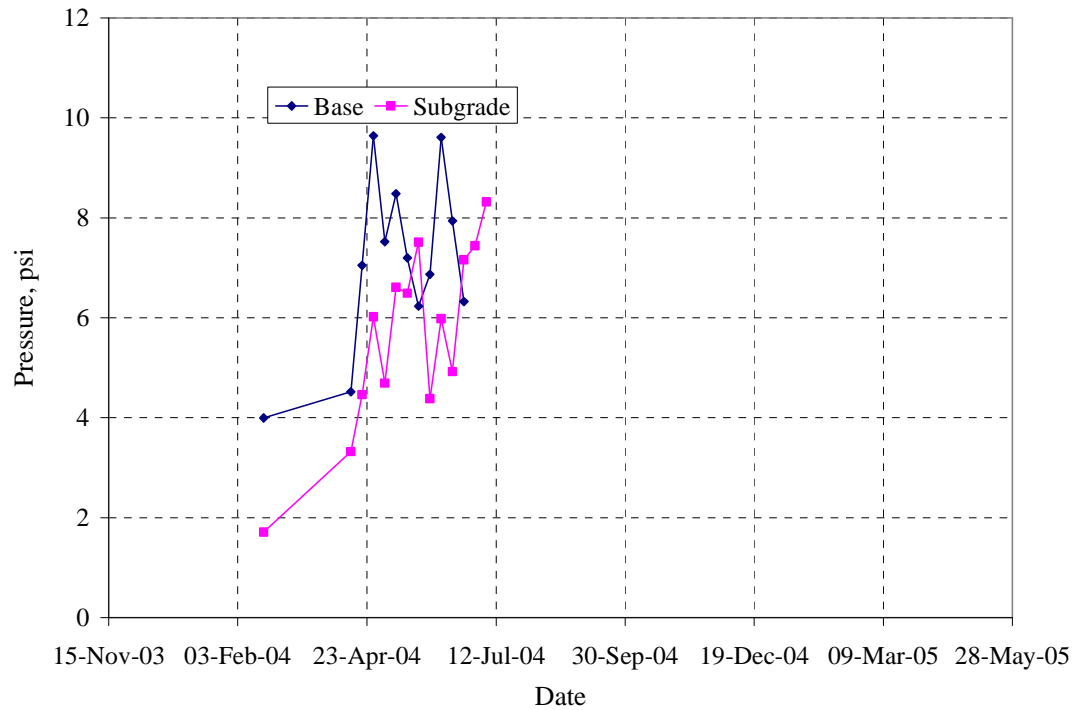


Figure 4.15 Trend of Base and Subgrade Pressures in Section N8-Box Trailer.

As expected, the base pressure was typically more than the subgrade pressure. Results showed that the percentage reduction in pressure between base and subgrade was approximately 30-45% in most of the test sections. All structural sections showed similar trends in pressure response. The fluctuations observed in Figures 4.2 to 4.15 between successive measurements in the same season for all test sections, were due to temperature variation at the time of testing, since data were collected at different time of the day in successive weeks. Therefore, it is important to include temperature as a primary factor in the pressure prediction model as will be explained later.

By using the maximum pressure value out of three truck passes in the analysis, the natural wheel wander effects were minimized. For triple trailer response, a maximum pressure value out of twelve passes was taken for analysis (4 triple trailers x 3 passes). For the box trailer, the maximum pressure out of three passes was considered in the analysis. A special study was conducted at the Test Track on October 13, 2004 to check the sufficiency of three truck passes in section N7. Ten passes of both triple and box trailer responses were captured from the field. Figures 4.16 and 4.17 show the base and subgrade pressure for different passes, respectively.

From the figures it was evident that the responses were fairly consistent with respect to number of passes. Within three passes the pressure variability was captured. Beyond three passes, no additional information was drawn from the data. From both figures, compared to other triple trailers, triple trailer 4 response was varying between passes which was observed during the whole duration of the Test Track cycle. This purely depended on the driving habits of the specific truck driver which was observed during the data collection from the field. This did not make any effect on the study since the maximum pressure response out of all four triple trailers was used in the study for analysis. As expected when the maximum pressure response was plotted against pass numbers (Figure 4.18), the pressure was consistent between passes and beyond three passes no additional information was drawn. This supported the decision of using the maximum response out of three truck passes.

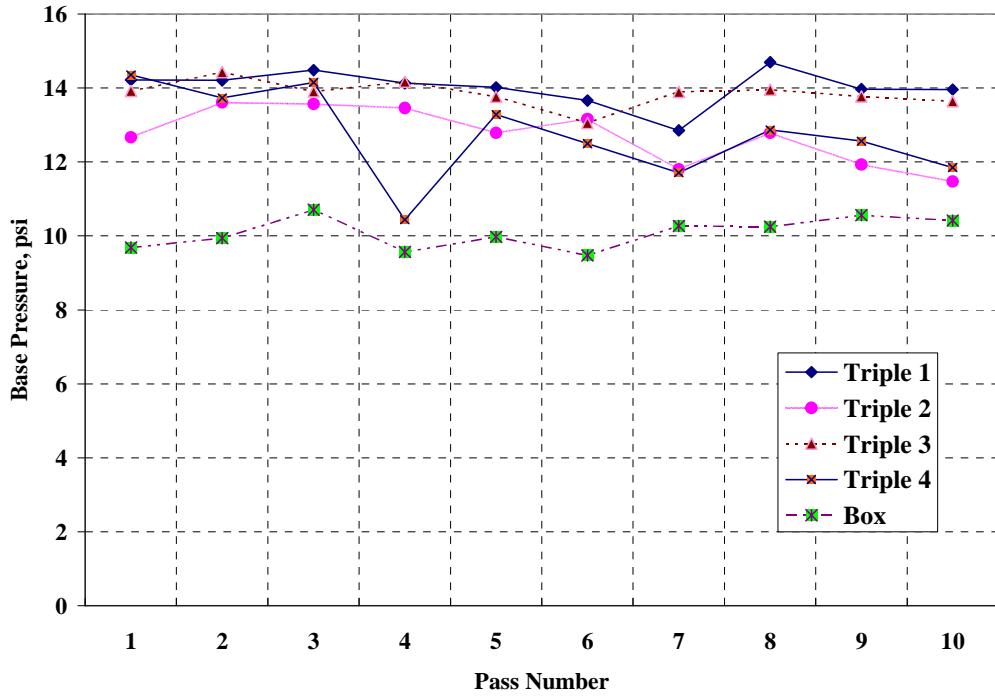


Figure 4.16 Base Pressure by Truck and Pass.

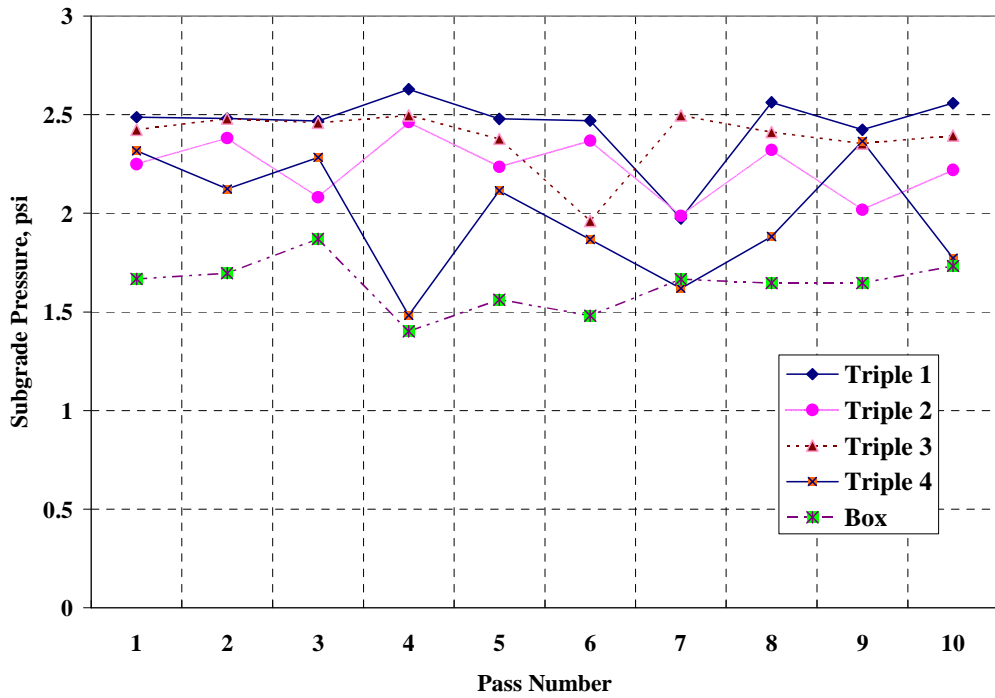


Figure 4.17 Subgrade Pressure by Truck and Pass.

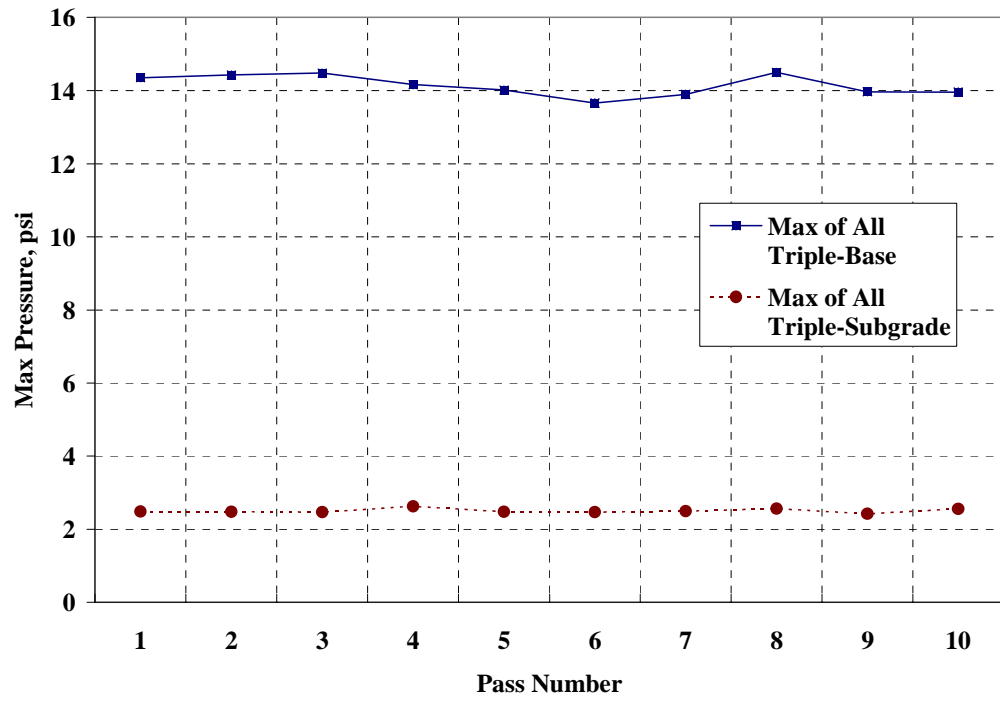


Figure 4.18 Maximum Base and Subgrade Pressure Response for Truck Pass.

4.3 PRESSURE PREDICTION MODEL

Collecting and processing high speed data from the Test Track is a voluminous work and it is impractical to collect data continuously throughout the day. However, the environmental data were available for every hour throughout the duration of the Test Track cycle. Therefore, an effort was made in this study to develop models that would predict the pavement response in terms of vertical pressure at any point of time of the day, by knowing the pavement temperature and thickness.

The base and subgrade pressures were plotted against pavement temperature at 2” from the surface. A good correlation was found between the measured temperature at 2” from the top of HMA surface and the measured pressures. In other related studies also (Gokhale et al., 2005; Kim et al., 2000) temperature measured at 2” gave a very good correlation with pavement response and performance.

Before choosing the 2” temperature, temperatures at different depths (surface, interpolated mid depth of HMA temperature, 4” from surface, and temperature at 10” from HMA top) were analyzed. However the pavement temperature measured at 2” from the HMA surface gave a good correlation with measured pressure values than temperatures measured at other locations in most of the test sections. So it was decided to use the temperature at 2” from the surface for pressure data related analysis. By using the collected pressure data from the Test Track, a pressure prediction model was developed using pressure as a function of temperature and HMA thickness. When thickness and temperature were included in the function for pressure prediction, a very good fit was observed for all sections rather than considering temperature alone.

Having separate models to predict pressures in each section would be advantageous and the model would be very accurate on a section by section basis. However, test sections N1, N2 and N8, failed very early during the test cycle, and there were not enough pressure data from those sections to build a pressure prediction model. In the Test Track, each test section had different HMA thicknesses and different binder modification. So, in order to accommodate sections N1, N2 and N8 in the study, it was decided to group modified, unmodified and stone matrix asphalt (SMA) sections separately. By doing so, the limited data from those test sections (N1, N2 and N8) were used in the model and the developed model helped to predict pressures in those test sections.

By grouping the sections, different HMA thicknesses were also brought into the pressure prediction equation to give a good fit between the measured and the predicted pressures. A preliminary mechanistic analysis was conducted to study the effects of varying HMA thickness on pressure response. The computed pressure values had a nonlinear relationship with HMA thickness as shown in Figure 4.19.

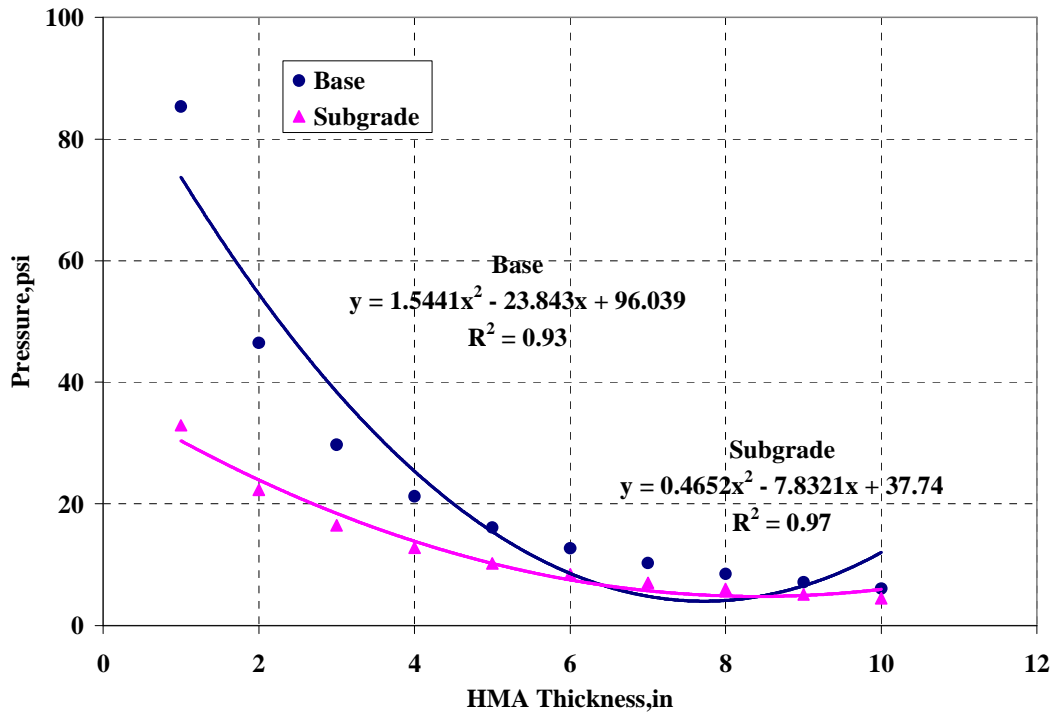


Figure 4.19 Example shows the HMA Thickness and Pressure Relation

As shown earlier in Figure 4.1, the pressure responses for varying temperature also suggested a non-linear relationship among the variables. So a non-linear least square regression equation was built by having pressure as a function of pavement temperature and HMA thickness. The basic form of the pressure prediction model was:

$$P_{base,subgrade} = K_0 + K_1 * T^2 + K_2 * T + K_3 * H^2 + K_4 * H \quad (4.1)$$

Where:

$P_{base,subgrade}$ = Vertical pressure over the top of base or subgrade, psi

H =HMA thickness, in

T = Pavement temperature at 2" from top of HMA, °F

K_0, K_1, K_2, K_3, K_4 = Regression constants

The preliminary model results are given in Tables 4.1 and 4.2.

Table 4.1 Pressure Prediction Model Coefficients for Triple Trailer Truck

Coefficients	Base Pressure			Subgrade Pressure		
	Unmodified	Modified	SMA	Unmodified	Modified	SMA
K ₀	31.2088	50.6896	10.320	13.2399	34.4752	4.7975
K ₁	-0.0003	0.0010	0.0011	0.0008	0.0007	0.0010
K ₂	0.1540	-0.0705	-0.0450	-0.0270	-0.0621	-0.0347
K ₃	0.5038	0.7616	0.1457	0.1032	0.4333	-0.4742
K ₄	-8.3668	-12.0968	-2.039	-2.2165	-7.3735	3.0303
R ²	0.88	0.88	0.80	0.93	0.90	0.95

Table 4.2 Pressure Prediction Model Coefficients for Box Trailer Truck

Coefficients	Base Pressure			Subgrade Pressure		
	Unmodified	Modified	SMA	Unmodified	Modified	SMA
K ₀	29.6513	50.8963	9.7870	13.3125	32.5737	4.4874
K ₁	0.0005	0.0016	0.0014	0.0007	0.0006	0.0013
K ₂	-0.0238	-0.1605	-0.1128	-0.0498	-0.0464	-0.1129
K ₃	0.4073	0.7129	0.4715	0.1123	0.4113	-0.2557
K ₄	-6.9187	-11.3306	-3.9148	-2.1636	-7.0256	1.9554
R ²	0.77	0.89	0.92	0.80	0.88	0.88

Statistical tests were conducted on the developed model and the p-value, t-ratio and ANOVA tables were built for each model. From the results, the model regression constants K₀, K₁, and K₃ were found to be highly significant (p-value <0.05). The p-values for K₂ and K₄ terms exceeded the significance level of 5%. So it was decided to remove those terms from the model. The final model results are given in Tables 4.3 and 4.4. The final pressure prediction model form was:

$$P_{base,subgrdae} = K_0 + K_1 * T^2 + K_3 * H^2 \quad (4.2)$$

Table 4.3 Final Pressure Model Coefficients for Triple Trailer

Coefficients	Base Pressure			Subgrade Pressure		
	Unmodified	Modified	SMA	Unmodified	Modified	SMA
K_0	3.380	2.749	1.282	4.211	3.860	14.198
K_1	6.34×10^{-4}	6.85×10^{-4}	7.14×10^{-4}	5.96×10^{-4}	3.44×10^{-4}	7.71×10^{-4}
K_3	-8.50×10^{-3}	-1.45×10^{-2}	0.00	-4.30×10^{-2}	-3.33×10^{-2}	-2.6×10^{-1}
R^2	0.86	0.74	0.70	0.92	0.77	0.95

Table 4.4 Final Pressure Model Coefficients for Box Trailer

Coefficients	Base Pressure			Subgrade Pressure		
	Unmodified	Modified	SMA	Unmodified	Modified	SMA
K_0	2.704	0.625	1.143	2.933	3.404	7.413
K_1	6.42×10^{-4}	5.96×10^{-4}	7.14×10^{-4}	3.86×10^{-4}	3.62×10^{-4}	5.64×10^{-4}
K_3	-1.84×10^{-2}	0.00	0.00	-2.34×10^{-2}	-2.90×10^{-2}	-1.3×10^{-1}
R^2	0.81	0.87	0.78	0.78	0.88	0.86

The model coefficients tabulated above for both triple and box trailers had a p-value less than 0.05. This showed that the probability of the model parameters reaching the value of zero is less than 5%. The complete statistical output for all models shown in Table 4.3 and 4.4 is given in Appendix A.

In SMA sections (sections N7 & N8), the K_3 term did not play a significant role in the base pressure prediction. This was expected since the in-situ HMA thickness in those two sections did not vary much and the pressure values also did not change significantly between them.

The measured pressure value was less for modified sections when compared to the unmodified sections at a same temperature and HMA thickness. To explain this, in the model, a temperature value of 70⁰F and a HMA thickness of 6” were assumed. For this case, the model for modified binder sections showed a base pressure value of 5.58 psi for triple trailer loading; whereas the unmodified binder sections had a base pressure of

6.18 psi. This behavior was also an expected one, considering the difference in performance between modified and unmodified binder sections as explained in the next chapter.

With the help of the models given in Tables 4.3 and 4.4, by knowing the temperature and thickness of the section, one can predict the base and subgrade pressures accurately. When the model-derived pressure values were plotted against the field pressure data, a good fit was observed ($R^2 = 0.70$ to 0.95) for all sections. The pressure prediction coefficients for triple and box trailers were different. This behavior was expected since both trucks have different load configuration and magnitude. From these models, for a given temperature and HMA thickness, the pavement pressure responses can be predicted with reasonable accuracy at any point of time of a day.

Figures 4.20 to 4.25 depict the relation between the measured pressures from the Test Track and the model predicted pressures for modified, unmodified and SMA test sections and for both truck types.

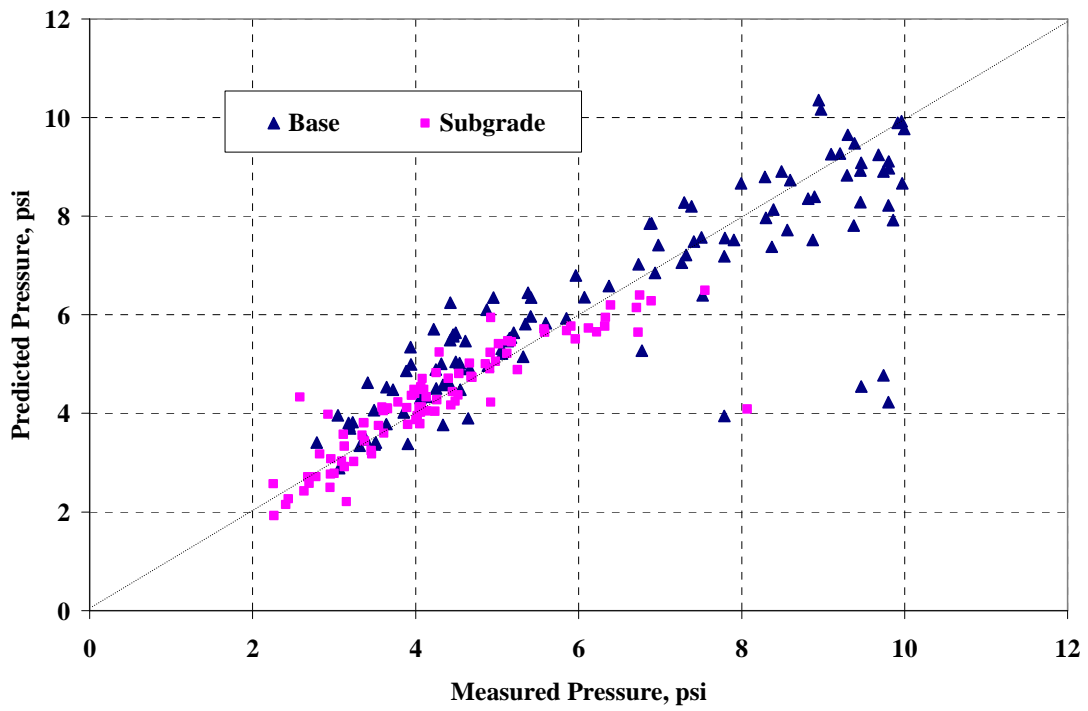


Figure 4.20 Measured and Predicted Pressures - Modified binder Sections (Triple).

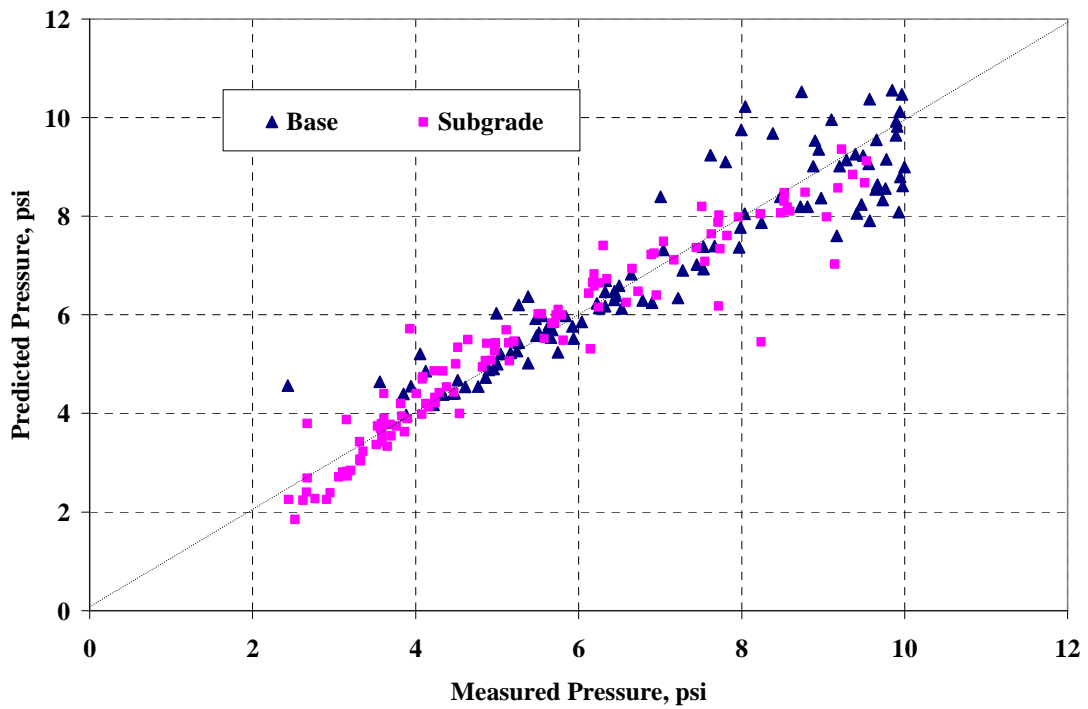


Figure 4.21 Measured and Predicted Pressures - Unmodified Test Sections (Triple).

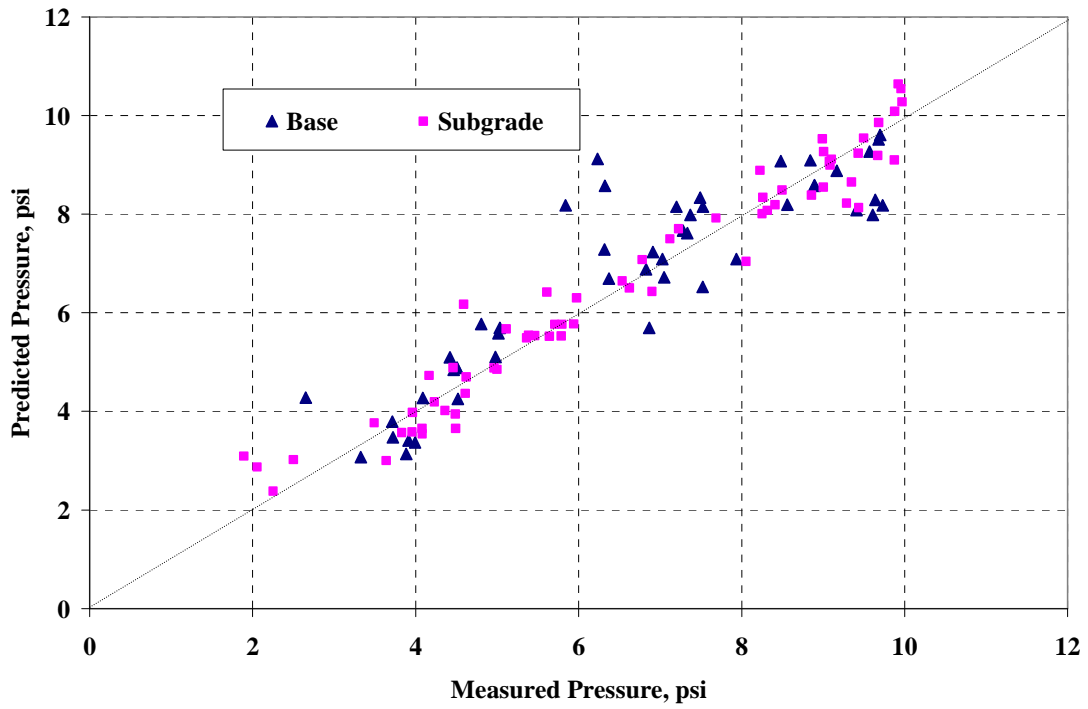


Figure 4.22 Measured and Model Predicted Pressures - SMA Test Sections (Triple).

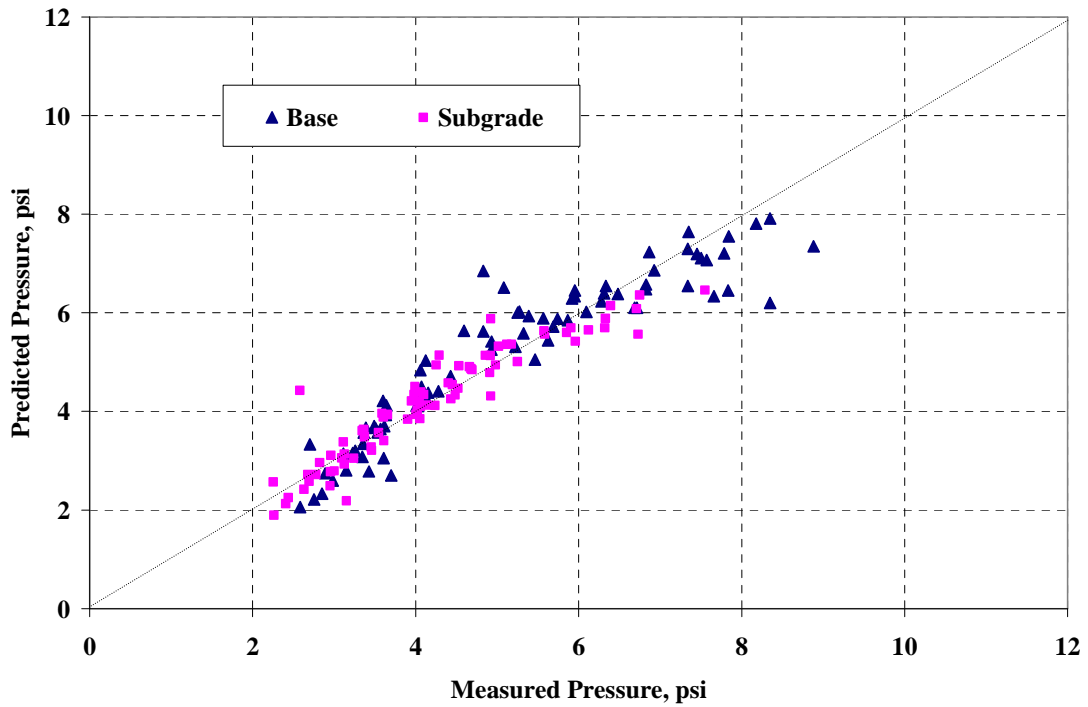


Figure 4.23 Measured and Predicted Pressures – Modified Test Sections (Box).

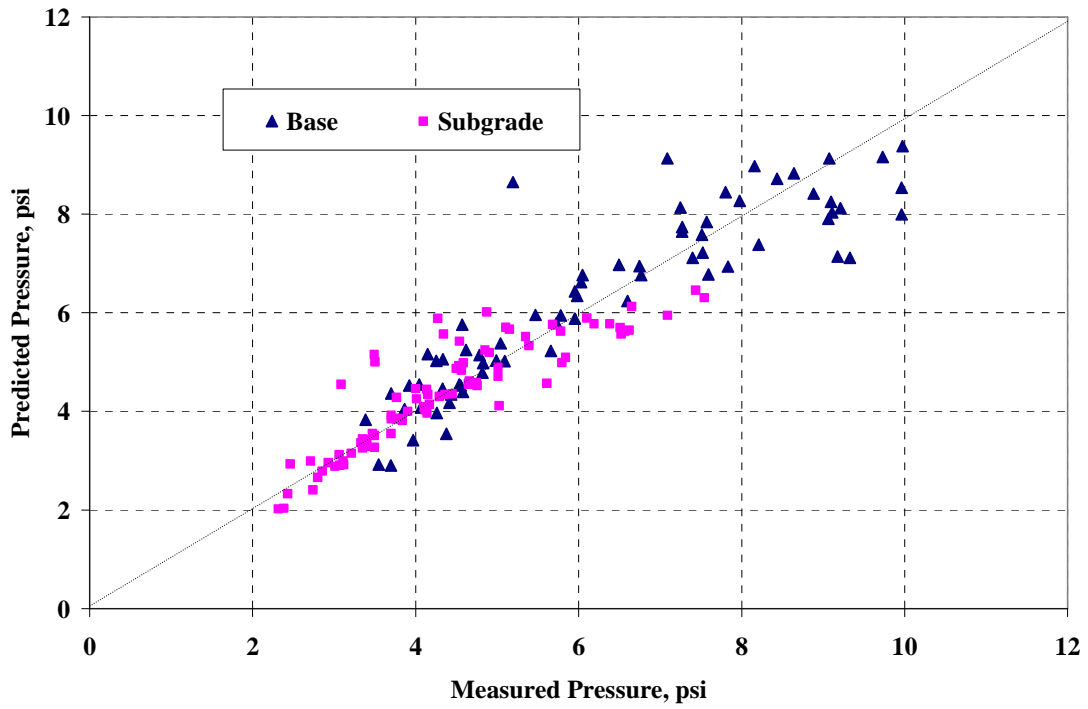


Figure 4.24 Measured and Predicted Pressures - Unmodified Test Sections (Box).

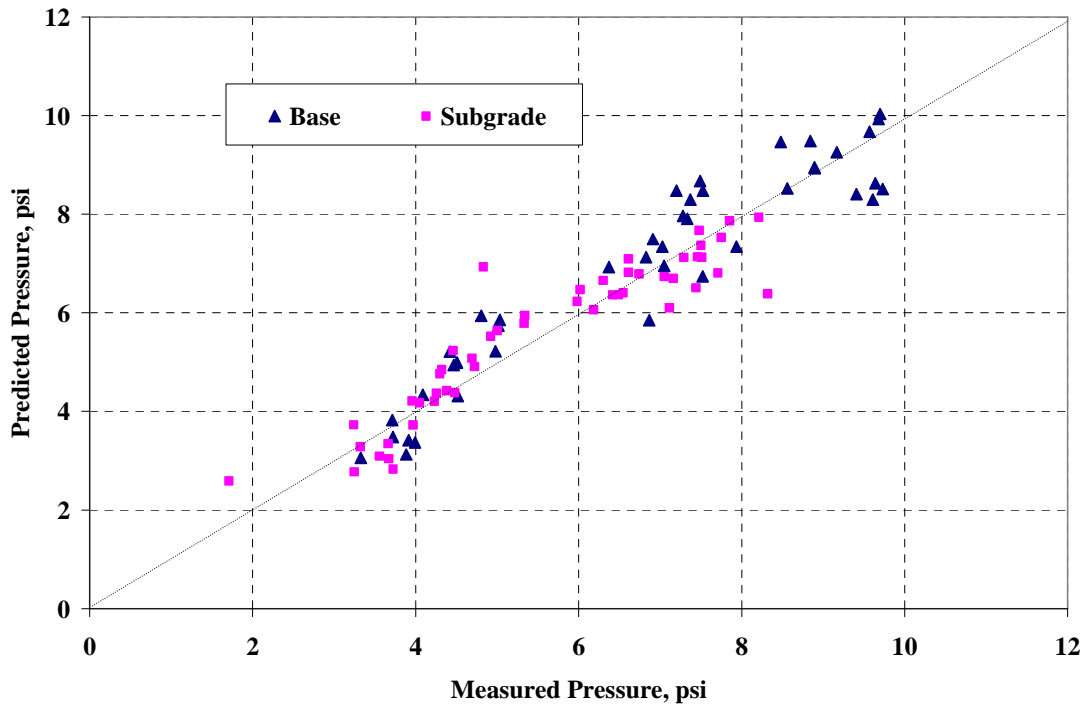


Figure 4.25 Measured and Predicted Pressures - SMA Test Sections (Box).

4.4 THEORETICAL PRESSURE CALCULATION

4.4.1 Material Characterization

Central to the main objectives of the structural study is the accurate characterization of material properties. For example, the validation of a mechanistic pavement model requires accurate material properties as inputs to the model. Regardless of the pavement design approach, it is important to characterize relevant material properties as they have a direct impact on the mechanistic pavement response of component pavement layers (Timm et al., 2006).

4.4.2 Selection of Pavement Cross Section

As mentioned in the previous chapter, FWD tests were conducted periodically at three random locations per test section to measure the material properties (layer modulus). The pavement layer modulus values were backcalculated from the deflection data obtained from FWD testing. During the backcalculation procedure, different pavement cross sections were investigated and the finally selected cross section for back calculation is shown in Figure 4.26.

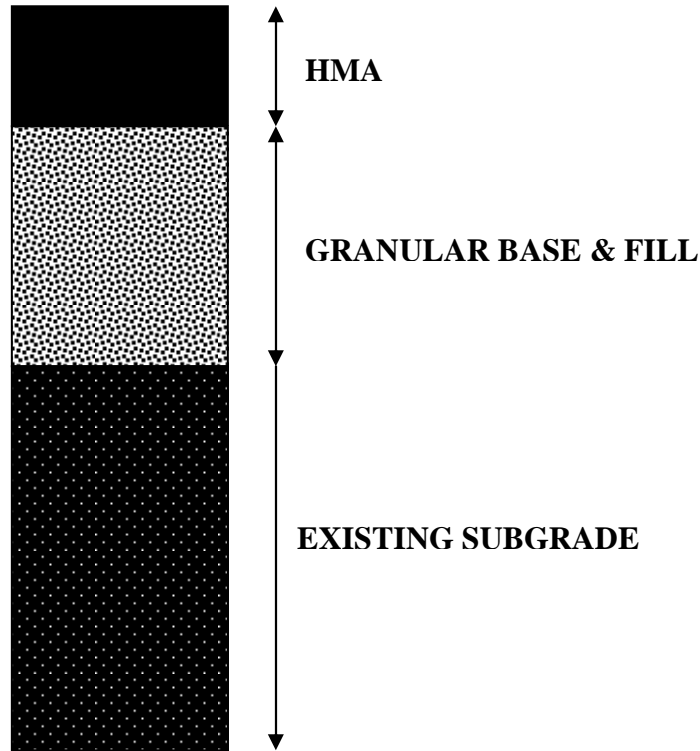


Figure 4.26 Pavement Cross Section for Backcalculation

To check the validity of the selected cross section, on April 2004, FWD testing was conducted on top of the instrumentation array in all test sections. The collected pavement responses were compared with the theoretical pavement responses. For theoretical pavement responses the backcalculated modulus values from the selected cross sections were used. The good match between predicted and measured responses in terms of vertical pressure and strain confirmed the validity of the selected cross section. The selected cross section produced lowest percentage of error (lowest RMS error), most repeatable and also the backcalculated modulus values matched well with laboratory test results. The results are documented elsewhere (Timm and Priest, 2006).

4.4.3 HMA Modulus Characterization

It is important to link the material properties to their mechanistic response whenever the loadings are applied on the pavement. Like pressure, HMA modulus also has a very good correlation with temperature. After examining modulus-temperature relationships representing temperatures obtained from various depths in the structure, the best correlation was found between the HMA modulus and the temperature measured at 2” below the pavement surface. The modulus data reported in this study were the backcalculated average modulus values of both inside and outside wheel paths at the three random locations in each test section.

The backcalculated HMA moduli were plotted versus HMA temperature to establish modulus-temperature relationships for section-specific HMA moduli according to:

$$E = C_1 e^{C_2 T} \quad (4.3)$$

Where:

E= HMA modulus, psi

T = Temperature at 2” from top of HMA, °F

C₁, C₂ = Regression coefficients

From the above equation, the HMA modulus can be found given the temperature at any time of the day. The HMA was most affected by seasonal changes, which was expected since it is well known that HMA modulus has a strong dependence upon temperature. Figure 4.27 shows the HMA modulus values for varying pavement temperatures.

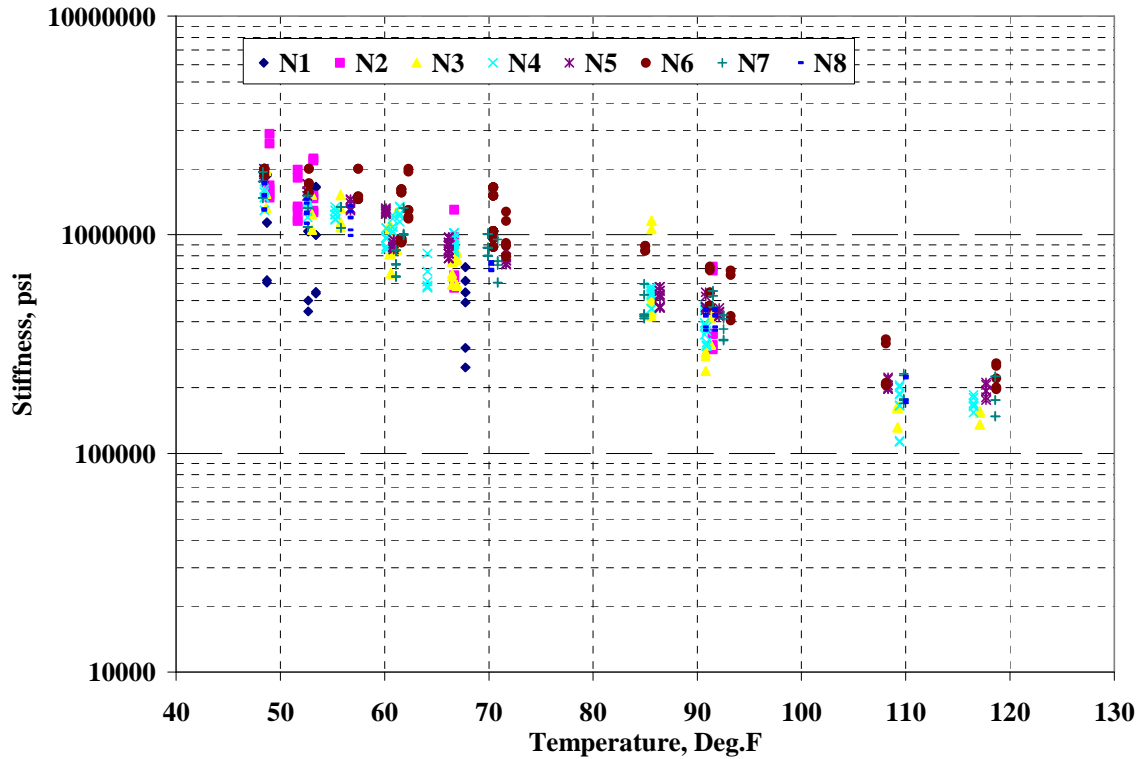


Figure 4.27 HMA Modulus vs. Temperature Relationship.

It is to be noted that sections N1 and N2 had limited pre-cracking backcalculated data with a small temperature range because the sections started showing signs of distress in early March and June 2004, respectively. However extrapolation was carried out since the trend in modulus for varying temperature was similar to other test sections. The model coefficients (C_1 , C_2) for all test sections are given in Table 4.5. The model statistics such as t-ratio, p-value and R^2 were also given in the table. As expected the temperature was negatively correlated to HMA modulus.

Table 4.5 HMA Modulus Prediction Model Coefficients

Test Section	C ₁			C ₂			R ²
	Value	t-ratio	p-value	Value	t-ratio	p-value	
N1	11.95x10 ⁶	0.98	0.33	-0.0466	-2.40	0.02	0.30
N2	14.08x10 ⁶	2.15	0.04	-0.0414	-4.73	0.00	0.66
N3	7.77x10 ⁶	6.73	0.00	-0.0346	-14.28	0.00	0.73
N4	7.04 x10 ⁶	11.97	0.00	-0.0315	-23.19	0.00	0.89
N5	10.51 x10 ⁶	12.54	0.00	-0.0371	-28.73	0.00	0.92
N6	7.23 x10 ⁶	7.66	0.00	-0.0270	-13.12	0.00	0.72
N7	6.50 x10 ⁶	9.36	0.00	-0.0302	-17.77	0.00	0.80
N8	6.60 x10 ⁶	10.82	0.00	-0.0309	-18.80	0.00	0.95

Similar correlation between HMA temperature and modulus were found from the MnRoad research project. In their study, the temperature at 1/3 HMA depth were strongly correlated to the modulus (Alvarez and Thompson, 1998). The backcalculated HMA modulus and temperature relationship developed to calibrate fatigue transfer functions from the NCAT Test Track data also had a same trend and similar to the one given in equation 4.3. In that study, the HMA mid-depth temperature was strongly related to the HMA modulus (Priest, 2005; Priest and Timm, 2006).

From Table 4.5, it is clear that the model coefficients C_1 and C_2 were highly significant with a p-value less than 0.05 with the exception of section N1. It is to be noted that section N1 had very low HMA modulus at higher temperature ranges with poor R^2 ($R^2 = 0.30$). A few factors were believed to be a reason for this observation. The first factor was the presence of distress in the test section. The fatigue cracking was observed in this section with pumping of fines on April 8, 2004. Though the cracking cut-off date was March 22, 2004, the cracks that were not clearly visible in the section could have contributed to higher moduli variability. Another reason being, that the test section itself might have been built with greater variation. Finally, the limited amount of pre-cracked FWD data from the section with small range of temperature (maximum temperature of 67⁰F and minimum temperature of 48⁰F) could also have resulted in this variation.

Tables 4.6 and 4.7 tabulate the HMA modulus values used in the mechanistic analysis for varying temperatures.

Table 4.6 Backcalculated Modulus Values for Modified Binder Sections

Temp, F	Section Specific HMA Modulus, ksi		
	N1	N4	N5
30	2956.314	2740.80	3458.51
40	1855.665	2000.92	2387.46
50	1164.793	1460.77	1648.09
60	731.1353	1066.43	1137.70
70	458.9304	778.54	785.37
80	288.0686	568.37	542.15
90	180.8194	414.94	374.25
100	113.4995	302.93	258.35
110	71.24314	221.15	178.34
120	44.719	161.45	123.11

Table 4.7 Backcalculated Modulus Values for Unmodified & SMA Binder Sections

Temp, F	Section Specific HMA Modulus, ksi				
	N2	N3	N6	N7	N8
30	4065.43	2753.54	3221.57	2632.43	2616.42
40	2686.86	1948.03	2460.05	1947.14	1921.48
50	1775.76	1378.16	1878.54	1440.25	1411.12
60	1173.61	975.00	1434.48	1065.32	1036.32
70	775.64	689.77	1095.40	787.99	761.07
80	512.63	487.99	836.47	582.85	558.92
90	338.80	345.24	638.74	431.12	410.47
100	223.91	244.24	487.75	318.89	301.45
110	147.99	172.79	372.46	235.88	221.38
120	97.80	122.24	284.42	174.47	162.58

4.4.4 Base Modulus

From all three random locations within a test section, the backcalculated average base modulus was considered as shown in Figure 4.28 with error bars indicating \pm one standard deviation.

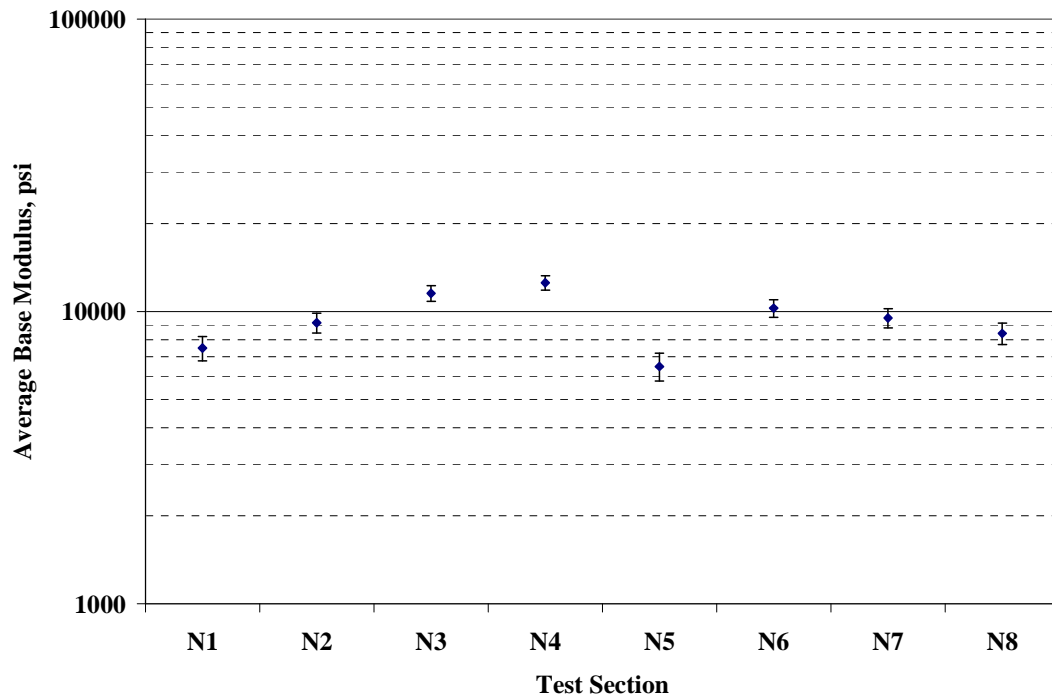


Figure 4.28 Backcalculated Average Base Modulus by Section.

An ANOVA test was conducted to compare the base modulus with other section modulus at a confidence level of 95% to study the differences in base modulus between test sections. The null hypothesis that all section modulus were equivalent was rejected (F-statistic = 71.57, p-value = 0.00). This shows that the modulus values between different sections were statistically significantly different. Considering this, it was decided to use the section specific base modulus in this study. Though the reasons for

this variability between the sections were not known, it was believed that the variability resulted from natural spatial variation between test sections.

The section specific base modulus values used in the mechanistic analysis are given in Figure 4.29.

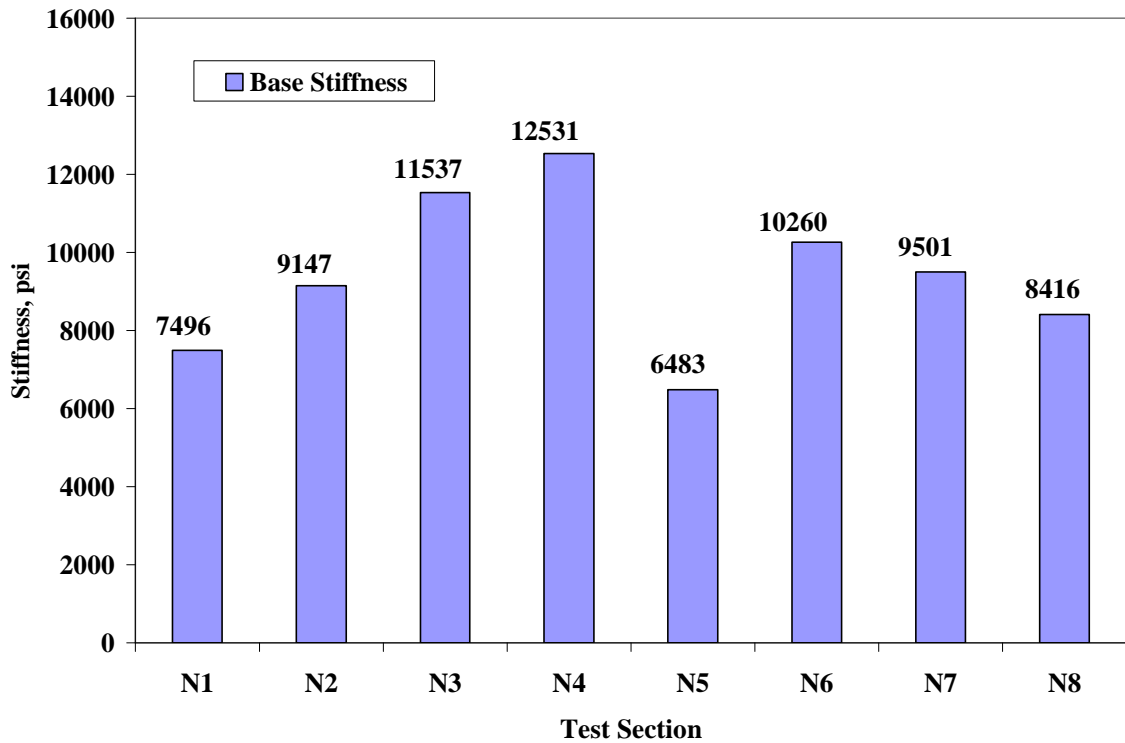


Figure 4.29 Backcalculated Base Modulus Values Used in Mechanistic Analysis.

It should be noted that the base modulus was lower than expected, but an extensive laboratory and field study utilizing triaxial resilient modulus and FWD testing on top of embedded instrumentation demonstrated that the values were reasonable. The laboratory and field study results are documented elsewhere (Timm and Priest, 2006). As expected, the HMA thickness played a significant role in defining the base modulus values through confinement, as observed by the trend in the base modulus with respect to HMA thickness in the test sections.

4.4.5 Subgrade Modulus

The backcalculated average subgrade modulus along with error bars, indicating \pm one standard deviation, in each section is given in Figure 4.30.

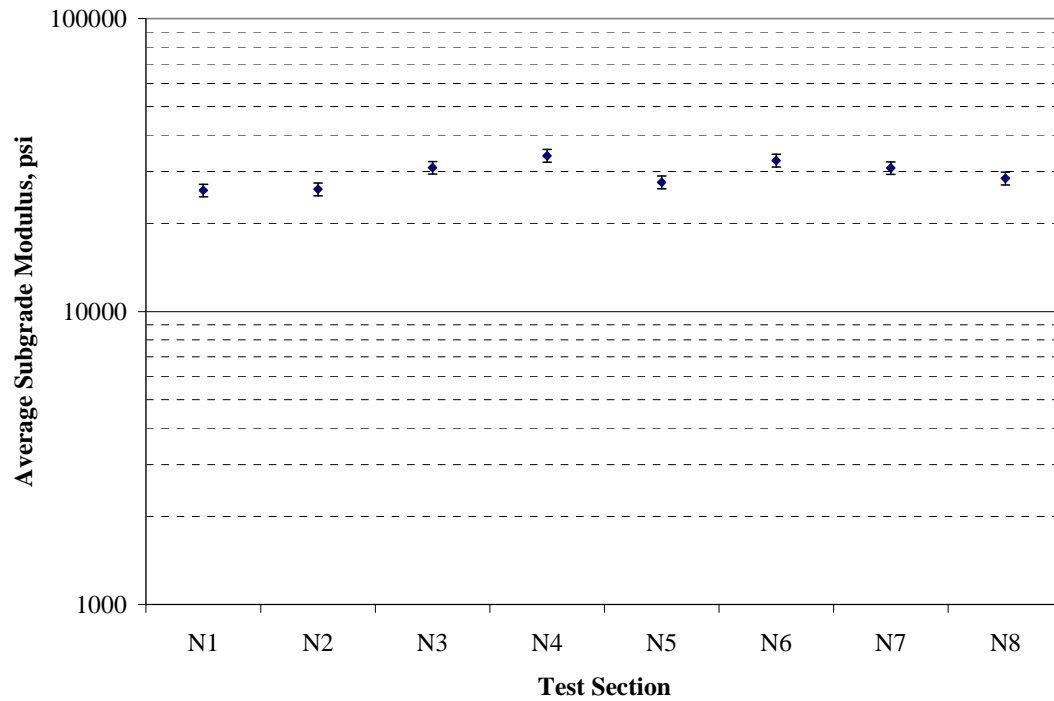


Figure 4.30 Backcalculated Average Subgrade Modulus by Section.

From Figure 4.30, there seems to be no clear distinctions in moduli between tests sections. The average subgrade modulus between test sections varied between 25830 psi to 33987 psi; where the average of all section moduli was found to be 30000 psi. The subgrade moduli did not show large differences due to seasonal variation and it maintained a modulus near 30,000 psi throughout the two-year research cycle in all test sections. The small differences between sections were attributed to natural spatial variability, not necessarily depend upon particular pavement parameters.

For a statistical check, ANOVA test was conducted to compare the subgrade modulus of all test sections at a confidence level of 95% to determine if there are any differences between the test sections. The null hypothesis that all section average moduli were equivalent was rejected (F-statistic = 52.83, p-value = 0.00). This shows that the subgrade modulus between different sections were different.

However, there was no appreciable practical difference in the mechanistic pavement response values when a subgrade modulus of 30,000 psi was used instead of 26,000 psi or 34,000 psi. This is explained by Figures 4.31 and 4.32. Here base and subgrade pressures were computed, using WESLEA, with different subgrade moduli at a constant HMA (700 ksi at 70⁰F) and base moduli (10ksi) for three different HMA thicknesses (5", 7" and 9"). The steer axle was assumed with an axle load of 10,000 lb with a tire pressure of 100 psi.

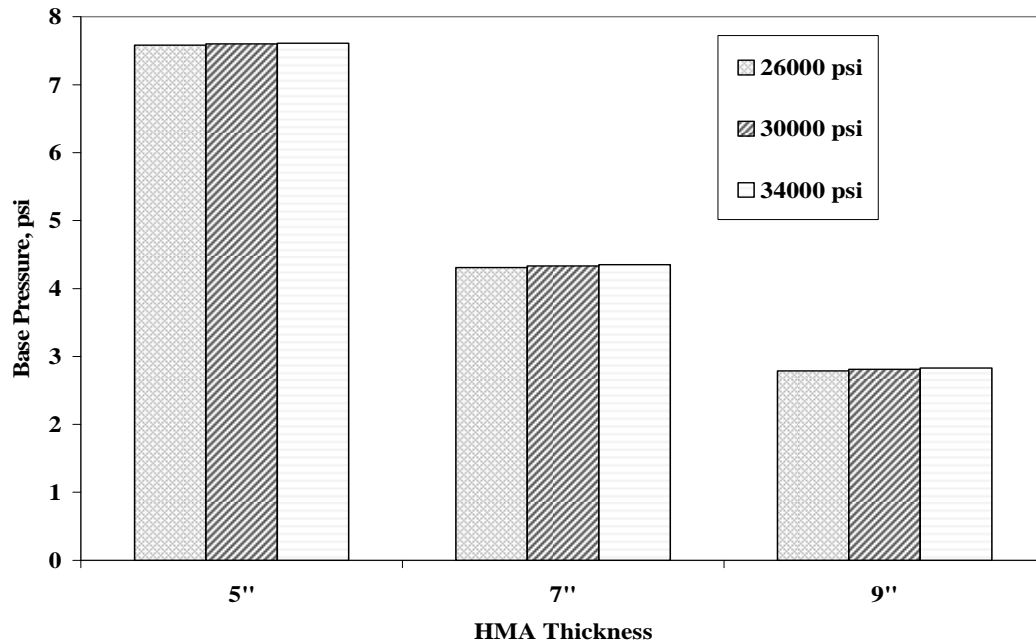


Figure 4.31 Computed Base Pressure for Varying Subgrade Moduli.

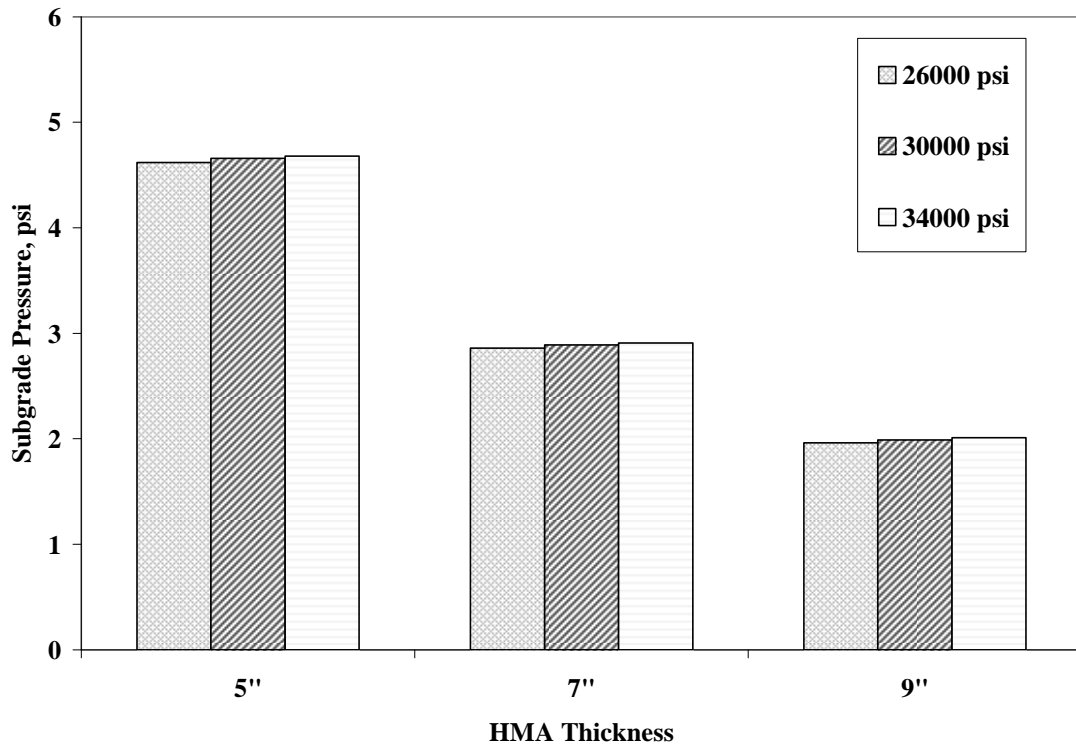


Figure 4.32 Computed Subgrade Pressure for Varying Subgrade Moduli.

From an engineering standpoint there was not any appreciable practical difference in the mechanistic response of pavement layers when the subgrade modulus was varied between 26,000 psi to 34,000 psi. Therefore, it was decided to use all section average subgrade moduli of 30,686 psi in this study for the computation of pavement response in terms of vertical pressure.

4.4.6 Pressure Computation

To validate load response model, theoretically calculated layered elastic responses need to be compared with measured pressures from the field. For that purpose, theoretical pressures have to be calculated first. For theoretical pressure calculation, a layered elastic analysis software package 'WESLEA' (**W**aterways **E**xperiment **S**tation **L**ayered **E**lastic **A**nalysis) was used. The modulus values that were presented earlier were used as material inputs. The typical Poisson ratio values of 0.35, 0.40 and 0.45 were used for HMA, base and subgrade materials, respectively (Timm et al., 1998).

The HMA modulus values in Tables 4.4 and 4.5 were used to calculate theoretical pressure in the pavement while using the layered elastic software package as will be explained below. To have a broad range of pavement temperature which can represent the Test Track temperatures over the 2-year period, temperatures were considered from 30°F to 120°F at 10 degree increments while computing the pavement response.

The WESLEA simulations were run for different truck axles (steer, tandem and single) and for test track configuration. In the 2003 Test Track cycle, exact locations of each axle were not able to be tracked, since there was no facility to point out the exact location of each axle in a truck with respect to the instrumentation array. As a result, an average of a single truck response was considered in the study instead of individual axle response. It is believed that installation of advanced facilities such as non-contact laser to track the axle location, installing axle sensing trips in each section before and after the instrumentation array would be a ideal solution to find out the truck axle location on the pavement. To account for different axles in a truck, the average pressure value for a truck pass (σ_{avg}) was calculated by:

$$\overline{\sigma}_{avg} = \frac{\sigma_{st}n_{st} + \sigma_t n_t + \sigma_s n_s}{N_T} \quad (4.4)$$

Where:

$\sigma_{st}, \sigma_t, \sigma_s$ = Calculated pressures (base, subgrade) for steer, tandem and single axles, respectively

n_{st}, n_t, n_s = Number of steer, tandem and single axles in a truck, respectively

N_T = Total number of axles = $n_{st} + n_t + n_s$

4.5 VALIDATION OF LAYERED ELASTIC RESPONSE MODEL

The theoretically-calculated pressure values were plotted against the measured pressures from the Test Track in Figures 4.33 and 4.34 corresponding to the triple and box trailer vehicles, respectively for a wide range of temperatures. The figures include all the data from each of the test sections collected before cracking was observed in each test section.

From the figures given below, it is quite clear that both theoretical and measured pressures are close to each other. Since these values are reasonably close to each other, it can be claimed that layered elastic analysis can be used to predict stresses in pavement layers within 2 psi difference in most cases. However when the pavement temperatures increased more than 100°F or the pressure value is more than 12 psi in base and about 7 psi in subgrade, the deviation between measured and predicted pressure value increased. Similar observations were found from the MnRoad study (Chadbourn et al., 1997), Virginia smart road study (Al-Qadi et al., 2004), and the study conducted at NCAT with FWD loading (Barrett and Timm, 2005).

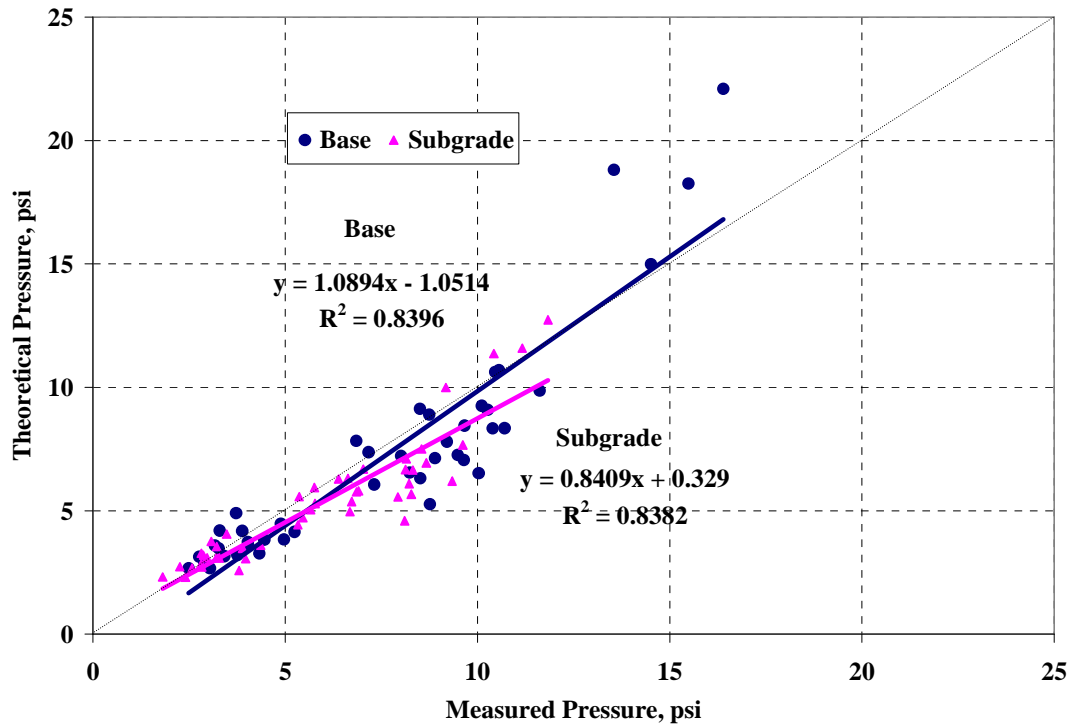


Figure 4.33 Measured and Theoretical Pressure Comparison for Triple Trailer.

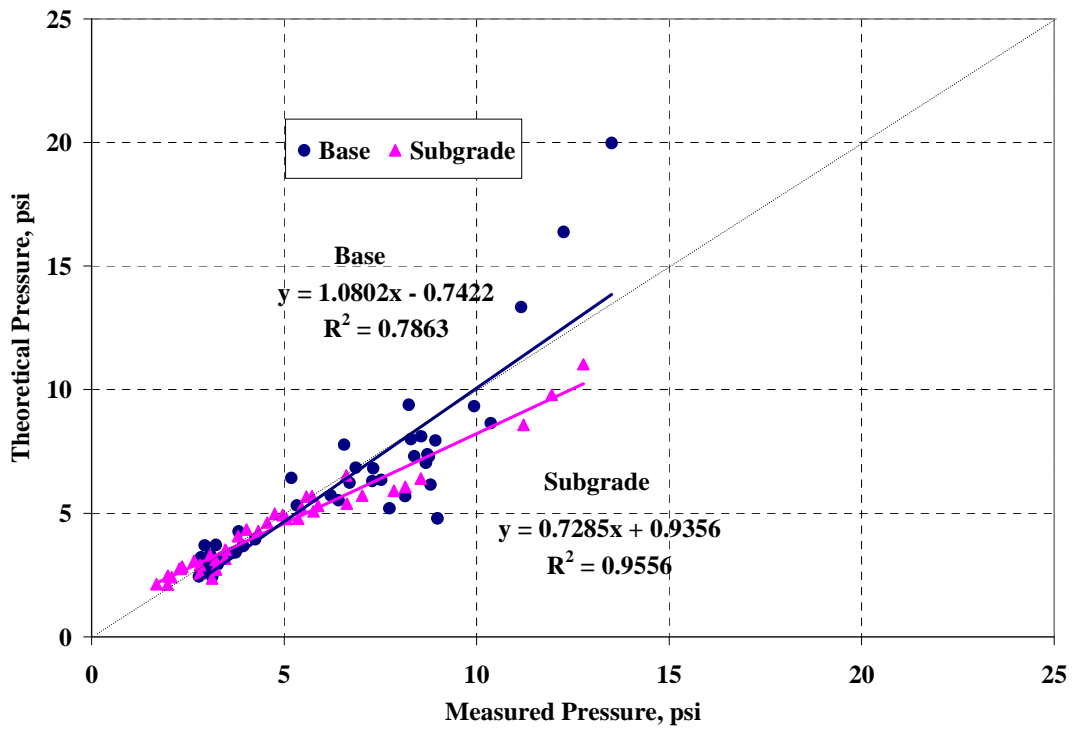


Figure 4.34 Measured and Theoretical Pressure Comparison for Box Truck.

4.6 SUMMARY AND CONCLUSION

The collected dynamic pavement response in terms of vertical pressure, collected over the period of two years was validated. Then a pressure prediction model was built to predict vertical pressure over the top of base and subgrade layers at any point of time, given the temperature and HMA thickness. With the help of backcalculated material properties, the theoretical pavement response was computed using the layer elastic analysis package 'WESLEA'. The predicted pressure and theoretical pressure responses were compared for a long range of temperature and the theoretical load response model was validated.

From obtained results, it was concluded that layered elastic analysis is a reasonable approximation of actual pavement responses under dynamic wheel load up to certain pressure values. However, at higher pressures (more than 12 psi in the base and about 7 psi in subgrade) which are resulting from higher pavement temperatures, some deviations were observed between predicted and measured responses in this study.

To alleviate such problems, the need for an advanced model which can account for non-linearity of pavement materials at higher pressures to predict pavement responses is recommended. In general, the results from layered elastic back and forward-calculation compared well with measured pavement responses obtained from the NCAT Test Track data. Even for dynamic truck loading, the layered elastic method is suitable in predicting pavement responses for different environmental, loading conditions. So this model can be used to compute pavement responses with confidence.

CHAPTER 5

RUT PREDICTION MODEL DEVELOPMENT

5.1 BACKGROUND

Accurate prediction of pavement rutting under the actions of traffic load and changing environmental conditions are critical for an efficient pavement design. Typically, M-E design uses two different calibrated transfer functions for rutting and fatigue crack prediction, respectively. Historically, various mathematical equations and models were developed by researchers to predict pavement performance. These equations illustrated the effect of various factors on pavement performance. Their usefulness in practice might be limited by the scope of the data base used in model development and the assumptions made (Huang, 2004). Further, most of these models were developed from laboratory data and then calibrated to field conditions using shift factors.

Historically, two different approaches have been used to limit rutting in pavement layers. One approach limited the vertical compressive strain on top of the subgrade thereby reduced the rutting. Another approach limited the total accumulated permanent deformation on the pavement surface based on the permanent deformation of each individual layer (Huang, 2004; El-Basyouny et al., 2005).

Rutting normally occurs in three stages (primary, secondary and tertiary) and a comprehensive rut prediction model should be able to predict all three. However, at the tertiary stage, fatigue cracking (macro cracking) can sometimes precede rutting and there is no need to model the tertiary stage of rutting (Zhou et al., 2003). The present mechanistic-empirical pavement design guide (MEPDG) models only the secondary stage of rutting; the primary stage was extrapolated from the secondary stage.

While most rutting transfer functions have relied upon vertical strains to predict rutting, recent lab studies showed better correlation of shear strain along the edge of the tire to HMA rutting and indicated that the magnitude of shear strain is strongly related to permanent deformation accumulation. However the shear strain approach has not been brought to model form and calibrated with large data set to predict rutting (Long, 2001). Therefore, there is a need to further explore the ability of HMA shear strain to predict rut progression and compare with the conventional vertical strain approach. There is also a need to assess the capabilities of a vertical strain versus shear strain approach in the context of M-E design.

5.2 RUTTING PROGRESSION IN THE NCAT TEST TRACK

As discussed in Chapter 2, flexible pavement rutting is categorized in three stages namely, primary, secondary and tertiary stage. As of November 2005, both primary and secondary stages of rutting were observed in structural study sections and none of the sections had reached the tertiary stage. In the primary stage the rutting accumulated quite rapidly. Later, the progression rate decreased and reached a constant value in the secondary stage. The tertiary stage did not occur, even after the application of 10 million ESAL. It is expected that further load applications of another 10 million ESALs during the 2006 traffic cycle will increase rutting which may lead to tertiary stage.

Figure 5.1 shows the progression of measured rutting using dipstick profiler in the NCAT Test Track structural sections. After a certain period of loading, the rutting did not show any appreciable increase. A similar rut progression trend was also seen in the AASHO Road Test (HRB, 1962) as number of axle applications increased, the rutting rate decreased (Thompson, 1993).

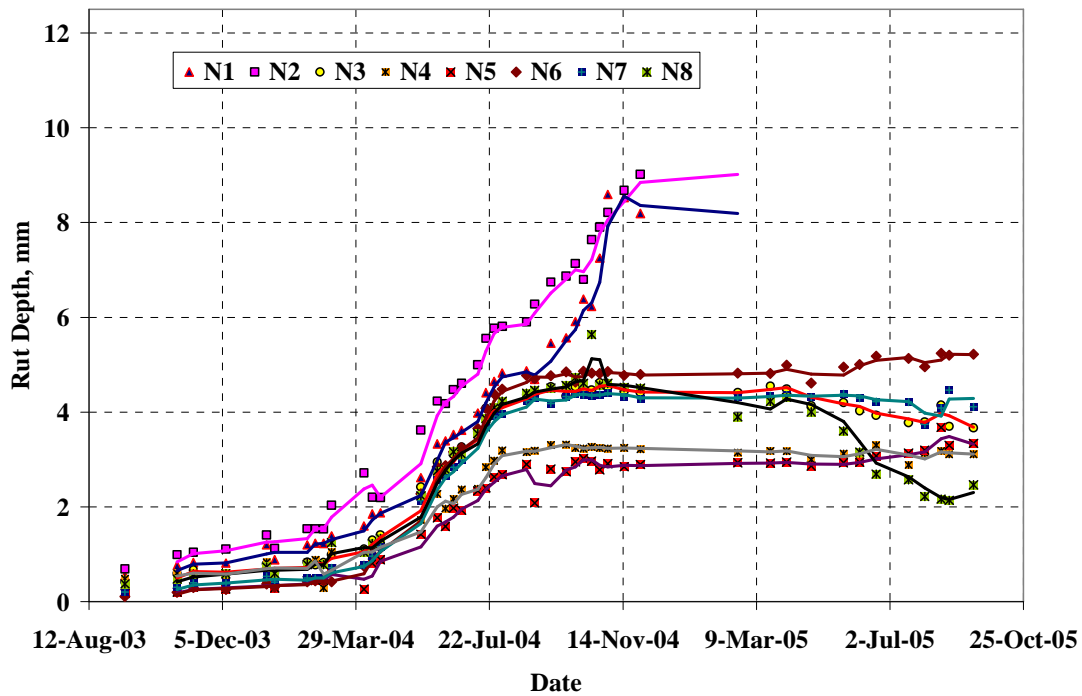


Figure 5.1 Rutting Progression in Structural Test Sections.

From the figure, it is clearly visible that for same number of load repetitions and thickness, the modified and unmodified binder sections performed differently in terms of rutting. Modified binder sections (N1, N4, and N5) have less rutting when compared to unmodified binder sections (N2, N3, N6, N7, and N8) for the same HMA thickness. Several research studies (Maccarrone et al., 1997; Immanuel, 2003; Immanuel, 2004) showed that modified binders exhibit better rutting performance even at higher pavement service temperatures.

It was observed from the thicker sections (7 and 9 in.) that the differences in measured rutting were not differentiated by HMA layer thickness, but by binder modification. For example, sections N4 and N5 have similar rut depths despite N4 having an HMA thickness 2 in. greater than N5. It should also be noted that all the

sections performed very well with respect to rutting, with the maximum below 10 mm. Further, section N8 deserves special mention. In the spring of 2005, a portion of N8 was milled and inlayed with new mix due to extensive fatigue cracking. However, data collection continued on the section and the apparent drop in rut depth was due to the surface repair.

Since the sections shown in Figure 5.1 were grouped primarily by binder modification with respect to rutting performance in the field, it was expected that the developed rut prediction model would also differentiate rutting between modified and unmodified sections.

5.3 MODEL METHODOLOGY: VERTICAL STRAIN BASED MODEL

One of the main objectives of this study was to build an M-E based rut prediction model. To achieve this, a conventional vertical strain approach similar to the one that is being used in the present MEPDG was developed to model the HMA rutting at the Test Track. The brief methodology is given in the form of flow chart in Figure 5.2.

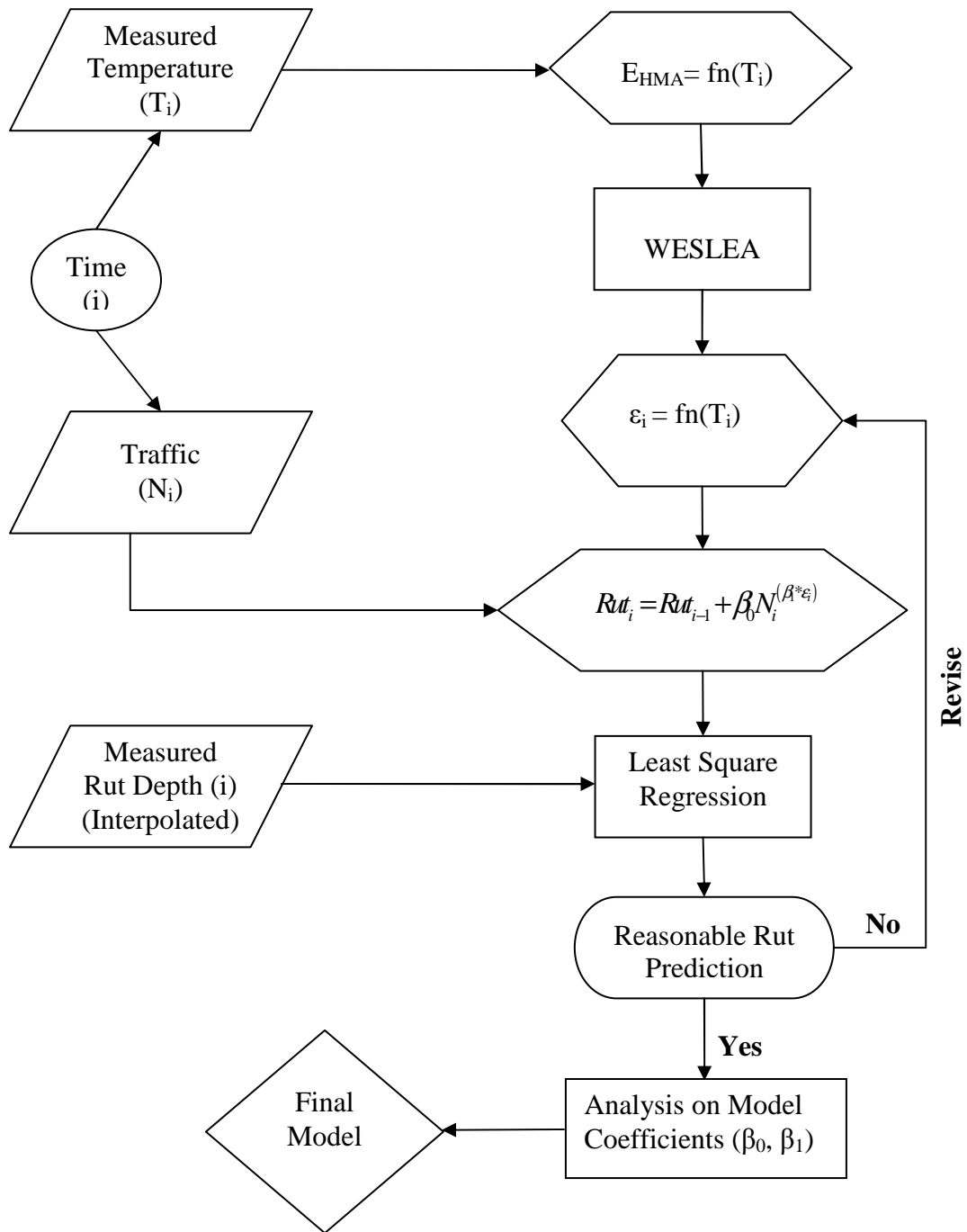


Figure 5.2 Vertical Strain Based Rut Prediction Methodology Flow Chart.

Here, the time stamp (i) is used to link variables such as measured temperature (T_i) and traffic (N_i) for a particular period. The measured pavement temperature plays a vital role in establishing the HMA modulus value which had a major influence on the mechanistic response of pavements in terms of vertical strain.

The calculated vertical strain on the top of granular layers for a particular time (ϵ_i , γ_i) and number of axle passes at that time (N_i) were used as the independent variables in the rut prediction models. The total measured rut depth (Rut_i) at a particular time was calculated as a sum of the previous total rutting plus additional incremental rutting caused by traffic (N_i) at the calculated strain level (ϵ_i or γ_i) in the current time increment. The non-linear regression coefficients were then analyzed for their validity in the developed rut prediction model.

5.4 VERTICAL STRAIN BASED RUTTING MODEL DEVELOPMENT

5.4.1 Need for Base and Subgrade Strain Calculation

As mentioned in the methodology, there is a need to include the measured vertical strain responses on the top of granular layers in the rut prediction model development.

However in the Test Track there was no instrumentation available to measure vertical strains in these layers. While it would be advantageous to also measure vertical strain, these types of gauges were not used because of prohibitively high cost (Timm et al., 2004). Since the layered elastic model predicts the pavement responses reasonably well and the model was validated successfully in the previous chapter, it was decided to use the same layered elastic analysis program, WESLEA, to calculate vertical strains at the top of base and subgrade layers.

Literature (Monismith, 1992) shows that for rutting evaluation, linear elastic analysis is a reasonable tool when the pavement surface temperature does not go beyond 40°C (~110°F). Since the maximum pavement temperature measured in the Test Track lies within 120°F, it is reasonable to use linear elastic model to predict pavement strains which can be used to build the rut prediction model. Also, this is the current state-of-practice for M-E pavement design (ERES, 2004).

5.4.2 Strain Prediction Models

A unique approach was adopted to calculate the pavement response for a truck pass after studying the typical pavement response trace collected from the embedded instrumentation at the Test Track. Using the same material properties and load configurations that were used earlier for theoretical pressure calculation, the vertical strain at the top of base and subgrade was calculated by using WESLEA. The WESLEA simulations were run for different truck axles (steer, tandem and single) and the average vertical strain (base, subgrade) value for a single truck pass (ϵ_{avg}) was calculated by:

$$\overline{\epsilon}_{avg} = \frac{\epsilon_{st}n_{st} + \epsilon_t n_t + \epsilon_s n_s}{N_T} \quad (5.1)$$

Where:

ϵ_{st} , ϵ_t , ϵ_s = Calculated strain (base, subgrade) for steer, tandem and single axles,

respectively

n_{st} , n_t , n_s = Number of steer, tandem and single axles in a truck, respectively

N_T = Total number of axles = $n_{st} + n_t + n_s$

To predict vertical strain on the top of base and subgrade layers at any point of time for a given pavement temperature, WESLEA simulations were run for a wide range of temperatures (30°F to 120 °F), representative of pavement temperatures at the Test Track, and the strain responses were computed for the truck loading. Then a model (Equation 5.2) was built to predict vertical strain on the top of base and subgrade layers as a function of pavement temperature for both triple and box trailer. The basic form of the vertical strain prediction model was:

$$\varepsilon = \alpha_1 e^{\alpha_2 * T} \quad (5.2)$$

Where:

ε = Vertical strain (base, subgrade), microstrain

T = Temperature at 2" from top of HMA, °F

α_1, α_2 = Regression coefficients

During the development of rut prediction model, the pavement layer vertical subgrade strain had to be linked with the traffic at every hour as will be explained below. Figures 5.3 to 5.6 show the relation between the vertical strain (base, subgrade) and temperature relationship for both triple and box trailers. It is to be noted here that for section N1, for temperatures higher than 70⁰ F, the vertical strain was not calculated since the backcalculated modulus values were highly variable and not very reliable at higher temperatures.

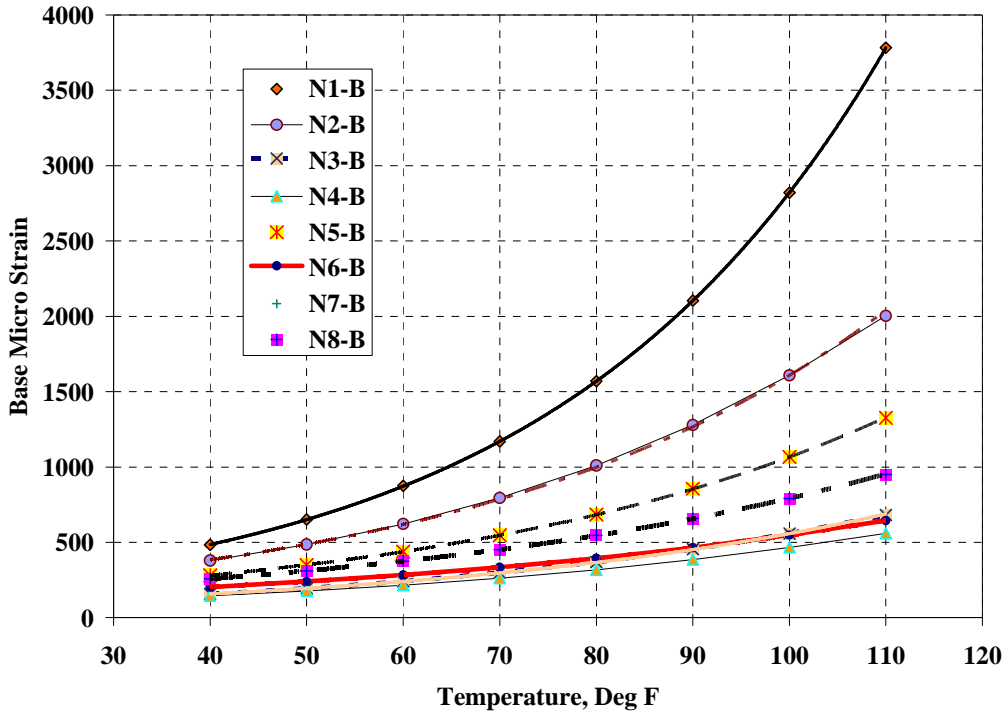


Figure 5.3 Base Strain Vs Temperature (Eq 5.2) - Triple Trailer.

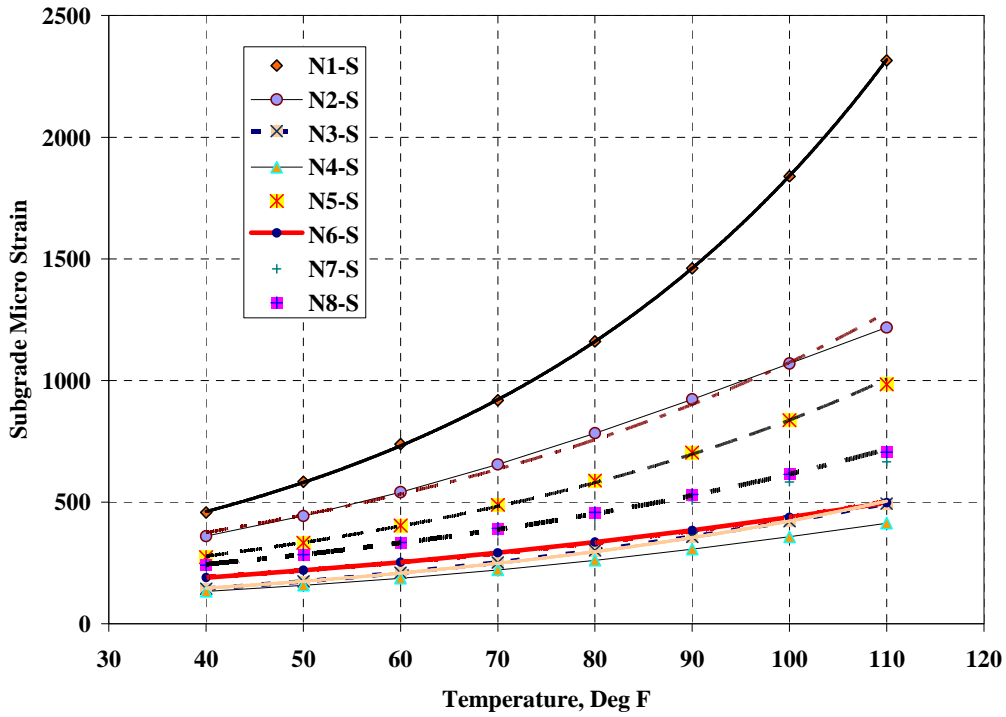


Figure 5. 4 Subgrade Strain Vs Temperature (Eq 5.2) - Triple Trailer.

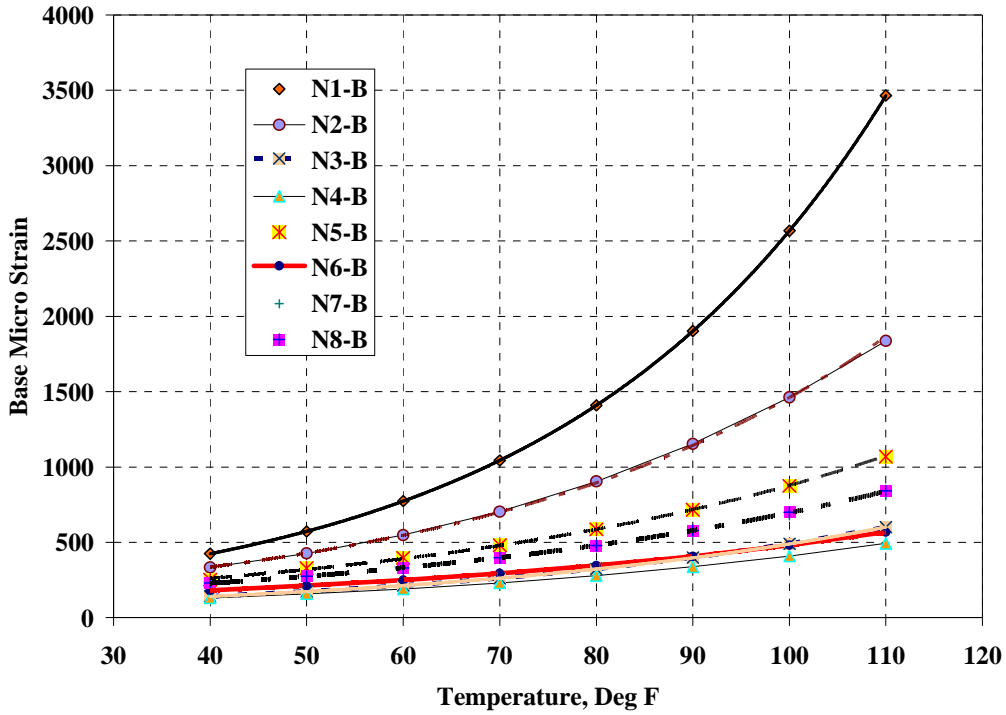


Figure 5.5 Base Strain Vs Temperature (Eq 5.2) - Box Trailer.

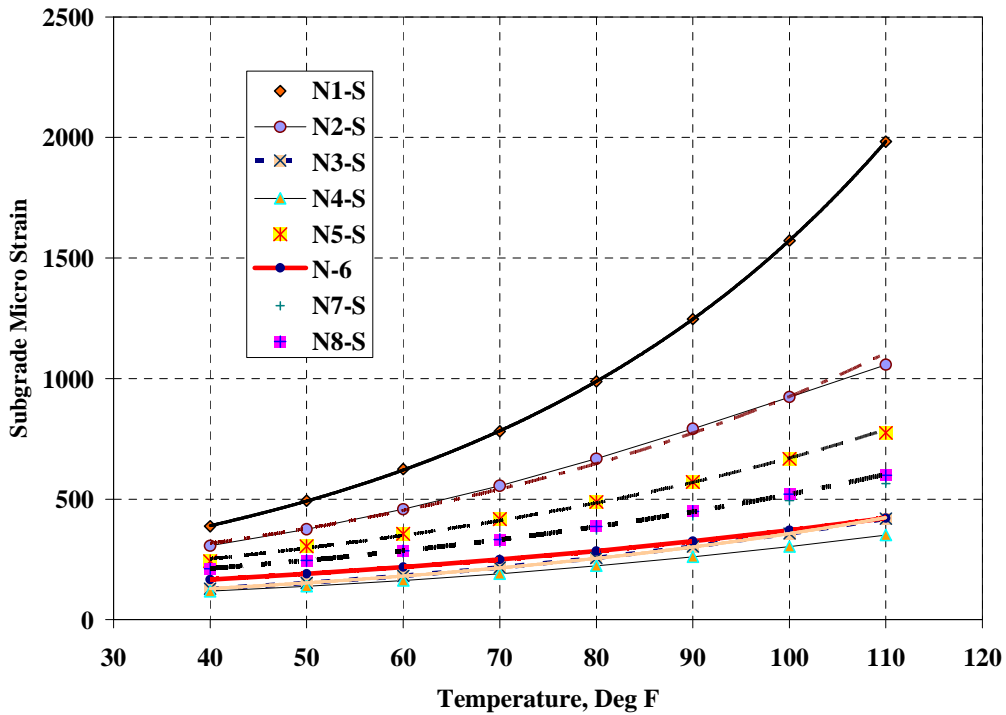


Figure 5.6 Subgrade Strain Vs Temperature (Eq 5.2) - Box Trailer.

Table 5.1 gives the non-linear regression equation results for computing base and subgrade vertical strain under truck loading. As expected, the data show the effect of thickness where the α_1 terms are highest for the thinnest sections and lowest for the thickest. Strain prediction coefficients for box trailers were lower than triple trailer model coefficients and the strains for box trailers were always lower than the triple trailer, because of differences in loading. This behavior was in tune with the theory that higher load magnitude produces more strain in a structure.

Table 5.1 Vertical Strain Model Results for Triple and Box Trailer

Section	Triple trailer				Box trailer			
	Base		Subgrade		Base		Subgrade	
	α_1	α_2	α_1	α_2	α_1	α_2	α_1	α_2
N1	150.32	0.0293	184.00	0.0230	127.86	0.030	154.37	0.0232
N2	154.22	0.0233	201.37	0.0166	130.21	0.0241	166.37	0.0170
N3	69.57	0.0208	74.70	0.0173	69.55	0.0207	66.59	0.0168
N4	68.95	0.0191	72.03	0.0160	61.43	0.0189	64.64	0.0154
N5	116.19	0.0221	138.41	0.0179	118.59	0.0200	136.13	0.0159
N6	105.76	0.0164	112.07	0.0136	93.67	0.0164	99.03	0.0132
N7	124.47	0.0181	135.21	0.0146	108.20	0.0183	116.75	0.0144
N8	123.07	0.0186	135.14	0.0151	107.67	0.0187	117.88	0.0148

5.4.3 Trucking Data

As mentioned in Chapter 3, the category of the vehicle (box, triple), and the number of laps each category of vehicle traveled were recorded at every hour. The total number of axle passes for a particular vehicle category was calculated by multiplying the number of laps per hour and the total number of axles in that vehicle (box: 5 axles, triple: 8 axles). The cumulative axle passes at any point of time was then calculated by cumulatively adding the number of total axle passes until that point of time. The trucking data were linked with the environmental database with the help of the time stamp and thereby at

any given time, the vertical strain produced by a certain number of axle passes was available for model development.

5.5 VERTICAL STRAIN BASED RUT PREDICTION MODEL RESULTS

5.5.1 Rut Prediction Model Form

When the mechanistic responses are combined with the number of axle passes, it explains the rutting mechanism clearly. For example, 100 axle passes at a strain value of 400 will have less effect on the pavement than the same number of axle passes at a strain of 800. Accumulation of axle load passes also increases the rutting in pavement. So it was believed that with the help of load cycles and dynamic pavement response in terms of vertical strain, the nature of rutting can be modeled.

The rut measurements made on a weekly basis were linearly interpolated to have a rutting value for each hour of each day in the experiment. As mentioned previously, from the trucking database, the total number of axle passes for every hour for both trucks were calculated from the total number of laps per hour. The vertical strain on the top of the granular pavement layers was calculated at every hour by substituting the measured temperature in the developed vertical strain prediction model (Equation 5.2).

By relating the measured hourly rutting to the vertical strain on the top of base granular layers and the total number of axle passes, rut prediction models were developed by performing a non-linear regression. The basic form of the vertical strain based rut prediction model is given in Equation 5.3. The rut prediction results showed that the accuracy of the prediction was not affected by the selection of strain location (top of base or top of subgrade). So, either base or subgrade strains can be used in the model. The

developed model form is given in Equation 5.3. Historically vertical stress over the top of subgrade has been correlated strongly to rut performance, so to be in consistent with that theory, the vertical strain over the top of subgrade layer was used in the developed model.

$$Rut_i = Rut_{i-1} + \beta_0 N_i^{(\beta_1 \epsilon_i)} \quad (5.3)$$

Where,

Rut_i = Rutting at time 'i'

Rut_{i-1} = Rutting at time 'i-1'

N_i = Total number of axle passes at time 'i'

ϵ_i = Vertical base or subgrade strain calculated at time 'i' from strain prediction models

β_0, β_1 = Regression constants for traffic and strain respectively

Table 5.2 gives the regression constants for the developed rutting model.

Table 5.2 Subgrade Vertical Strain Based Rut Prediction Model Coefficients

Section	β_0	β_1	R^2
N1	1.90×10^{-4}	1.05×10^{-4}	0.94
N2	2.33×10^{-4}	1.85×10^{-4}	0.99
N3	5.62×10^{-5}	8.02×10^{-4}	0.82
N4	4.09×10^{-5}	9.37×10^{-4}	0.84
N5	7.32×10^{-5}	3.11×10^{-4}	0.89
N6	5.57×10^{-5}	8.70×10^{-4}	0.89
N7	7.22×10^{-5}	5.27×10^{-4}	0.87
N8	9.79×10^{-5}	4.71×10^{-4}	0.94

When an ANOVA test was performed in the developed model with a confidence level of 95% , both model coefficients were proved to be significant in all test sections, as evident by the low p-value (p-value = 0.00). In sections N1 and N2, after some point of time, the sections failed because of fatigue, so the measured rutting was a result of

excessive fatigue cracking which resulted in pumping of fine materials from base. The effect of thickness is readily apparent in this model. For example, the β_0 terms in the vertical strain model are an order of magnitude higher for N1 and N2 compared to the other sections.

The positive coefficients for both traffic and strains show that increase in number of axle passes and strain levels will increase the rutting which is in tune with the theory. Figures 5.7-5.14 show the predicted rutting from the model and the measured rutting from the Test Track for increasing axle passes. Overall, the vertical strain based rut prediction model satisfactorily predicted field rutting.

In some sections, at higher axle passes, the model predicts an upward trend in rutting, however in the field the measured rutting generally levels off or even decreases. It is believed that during the end of the Test Track cycle, those sections (N7, N8) that showed decrease in rutting trend had fatigue failures which could have affected the measured rutting. Since the trucks were veering around sections N1 and N2 after they failed in fatigue, and the trucks wander could have affected the measured rutting in section N3.

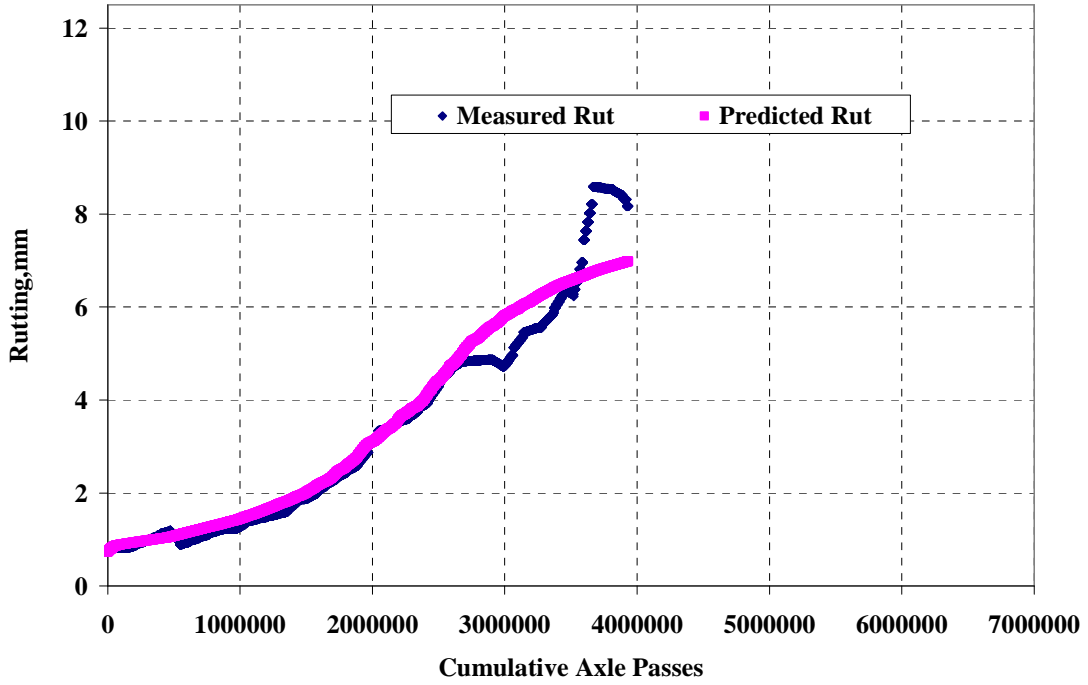


Figure 5.7 Predicted and Measured Rutting for Section N1.

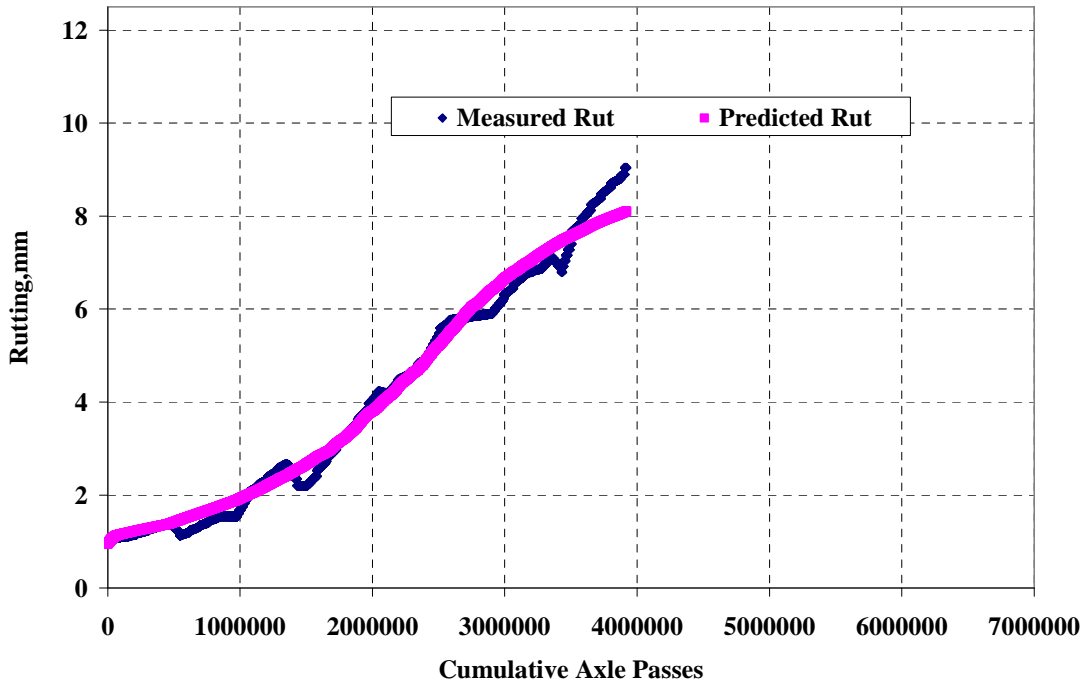


Figure 5.8 Predicted and Measured Rutting for Section N2.

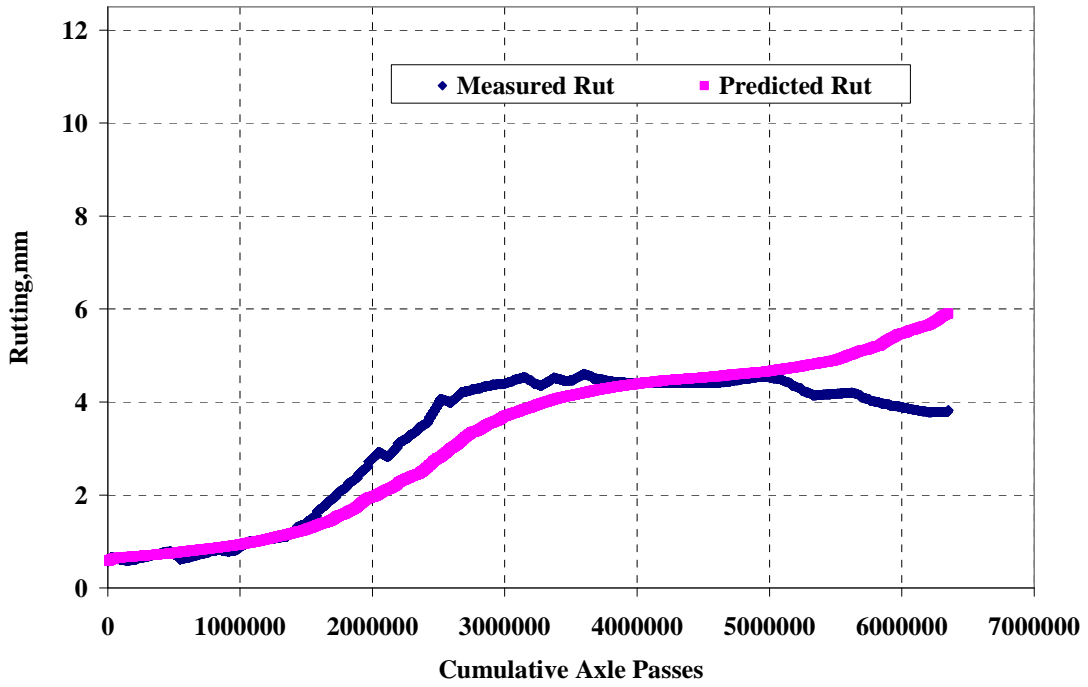


Figure 5.9 Predicted and Measured Rutting for Section N3.

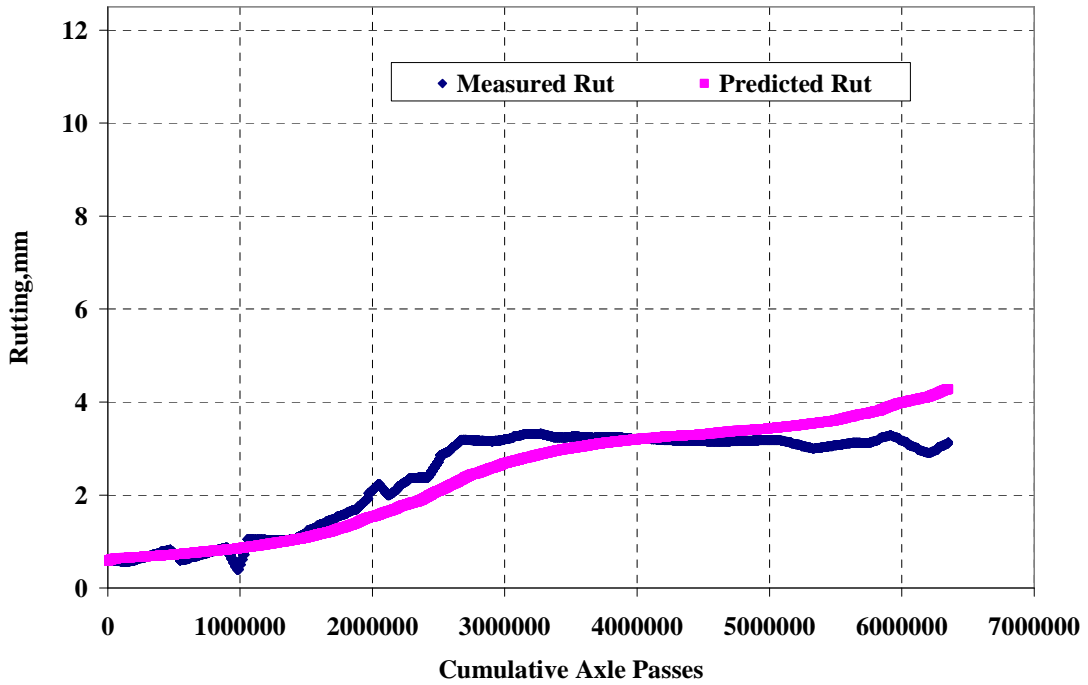


Figure 5.10 Predicted and Measured Rutting for Section N4.

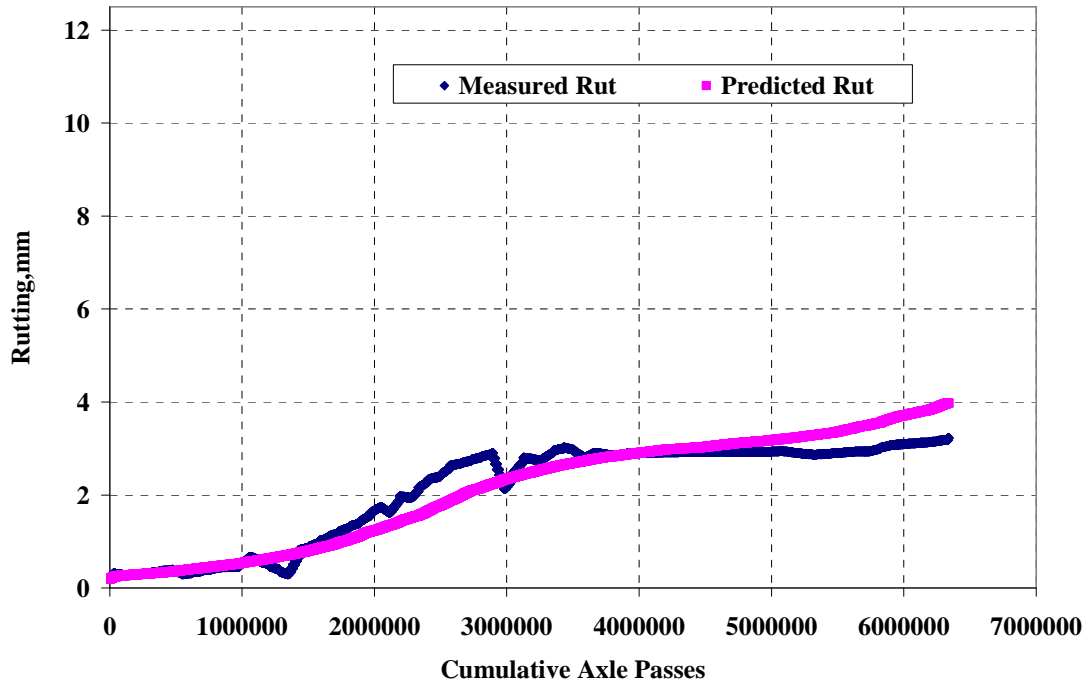


Figure 5.11 Predicted and Measured Rutting for Section N5.

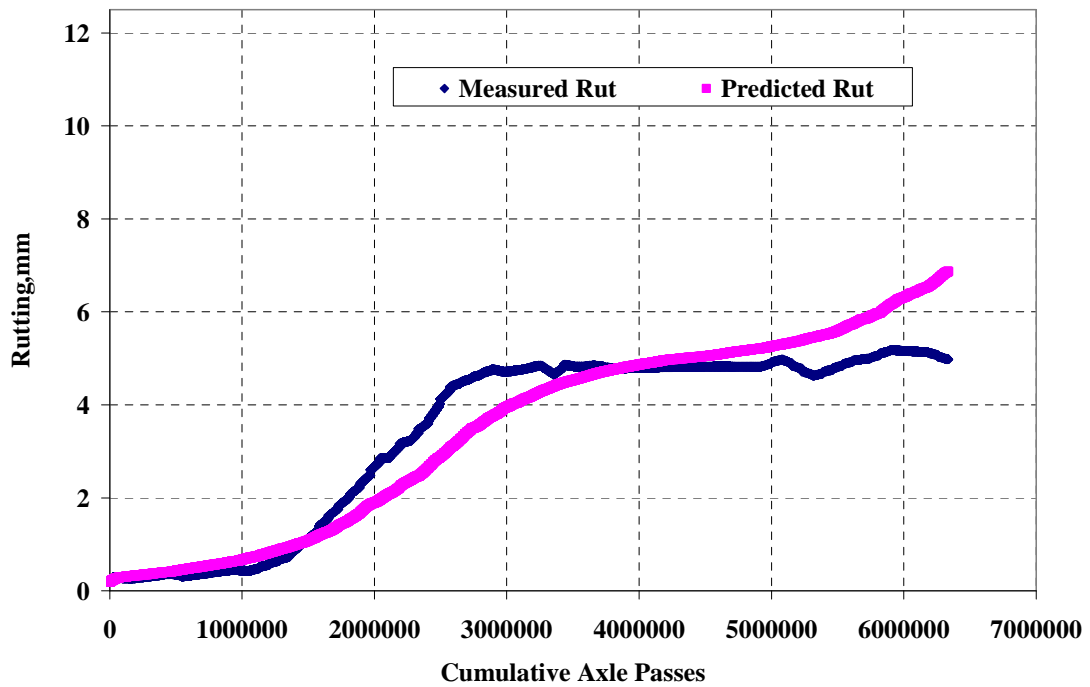


Figure 5.12 Predicted and Measured Rutting for Section N6.

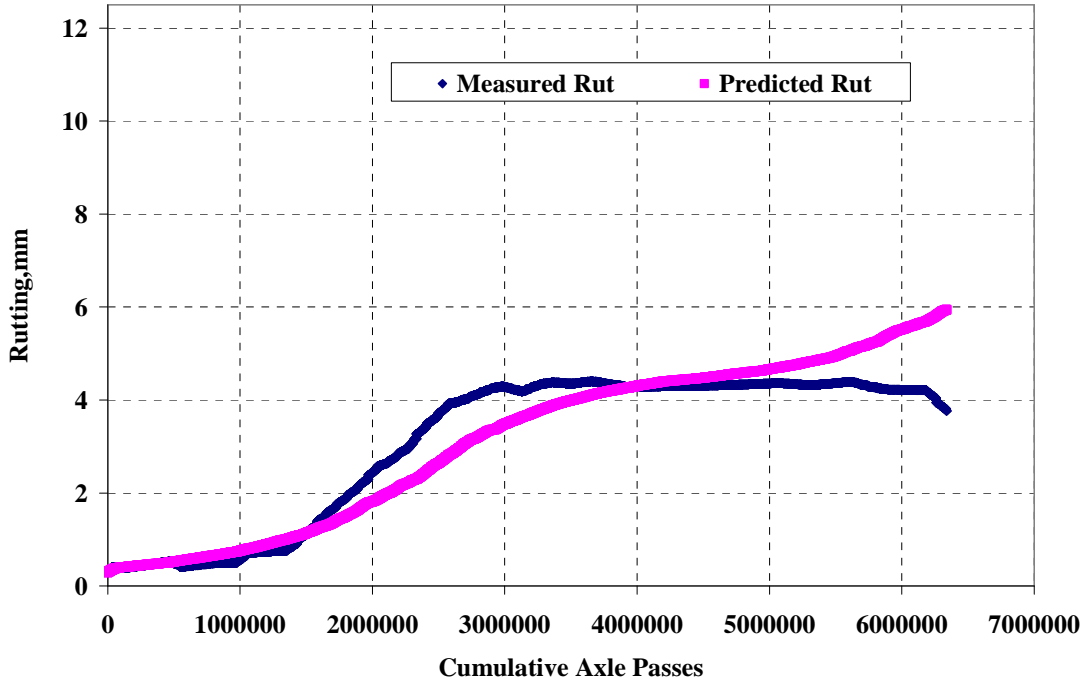


Figure 5.13 Predicted and Measured Rutting for Section N7.

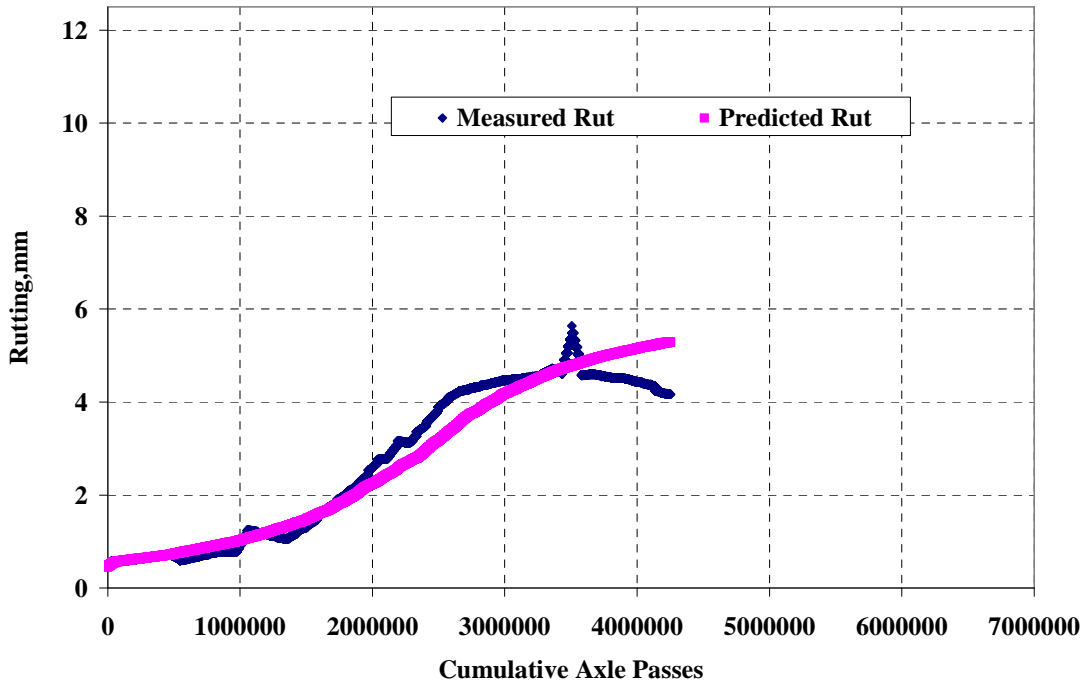


Figure 5.14 Predicted and Measured Rutting for Section N8.

5.5.2 Analysis on Model Coefficients

A developed model may yield good prediction, even if the model coefficients do not make proper engineering sense. So in order to evaluate the model coefficients for their validity in the model to make proper sense in the prediction a relationship between the rutting model coefficients and the in-situ HMA thickness was established (Figure 5.15).

This plot shows that for increase in HMA thickness, the strain coefficient increases and the traffic coefficient decreases. For example, in the 9" modified HMA section N4, the strain coefficient value ($\beta_1 = 9.37 \times 10^{-4}$) was higher than section N7 ($\beta_1 = 5.27 \times 10^{-4}$) which had 7" HMA thickness. The strain model coefficient (β_1) should have been lower for thick pavement sections, since they had less rutting. However, in the vertical strain approach as the thickness of HMA increased, the vertical strain coefficient (β_1) also increased.

It is believed that the strain and traffic coefficients compensate for each other while predicting the rutting and the strain model coefficients were influenced only by the HMA thickness. To produce higher amount of rutting in thick pavements, the number of traffic applications should be higher, i.e., the traffic coefficient should have a higher number. Despite accurate prediction of rut depths, the model coefficients did not explain the field measured rutting mechanism from a conceptual standpoint.

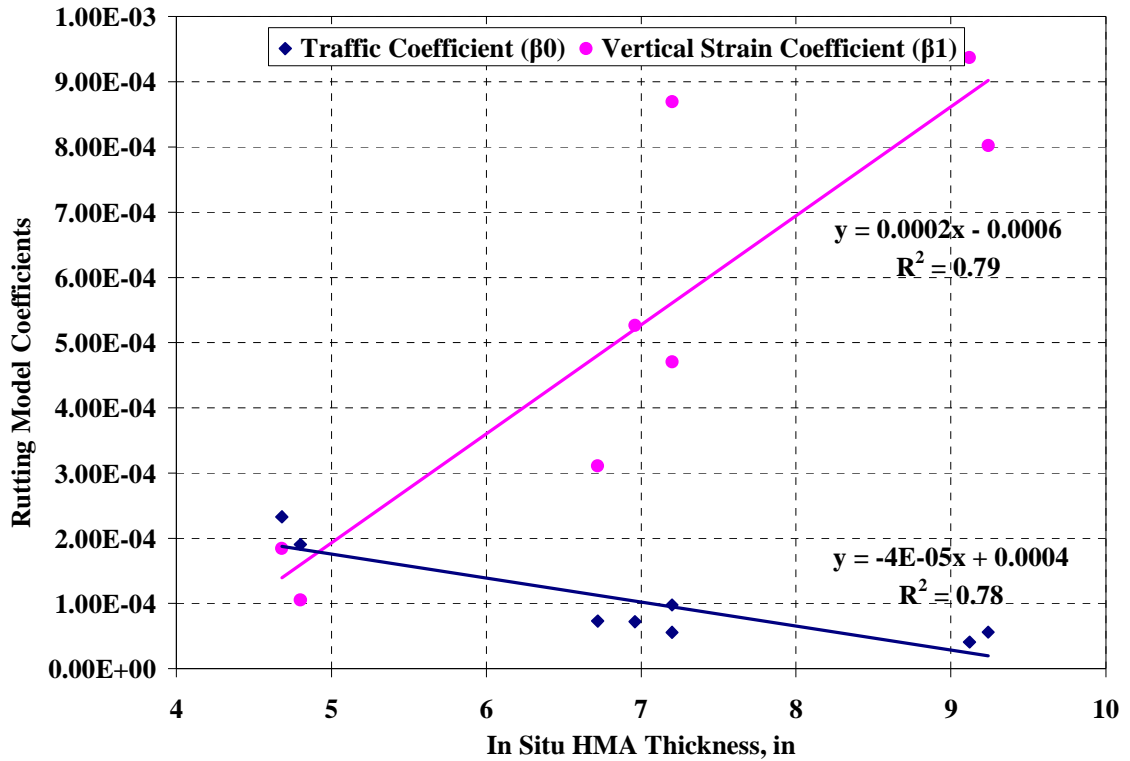


Figure 5.15 HMA Thickness vs Rutting Model Coefficients.

Figure 5.16 shows that the model coefficients did not relate well with modified and unmodified sections, and there were no distinguished differences between modified section model coefficients and unmodified section model coefficients. Though, the developed model did a very good job of predicting the pavement rutting on section by section basis, it failed to explain the field rutting behavior observed in the test sections from a materials standpoint.

On an additional note, a similar occurrence happened while validating the developed model to predict asphalt layer rutting in the MEPDG. The model predicted higher HMA rut depth as the thickness of the HMA increased. This limitation was then overcome by calibrating the model using trench studies from the Mn/Road project (El-

Basyouny et al., 2005). So analysis on model coefficients to check whether they make proper sense is very important.

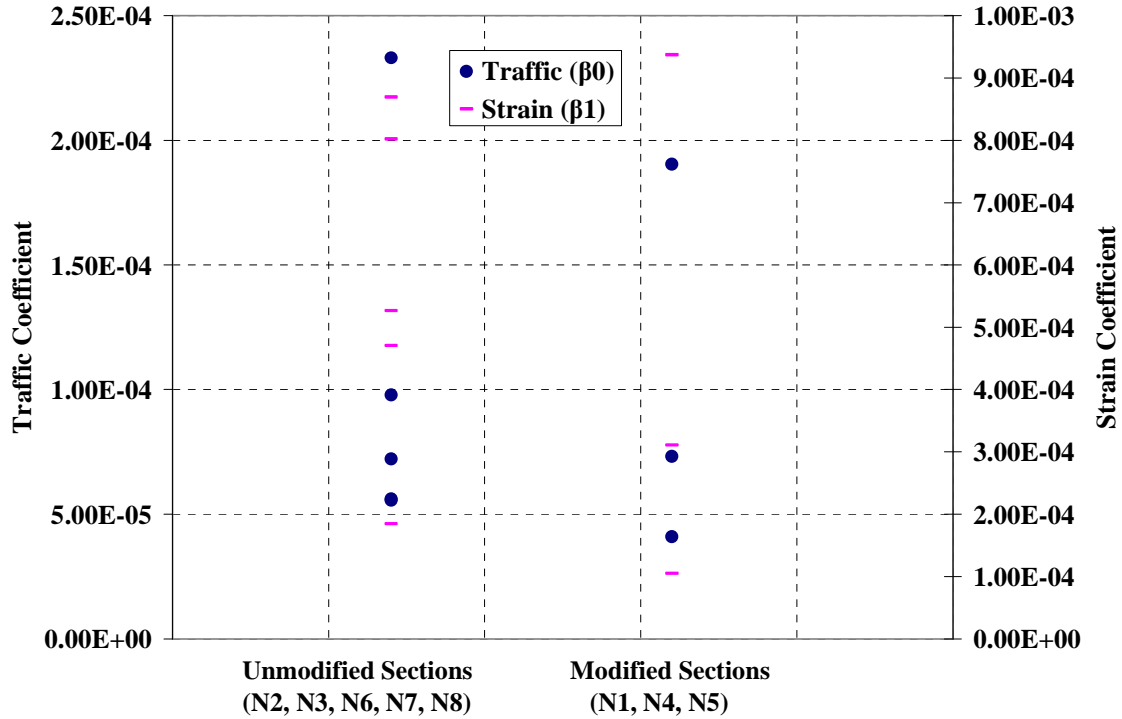


Figure 5.16 Rutting Model Coefficients for Modified and Unmodified Sections.

Having different individual models to explain the rutting mechanism in each section is not a viable solution in the field. This methodology requires development of individual models whenever materials or pavement thickness changes which is practically an impossible and time consuming process.

To alleviate this problem, an effort was made to replicate the field observed behavior by grouping all modified, unmodified sections separately. As explained earlier, the rutting appeared to be grouped by binder modification. Therefore, it was logical to perform model calibration with grouped sections.

To develop a generalized model for rut prediction in modified (N1, N4 and N5) and unmodified sections (N2, N3, N6 and N7), an effort was made to develop one unique equation to minimize the error for all sections within the group. When sections were grouped, the non-linear regression could not be successfully computed. In other words, there was not a single set of coefficients that could reasonably predict rut progression in all the unmodified and modified sections, respectively when the vertical strain criteria was considered. Further the model coefficients did not make any engineering sense, and both traffic and strain coefficients were negative. The combined model failed to predict rutting and it could not model the primary and secondary stages of rutting observed at the Test Track.

Despite accurate prediction of rut depths on a section-by-section basis, the vertical strain model coefficients did not explain the field rutting mechanism and they did not distinguish rutting between modified and unmodified sections. However, in the field, modified sections had lower rutting than unmodified sections. After extensive literature review, in order to alleviate such problems, modeling the rutting by considering the shear strain response was attempted as a next step in this study.

5.6 SHEAR STRAIN BASED RUTTING MODEL DEVELOPMENT

5.6.1 Background

Since the vertical strain based rut prediction model fails to explain the rutting phenomenon in the field, it is believed that the rutting phenomenon could be a result of another related mechanistic response within the HMA layers. Researchers (Theyse et al., 2006; Kim et al., 2000) have shown that it is difficult to control the pavement rutting only by controlling the vertical compressive strain on the top of roadbed soil. The models built from subgrade strain approach have limitations and they normally have large scatter between predicted and measured rutting (Ali, 1998). Literature shows that limiting subgrade strain approach does a reasonably well in predicting base and subgrade rutting but fails to predict the HMA layer rutting accurately. Studies have shown that in most of the pavements rutting occurred as a result of shear deformation and not by excessive subgrade vertical strain.

From these earlier studies, it is expected that analyzing other mechanistic responses (shear stress, shear strain) in the HMA layer and correlating them to the measured rutting could explain the rutting phenomenon in the Test Track sections. Laboratory study results indicated that the rate of accumulation of permanent deformation is strongly related to the magnitude of shear strain. Some studies (Long, 2001; Epps et al., 1997) proposed a correlation of shear strain at 2" depth below the edge of the tire to the pavement rutting. However the method had not been calibrated with a large data set. So it was decided to make an effort to build a fully field calibrated model with a large data set (approximately 12,000 data points per section) in this study.

5.6.2 Methodology

The procedure to build shear strain based model was similar to the previous model, except the mechanistic response was substituted with maximum shear strain.

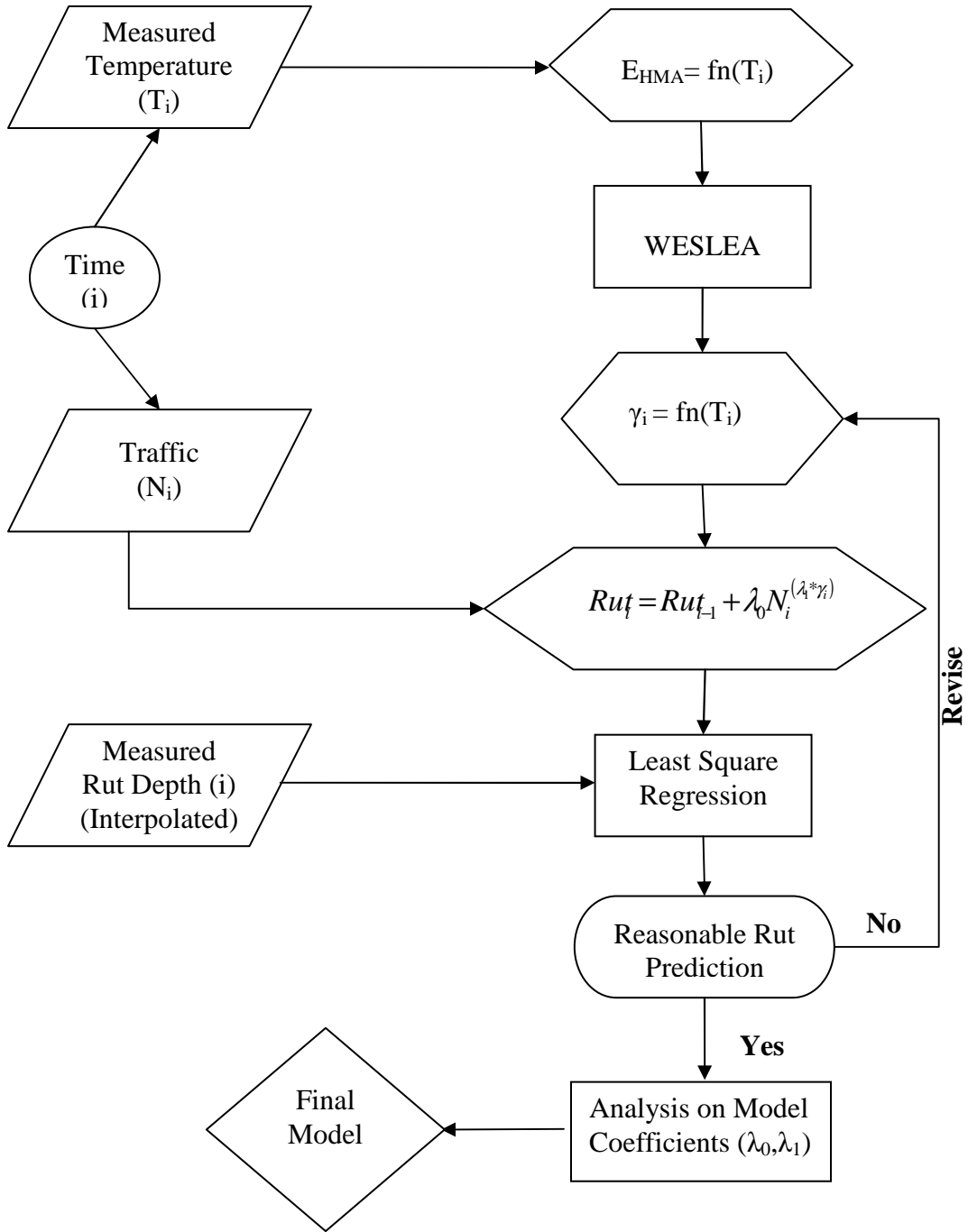


Figure 5.17 Shear Strain Based Rut Prediction Methodology Flow Chart.

5.6.3 Maximum Shear Strain Computation

The shear strain computation was similar to the vertical strain computation approach. However the shear strain was computed at different depths in the HMA layer and the maximum shear strain was observed at about 1” from the surface, at the edge of the tire. The used mechanistic model WESLEA provides many pavement responses in terms of stress, strain, deflection etc., it does not compute shear strain. However; WESLEA computes the shear stress and using Equation 5.4, the shear strain for a single axle load was calculated;

$$\gamma = \frac{2\tau(1 + \nu)}{E} \quad (5.4)$$

Where:

γ = Shear strain, microstrain

τ = Shear stress measured along the edge of a tire, psi

ν = Poisson ratio of HMA, taken as 0.35 for this study

E = HMA modulus, psi

It should be noted that strain profiles representing strains at 0.1” depth increments were first examined and found that the maximum typically occurred at 1” depth. For the majority of test sections, the maximum shear strain was found between 0.5-1”. However to be consistent between sections, the maximum shear strain at 1” was selected.

A typical shear strain profile at different depths calculated for a test section (N1) is given in Figure 5.18. At 1" the shear strain reaches its maximum value and beyond 1" the value starts decreasing. Recently this was also shown with finite element modeling by researchers at the University of Illinois at Urbana Champaign (Yoo and Al-Qadi, 2007) wherein the maximum shear strain was found to be at about 20mm (~1").

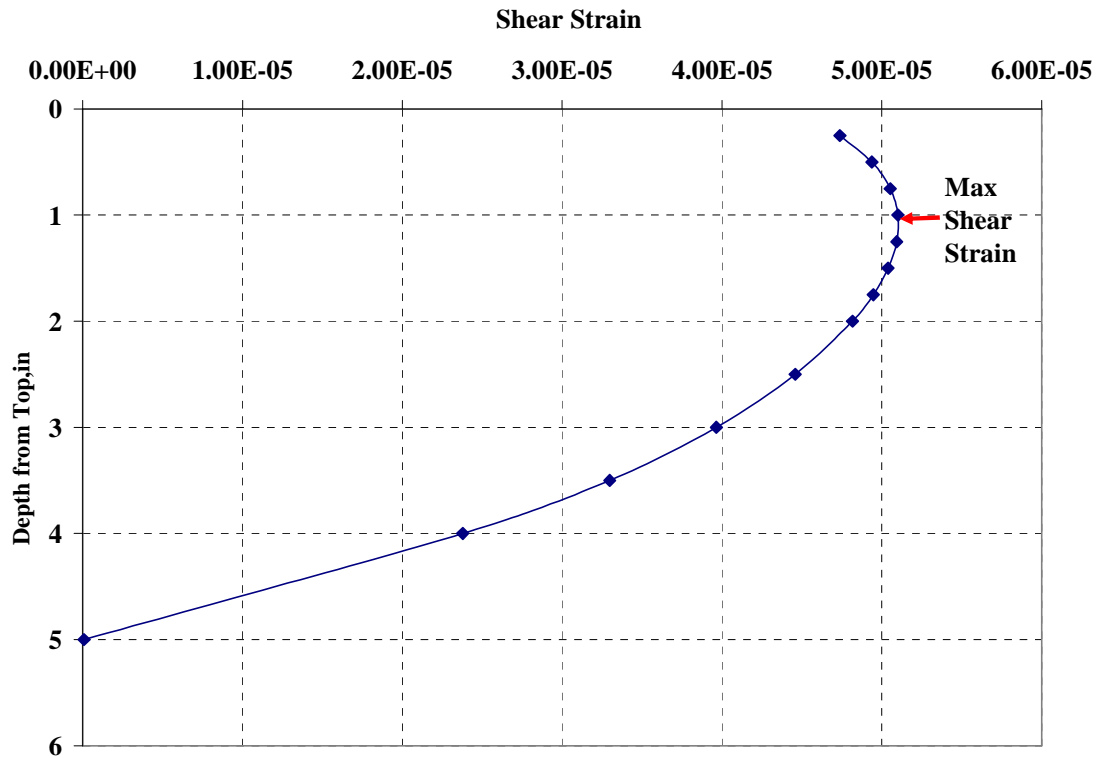


Figure 5.18 Typical Shear Strain Profile (Section N1 at 40 Deg F-Triple Trailer).

A similar approach adopted to compute vertical strain for a single truck pass was followed to compute shear strain. The shear strain for a truck pass was:

$$\overline{\gamma}_{avg} = \frac{\gamma_{st}n_{st} + \gamma_t n_t + \gamma_s n_s}{N_T} \quad (5.5)$$

Where:

$\gamma_{st}, \gamma_t, \gamma_s$ = Calculated maximum shear strain in HMA at 1” depth for steer, tandem and single axles, respectively

n_{st}, n_t, n_s = Number of steer, tandem and single axles in a truck, respectively

N_T = Total number of axles = $n_{st} + n_t + n_s$

Following the procedure outlined for vertical strain, the shear strain as a function of temperature was:

$$\gamma = ae^{b*T} \quad (5.6)$$

Where:

γ = Maximum shear strain at 1” from the top of HMA layer, microstrain

T = Temperature at 2” from top of HMA, °F

a, b = Regression coefficients

The Figures 5.19 and 5.20 show the shear strain versus temperature relation for both triple and box trailers.

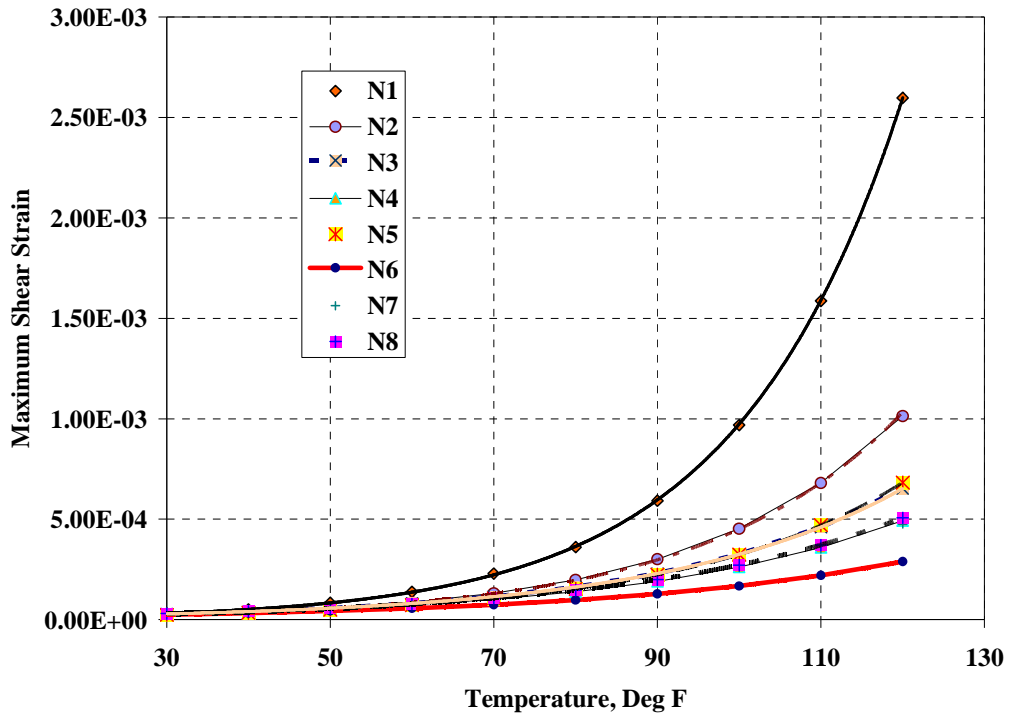


Figure 5.19 Maximum Shear Strain Vs Temperature Relation (Triple Trailer).

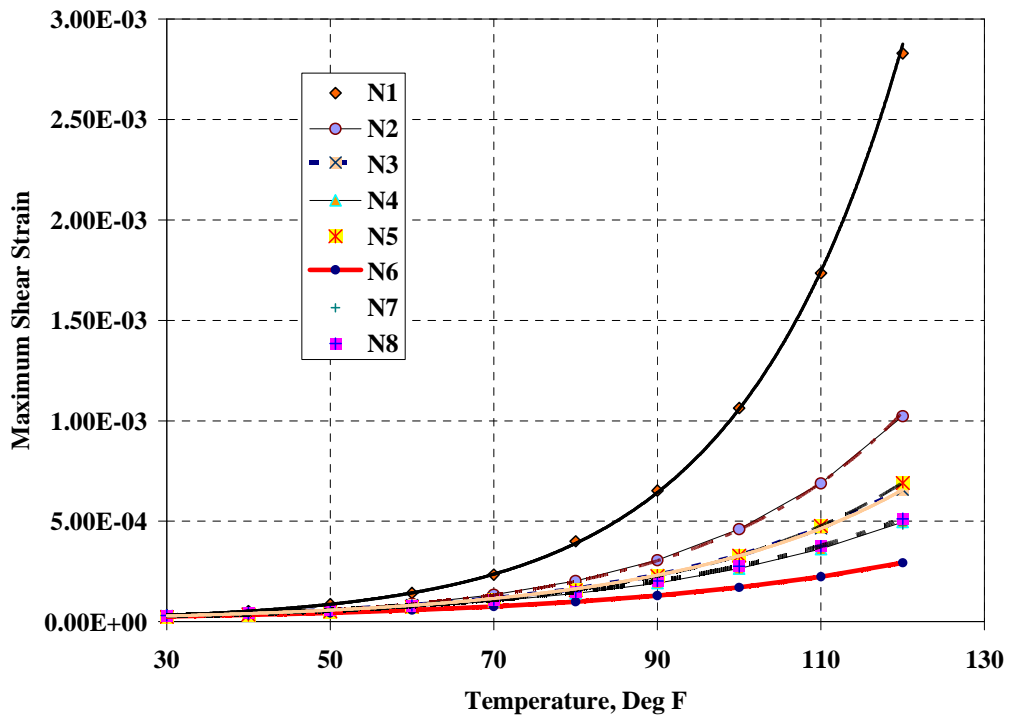


Figure 5.20 Maximum Shear Strain Vs Temperature Relation (Box Trailer).

Table 5.3 gives the results of the shear strain prediction model to predict maximum shear strain for triple and box trailer trucks. Unlike the vertical strain models (Table 5.1) there was not a clear effect of thickness in the model coefficients. There was also not a clear distinction between modified and unmodified test sections. For example, the model coefficients for N1 and N2 are very similar, meaning they experienced approximately the same shear strain level at a given temperature. This would imply that N1 experienced less rutting because the asphalt material was more shear strain resistant.

Table 5.3 Shear Strain Model Results for Triple and Box Trailer

Section	Triple trailer		Box trailer	
	a	b	a	b
N1	7×10^{-6}	0.0493	8×10^{-6}	0.0489
N2	7×10^{-6}	0.0414	7×10^{-6}	0.0411
N3	1×10^{-5}	0.0348	1×10^{-5}	0.0347
N4	1×10^{-5}	0.0316	1×10^{-5}	0.0315
N5	8×10^{-6}	0.0373	8×10^{-6}	0.0372
N6	1×10^{-5}	0.0271	1×10^{-5}	0.0271
N7	1×10^{-5}	0.0303	1×10^{-5}	0.0302
N8	1×10^{-5}	0.0311	1×10^{-5}	0.0310

5.7 RUT PREDICTION MODEL: SHEAR STRAIN APPROACH

The same approach described for vertical strain based model building was used to develop the shear strain based rut prediction model:

$$Rut_i = Rut_{i-1} + \lambda_0 N_i^{(\lambda_1 * \gamma_i)} \quad (5.7)$$

Where,

γ_i = shear strain in HMA calculated at time 'i' from the shear strain prediction model

λ_0, λ_1 = Regression constants for traffic and shear strain in HMA respectively

The model result is given below in Table 5.4.

Table 5.4 Shear Strain Model Coefficients

Section	λ_0	λ_1	R^2
N1	2.88×10^{-4}	197.33	0.94
N2	3.64×10^{-4}	465.83	0.98
N3	0.89×10^{-4}	1064.33	0.84
N4	1.09×10^{-4}	980.00	0.85
N5	4.18×10^{-4}	1199.97	0.88
N6	2.23×10^{-4}	1301.24	0.89
N7	1.10×10^{-4}	1531.59	0.88
N8	1.12×10^{-4}	1499.81	0.94

In the model both traffic and shear strain coefficients were found to be highly significant when ANOVA tests were conducted at a significance level of 5%. The very high t-ratio value and the p-value approaching zero in all test sections proved that both model variables were very significant. From the results, it is evident that the λ_1 terms are much lower for N1 and N2 when compared to the other sections. This is compensated by λ_0 terms being higher than all, but section N5. From the R^2 values, it can be seen that this approach predicts HMA rutting with good accuracy. Also, the coefficients are all positive, which is theoretically sound, since one would expect rutting to increase with increases in load applications or strain levels. Figures 5.21-5.28 show the capability of the model to accurately model the field rutting.

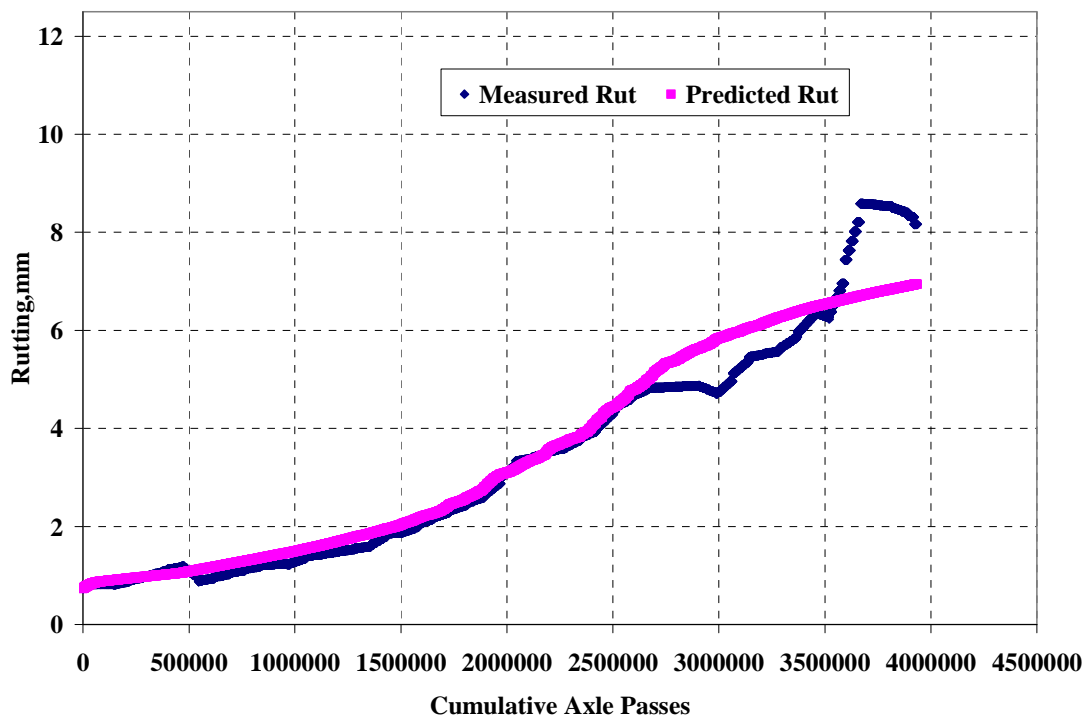


Figure 5.21 Shear Strain Model: Predicted and Measured Rutting for Section N1.

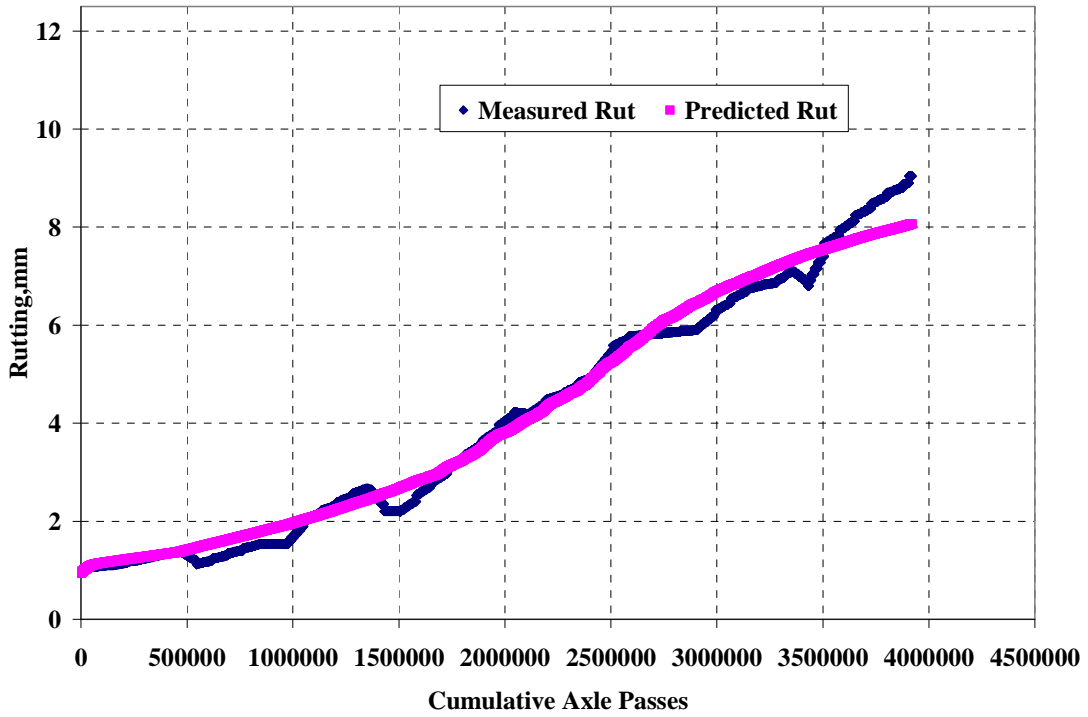


Figure 5.22 Shear Strain Model: Predicted and Measured Rutting for Section N2.

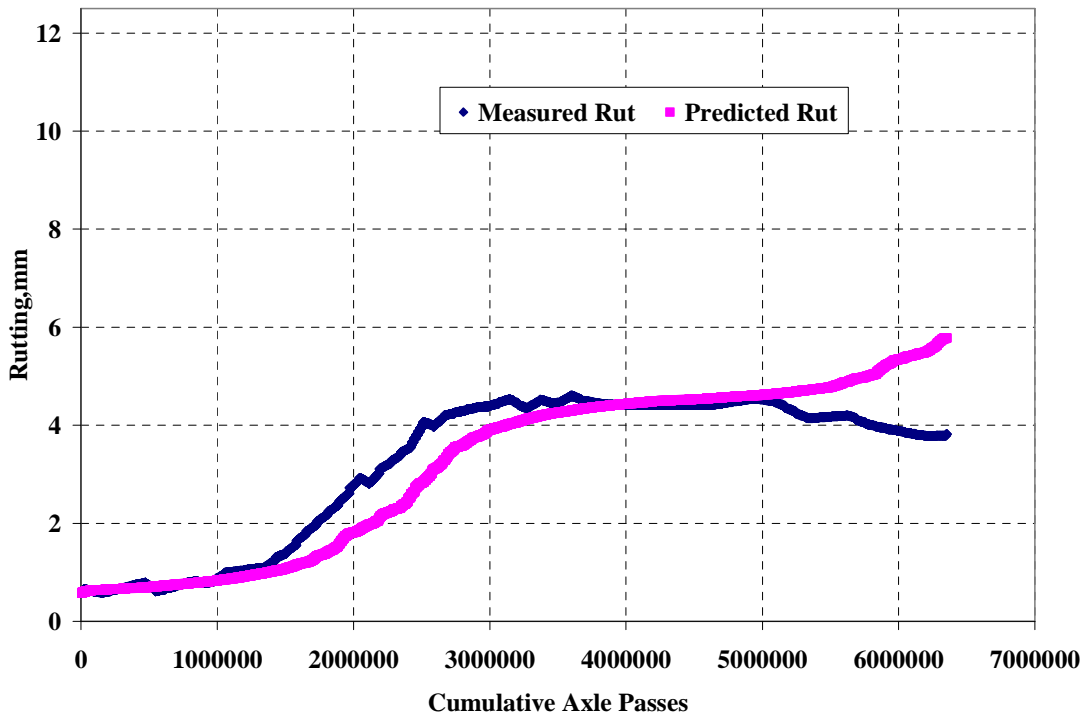


Figure 5.23 Shear Strain Model: Predicted and Measured Rutting for Section N3.

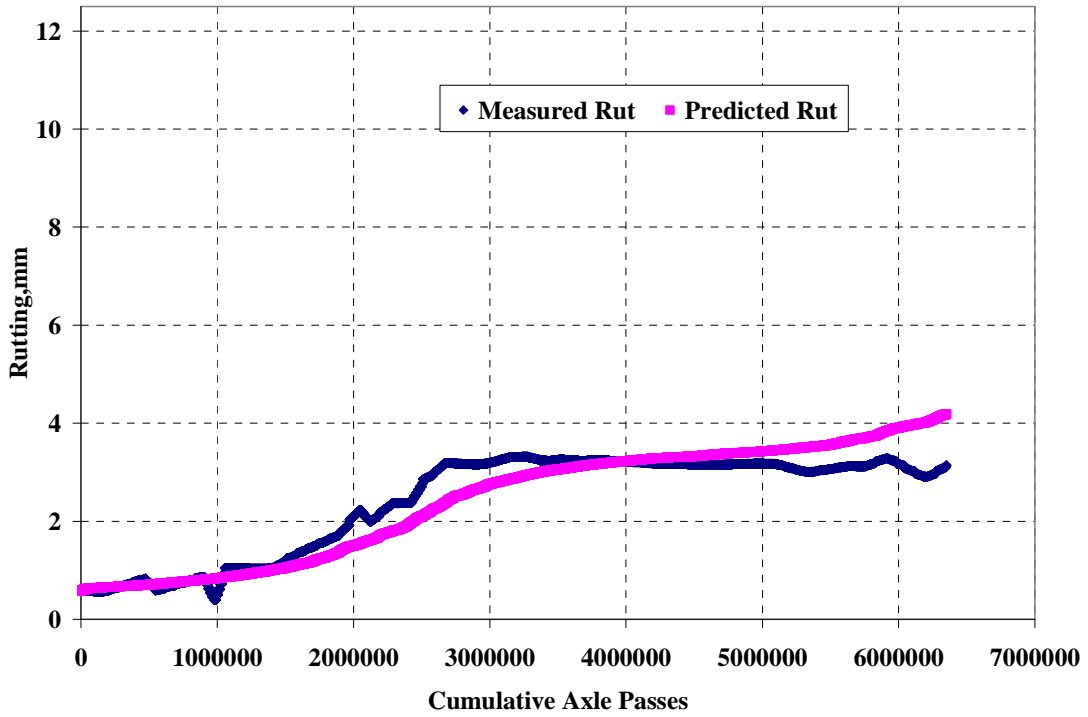


Figure 5.24 Shear Strain Model: Predicted and Measured Rutting for Section N4.

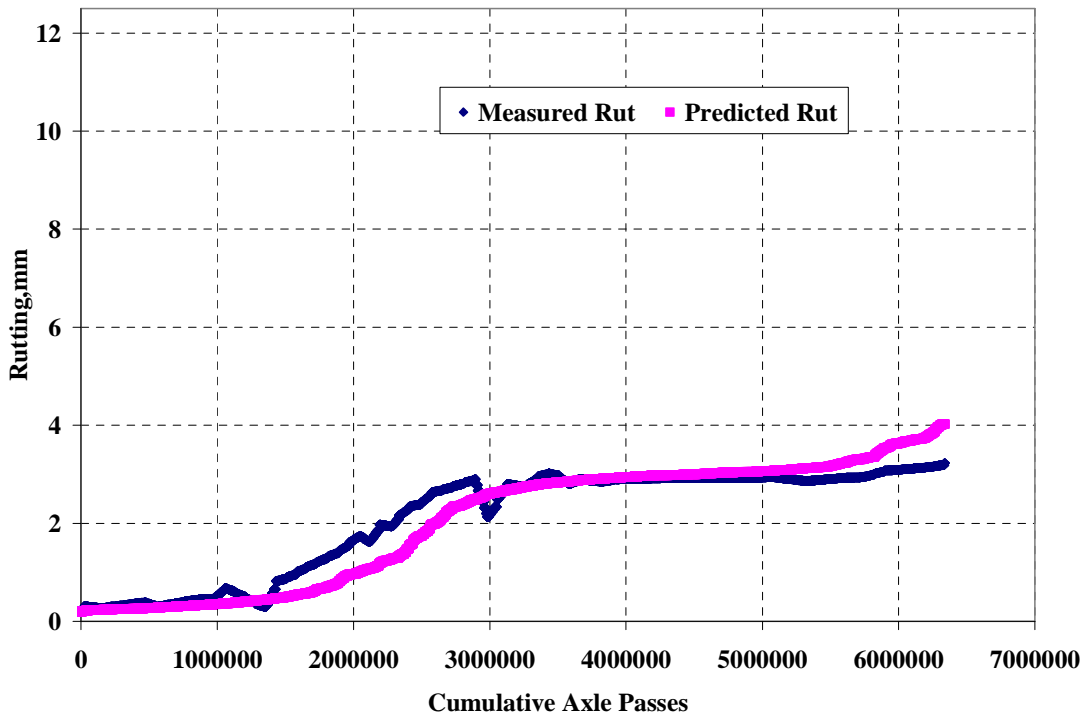


Figure 5.25 Shear Strain Model: Predicted and Measured Rutting for Section N5.

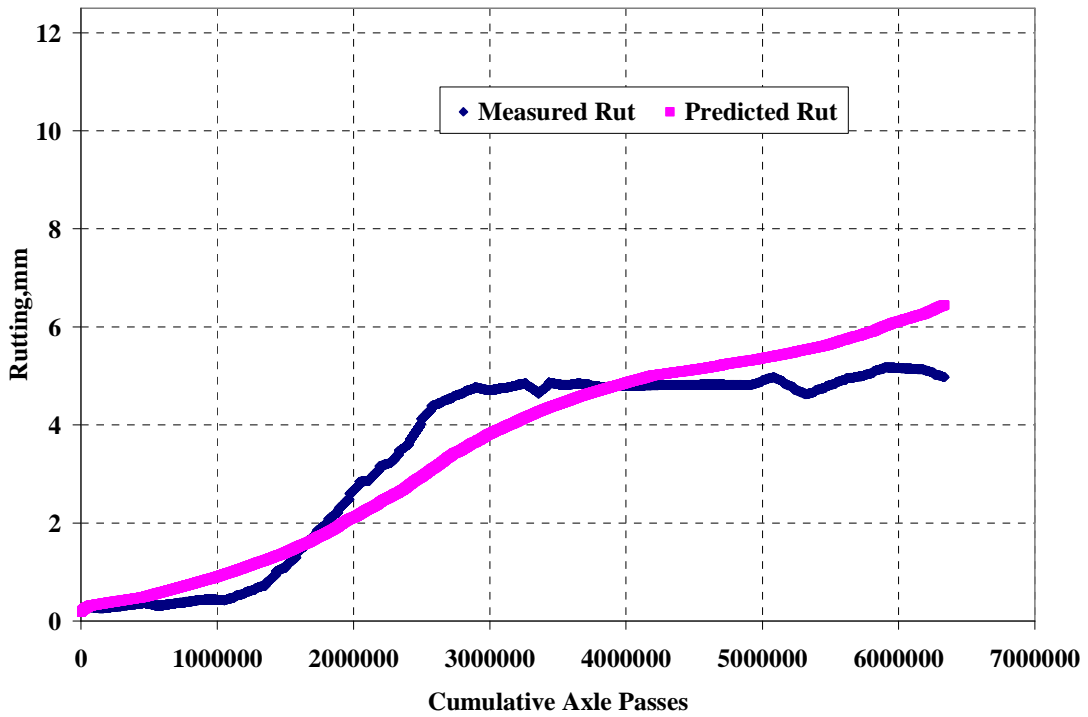


Figure 5.26 Shear Strain Model: Predicted and Measured Rutting for Section N6.

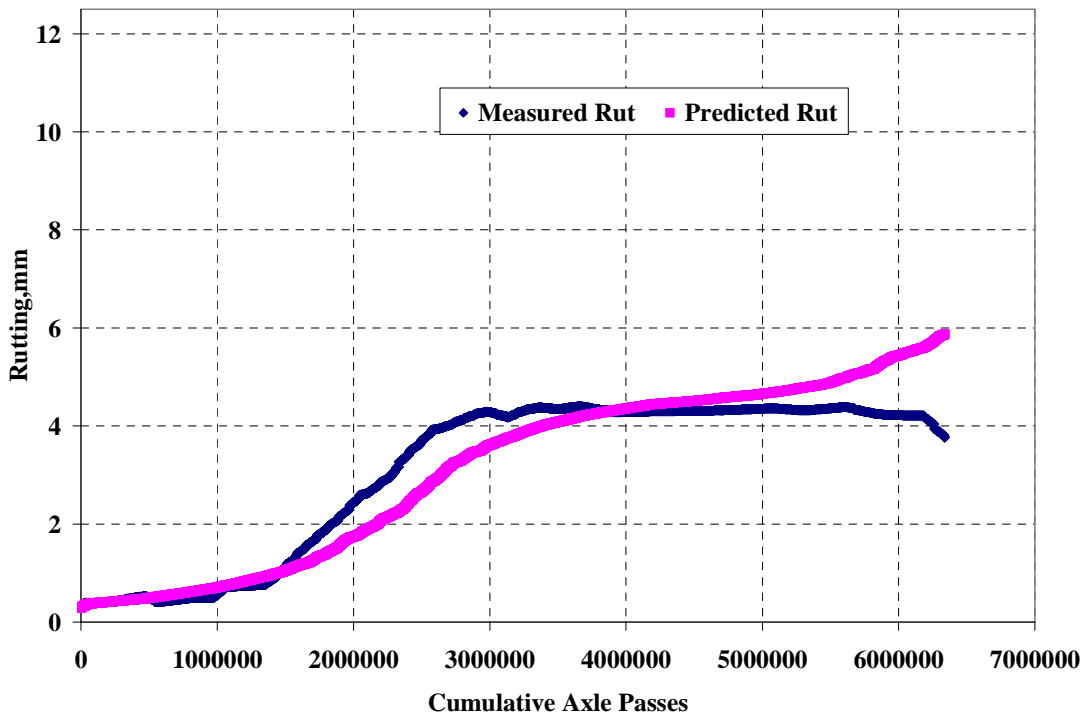


Figure 5.27 Shear Strain Model: Predicted and Measured Rutting for Section N7.

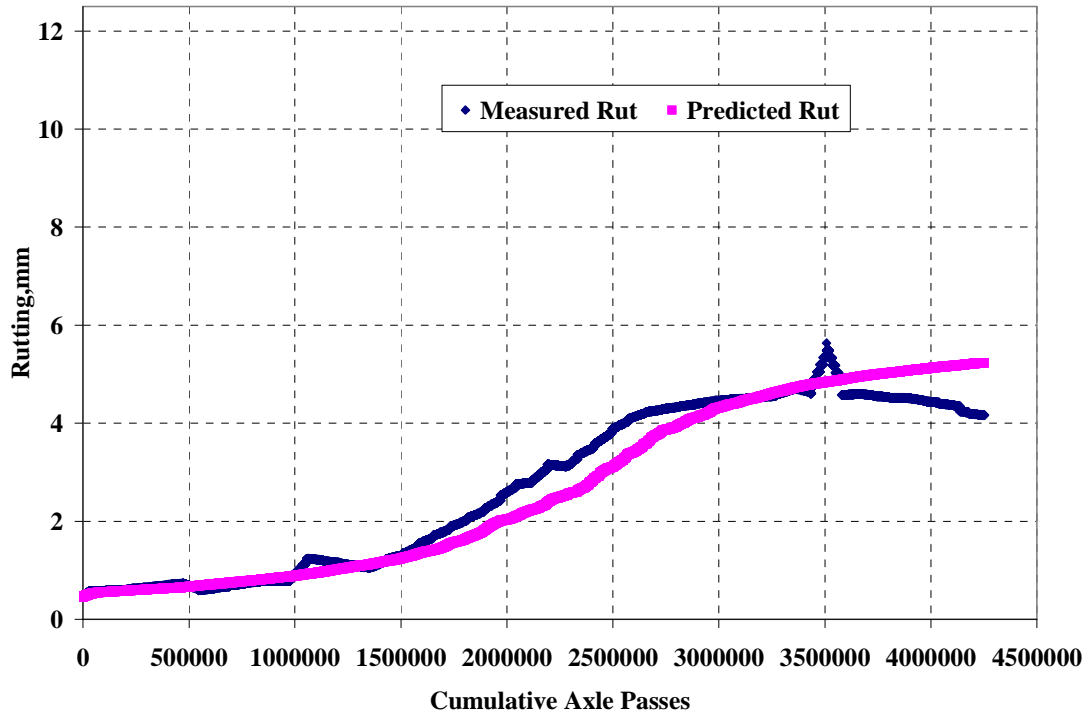


Figure 5.28 Shear Strain Model: Predicted and Measured Rutting for Section N8.

5.7.1 Analysis of Model Coefficients

After determining the coefficients from the non-linear regression, the model coefficients (λ_0, λ_1) were analyzed for their validity. This step was performed to make sure that the developed models did not predict unrealistic rutting. Initially, the model coefficients were analyzed on a section-by-section basis. From Figure 5.29, there appears to be no clear trend in the model coefficients for increasing HMA thickness.

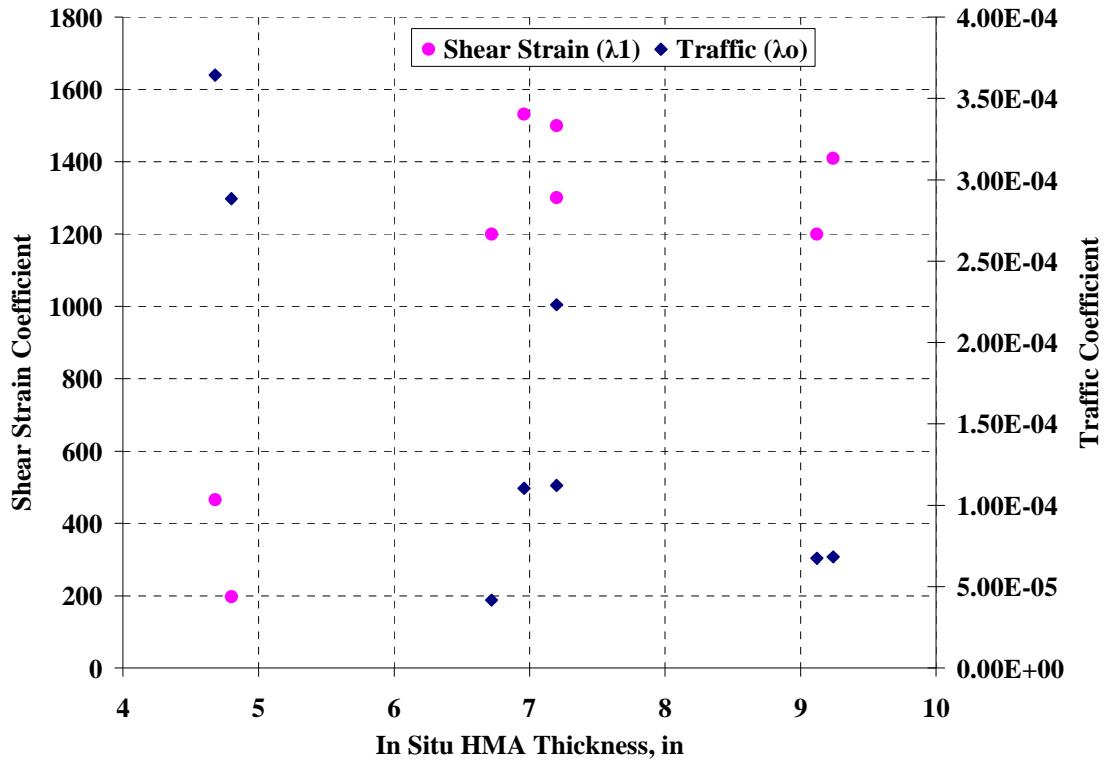


Figure 5.29 HMA Thickness vs Shear Strain Based Rutting Model Coefficients.

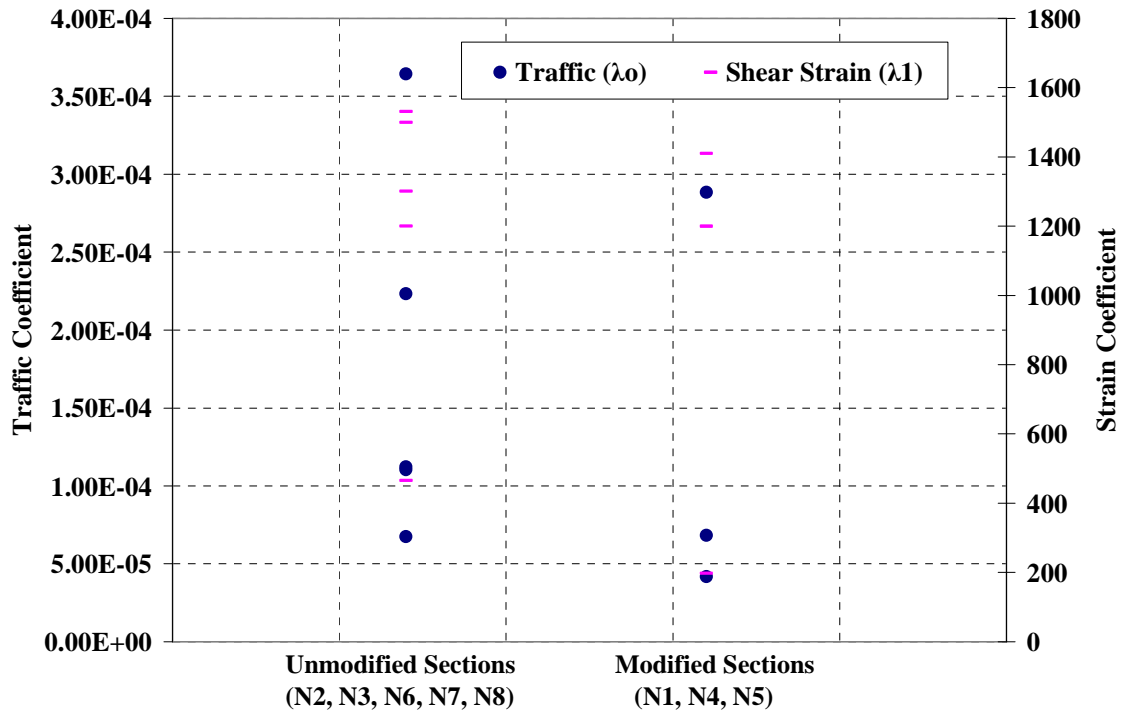


Figure 5.30 Shear Strain Based Model Coefficients for Modified and Unmodified Sections.

From Figure 5.30, there did not appear to be an obvious grouping of coefficients as a function of binder modification. Specifically, when comparing coefficients between paired sections (e.g., N1 vs. N2 or N3 vs. N4) there were no consistent trends in the coefficients (e.g., N1 lower than N2 and N4 lower than N3). Therefore, there was a need to perform further model calibration using one model to predict rutting performance for modified sections and one model for unmodified sections by combining data. However, when comparing coefficients between paired sections (e.g., N1 vs. N2 or N3 vs. N4) there were no consistent trends in the coefficients (e.g., N1 lower than N2 and N4 lower than N3).

5.7.2 Grouped Model Based on Binder Modification

To develop a generalized model by grouping data for rut prediction in modified (N1, N4 and N5) and unmodified sections (N2, N3, N6 and N7), one equation was developed to minimize the error for all sections within the group.

This resulted in two individual models, one to predict rutting in modified sections (Equation 5.8) and the other to predict rutting in unmodified sections (Equation 5.9). The final model forms are:

$$\text{Modified: } Rut_i = Rut_{i-1} + 1.37 \times 10^{-4} N_i^{(242\gamma_i)}; R^2=0.92 \quad (5.8)$$

$$\text{Unmodified: } Rut_i = Rut_{i-1} + 3.05 \times 10^{-4} N_i^{(459\gamma_i)}; R^2=0.80 \quad (5.9)$$

ANOVA test was conducted on the final rut prediction model given in equations 5.8 and 5.9 at a significance level of 5%. The low p-value (p-value = 0.00) showed that both model variables are highly significant in the model.

When the sections were grouped for the shear strain approach, the resulting model predicted rutting reasonably well and closely tracked the measured Test Track rutting as shown in Figures 5.31-5.33.

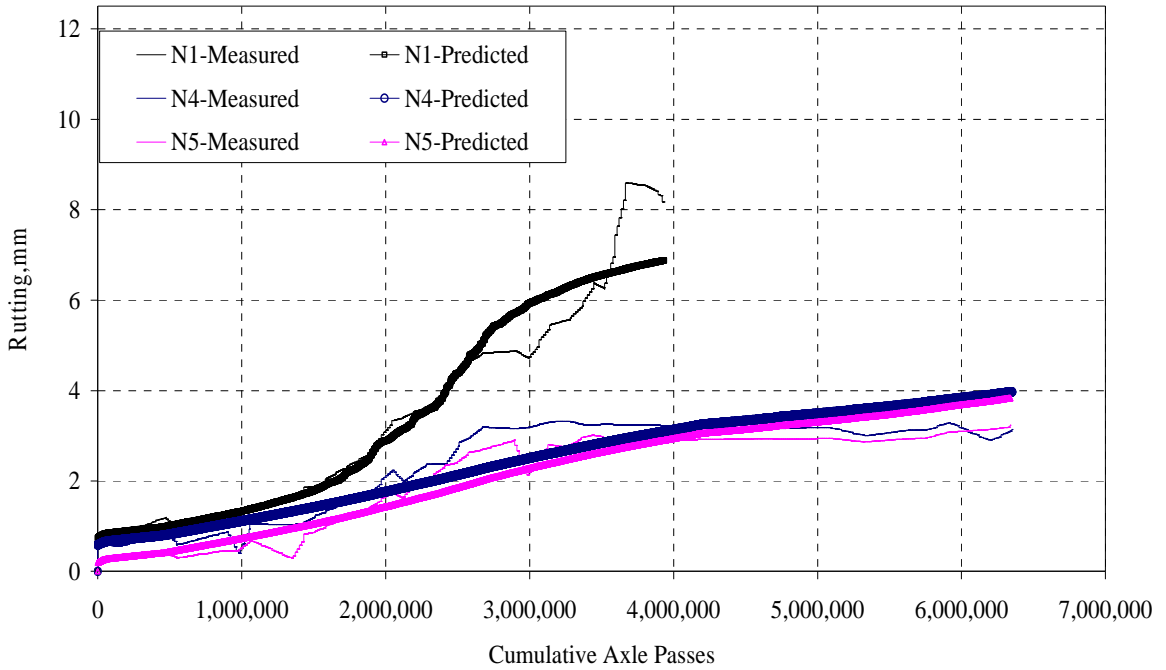


Figure 5.31 Shear Strain: Rut prediction for Modified Sections (N1, N4, N5).

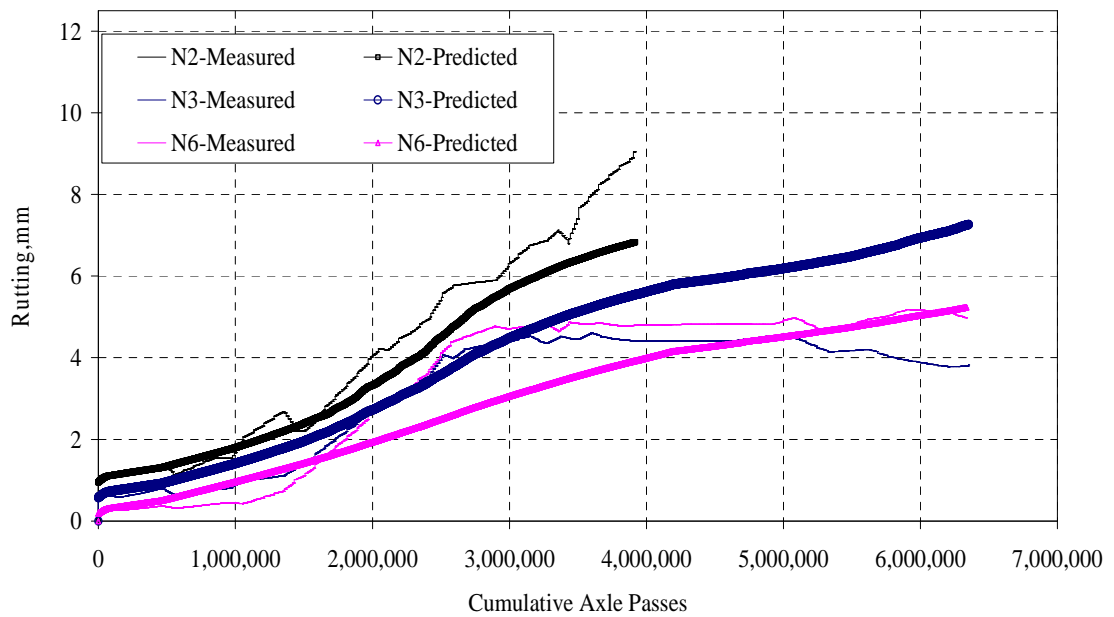


Figure 5.32 Shear Strain: Rut Prediction For Unmodified Sections (N2, N3, N6).

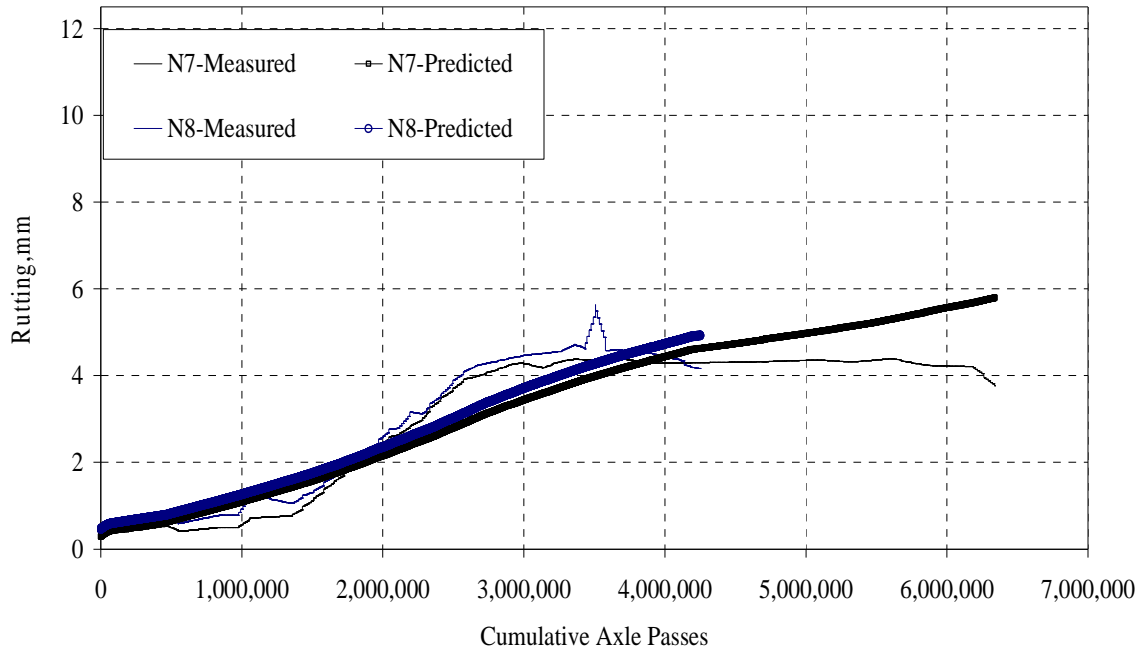


Figure 5.33 Shear Strain: Rut Prediction For SMA Sections (N7 and N8).

It is to be noted that the traffic and shear strain coefficients for the modified model was smaller than the unmodified section model results, which makes sense since less rutting was observed in the modified sections. The generalized models predict rutting with reasonably good accuracy, typically within 1 mm of measured. The two worst cases were N3 and N7 where the model predicted several more mm of rutting than measured. This may be due to testing conditions at the Test Track. When sections N2 and N8 began to show severe fatigue cracking, trucks were forced to veer around these sections. Consequently, the traffic pattern in the adjacent sections (N3 and N7) likely changed as well since the drivers required significant distance to safely make the lane transition. Had the vehicles maintained their original lane placement, the rut depths in sections N3 and N7 could have been greater.

5.8 SUMMARY

In this chapter, the development of a vertical strain based rut prediction model was explained. The model predicted rutting on a section-by-section basis. However the conventional model approach failed to distinguish the field measured rutting between the sections that were differentiated by binder modification. The combined data based on binder modification, failed to yield a sensible model.

After this, an attempt was made to incorporate maximum shear strain response in HMA layer into the model rather than vertical strain. An effort was made to validate the lab proven concept on the use of shear strain to predict HMA rutting was done successfully with the help of field data. This new approach predicted rutting in individual sections. When the data were grouped to reflect the field measured rutting, it resulted in two different models, one to predict rutting in modified binder sections and another to predict rutting in unmodified sections.

Though, it will be highly advantageous to include construction variables such as air voids, asphalt content in the developed model to predict field rutting, this present study was not designed to include those variables, since the test sections were built to study two important variables, HMA thickness and binder modification. All other variables were kept constant between test sections in this research cycle.

CHAPTER 6

CONCLUSIONS AND RECOMMENDATIONS

6.1 CONCLUSIONS

Accurate prediction of pavement rutting and an accurate load response model are critical for an efficient M-E pavement design. The conclusions of this research to address these two main components of M-E design are given below. The limitations and recommendations for further study are also presented. To fulfill the first objective of this research effort, the load response model was validated with respect to field measured pavement response. Then, a fully field calibrated M-E based rut prediction model was built to accomplish the second objective.

Regarding the load response model validation, the following conclusions were made:

1. From the results obtained, layered elastic analysis is a reasonable approximation of actual pavement responses under dynamic wheel loads. In general, the results from layered elastic back and forward-calculation compared well with measured pavement responses obtained from the NCAT Test Track data. Since the use of layered elastic analysis approach was validated successfully with respect to field responses, this model can be used to compute pavement responses with more confidence in the M-E design approach.

2. The weekly dynamic response data collection efforts were proven to be sufficient to develop dynamic response prediction models (in terms of pressure) which can predict vertical pressure at any time of a day.
3. It was shown in this study that three passes of each test vehicle was sufficient enough to get the maximum pavement response. To capture maximum pressure response and to get full range of variability, it is suggested to continue recording three passes in future test cycles.
4. Though the FWD data collection efforts by ALDOT personnel were satisfactory to establish links between temperature and layer modulus, more FWD data at varying pavement temperatures before the pavement experiences any distress would result in a very accurate material characterization. So it is suggested to collect more FWD data at frequent intervals in future research cycles.

Below are the conclusions regarding the development of rut prediction model from this study:

1. Both the vertical strain and shear strain approaches could accurately predict rutting on a section-by-section basis. However, the vertical strain approach could not accurately predict rutting when sections were grouped according to binder modification.
2. The shear strain approach accurately predicted field rutting when sections were grouped according to binder modification. The final suggested models to predict HMA rutting in modified and unmodified binder sections are:

For modified pavement sections;

$$Rut_i = Rut_{i-1} + 1.37 \times 10^{-4} N_i^{(242\gamma_i)}$$

For unmodified pavement sections;

$$Rut_i = Rut_{i-1} + 3.05 \times 10^{-4} N_i^{(459\gamma_i)}$$

Where,

Rut_i = Rutting at time 'i'

Rut_{i-1} = Rutting at time 'i-1'

N_i = Total number of axle passes at time 'i'

γ_i = shear strain in HMA calculated at time 'i' from the shear strain prediction model

3. Distinguishable difference in rut performance was observed between modified and unmodified binder sections. Modified binder sections had less rutting when compared with unmodified sections.
4. The developed model was entirely from field data. This shear strain approach to model HMA rutting can be readily incorporated into the M-E design after performing additional field verification studies.
5. As theorized by laboratory rut-performance tests such as the Asphalt Pavement Analyzer, mixes exhibiting higher shear resistance should perform better in terms of HMA rutting. From this study, it was concluded that shear strain in the HMA layer can be successfully used to predict surface rutting. The laboratory derived shear strain approach developed by researchers to predict HMA rutting was proved with a large set of field data in this research.

6.2 LIMITATIONS AND RECOMMENDATIONS

Given the above conclusions, there are some limitations and recommendations to be made:

1. Though the approach adopted in this study to account for pressure response for a single truck pass instead of considering each truck axle separately, is valid on an engineering standpoint, for more accurate analysis capturing each axle response is recommended. In the 2003 test cycle, there was no way to capture the exact location of each axle pass with respect to the instrumentation array. In future test cycles, advanced methods such as installing axle sending strips immediately before and after the instrumentation array and use of non-contact lasers to capture exact location of each axle need to be explored
2. The layered elastic model was validated for southeast climatic regions. However, when the pavement experiences higher pressure, which results from higher pavement temperature, some deviations were observed between predicted and measured responses in this study. While keeping this in mind, for other climatic regions where higher temperatures are expected for a longer duration, the layer elastic model needs to be validated and if required an advanced model that can account for non-linearity of pavement materials at higher pressures is recommended.

3. The shear strain based rut prediction model is applicable only when HMA layer rutting is the leading source of pavement rutting. In practice, where rutting is seen in other underlying layers, it may be necessary to use a shear strain model in conjunction with vertical strain models in underlying layers to completely capture total rutting.
4. The M-E based field-calibrated rut model was developed from a limited number of test sections. Further refinement of the model with more test sections with different layer configuration and material properties is suggested. A large data set exists from the 2000 Test Track research cycle. It is suggested that the shear strain approach be applied to those sections for validation purposes. The same approach can be used to predict HMA layer rutting in the 2006 Test Track research cycle and the result can be compared with field results in future.
5. The FWD backcalculated modulus used to calculate pavement responses does not differentiate between various lift thickness in the HMA layer and each lift thickness may contain different mix components. Since HMA rutting was visible in the topmost layer, it is recommended to explore various possibilities to accurately measure different lift layer modulus from the field in future.

6. It is recommended to expand the rut prediction capabilities of the developed model to include the effects of change in asphalt content, air voids and other related mix criteria. This can be done by building more sections with more experimental variables such as varying asphalt content, air voids, change in aggregate gradation and compaction efforts and developing rut prediction models as per the model development procedure followed in this study. It should be noted that the research efforts presented in this dissertation had only two primary experimental variables, HMA thickness and binder modification.
7. It should be noted that the rutting model this study was based upon moderate climate conditions in East-Central Alabama. Therefore, the model should not be applied to low temperature regions where the pavement temperature goes below 20°F and at very high temperature regions where the pavement temperature often goes above 110°F. Calibration for low, high temperature regions and further validation of this shear strain based rut prediction model is recommended.

REFERENCES

1. Ali, H.A., Tayabji, S.D., and Torre, F.L., “Calibration of Mechanistic-Empirical Rutting Model for In-Service Pavements”, Transportation Research Record 1629, 1998, pg 159-168.
2. Allen, D., Deen, R.C., “Rutting Models for Asphaltic Concrete and Dense Graded Aggregate from Repeated Load Tests”, Proceedings of the Association of Asphalt Paving Technologists, Louisville, Kentucky 1980
3. Al-Qadi, I. L., Elseifi, M. and Yoo, P.J., “In-Situ Validation of Mechanistic Pavement Finite Element Modeling,” Proceedings of the 2nd International Conference on Pavement Accelerated Facilities, Minneapolis, Minnesota, 2004.
4. Alvarez, C. and M.R. Thompson. “Mechanistic-Empirical Evaluation of the Mn/Road Mainline Flexible Pavement Sections,” Project IHR-535, Illinois Cooperative Highway and Transportation Research Program, University of Illinois, Urbana, IL, 1998.
5. Archilla, A.R., and Madanat, S., “Statistical Model of Pavement Rutting in Asphalt Concrete Mixes”, Transportation Research Record 1764, 2001, pp. 70-77.

6. Austroads 2001., “A Guide to the Design of Road Pavements (Final Draft): An Austroads publication”, New South Wales, Australia, 2001.
7. Bao, W., “Calibration of Flexible Pavements Structural Model Using Mn/Road Data”, Published M.S thesis, University of Minnesota, Minnesota, 2000.
8. Barenberg, E.J., and Zollinger, D.G., “Validation of Concrete Pavement Responses Using Instrumented Pavements”, Transportation Research Record 1286, TRB, National Research Council, Washington D.C., 1990, pp. 67-77.
9. Barksdale, R. D.,”Laboratory Evaluation of Rutting in Base Course Materials” Proceedings of the Third International Conference on the Structural Design of Asphalt Pavements, London, 1972.
10. Barrett, W.E. and Timm, D.H., “Theoretical vs Measured Pavement Responses Under Dynamic Loading,” 7th International Conference on the Bearing Capacity of Roads, Railways and Airfields, Trondheim, Norway, 2005.
11. Battiato, G., Ronca, G., Verga, C., “Moving Loads on a Viscoelastic Double Layer: Prediction of Recoverable and Permanent Deformations” Proceedings of the Third International Conference on the Structural Design of Asphalt Pavements, London, 1977.
12. Bissada, A.F., Hamdanl, S.K., Guirguis, H.R., “Design Criteria of Asphalt Pavement Structures at High Service Temperatures”, Proceedings of the Fifth International Conference on the Structural Design of Asphalt Pavements, Michigan, USA, 1982, pp. 142-155.

13. Blab, R., and Harvey, J.T., “Viscoelastic Rutting Model with Improved Loading Assumptions”, Proceedings of the Ninth International Conference on the Structural Design of Asphalt Pavements, Copenhagen, Denmark, 2002.
14. Brown, E. R., Cooley, L. A., Hanson, D., Lynn, C., Powell, R. B., Prowell, B., and D. Watson., “NCAT Test Track Design, Construction, and Performance”, NCAT Report 02-12, National Center for Asphalt Technology, 2002.
15. Brown, E.R., Prowell. B., Cooley, A., Zhang, J., and Powell, R.B., “Evaluation of Rutting on the 2000 NCAT Test Track”, Journal of Association of Asphalt Paving Technologists. Vol. 73, 2004, pp. 287-336
16. Brown, S.F., and Bell, C.A., “The Prediction of Permanent Deformation in Asphalt Pavements” Proceedings of the Association of Asphalt Paving Technologists, Volume 48, 1979, pp. 438-476.
17. Chadbourn, Bruce A., Newcomb D.E., and Timm, D.H., “Measured and Theoretical Comparisons of Traffic Loads and Pavement Response Distributions,” Proceedings of the Eighth International Conference on Asphalt Pavements, Seattle, WA, 1997, pp. 229-238.
18. Chen, D.H., Bilyeu, J., Scullion, T., Lin D.F., and Zhou, F., “Forensic Evaluation of Premature Failures of Texas Specific Pavement Study-1 Sections”, Journal of Performance of Constructed Facilities, ASCE, 2003, pp. 67-74.

19. Claessen, A., Edwards, J. M., Sommer, P., Uge P., “Asphalt Pavement Design - The Shell Method”, Proceedings of the Fourth International Conference on the Structural Design of Asphalt Pavements, Michigan, USA, 1977, pp. 39-72
20. Das, A., “Some suggestions to improve the Mechanistic-Empirical bituminous pavement design in Indian context”, Proceedings of 1st International Symposium on Design and Construction of Long Lasting Asphalt Pavements, Auburn, 2004, pp.199-215.
21. Dawley, C.B., Hogenwiede, B.L., and Anderson, K.O., “Mitigation of Instability Rutting of Asphalt Concrete Pavements in Lethbridge, Alberta, Canada”, Journal of Association of Asphalt Paving Technologists. Vol. 59, 1990, pp. 481-508.
22. Dormon, G.M., “The Extension to Practice of a Fundamental Procedure for the Design of Flexible Pavements”, Proceedings of the First International Conference on the Structural Design of Asphalt Pavements, Ann Arbor, Michigan, USA, 1962, pp. 785-793.
23. Dormon, G.M., and Edwards, J.M., “Developments in the Application in Practice of a Fundamental Procedure for the Design of Flexible Pavements”, Proceedings of the Second International Conference on the Structural Design of Asphalt Pavements, Ann Arbor, Michigan, 1967, pp. 99-108.
24. Drakos, C.A., Roque, R., and Birgisson, B., “Effect of Measured Tire Contact Stresses on near Surface Rutting”, Journal of the Transportation Research Board, TRR 1764, Washington DC, 2001, pp. 59-69.

25. El-Basyouny, M.M., Witczak, M., and Kaloush, K., “Development of the Permanent Deformation Models for the 2002 Design Guide”, 84th Annual Meeting of the Transportation Research Board, Available in TRB 2005 Annual Meeting CD-ROM., 2005.
26. El-Basyouny, M.M., Witczak, M.W., El-Badawy, S., “Verification for the Calibrated Permanent Deformation Models for the 2002 Design Guide” Journal of the Association of Asphalt Paving Technologies, Volume 74, 2005, pp. 601-652.
27. Elseifi, M.A., Al-Qadi, I.L., and Yoo, P.J, “Viscoelastic Modeling and Field Validation of Flexible Pavements”, Journal of Engineering Mechanics, ASCE, 2006,pp. 172-178.
28. Epps, A., Walubita, L.F., and Bangera, N.U., “Pavement Response and Rutting for Full-Scale and scaled APT”, Journal of Transportation Engineering, ASCE, 2003, p.p. 451-461.
29. Epps, J., Monismith, C.L., Seeds, S.B., Ashmore, S.C., Mitchell T.M., “Westrack Full-Scale Test Track: Interim Findings:1997” Accessed online on June 14, 2006, <http://www.westrack.com/isap.pdf>.
30. Epps, J.A., A. Hand, S. Seeds, T. Schulz, S. Alavi, C. Ashmore, C.L. Monismith, J.A. Deacon, J.T. Harvey, R. Leahy, “Recommended Performance-Related Specification for Hot-Mix Asphalt Construction: Results of the Westrack Project” NCHRP Report 455, Transportation Research Board, National Research Council, 2002.

31. ERES Consultants Division, "Guide for Mechanistic-Empirical Pavement Design of New and Rehabilitated Pavement Structures", Final Report, NCHRP 1-37A, 2004.
32. Fang, H., Haddock, J.E., White, T.D and Hand, A.J., "On the Characterization of Flexible Pavement Rutting Using Creep Model Based Finite Element Analysis", *Finite Elements in Analysis and Design* 41 (2004), 49-73, Also available online at www.sciencedirect.com.
33. FHWA, Lead States Group, Available online, <http://www.fhwa.dot.gov/pavement/dgit/leadstates/>, Accessed on May 31, 2006.
34. Finn, F., Saraf, C., Kulkarni, R., Nair, K., Smith, W., Abdullah, A., "The Use of Distress Prediction Subsystems for the Design of Pavement Structures", *Proceedings of the Fourth International Conference on the Structural Design of Asphalt Pavements*, Michigan, USA, 1977, pp. 3-37
35. Fwa, T.F., Tan, S.A., Zhu, L.y., "Rutting Prediction of Asphalt Pavement Layer Using C- Φ Model", *Journal of Transportation Engineering*, ASCE, 2004, pp. 675-683.
36. Geokon, "Instrumentation Manual Model 3500/3510 Earth Pressure Cells," 2006.
37. Goetz, W., McLaughlin, J., and Wood, L., "Load Deformation Characteristics of Bituminous Mixtures Under Various Conditions of Loading", *Proceedings of Association of Asphalt Paving Technologists*, Volume 26, 1957.

38. Gokhale, S., Choubane, B., Byron, T., Tia, M., “Rut Initiation Mechanisms in Asphalt Mixtures as Generated Under Accelerated Pavement Testing”, Transportation Research Record 1940, 2005, pp. 136-145.
39. Gusfeldt, K.H., and Dempwolff, K.R., Deutsche Shell, A.G., and Wilhelmsburg., “Stress and Strain Measurements in Experimental Road Sections Under Controlled Loading Conditions”, Proceedings of the Second International Conference on the Structural Design of Asphalt Pavements, Ann Arbor, Michigan, 1967, 1967, pp. 663-669
40. Hajek, J.J., Smith, K.L., Rao, S.P, and Darter, M.I., “Adaptation and Verification of AASHTO Pavement Design Guide for Ontario Conditions”, Ontario Ministry of Transportation report MI-183, 2001.
41. Hand, A. J., Epps, J. A., and P. E. Sebaaly, .Development of APT Based Permanent Deformation Prediction Models Translatable to Other Environments., Accelerated Pavement Testing International Conference, Reno, NV, 1999.
42. Harvey, J., and Popescu, L., “Accelerated Pavement Testing of Rutting Performance of Two Caltrans Overlay Strategies”, Transportation Research Record 1716, Paper No 00-0427, 2000, pp. 116-125.
43. Hicks, R.G., and Finn, F.N., “Analysis of Results from the Dynamic Measurements Program on the San Diego Test Road”, Proceedings of the Association of Asphalt Paving Technologists, Volume 39, 1970, pp. 153-185.
44. Hildebrand, G., “Verification of Flexible Pavement Response from a Field Test”, Danish Road Institute, Report 121, 2002.

45. Hornych, P., Kerzreho, J.P., and Salasca, S., “Prediction of the Behaviour of a Flexible Pavement Using Finite Element Analysis with Non-Linear Elastic and Visco-Elastic Models”, Proceedings of the Ninth International Conference on the Structural Design of Asphalt Pavements, Copenhagen, Denmark, 2002.
46. HRB, “The AASHO Road Test”, Report 5, Pavement Research Special Report 61E, National Academy of Sciences – National Research Council, Washington DC, 1962.
47. Huang, Y.H., “Pavement Analysis and Design” Second Edition, Prentice Hall, NJ, 2004.
48. Huang, Y.H., “Stresses and Displacements in Viscoelastic Layered Systems under Circular Loaded Areas” Proceedings of the Second International Conference on the Structural Design of Asphalt Pavements, Ann Arbor, Michigan, 1967, pp. 225-244
49. Hugo, F., and Epps, A., “Significant Findings from Full-Scale Accelerated Pavement Testing” NCHRP 325 Synthesis 325, Transportation Research Board, Washington D.C, 2004.
50. Immanuel, S. S., and D. H. Timm. Measured and Theoretical Pressures in Base and Subgrade Layers under Dynamic Truck Loading. Proceedings of Airport and Highway Specialty Conference, American Society of Civil Engineers, Atlanta, GA, 2006, pp 155-166.
51. Immanuel, S.S., “Performance Study of Bituminous Mixes under Different Testing Temperatures in Laboratory Conditions” M.E thesis, Anna University, Chennai, India. 2003.

52. Immanuel, S.S., "Performance Study of Bituminous Mixes under Different Testing Temperatures in Laboratory Conditions" M.E thesis, Anna University, Chennai, India, 2004.
53. Ioannides, A.M., "Full Mechanistic performance modeling: a contradiction of terms?" Proceedings of the Seventh International Conference on the Structural Design of Asphalt Pavements, Nottingham, UK, 1992.
54. Kenis, W.J., "Predictive Design Procedures - A Design Method for Flexible Pavements Using the VESYS Structural Subsystem", Proceedings of the Fourth International Conference on the Structural Design of Asphalt Pavements, Michigan, 1977, pp. 101-130.
55. Kim, H.B., Buch, N., Park, D.Y., "Mechanistic-Empirical Rut Prediction Model for In-Service Pavements", Transportation Research Record 1730, Paper no. 00-0165, 2000, pp. 99-109.
56. Kirwan, R.W., Snaith, M,N, Glynn, T.E., "A Computer Based Subsystem for the Prediction of Pavement Deformation" Proceedings of the Third International Conference on the Structural Design of Asphalt Pavements, London, 1977.
57. Klomp, A. I. G., and TH. W. Niesman, Koninklijk, "Observed and Calculated Strains at Various Depths in Asphalt Pavements", Proceedings of the Second International Conference on the Structural Design of Asphalt Pavements, Ann Arbor, Michigan, 1967, pp. 671-685.

58. Krukar, M., and Cook, J.C., “Practical Design Applications on Washington State University Test Track Results”, Proceedings of the Third International Conference on the Structural Design of Asphalt Pavements, London, UK, 1972, pp. 866-875.
59. Leahy, R. B., “Permanent Deformation Characteristics of Asphalt Concrete”, Ph.D. Dissertation, University of Maryland, College Park, Maryland, 1989.
60. Long, F.M., “Permanent Deformation of Asphalt Concrete Pavements: A Nonlinear Viscoelastic Approach to Mix Analysis and Design” PhD Dissertation, University of California, Berkeley, California, 2001.
61. LTPP, “Distress Identification Manual for the Long-Term Pavement Performance Program”, Fourth Revised Edition FHWA-RD-03-031, 2003.
62. Maccarrone, S., Ky, A.V., Gnanaseelan, G.P., “Permanent Deformation and Fatigue Properties of Polymer Modified Asphalt Mixes” Proceedings of the Eighth International Conference on Asphalt Pavements, Seattle, WA, 1997, pp. 1545-1554.
63. Madanat, S.M., Prozzi, J. A., and Han, M., “Effects Of Performance Model Accuracy On Optimal Performance Design”, Journal of Computer-Aided Civil and Infrastructure Engineering, No. 17, 2002, pp. 22-30.
64. Meyer, F.R., Hass, R.C., “A Working Design Subsystem for Permanent Deformation in Asphalt Pavements” Proceedings of the Third International Conference on the Structural Design of Asphalt Pavements, London, 1977.

65. Monismith, C.L., “Analytically Based Asphalt Pavement Design and Rehabilitation: Theory to Practice, 1962-192”, Transportation Research Record 1354, 1992, pp. 5-26.
66. Monismith, C.L., “Evolution of Long Lasting Asphalt Design Methodology: A Perspective”, Distinguished lecture, presented at International Symposium on Design and Construction of Long Lasting Asphalt Pavements, Auburn University, Alabama, 2004.
67. Monismith, C.L., Finn, F., “Distortion mode of distress for asphalt pavements: Moderators summary report of papers presented for discussion at session III – Design theory”, Proceedings of the Third International Conference on the Structural Design of Asphalt Pavements, London.
68. Newcomb D.E., and Von Quintus, H., “Wanted Transfer Functions- Experience Needed”, Hot Mix Asphalt Technology, December, 2002.
69. Nijboer, L.W., “Testing Flexible Pavements Under Normal Traffic Loadings by Means of Measuring Some Physical Quantities Related to Design Theories”, Proceedings of the Second International Conference on the Structural Design of Asphalt Pavements, Ann Arbor, Michigan, 1967, pp. 689-705.
70. Park, D.W., “Characterization of permanent deformation in asphalt concrete using a laboratory prediction method and an elastic visco plastic model”, PhD Dissertation, Texas A&M University, College Station, Texas, 2004.

71. Peattie, K.R., "A Fundamental Approach to the Design of Flexible Pavements", Proceedings of the First International Conference on the Structural Design of Asphalt Pavements, Ann Arbor, Michigan, 1962.
72. Pister, K.S., Westmann, R.A., "Analysis of Visco-elastic pavements subjected to moving loads", Proceedings of the First International Conference on the Structural Design of Asphalt Pavements, Ann Arbor, Michigan, USA, 1962, pp. 522-529.
73. Powell, R. B., "As-Built Properties of Experimental Sections on the 2000 NCAT Pavement Test Track", NCAT Report 01-02, National Center for Asphalt Technology, Auburn, 2002.
74. Powell., B., "Predicting Field Performance on the NCAT Pavement Test Track" PhD Dissertation, Auburn University, Auburn, 2006.
75. Priest, A.L., "Calibration of Fatigue Transfer Functions for Mechanistic-Empirical Flexible Pavement Design." M.S thesis, Auburn University, Auburn, Alabama, 2005.
76. Priest, A.L., and Timm, D. H., "Methodology and Calibration of Fatigue Transfer Functions for Mechanistic-Empirical Flexible Pavement Design", Publication NCAT 06-03. National Center for Asphalt Technology, Auburn University, Auburn, Alabama, 2006.
77. Romain, J.E., "Rut Depth Prediction in Asphalt Pavements", Proceedings of the Third International Conference on the Structural Design of Asphalt Pavements, London, UK, 1972, pp. 705-710.

78. Ros, J., Pronk, A.C., Eikelboom, J., “The Performance of Highway Pavements in the Netherlands and the Application of Linear Elasticity Theory to Pavement Design”, Proceedings of the Fifth International Conference on the Structural Design of Asphalt Pavements, Michigan, 1982, pp. 285-302.
79. Seeds, S.B., “Flexible Pavement Design; Summary of the State of the Art”, A2B03 Committee on Flexible Pavement Design Millennium paper, TRB, Washington DC, 2000.
80. Shook, J.E., Finn, F.N., Witczak, M.W., Monismith, C.L., “Thickness Design of Asphalt Pavements - The Asphalt Institute Methods”, Proceedings of the Fifth International Conference on the Structural Design of Asphalt Pavements, Michigan, USA, 1982, pp. 17-44.
81. Siddharthan, R.V., Sebaaly, P.E., El-Desouky, M.M., and El-Mousl, M., “Development and Validation of a Pavement Response Evaluation Model”, Proceedings of the Ninth International Conference on the Structural Design of Asphalt Pavements, Copenhagen, Denmark, 2002.
82. Skok, E.L., and Finn, F.N., “Theoretical Concepts Applied to Asphalt Concrete Pavement Design”, Proceedings of the First International Conference on the Structural Design of Asphalt Pavements, Ann Arbor, Michigan, 1962, pp. 412-440.
83. Sousa, J. B., Craus, J., and C. L. Monismith., “Summary Report on Permanent Deformation in Asphalt Concrete”, Report SHRP-A/IR-91-104, Strategic Highway Research Program, National Research Council, Washington, DC, 1991.

84. Sousa, J. B., Weissman, S., Sackman, J., Monismith, C. L., “A Nonlinear Elastic Viscous with Damage Model to Predict Permanent Deformation of Asphalt Concrete Mixtures.” TRR 1384, Transportation Research Board, National Research Council, Washington D.C., 1993, pp 80-93.
85. Sousa, J., and Monismith, C.L., “Permanent deformation response of asphalt aggregate mixes.” SHRP-A-415, Strategic Highway Research Program, National Research Council, Washington, D.C, 1993.
86. Southgate, H.F., and Deen, R.C., “Flexible Pavement Designs Based on Work”, Journal of Association of Asphalt Paving Technologists. Vol. 57, 1988, pp. 389-413.
87. Sukumaran, B., Mike Willis and Nishanth Chamala, “Three-dimensional finite element analysis of flexible pavements,” FAA Worldwide Airport Technology Conference, Atlantic, New Jersey, 2004.
88. Terrel, R.L., and Krukar, M., “Evaluation of Test Tracking Pavements”, Proceedings of the Association of Asphalt Paving Technologists, Volume 39, 1970, pp. 273-296.
89. Theyse, H L., De Beer, M. and Rust, F. C., “Overview of South African Mechanistic Pavement Design Method,” Transportation Research Record, No. 1539, Transportation Research Board, 1996, pp. 6 – 17.
90. Theyse, H.L., Hoover, T.P., Harvey, J.T., Monismith, C.L., and Coetzee, N.F., “A Mechanistic-Empirical Subgrade Design Model Based on Heavy Vehicle Simulator Test Results” Pavement Mechanics and Performance, Geotechnical Special Publication No. 154, China, 2006.

91. Thompson, M.R., and Nauman, D., “Rutting Rate Analysis of the AASHTO Road Test Flexible Pavements”, Transportation Research Record 1384, 1993, pp. 36-48.
92. Thrower, E.N., “Methods of Predicting Deformation in Road Pavements” Proceedings of the Third International Conference on the Structural Design of Asphalt Pavements, London, 1977.
93. Thrower, E.N., Lister, N.W., and Potter, J.E., “Experimental and Theoretical Studies of Pavement Behavior Under Vehicular Loading in Relation to Elastic Theory”, Proceedings of the Third International Conference on the Structural Design of Asphalt Pavements, London, UK, 1972, pp. 521-535.
94. Timm, D. H., and Priest, A.L., “Wheel Wander at the NCAT Test Track”, NCAT Report 05-02. National Center for Asphalt Technology, Auburn University, Auburn, Alabama, 2005.
95. Timm, D.H., Birgisson, B., Newcomb, D.E., “Development of Mechanistic-Empirical Pavement Design in Minnesota”, Transportation Research Record 1629, Paper No 98-0365, 1998, pp. 181-188.
96. Timm, D.H., and Newcomb, D.E., “Calibration of Flexible Pavement Performance Equations for Minnesota Road Research Project”, Transportation Research Record 1853, Paper No 03-2012, 2003, p.p 134-142.
97. Timm, D.H., and Priest, A.L., “Material Properties of the 2003 NCAT Test Track Structural Study” Report No. 06-01, National Center for Asphalt Technology, Auburn University, Alabama, 2006.

98. Timm, D.H., Priest, A.L., McEwen, T.V., "Design and Instrumentation of the Structural Experiment at the NCAT Test Track." Report No. 04-01, National Center for Asphalt Technology, Auburn University, Alabama, 2004.
99. Ullidtz, P., "Deterioration Models for Managing Flexible Pavements", Transportation Research Record 1655, Paper no 99-0039, 1999, pp. 31-34.
100. Ullidtz, P., "Analytical Tools for Design of Flexible Pavements", Keynote Address delivered at the 8th ISAP Conference held in Copenhagen, 2002.
101. Waterhouse, A., "Stresses in Layered Systems under Static and Dynamic Loading", Proceedings of the Second International Conference on the Structural Design of Asphalt Pavements, Ann Arbor, Michigan, USA, 1967, pp. 291-308.
102. Whiffin, A.C., Lister, N.W., "The Application of Elastic Theory to flexible Pavements", Proceedings of the First International Conference on the Structural Design of Asphalt Pavements, Ann Arbor, Michigan, 1962, pp. 499-521.
103. WSDOT, 2003. "Washington State Pavement Design Guide", Available online, <http://training.ce.washington.edu/WSDOT/>, Accessed on May 30, 2006.
104. Yoo, P.j., and Al-Qadi, I.L., "Effect of Transient Dynamic Loading on Flexible Pavements", Paper available in 86th Annual TRB Meeting CD-ROM. Washington DC., 2007.

105. Zhou, F., Scullion, T., “Discussion: Three Stages of Permanent Deformation Curve and Rutting Model”, *International Journal of Pavement Engineering*, Volume 3, Number 4, 2002, pp. 251-260.
106. Zhou, F., Scullion, T., and Sun, L., “Verification and Modeling of Three-Stage Permanent Deformation Behavior of Asphalt Mixes”, *Journal of Transportation Engineering*, ASCE, 2004, pp. 486-494.

APPENDIX
PRESSURE PREDICTION MODEL STATISTICS

TRIPLE TRAILER

SUMMARY OUTPUT (Modified Base-Triple)

<i>Regression Statistics</i>	
Multiple R	0.8579
R Square	0.7360
Adjusted R Square	0.7312
Standard Error	1.1972
Observations	113

ANOVA					
	<i>df</i>	<i>SS</i>	<i>MS</i>	<i>F</i>	<i>Significance F</i>
Regression	2	439.6044	219.8022	153.3436	0.0000
Residual	110	157.6736	1.4334		
Total	112	597.2780			

	<i>Coefficients</i>	<i>Standard Error</i>	<i>t Stat</i>	<i>P-value</i>	<i>Lower 95%</i>
Intercept	2.7494	0.4418	6.2229	0.0000	1.8738
Temp^2	0.0007	0.0000	17.3843	0.0000	0.0006
Thick^2	-0.0145	0.0053	-2.7346	0.0073	-0.0250

SUMMARY OUTPUT (Unmodified Base-Triple)

<i>Regression Statistics</i>	
Multiple R	0.9266
R Square	0.8587
Adjusted R Square	0.8559
Standard Error	0.7672
Observations	107.0000

ANOVA

	<i>df</i>	<i>SS</i>	<i>MS</i>	<i>F</i>	<i>Significance F</i>
Regression	2	371.8964	185.9482	315.9017	0.0000
Residual	104	61.2172	0.5886		
Total	106	433.1135			

	<i>Coefficients</i>	<i>Standard Error</i>	<i>t Stat</i>	<i>P-value</i>	<i>Lower 95%</i>
Intercept	3.3802	0.3835	8.8133	0.0000	2.6196
Temp^2	0.0006	0.0000	25.0173	0.0000	0.0006
Thick^2	-0.0085	0.0048	-1.7807	0.0779	-0.0180

SUMMARY OUTPUT (SMA Base-Triple)

<i>Regression Statistics</i>	
Multiple R	0.8373
R Square	0.7011
Adjusted R Square	0.6947
Standard Error	1.2978
Observations	49

ANOVA					
	<i>df</i>	<i>SS</i>	<i>MS</i>	<i>F</i>	<i>Significance F</i>
Regression	1	185.6650	185.6650	110.2264	0.0000
Residual	47	79.1666	1.6844		
Total	48	264.8316			

	<i>Coefficients</i>	<i>Standard Error</i>	<i>t Stat</i>	<i>P-value</i>	<i>Lower 95%</i>	<i>Upper 95%</i>
Intercept	1.2819	0.5543	2.3127	0.0252	0.1668	2.3970
Temp^2	0.0007	0.0001	10.4989	0.0000	0.0006	0.0009

SUMMARY OUTPUT (Modified Subgrade-Triple)

<i>Regression Statistics</i>	
Multiple R	0.8752
R Square	0.7660
Adjusted R Square	0.7607
Standard Error	0.6212
Observations	90

ANOVA					
	<i>df</i>	<i>SS</i>	<i>MS</i>	<i>F</i>	<i>Significance F</i>
Regression	2	109.9411	54.9706	142.4349	0.0000
Residual	87	33.5763	0.3859		
Total	89	143.5174			

	<i>Coefficients</i>	<i>Standard Error</i>	<i>t Stat</i>	<i>P-value</i>	<i>Lower 95%</i>
Intercept	3.86E+00	2.77E-01	1.39E+01	7.74E-24	3.31E+00
Temp^2	3.44E-04	2.47E-05	1.39E+01	8.44E-24	2.95E-04
Thick^2	-3.33E-02	3.20E-03	1.04E+01	6.07E-17	-3.97E-02

SUMMARY OUTPUT (Unmodified Subgrade-Triple)

<i>Regression Statistics</i>	
Multiple R	0.9571
R Square	0.9161
Adjusted R Square	0.9145
Standard Error	0.5812
Observations	114

ANOVA					
	<i>df</i>	<i>SS</i>	<i>MS</i>	<i>F</i>	<i>Significance F</i>
Regression	2	409.1036	204.5518	605.6522	0.0000
Residual	111	37.4889	0.3377		
Total	113	446.5926			

	<i>Coefficients</i>	<i>Standard Error</i>	<i>t Stat</i>	<i>P-value</i>	<i>Lower 95%</i>
Intercept	4.2108	0.2075	20.2943	0.0000	3.7996
Temp^2	0.0006	0.0000	31.7989	0.0000	0.0006
Thick^2	-0.0430	0.0026	-16.4515	0.0000	-0.0482

SUMMARY OUTPUT (SMA Subgrade-Triple)

<i>Regression Statistics</i>	
Multiple R	0.9759
R Square	0.9524
Adjusted R Square	0.9509
Standard Error	0.5258
Observations	66

ANOVA					
	<i>df</i>	<i>SS</i>	<i>MS</i>	<i>F</i>	<i>Significance F</i>
Regression	2	348.6938678	174.3469	630.5692	2.17935E-42
Residual	63	17.41895572	0.276491		
Total	65	366.1128235			

	<i>Coefficients</i>	<i>Standard Error</i>	<i>t Stat</i>	<i>P-value</i>	<i>Lower 95%</i>
Intercept	14.1982	2.0514	6.9214	0.0000	10.0989
Temp^2	0.0008	0.0000	35.3571	0.0000	0.0007
Thick^2	-0.2591	0.0416	-6.2295	0.0000	-0.3422

BOX TRAILER

SUMMARY OUTPUT (Modified Base-Box)

<i>Regression Statistics</i>	
Multiple R	0.7411
R Square	0.5493
Adjusted R Square	0.5380
Standard Error	1.2368
Observations	83

ANOVA					
	<i>df</i>	<i>SS</i>	<i>MS</i>	<i>F</i>	<i>Significance F</i>
Regression	2	149.1344	74.5672	48.7483	0.0000
Residual	80	122.3709	1.5296		
Total	82	271.5053			

	<i>Coefficients</i>	<i>Standard Error</i>	<i>t Stat</i>	<i>P-value</i>	<i>Lower 95%</i>
Intercept	2.5107	0.5579	4.5001	0.0000	1.4004
Temp^2	0.0005	0.0001	9.8029	0.0000	0.0004
Thick^2	-0.0141	0.0065	-2.1571	0.0340	-0.0271

SUMMARY OUTPUT (Unmodified Base-Box)

<i>Regression Statistics</i>	
Multiple R	0.9005
R Square	0.8110
Adjusted R Square	0.8053
Standard Error	0.8723
Observations	70

ANOVA					
	<i>df</i>	<i>SS</i>	<i>MS</i>	<i>F</i>	<i>Significance F</i>
Regression	2	218.6996	109.3498	143.7165	0.0000
Residual	67	50.9784	0.7609		
Total	69	269.6780			

	<i>Coefficients</i>	<i>Standard Error</i>	<i>t Stat</i>	<i>P-value</i>	<i>Lower 95%</i>
Intercept	2.7042	0.5521	4.8981	0.0000	1.6022
Temp^2	0.0006	0.0000	16.8263	0.0000	0.0006
Thick^2	-0.0184	0.0067	-2.7319	0.0080	-0.0318

SUMMARY OUTPUT (SMA Base-Box)

<i>Regression Statistics</i>	
Multiple R	0.8841
R Square	0.7816
Adjusted R Square	0.7764
Standard Error	1.1298
Observations	44

ANOVA

	<i>df</i>	<i>SS</i>	<i>MS</i>	<i>F</i>	<i>Significance F</i>
Regression	1	191.7986	191.7986	150.2712	0.0000
Residual	42	53.6067	1.2763		
Total	43	245.4053			

	<i>Coefficients</i>	<i>Standard Error</i>	<i>t Stat</i>	<i>P-value</i>	<i>Lower 95%</i>
Intercept	1.14265	0.50061	2.28252	0.02759	0.13238
Temp^2	0.00076	0.00006	12.25852	0.00000	0.00064

SUMMARY OUTPUT (Unmodified Subgrade-Box)

<i>Regression Statistics</i>	
Multiple R	0.8859
R Square	0.7849
Adjusted R Square	0.7796
Standard Error	0.5836
Observations	85

ANOVA

	<i>df</i>	<i>SS</i>	<i>MS</i>	<i>F</i>	<i>Significance F</i>
Regression	2	101.9008	50.9504	149.5943	0.0000
Residual	82	27.9284	0.3406		
Total	84	129.8293			

	<i>Coefficients</i>	<i>Standard Error</i>	<i>t Stat</i>	<i>P-value</i>	<i>Lower 95%</i>
Intercept	2.9336	0.2765	10.6107	0.0000	2.3836
Temp^2	0.0004	0.0000	16.2682	0.0000	0.0003
Thick^2	-0.0234	0.0033	-7.0178	0.0000	-0.0301

SUMMARY OUTPUT (Modified Subgrade-Box)

<i>Regression Statistics</i>	
Multiple R	0.9359
R Square	0.8758
Adjusted R Square	0.8726
Standard Error	0.4335
Observations	79

ANOVA

	<i>df</i>	<i>SS</i>	<i>MS</i>	<i>F</i>	<i>Significance F</i>
Regression	2	100.7643	50.3821	268.0531	0.0000
Residual	76	14.2846	0.1880		
Total	78	115.0489			

	<i>Coefficients</i>	<i>Standard Error</i>	<i>t Stat</i>	<i>P-value</i>	<i>Lower 95%</i>
Intercept	3.4044	0.2183	15.5955	0.0000	2.9696
Temp^2	0.0004	0.0000	19.8029	0.0000	0.0003
Thick^2	-0.0290	0.0024	-11.9393	0.0000	-0.0339

SUMMARY OUTPUT (SMA Subgrade-Box)

<i>Regression Statistics</i>	
Multiple R	0.9292
R Square	0.8634
Adjusted R Square	0.8575
Standard Error	0.6239
Observations	49

ANOVA

	<i>df</i>	<i>SS</i>	<i>MS</i>	<i>F</i>	<i>Significance F</i>
Regression	2	113.1795	56.5897	145.4040	0.0000
Residual	46	17.9027	0.3892		
Total	48	131.0822			

	<i>Coefficients</i>	<i>Standard Error</i>	<i>t Stat</i>	<i>P-value</i>	<i>Lower 95%</i>
Intercept	7.4130	2.8762	2.5774	0.0132	1.6235
Temp^2	0.0006	0.0000	17.0458	0.0000	0.0005
Thick^2	-0.1249	0.0587	-2.1259	0.0389	-0.2431